Role of the cadherin-catenin complex and of tetraspanins in the formation and functionality of Tunneling Nanotubes

Roberto Notario Manzano

Sorbonne Université

ED 394 - Physiologie, physiopathologie et thérapeutique

Trafic membranaire et pathogenèse / Institut Pasteur

Role of the cadherin-catenin complex and of tetraspanins in the formation and functionality of Tunneling Nanotubes

Par Roberto Notario Manzano

Thèse de doctorat de Sorbonne Université

Dirigée par Dr. Christel Brou

Dans le laboratoire de Pr. Chiara Zurzolo

Présentée et soutenue publiquement le 23 Novembre 2022

Devant un jury composé de:

Xavier HOUARD, Professeur des Universités, Président du Jury

Corinne ALBIGES-RIZO, Directrice de recherche, Rapporteur

Marie-Luce VIGNAIS, Chargée de recherche, Rapporteur

Clotilde THÉRY, Directrice de recherche, Examinatrice

Christel BROU, Directrice de recherche, Directrice de thèse

Chiara ZURZOLO, Directrice de recherche, Responsable de structure, Invitée

A la chica de ayer,

que pronto volverá.

Section 1: Preface

Acknowledgments

This PhD study was carried out in 2019-2022 in the Membrane Traffic and Pathogenesis Unit, within the Department of Cell Biology & Infection of the Institut Pasteur.

First of all, I would like to express my appreciation to each member of my thesis jury for accepting to be part of this defense and work. I am grateful to Pr. Xavier Houard to be the president of my jury, also thanks to Dr. Corinne Albiges-Rizo and Dr. Marie-Luce Vignais for accepting to review this manuscript. I am also thankful to Dr. Clotilde Théry to accept to be the examiner.

I would like to thanks all my lab team. I really thank the head of the lab Chiara Zurzolo for giving me the opportunity to be in her lab and for her trust on me. So che tutto ciò che avete fatto è sempre stato per me, per migliorarmi come scienziato, e apprezzo tutto il tempo che avete dedicato a me, grazie mille. I would especially like to thank my thesis supervisor, Christel Brou. Tu m'as appris beaucoup de choses, d'un point de vue scientifique ou plus personnel, et tu ne peux pas imaginer à quel point cela m'a fait grandir. Ce fut un plaisir de travailler avec toi pendant tout ce temps et d'apprendre de toi. Les discussions sans fin sur les expériences et toutes les leçons que j'ai apprises de toi vont me manquer. I would also like to thank all the members of my lab, those still present and those who are no longer in the lab, Sylvie, Stéphanie, Parisa, Michael, Maura, Inés, Olga, Thea, Lalitya, Sevan, Malala, Nathaly, Kinga, Ranabir, Shiyu, Dandan, Harsh, Diego, Aysegul, Reine (merci beaucoup Reine d'être toujours prête à aider avec le sourire, je pense que tu es le membre le plus indispensable du laboratoire), and many other (honestly, I don't even count how many people have passed through here in these three years). I would like to specially thank Anna, with whom I entered the lab as her student and over time we continued to work together as colleagues, questa tesi è anche un po' parte di te, and Nina, who accompanied me for more than two years and who made my stay much more fun thanks to her incredibly positive personality, знаш да те веома ценим и надам се да се никада нећеш променити.

Also, I am very grateful to all my comité de suivi de thèse members, Célia Caillet-Saguy, Remi Piedagnel, René-Marc Mège and Eric Rubinstein, who besides being a member of the committee has been our collaborator and to whom I am very grateful for all the knowledge that he has been able to transmit to me.

Un gracias infinito a todas esas personas con la que he compartido mi vida en Paris durante todo este tiempo: Juanma, Carlos, Raquel, Ivan, Júlia, Sebas, Laura, Livier, Rocio, Alicia, Catarina, Hugo, Anna, María, Cristina, Ruben, Neris, Egill, David, Agus, Markel, Samu, Laura, Frank, Pedro y Pablo. No querria terminar este pequeño pero no menos importante parrafo mencionando a cuatro personas especiales para mi. Alejandro (eres demasiado inteligente, contratame cuando tengas tu grupo), me has hecho pasar grandes momentos aqui y siempre has estado ahi en momentos en los que se te necesitaba. Clari, que habriamos hecho sin tí!, siempre has estado ahí y nunca nos has fallado a los dos y mucho menos a mí, solo tengo palabras de agradecimiento para tí. Y Lorea y Haser, creo que hemos construido una relacion especial entre los 4 y de verdad aprecio mucho vuestra amistad! Eskerrik asko Lorea beti hor egoteagatik (nahiz eta beti berandu iristen den) eta nigatik benetako kezka agertzeagatik eta biok hainbeste zaintzeagatik (probablemente esté escrito como la mierda por que el traductor no funciona bien con el euskera pero es lo que hay, tampoco tú lo hablas muy bien…). Haser, benim için gerçek bir dost oldun ve ne kadar sadık ve iyi bir insan olduğunu gerçekten takdir ediyorum, seninle anlaşmak ve seni arkadaşım olarak görmek çok kolay oldu (I say the same as Lorea, if it is not well written it is not my fault, it is the translator's).

También quería agradecer a toda mi familia su apoyo y sobre todo a mis padres, sin ellos jamás hubiera llegado a este punto, gracias por apoyarme y ayudarme en todo lo que he necesitado a lo largo de todos estos años. No es ninguna mentira que sin ellos no podria haber hecho esta tesis por que siempre confiaron en mi y me apoyaron en todos los pasos que dí.

“Es igual que en los grandes cuentos, los cuentos que eran importantes, estaban llenos de oscuridad y peligro, a veces uno no querría saber el fin, porque, ¿cómo podría ser un final feliz?, ¿cómo podría ser el mundo como antes cuando han pasado tantas cosas malas? Pero al final, las sombras sólo son, transitorias, aún la oscuridad debe terminar. Vendrá un nuevo día, cuando el sol brille iluminará hasta la claridad. Esos eran los cuentos que permanecían, que tenían significado, aunque fuera demasiado pequeño para entender por qué. Pero, creo que si lo entiendo, ahora lo sé, porque la gente en ellos tuvo ocasión de dar la vuelta y nunca lo hizo, siguió caminando porque tenía algo de lo cual aferrarse”. Rebe, 12 años desde que nos conocemos, 9 desde que estamos juntos. Como casi todo durante este tiempo, esta aventura la empezamos juntos, y aunque

puede haber gente a la que esto le agobiaría, yo no veo como podria haber hecho esto sin ti. Cuantas cosas hemos pasado juntos y cuantas nos quedan por pasar, si he podido estar a gusto en París o en el doctorado ha sido sin lugar a dudas por tenerte a mi lado y no me arrepiento de ninguna decision tomada por que siempre ha sido pensando en los dos. No vamos a mentir, no hemos disfrutado estos ultimos años tanto como en otros momentos, pero ojala todo el mundo pudiese sentir lo que siento yo y es que hasta los malos momentos a tu lado merecen la pena vivirlos. Sin duda alguna, cada segundo invertido en esta tesis esta dedicado a ti, a tu sacrificio para que yo hiciese este trabajo. Da igual lo que hemos pasado, da igual lo que viene, contigo todo ha merecido, merece y merecerá la pena.

Thank you very much, merci beaucoup, muchísimas gracias to all the people that have shared this journey with me.

Summary

Intercellular communications are fundamental for proper development and survival of any organism. The mechanisms of communication between cells can be varied, including exchange of information and material either through the secretion of substances or ligands at a distance such as paracrine, autocrine or endocrine communication, or through cell-to-cell contact communication such as through synapses or gap junctions.

Within this last group of mechanisms of cell-to-cell communication through direct contact is included a novel structure discovered in 2004, the Tunneling Nanotubes or TNTs. TNTs are membranous cellular structures with a basic composition of actin filaments that extend from one cell to another forming an open channel or tunnel thus allowing the exchange of cellular material between these two connected cells. These structures are involved in the development and propagation of different diseases, such as different types of cancers or neurodegenerative diseases like Alzheimer's disease or Parkinson's disease.

In order to better understand these structures, my thesis project is based on the study of the major processes of TNT formation such as the protrusive activity of the membrane, the adhesion of these structures with the opposing cell and the subsequent possible fusion of the TNTs to form these open tunnels. Specifically, my research is focused on studying the role of different proteins such as the cadherin-catenin complex or the tetraspanins and their possible role in these processes of TNTs formation.

Regarding the cadherin-catenin complex in the regulation of TNTs, I have shown how N-cadherin controls the architecture of TNTs at the ultrastructural level (based on individual TNTs or iTNTs) by increasing the parallel and straight ordering of TNTs from one cell to the other. Furthermore, N-cadherin is able to regulate the adhesion process of TNTs with the opposing cell, thus controlling the stability of these structures and promoting their increased durability presumably then facilitating the transfer of cargo by TNTs. Furthermore, I have been able to show how N-cadherin does not act alone in the regulation of TNTs, but collaborates with alpha-catenin, one of its associated proteins, acting alpha-catenin downstream and in the same pathway as N-cadherin. On the other hand, I have also studied the role of tetraspanins CD9 and CD81, two molecules well known for their functions in different membrane protrusion and membrane fusion

processes, in the formation and functionality of TNTs. Here I have been able to show how these two tetraspanins act in the formation of TNTs and have complementary functions: CD9 being involved in the initiation of the TNT formation process, i.e. the evagination of the membrane protrusion as well as its extension towards the opposing cell, while CD81 seems to be involved in the membrane fusion process of TNTs with the opposing cell.

Therefore, my project has contributed to the basic knowledge of structures whose understanding is a necessary step to understand the development and progression of several pathologies.

Résumé

Les communications intercellulaires sont fondamentales dans le maintien du bon développement et de la survie de tout organisme. Les mécanismes de communication entre les cellules peuvent être variés, permettant l'échange d'informations et de matériel soit par la sécrétion de substances ou de ligands à distance par communication paracrine, autocrine ou endocrine, soit par contact direct entre cellules grâce aux synapses ou aux gap-jonctions.

Parmi les mécanismes de communications intercellulaires par contact direct s'intègre une nouvelle structure découverte en 2004, les Tunneling Nanotubes ou TNT. Les TNT sont des structures cellulaires membraneuses à base de filaments d'actine qui relient deux cellules en formant un canal ouvert ou tunnel, permettant ainsi l'échange direct d'éléments cellulaires entre les deux cellules connectées. Ces structures sont impliquées dans le développement et la propagation de différentes maladies, telles que différents types de cancers ou de maladies neurodégénératives comme la maladie d'Alzheimer ou la maladie de Parkinson.

Afin de mieux comprendre ces structures, mon projet de thèse s'appuie sur l'étude des processus majeurs de formation des TNT tels que l'activité protrusive de la membrane, l'adhésion de ces structures avec la cellule opposée et la possible fusion ultérieure des TNT pour former ces tunnels ouverts. En particulier, mes recherches portent sur l'étude du rôle de différentes protéines telles que le complexe cadhérine-caténine ou les tétraspanines et leur rôle éventuel dans ces processus de formation des TNT.

En ce qui concerne le complexe cadhérine-caténine dans la régulation des TNT, j'ai montré que la N-cadhérine contrôle l'architecture des TNTs au niveau ultrastructural (c'est à dire sur les TNTs individuels ou iTNTs) en augmentant l'ordre parallèle et droit des TNT d'une cellule à l'autre. De plus, la N-cadhérine est capable de réguler le processus d'adhésion des TNT avec la cellule opposée, contrôlant ainsi la stabilité de ces structures et favorisant leur durabilité accrue, et par là-même facilitant vraisemblablement le transfert des cargos par les TNT. De plus, j'ai pu montrer comment la N-cadhérine n'agit pas seule dans la régulation des TNTs, mais collabore avec l'alpha-caténine, une de ses protéines associées, faisant agir l'alpha-caténine en aval et dans la même voie que la N-cadhérine.

D'autre part, j'ai également étudié le rôle des tétraspanines CD9 et CD81, deux molécules bien connues pour leurs fonctions dans différents processus de protrusion membranaire et de fusion membranaire, dans la formation et la fonctionnalité des TNT. Ici, j'ai pu montrer comment ces deux tétraspanines ont des fonctions complémentaires dans les TNT puisque CD9 semble être impliqué dans l'initiation du processus de formation du TNT, c'est-à-dire l'évagination de la protrusion membranaire ainsi que son extension vers la cellule opposée, tandis que CD81 semble être impliqué dans le processus de fusion membranaire des TNT avec la cellule opposée.

Mon projet a donc contribué à la connaissance fondamentale de structures dont la compréhension est une étape nécessaire pour comprendre le développement et la progression de plusieurs pathologies.

Résumé de la thèse

La communication intercellulaire pourrait être définie comme la capacité des cellules à communiquer avec elles-mêmes, les autres cellules ou l'environnement leur permettant de s'adapter et de répondre à une multitude de changements qui se produisent autour d'elles et comme pour tout type de communication il faut un émetteur, un récepteur et un message. On pourrait subdiviser les communications intercellulaires en communications indépendantes des contacts entre les cellules et dépendantes des contacts. Des exemples classiques de communications indépendantes des contacts sont la signalisation autocrine (lorsqu'un signal produit par une cellule est reçu par les récepteurs de cette même cellule), la paracrine (lorsqu'un signal secrété dans l'espace extracellulaire se lie à ou est capté par une cellule réceptrice qui se trouve dans le voisinage immédiat) ou la signalisation endocrinienne (qui se produit entre des cellules largement séparées au sein d'un organisme et le message étant transporté par le flux sanguin). D'autre part, des exemples de communications dépendantes du contact sont les pili (qui sont des projections de bactéries qui permettent le transfert horizontal de matériel génétique), les plasmodesmes (canaux aqueux formés par le réticulum endoplasmique des cellules des plantes), les cytonèmes (protrusions d'actine chez la Drosophile ou les vertébrés permettant le transport à distance de morphogènes) et les gap-jonctions (formées par des canaux qui relient deux cellules voisines, elles sont importantes pour le transport des ions et des petites molécules biologiques).

Mais, en 2004, dans le laboratoire de Hans-Hermann Gerdes, Rustom et ses collègues ont découvert un type de communication directe de cellule à cellule qui permet l'échange d'une grande variété de cargaisons entre les cellules, qu'ils appellent les tunneling nanotubes ou TNT.

Les TNT sont de minces tunnels membraneux non adhérents, allant de 50 à 700 nm de diamètre et jusqu'à 100 µm de long. Leur composition cytosquelettique est toujours à base d'actine, bien que certains types de cellules puissent contenir des microtubules ou des filaments intermédiaires. Ce qui définit vraiment les TNT, c'est leur capacité à transférer une grande variété de cargaisons telles que le calcium, les agents pathogènes, les organites ou les protéines mal repliées, et c'est cette capacité à transférer des cargaisons qui les rend impliqués dans différentes maladies telles que la maladie de Parkinson, la maladie d'Alzheimer ou dans la propagation de maladies infectieuses comme le Covid-19.

Au fil des années, différentes études ont montré que les TNT peuvent avoir diverses morphologies. Ainsi, aujourd'hui, on peut trouver des TNT qui suivent la description originale de Rustom et al., 2004, comme étant des structures ouvertes qui relient deux cellules distantes et qui peuvent être minces ou épaisses, mais on peut aussi trouver des TNT fermés à leur extrémité, se terminant typiquement par des gap-jonctions. Cependant, en 2019, notre laboratoire a découvert que les TNT, du moins dans les cellules neuronales, ne sont pas toujours composés d'un seul tube, mais peuvent être formés par un faisceau de TNT plus fins, appelés TNT individuels ou iTNT.

Dans ce travail, notre groupe a démontré que, bien que les TNT dans les cellules neuronales semblent être une structure unique en microscopie à fluorescence et à faible grossissement, en cryo-microscopie électronique ces TNT peuvent en fait être constitués d'un faisceau de TNT individuels (iTNT) dans lequel des cargaisons, telles que des vésicules, peuvent se trouver. En appliquant la microscopie électronique à faisceau ionique focalisé, notre laboratoire a démontré qu'ils peuvent en effet être ouvertes. Enfin, ils ont découvert que les iTNT sont reliés entre eux par des liens à l'échelle nanométrique positifs pour la N-cadhérine qui fonctionneraient vraisemblablement comme support du faisceau d'iTNT.

Malgré cette diversité morphologique et compositionnelle, il a été émis l'hypothèse que les TNT seraient formés par deux mécanismes distincts qui ne s'excluent pas mutuellement, la protrusion induite par l'actine et le mécanisme de délogement cellulaire. Dans le mécanisme piloté par l'actine, nous pouvons trouver l’une ou les deux cellules impliquées dans la formation de ces structures, ce qui entraînerait la croissance d'une protubérance de type filopode F-actine. Ensuite, la polymérisation de l'actine peut se produire pour provoquer l'allongement et la croissance de la protrusion vers la cellule réceptrice. Après allongement, la pointe de la protrusion établit un contact physique direct avec la cellule cible, impliquant éventuellement des molécules d'adhésion. Enfin, la fusion membranaire doit avoir lieu lors du contact cellule-cellule afin de permettre la continuité membranaire pour établir une connexion TNT ouverte. Selon le mécanisme de délogement cellulaire, les TNT proviendraient de deux cellules qui sont en contact très étroit et lorsque ces cellules migrent dans des directions opposées, elles laisseraient entre elles un TNT. Il est supposé, bien qu'il n'y ait pas encore de preuves, que les molécules d'adhésion cellulaire favoriseraient les étapes initiales de ce type de formation de TNT et

que la fusion TNT-membrane cellulaire pourrait se produire soit au début de ce processus, soit à un moment donné au cours de la formation. .

Bien que les TNT puissent être formés selon ces deux mécanismes, il est concevable que les mêmes processus de formation soient partagés dans les deux modèles mais pas dans le même ordre. Ce processus de formation commencerait avec une cellule dans un état inactif. Ensuite, les cellules pourraient être stimulées par divers signaux qui induiraient la courbure positive de la membrane nécessaire à la formation de TNT et seraient suivies d'une polymérisation de l'actine pour former des faisceaux d'actine initiaux capables de surmonter l'élasticité de la membrane, permettant un allongement supplémentaire du TNT. Ensuite, le TNT développé à partir d'une cellule atteindrait la cellule opposée, adhèrerait et fusionnerait avec sa membrane selon un mécanisme inconnu. Enfin, un TNT fonctionnel se formerait entre les deux cellules contenant des filaments d'actine, et pourrait maintenant échanger du matériel cellulaire. Ces derniers processus d'adhésion et de fusion des TNT avec les cellules antagonistes n'ayant pas été investigués, j'ai considéré qu'étudier des candidats pouvant avoir un rôle très important dans ces étapes de la formation des TNT pourrait élargir nos connaissances sur les TNT. J'ai choisi les cadhérines et les tétraspanines en se concentrant sur la N-cadhérine et sur les tétraspanines CD9 et CD81.

Concernant mon premier candidat, la famille des cadhérines est une superfamille de plus de 100 protéines avec plusieurs sous-familles qui partagent une fonction commune : être des molécules d'adhésion entre les cellules. Dans cette superfamille, les plus connues sont les cadhérines classiques E-cadhérine et N-cadhérine. Ces cadhérines forment ce que l'on appelle l'adhésome de cadhérine, un complexe d'adhésion cellule-cellule appelé jonction adhérente, composé de cadhérines et de molécules associées aux cadhérines : les cadhérines sont des molécules qui médient l'adhésion cellulaire homophile dépendante de Ca2+ et sont composées de : 5 éléments hautement conservés des ectodomaines avec lesquels les molécules de cadhérine interagissent entre elles, 1 seul passage transmembranaire et une queue cytoplasmique avec laquelle elles interagissent avec leurs molécules associées. Ces molécules associées aux cadhérines sont : la p120-caténine (qui contrôle le renforcement de l'adhésion à base de cadhérines, le regroupement de ces molécules et le recyclage), la β-caténine (impliquée dans la transmission des signaux mécaniques aux cadhérines et dans la voie Wnt) et l'α-caténine (qui relie la jonction

adhérente au cytosquelette d'actine et lie également et regroupe l'actine et les protéines liées à l'actine).

Malheureusement, le rôle des cadhérines et/ou des caténines dans les TNT n'a guère été étudié. Le premier rapport sur la présence du complexe cadhérine-caténine dans les TNT remonte à 2010, dans lequel Lokar et ses collègues ont trouvé dans les cellules urothéliales T24 à la fois la N-cadhérine et la β-caténine le long des TNT et ont émis l'hypothèse que le complexe cadhérine-caténine servirait comme 'ancrage des TNT avec la cellule opposée pour former ensuite un canal ouvert, mais aucun rôle fonctionnel autre que la présence de ces molécules n'a été étudié. Une autre cadhérine, dans ce cas ECAD également associée à la β-caténine, a été trouvée dans des cellules de testicule de porc enrichies dans la zone d'adhérence des TNT avec la cellule opposée et pourrait assurer une continuité cytoplasmique avec la cellule opposée, encore une fois sans affirmer le rôle de ces molécules. Notre laboratoire a récemment découvert que, au moins dans les cellules neuronales, la formation de TNT est régulée par une voie Wnt indépendante de la β-caténine, que les TNT sont constitués d'iTNT qui forment un faisceau et que cette structure semble être maintenue par des molécules de N-cadhérines. Cette année seulement, deux nouvelles études sont apparues concernant la N- cadhérine et les TNT. Dans l'une d'elles, ils affirment que la formation de TNT fermés est facilitée par la N-cadhérine et dans la seconde étude, ils ont découvert que la N-cadhérine détermine principalement la résistance à la traction et la résistance à la flexion des TNT. Par conséquent, j'ai commencé ce projet visant à fournir une étude plus complète sur le rôle de la N- cadhérine ainsi que du complexe cadhérine-caténine dans les TNT.

Par ailleurs, je souhaitais également apporter un éclairage sur d'autres molécules peu étudiées dans le cadre des TNT, comme c'est le cas de mes seconds candidats, les tétraspanines CD9 et CD81. Comme pour la N-cadhérine, les tétraspanines ont également été montrées sur les TNT, mais dans une seule étude qui montre leur présence sur les TNT des tétraspanines CD9 et CD81 lorsqu'elles étaient surexprimées dans les lymphocytes T. D'autre part, nous avons découvert au laboratoire grâce aux travaux de ma directrice de thèse le Dr Christel Brou utilisant l'analyse par spectrométrie de masse, que ces deux tétraspanines étaient abondamment représentées dans la fraction TNT parmi les protéines membranaires.

Les tétraspanines sont de petites protéines transmembranaires avec une grande variété de fonctions et partageant toutes une structure commune composée de : deux courtes queues cytoplasmiques, quatre domaines transmembranaires, un domaine intracellulaire et deux domaines extracellulaires, la boucle extracellulaire courte (small extracellular loop ou SEL) et la grande boucle extracellulaire (large extracellular loop ou LEL). Ce qui définit réellement les tétraspanines, c'est leur capacité à interagir avec une grande quantité de molécules différentes formant des domaines membranaires appelés«Tetraspanin-enriched microdomains» ou «Tetraspanin webs». Par conséquent, ces tétraspanines peuvent interagir avec d'autres tétraspanines, des partenaires de tétraspanines (comme les membres de la famille des immunoglobulines EWI-2 et CD9P-1), des intégrines ou former des complexes secondaires avec différentes molécules telles que les métalloprotéases, les intégrines ou le cytosquelette d'actine.

Cette diversité d'interactants est ce qui pourrait déterminer certaines des fonctions des tétraspanines. En général, les tétraspanines agissent dans une variété de processus cellulaires tels que dans la composition des vésicules extracellulaires (dans lesquelles CD63 peut être trouvé comme marqueur des exosomes et CD9 et CD81 dans les ectosomes), elles peuvent réguler l'établissement et le renforcement de l'adhésion des intégrines (en particulier CD151) ou réguler certains processus induits par des virus tels que la fusion, le bourgeonnement ou la libération (pour des virus tels que le virus du papillome humain, le VIH ou le virus de l'hépatite C). Spécifiquement pour les tétraspanines CD9 et CD81, ces deux tétraspanines ont été associées à la formation d'un autre type de protrusion. Il a été démontré qu'elles peuvent favoriser la formation de microvillosités et de jonctions de digitation, et cela est très probablement dû à leur forme moléculaire, puisque la structure en cône inversé de ces tétraspanines peut favoriser la flexion de la membrane. Un autre processus hautement régulé par ces tétraspanines est la fusion membranaire, car il a été démontré que CD9 et CD81 sont des régulateurs positifs de la fusion ovocyte- sperme mais des régulateurs négatifs de la fusion des cellules musculaires et de la formation de cellules géantes multinucléées.

Par conséquent, cela m'a indiqué que les tétraspanines CD9 et CD81 pourraient avoir une importance majeure dans certains processus de formation de TNT.

1. Régulation de la formation des TNT pas l'axe N-cadhérine/α-caténine

En ce qui concerne mon premier projet, j'ai cherché à caractériser le rôle possible de la N-cadhérine en tant que régulateur de la formation des TNT et d'autres processus liés à ces structures tels que la maintenance des faisceaux iTNT, l'adhésion ou la fusion des TNT. De plus j'ai voulu décrypter le rôle possible de l'effecteur en aval des cadhérines sur le cytosquelette d'actine, l'α-caténine, dans la régulation des TNT par la N-cadhérine.

Pour comprendre le rôle de la N-cadhérine sur les TNT, j'ai d'abord décidé d'inhiber (knock-down ou KD) cette protéine et j'ai étudié l'effet sur les TNT. Sur le KD de la N-cadhérine, j'ai observé que le pourcentage de cellules connectées par des TNT est augmenté. De manière surprenante et contrairement à ce que l'on pourrait attendre de l'augmentation des structures capables de transférer du matériel, lorsque j'ai vérifié la fonctionnalité des TNT dans des conditions de N-cadhérine KD par notre test de coculture, j'ai montré que le transfert de vésicules était significativement diminué par le KD de N -cadherin, montrant une déconnexion entre le nombre de TNT et la capacité de transfert. Pour mieux comprendre ce phénomène, j'ai surexprimé (overexpress ou OE) la N-cadhérine marquée à la GFP. Sur cet OE, j'ai observé le phénotype contraire du KD, avec une importante diminution des cellules connectées par des TNT mais une augmentation du transfert de vésicules. Par conséquent, la N-cadhérine diminue la formation de TNT alors qu'elle augmente leur fonction de transfert. Cet écart entre le nombre de TNT et le transfert de vésicules pourrait montrer un défaut de fusion ou d'adhésion des TNT avec la cellule opposée.

Ainsi, on s'est demandé quelle serait la structure de ces TNT. Dans ce but, en collaboration avec le Dr Anna Pepe, nous avons appliqué notre approche Correlative Cryo-EM pour étudier l'ultrastructure des TNT. Nous avons observé que sur le KD de la N-cadhérine, la structure parallèle et bien organisée du faisceau d'iTNT des conditions de contrôle était affectée, montrant des iTNT désordonnés qui se croisaient et de nombreux iTNT interrompus avec des extrémités fermées. Contrairement à cela, l'OE de la N-cadhérine a montré des iTNTs droits et parallèles. En analysant nos tomographies, nous avons classé les iTNTs en deux catégories selon leur continuité ou non d'une cellule à l'autre, ceux qui n'étaient pas interrompus ont été classés en « extension complète » et ceux interrompus en « extrémités fermées ». Dans les conditions de contrôle, nous avons observé que la majorité des iTNT s'étendaient complètement d'une cellule à l'autre. Cependant, lorsque nous avons KD N-cadhérine, ce phénotype a changé, montrant une

augmentation des iTNT fermés, avec un phénotype similaire dans les conditions OE. Ainsi, ces données suggèrent que notre hypothèse selon laquelle la N-cadhérine participe à l'organisation du faisceau d'iTNT semble être correcte. De plus, l'augmentation des iTNT fermés lorsque nous K/D N-cadhérine peut refléter que l'absence de cette protéine rend les TNT instables ou moins capables de fusionner.

Pour tester la possibilité que la N-cadhérine régule la stabilité des TNT, j'ai mesuré la durée des TNT déjà formés par imagerie sur cellules vivantes en faisant un enregistrement continu de ces TNT jusqu'à leur rupture. J'ai découvert que, sur les TNT provenant de cellules KD pour la N-cadhérine, la durée de ces structures avait tendance à être plus courte, alors que lorsque la N-cadhérine est surexprimée, les TNT avaient une plus longue durée. Ainsi, la N-cadhérine améliorerait la stabilité des TNT et les changements observés sur le transfert des vésicules pourraient être le résultat d'un changement de la stabilité des TNT provoqué par la N-cadhérine.

Connaissant l'importance de la N-cadhérine dans la régulation des TNT, j'ai décidé d'examiner le rôle possible que l'α-caténine, l'adaptateur des cadhérines au cytosquelette d'actine, pourrait jouer dans les TNT. Pour ce faire, et comme c'était le cas pour la N-cadhérine, j'ai décidé de KD ou OE α-caténine et de regarder l'effet sur le nombre de TNT et le transfert de vésicules. Le KD de l'α-caténine a montré une augmentation du nombre de cellules connectées par les TNT mais contrairement à cela, le transfert des vésicules a diminué. De façon remarquable, ces résultats étaient quasiment identiques à ceux obtenus avec la N-cadhérine KD. D'autre part, l'OE de l'α-caténine a montré une diminution du nombre de cellules connectées au TNT mais une augmentation du transfert des vésicules. Encore une fois, ces résultats étaient extrêmement similaires à ceux obtenus avec la N-cadhérine OE. Par conséquent, l'α-caténine a phénocopié l'effet de la N-CADHERIN sur les TNT. Mais on peut se demander s'il en serait de même à un niveau ultrastructural. Là encore, nous avons observé le même phénotype pour le KD de l'α-caténine que pour la N-cadhérine (iTNT désorganisés et iTNT fermés) et le même pour l'OE (avec des iTNT hautement organisés et parallèles). Dans ce cas, la quantification de la continuité des iTNT a révélé que dans les conditions KD, la plupart des iTNT étaient fermés alors que dans les conditions OE, ils s'étendent pour la plupart complètement d’une cellule à l’autre, ceci constituant un phénotype similaire mais encore plus aigu par rapport à la N-cadhérine KD ou OE. Ainsi, tous les résultats de l'α-caténine étaient parfaitement conformes à leurs

résultats respectifs de la N-cadhérine sur le nombre de TNT, le transfert de vésicules et l'ultrastructure, ce qui pourrait signifier que la N-cadhérine et l'α-caténine fonctionnent dans la même voie de régulation des TNT.

Ensuite, j'ai décidé d'étudier si la N-cadhérine et l'α-caténine pouvaient fonctionner dans la même voie dans la régulation des TNT. Dans ce but, j'ai KD α-caténine dans les cellules OE N-cadhérine (cellules qui forment peu de TNT mais transfèrent beaucoup de matériel) et j'ai trouvé que ce KD inversait l'effet de l'OE de N-cadhérine (bien que n'atteignant pas les niveaux des conditions sauvages). Par conséquent, j'ai montré ici que l'α-caténine agit en aval de la N-cadhérine sur la régulation du TNT.

Enfin, afin d'exclure si ces deux protéines étaient nécessaires dans les populations de cellules donneuses et acceptrices, j'ai effectué des expériences en utilisant des cellules qui étaient OE N-cadhérine par rapport aux cellules KD pour l'α-caténine. Ces expérimentations ont consisté en une coculture de ces deux populations et dans deux conditions différentes :

1) Utiliser les cellules OE N-cadhérine comme donneuses et donc avec des vésicules colorées et les co-cultiver avec des cellules acceptrices exprimant mCherry (servant à les distinguer des cellules GFP N-cadhérine) et transfectées avec un siRNA contrôle ou ciblant l'α-caténine.

2) Cellules donneuses exprimant mCherry et transfectées avec un siRNA contrôle ou ciblant l'α-caténine avec des vésicules colorées co-cultivées avec des cellules acceptrices OE N-cadhérine. Dans cette expérience, les résultats obtenus ont montré que peu importe que les cellules KD pour l'α-caténine soient utilisées comme donneuses ou acceptrices, elles diminuaient toujours le transfert de vésicules, ce qui signifie que la N-cadhérine et l'α-caténine étaient nécessaires dans les deux populations cellulaires. Nous avons également vérifié l'ultrastructure des TNT dans cette condition, des TNT formés entre les cellules OE N-cadhérine et les cellules KD pour l'α-caténine et nous avons constaté que les iTNT fermés étaient très courants, qu'il s'agisse de la cellule OE N-cadhérine ou la cellule KD pour l'α-caténine celle formant le TNT. En effet, la quantification de nos tomogrammes a montré que la grande majorité des iTNT formés par n'importe quelle cellule étaient fermés, ce qui signifie que le manque d'α-caténine altère le rôle de la N-cadhérine dans l'adhésion homophile sur les TNT.

En conclusion de ce projet, nous savons maintenant que le complexe cadhérine-caténine a un rôle majeur sur la régulation des TNT, la N-cadhérine étant un organisateur de la structure du TNT puisque l'absence de cette protéine entraîne des iTNT désordonnés. De plus, la N-cadhérine s'est avérée avoir une double fonction sur les TNT, puisque cette protéine diminue la formation de TNT tout en augmentant leur fonction de transfert. Et enfin, ici, j'ai montré que l'α-caténine est essentielle et travaille en aval de la N-cadhérine dans la régulation des TNT.

2. Régulation des TNT par les tétraspanines CD9 et CD81

En ce qui concerne mon deuxième projet, le rôle de CD9 et CD81 dans les TNT, mon objectif général était d'étudier le rôle possible de CD9 et CD81 sur la formation de TNT lié à leur capacité à induire une courbure membranaire et d'évaluer le rôle de ces tétraspanines sur la fonctionnalité des TNT par leur capacité à contrôler différents événements de fusion membranaire.

Pour comprendre quel rôle jouaient CD9 et CD81 sur les TNT, j'ai d'abord décidé d'inactiver (knock-out ou KO) ou OE CD9 et/ou CD81 et de vérifier le nombre de TNT que ces cellules formaient. Tout d'abord, j'ai trouvé que dans le KO de CD9, le nombre de TNT était diminué alors que le KO de CD81 n'affectait pas les cellules connectées par des TNT. Lorsque j'ai KO à la fois CD9 et CD81, ces cellules DKO doubles KO (DKO) ont montré une énorme réduction du % de cellules connectées par des TNT, encore plus faible que le simple CD9 KO. Pour explorer ces observations, j'ai OE CD9 ou CD81 et j'ai observé que CD9 OE, contrairement au KO, augmentait le nombre de TNT, alors que CD81 OE, comme c'était le cas pour le KO, n'affectait pas le nombre de TNT. Ces données signifieraient que CD9 pourrait réguler le processus de formation (et/ou de stabilité) des TNT alors que CD81 pourrait ne pas être impliqué dans ce processus. De plus, l'énorme diminution des TNT dans les cellules DKO par rapport au seul CD9 KO peut indiquer un rôle partiellement redondant de ces tétraspanines.

Une fois que j'ai évalué l'effet de ces tétraspanines sur la formation de TNT, j'ai ensuite étudié l'implication de CD9 et CD81 dans la fonctionnalité des TNT. Pour cela, j'ai utilisé notre test de coculture, en utilisant les cellules KO tétraspanines comme cellules donneuses et donc en colorant leurs vésicules. Les cellules CD9 KO ont montré une corrélation du transfert avec le nombre de TNT, puisque ce KO a diminué le transfert des

vésicules. Étonnamment, bien que ne modifiant pas le nombre de TNT, les cellules CD81 KO ont diminué le transfert de vésicules et les cellules DKO, comme c'était le cas pour le nombre de TNT, ont fortement diminué le transfert de vésicules à des niveaux inférieurs au KO unique respectif. Lors de l'utilisation des cellules OE CD9 ou CD81 dans ce même système de coculture, CD9 ou CD81 OE ont augmenté le transfert de vésicules. Par conséquent, ces données pourraient signifier que CD9 pourrait réguler la formation et la fonctionnalité des TNT tandis que CD81 semblerait jouer un rôle dans la fonction de transfert des TNT (peut-être en contrôlant la fusion des TNT avec les cellules réceptrices).

Sachant que CD9 peut être impliqué dans la formation des TNT, que la conformation moléculaire des molécules de CD9 peut induire une courbure membranaire et que le regroupement induit de CD9 peut être obtenu en traitant des cellules avec des anticorps spécifiques contre cette protéine qui pourraient conduire à la formation de protrusions telles que les microvillosités, j'ai postulé que CD9 pourrait être impliqué dans les étapes initiales de la formation et j'ai demandé si la promotion du regroupement de CD9 pouvait affecter le nombre et la fonction des TNT. L'incubation pendant 2 heures avec des anticorps anti-CD9 dans des cocultures de 24 heures utilisant des cellules WT a conduit à une augmentation du % de cellules connectées par des TNT qui était corrélée à une augmentation du transfert de vésicules. Lors de la répétition de ces séries d'expériences sur des cellules KO CD81, l'augmentation des TNT par les anticorps n'a pas été affectée par le manque de CD81 mais, cette augmentation des TNT n'a pas été accompagnée d'une augmentation du transfert de vésicule. Ces données suggèrent que, premièrement, le regroupement de CD9 pourrait induire la formation de TNT ou participer à la stabilité de ces structures et deuxièmement, que CD9 ne nécessite pas de CD81 pour former/stabiliser des TNT, mais que si CD81 n'est pas présent, la fonctionnalité des TNT est compromise.

Les données ci-dessus montrent que CD9 et CD81 régulent le transfert de matériel via TNT. Cependant, comme l'expression de CD9 est associée à un nombre accru de TNT, il reste à déterminer à ce stade si CD9 régule le transfert indépendamment de cet effet sur la formation/stabilisation de TNT. Pour répondre à cette question, nous avons KO CD81 dans les cellules OE CD9. La surexpression de CD9 était associée à une augmentation du % de cellules connectées par des TNT, qui n'a pas changé après le KO CD81, ce qui est cohérent avec le fait que CD81 ne joue pas de rôle dans la formation des TNT, du moins dans les cellules exprimant CD9. Cependant, le transfert dans les cellules OE CD9 n'était

pas sensible au KO CD81, contrairement aux cellules WT, suggérant que l'OE de CD9 peut compenser l'impact de l'absence d'expression de CD81 sur le transfert des vésicules. Auparavant, j'ai montré que CD81 OE ne stimule pas le nombre de TNT dans les cellules exprimant CD9. Pour déterminer si le CD81 peut remplacer le CD9 dans la stimulation/stabilisation du TNT, nous avons éliminé le CD9 dans les cellules CD81 OE. CD9 KO a réduit le nombre de TNT dans ces cellules CD81 OE. Ainsi, CD81 ne peut pas compenser CD9 pour la formation/stabilisation de TNT. La diminution du transfert de vésicule observée dans les cellules CD81 OE, CD9 KO est probablement une conséquence de cette diminution du nombre de TNT.

Par conséquent, ici, j'ai démontré que, à la fois CD9 et CD81 ont un rôle sur les TNT, mais ils peuvent agir sur différents processus ou étapes, avec CD9 régulant vraisemblablement la formation des TNT tandis que CD81 contrôlerait la fonctionnalité des TNT, peut-être en régulant la fusion du TNT avec la cellule adverse. Enfin, j'ai montré que CD9 OE peut compenser l'absence de CD81, mais pas l'inverse.

En conclusion de tous les résultats présentés, je propose le modèle hypothétique suivant pour la formation des TNT:

1) La première étape initiale consisterait en une cellule à l'état inactif contenant CD9, CD81 et N-cadhérine/α-caténine au niveau de la membrane

2) Lors de la réception d'un stimulus, ou peut-être spontanément, CD9 se regrouperait, pliant la membrane en raison de sa forme moléculaire. De plus, la polymérisation de l'actine pourrait aider au processus de déformation de la membrane, conduisant à la formation d'une microprotrusion .

3) Une fois cette microprotrusion formée, le regroupement et la polymérisation de l'actine conduiraient à la formation de filaments d'actine qui allongeraient la protubérance en formant un TNT en croissance. Ici, je propose que CD9, qui a initié ce processus, apporterait avec lui le complexe cadhérine/caténine et CD81.

4) Une fois que la pointe du TNT atteint la cellule opposée, ces deux membranes adhéreraient par adhésion homophile médiée par la N-cadhérine et l'α-caténine qui rapprocheraient les membranes.

5) Maintenant, le TNT continuerait à pousser sur la cellule opposée, produisant des forces de poussée, mais de par les forces de traction et de résistance dans la cellule opposée, de la même manière que ce qui a été observé dans la fusion des myoblastes, cela conduirait à la fusion. La fusion peut se produire en raison de l'action de CD9 et CD81 (bien caractérisés comme régulateurs des processus de fusion). Cette fusion pourrait se produire par l'action directe de CD9 et/ou CD81 se liant en trans avec une molécule fusogénique inconnue, ou ces tétraspanines pourraient être associées à leurs partenaires tétraspanines (également impliqués dans les processus de fusion) qui pourraient éventuellement interagir entre eux mais dans des membranes opposées ou avec une molécule fusogénique inconnue, conduisant à la fusion

6) Une fois la fusion effectuée, un TNT fonctionnel est présent, formant un canal ouvert entre les deux cellules qui peuvent désormais échanger des cargaisons.

Main index

Index of figures

Abbreviations

A

AB Antibody

ADAM A disintegrin and metalloproteinase domain-containing protein

AKT Protein kinase B

ALCAM Activated Leukocyte Cell Adhesion Molecule

APC Adenomatosis Polyposis Coli

Arp2/3 Actin Related Protein 2/3

B

βCaMKII β-Ca^{2+}-Calmodulin-dependent protein kinase II

C

Ca^{2+} Calcium

CAD Cath. a-differentiated

CD Cluster of differentiation

CD9P-1 CD9 partner 1

CDC42 Cell division control protein 42 homolog

CDH Cadherin

Cryo-EM Cryogenic Electron Microscopy

Cryo-ET Cryogenic Electron Tomography

D

DAPI 4′,6-diamidino-2-phenylindole

DFB Double Filopodial Bridge

DiD 1,1′-dioctadecyl-3,3,3′,3′-tetramethylindodicarbocyanine, 4-chlorobenzenesulfonate

DiI 1,1-dioctadecyl-3,3,3,3,3-tetramethylindocarbocyanine perchlorate

DiO 3,3-dioctadecyloxacarbocyanine perchlorate

E

EC Extracellular

ECAD Epithelial-Cadherin

ECL Enhanced luminol-based chemiluminescent

ECM Extracellular matrix

EDTA Ethylenediaminetetraacetic acid

EGFR Epidermal growth factor receptor

EGTA ethylene glycol-bis(β-aminoethyl ether)-N,N,N′,N′-tetraacetic acid

EM Electron microscopy

Eps8 Epidermal Growth Factor Receptor Pathway Substrate 8

ERM Ezrin-Radixin-Moesin

EV Extracellular vesicle

EWI Glutamyl-tryptophanyl-isoleucine (EWI) motif-containing

F

F-actin Filamentous actin

FAK Focal adhesion kinase

FCS Forward scatter

FGFR Fibroblast Growth Factor Receptor

FIB-SEM Focus ion beam scanning electron microscopy

FM Fluorescence microscopy

FRAP Fluorescence recovery after photobleaching

G

G-actin Globular actin

GFP Green Fluorescent Protein

GIT2 G Protein-Coupled Receptor Kinase Interacting Protein 2

GM130 Golgi matrix protein 130

GPI Glycosylphosphatidylinositol

GTP Guanosine Triphosphate

GTPase Guanosine Triphosphatase

H

H2B Histone 2B

HBEC-3 Human bronchial epithelial cells

HEK human embryonic kidney

HeLa Henrietta Lacks

HEPES 4-(2-hydroxyethyl)-1&piperazineethanesulfonic acid

HIV Human Immunodeficiency Virus

HPV Human papillomavirus

Htt Hungtintin

HUVEC Human umbilical vein endothelial cells

I

I-BAR Inverse Bin-Amphiphysin-Rvs

IF Immunofluorescence

Ig Immunoglobulin

IL-1 Interleukin-1

IP immunoprecipitation

IP3R Inositol triphosphate receptor

IP-TNT interpericyte Tunneling nanotube

IRSp53 Insulin Receptor Kinase Substrate of 53 kDa

ITG Integrin

iTNT individual tunneling nanotube

K

KD Knock down

kDa Kilodalton

KO Knock out

L

LAMP-1 Lysosomal-associated membrane protein 1

LEF Lymphoid enhancer factor

LEL Large Extracellular Loop

M

MDCK Madin-Darby Canine Kidney cells

MHC Major histocompatibility complex

miRNA microRNA

mRNA messenger RNA

MSC Mesenchymal Stromal Cells

mTOR mammalian Target Of Rapamycin

N

nanoFCM Nanoparticle Flow Cytometry

NCAD Neural-Cadherin

NCAM Neural Cell Adhesion Molecule

NPRAP Neural Plakophilin-Related ARM-repeat Protein

NPU Normal Porcine Urothelial cells

NRK Normal rat kidney

N-WASP neural Wiskott-Aldrich syndrome protein

O

OE Overexpression/overexpressing

P

PBS Phosphate Buffer Saline

PC12 Pheochromocytoma rat cells

PFA Paraformaldehyde

PI3K Phosphoinositide 3-kinase

PIP3 Phosphatidylinositol (3,4,5)-trisphosphate

PKCβII Protein kinase C βII

PrPSc Scrapie prion protein

PTGFRN Prostaglandin F2 receptor negative regulator

PTPμ Protein tyrosine phosphatase μ

PVDF Polyvinylidene difluoride

R

Rac1 Ras-related C3 botulinum toxin substrate 1

RACK1 Receptor for activated C kinase 1

Ral-A Ras related protein A

Rhes Ras Homolog Enriched in the Striatum

Rho Ras homolog

RNA Ribonucleic acid

RT Room Temperature

S

SARS-CoV-2 Severe acute respiratory syndrome coronavirus 2

SDS-PAGE Sodium dodecyl sulphate-polyacrylamide gel electrophoresis

SEL Short Extracellular Loop

SEM Scanning electron microscopy

SFB Single Filopodial Bridge

siRNA small interfering RNA

Src Sarcoma

ST Swine testicle cells

T

TAPA-1 Target of an Antiproliferative Antibody

TBS-T Tris-Buffered Saline - Tween

TCF T cell factor

TEM Transmission electron microscopy

TEMs Tetraspanin-enriched microdomains

TM Transmembrane

TM4SF Transmembrane 4 superfamily

TNT Tunneling Nanotube

U

UV Ultraviolet

V

VASP Vasodilator-stimulated phosphoprotein

W

WB Western Blot

WGA Wheat germ agglutinin

Wnt Wingless/Integrated

WT Wild type

Z

ZO-1 Zonula occludens-1

Section 2: Introduction

Chapter 1. Intercellular communication

Cell-to-cell communication is a crucial process in the maintenance of homeostasis and the development of simple or complex organisms. This is true whether they are single or multicellular organisms, cells isolated in their environment or cells forming tissues, organs and organisms. The ability of cells to communicate with themselves, other cells or the environment allows them to adapt and respond to a multitude of changes that occur around them and that condition their development and viability.

In a simplified way, and just as it happens between human beings and therefore cells are no exception, any type of communication requires a sender, a receiver and a message. This implies that in cells we always have a sender cell that sends a signal and a target cell that receives it. These signals can be of a wide variety of types generally subdivided into physical signals (if there is interaction that produces changes either between one cell and another or a cell and its environment), chemical signals (through neurotransmitters, hormones, growth factors) or electrical signals (such as changes in membrane potentials due to the passage of ions through membrane channels).

All these signals used to communicate between cells can in turn be divided into two main types of communication: long range communication and contact-dependent communication.

Long-range communication

As the name suggests, long-range communication involves a type of communication without direct contact through the secretion of molecules. This type of communication is especially critical in establishing organism-wide communication between widely separated parts of the organism, but cells that are not so far apart within an organism also secrete certain molecules to communicate with other cells or with themselves without the need to establish physical contact (*Alberts et al., 2015*; to be noted, this reference comes from a book whose last edition dates back to 2015 and therefore it is not the most updated information of today's knowledge, however, any mention of this book is of general and informative interest. Other references in the existing literature that are more up to date and/or accurate are presented together with this book). Therefore, according to this criteria, long-range communication can be classified according to the distance between

the cell that sends the message and the cell that receives it in: endocrine, paracrine and autocrine (*Figure 1*).

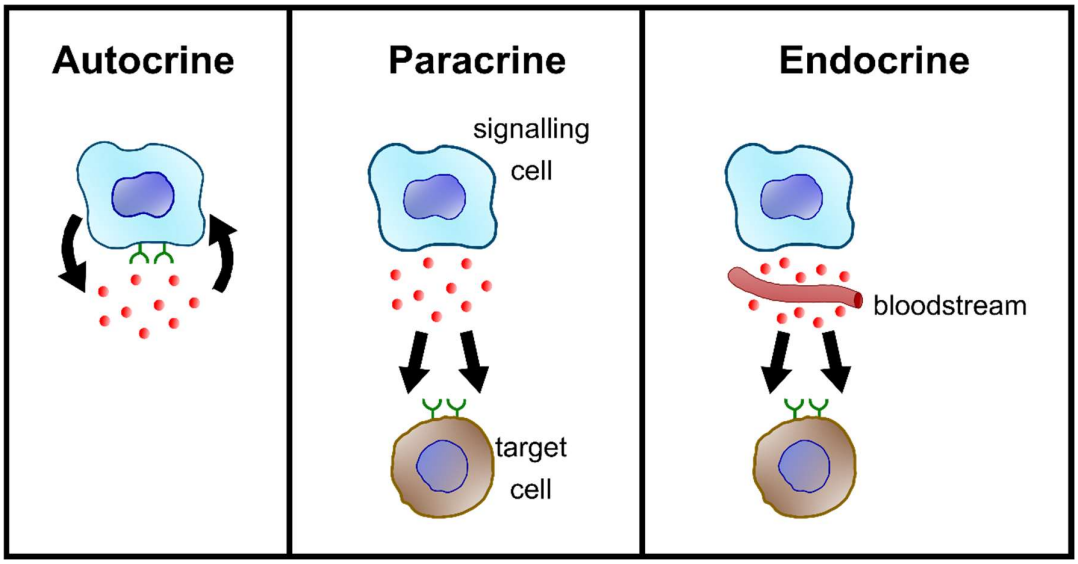

Figure 1. Long range intercellular communication.

This type of communication is defined by not establishing a direct physical contact between signaling and target cell and is classified depending on the distance between these two cells: autocrine if the signaling and target are the same cell, paracrine if the sender and receiver cells are in the immediate vicinity and endocrine if these two cells are far away from each other using the bloodstream as a route of communication between them.

Endocrine signaling

This type of signaling occurs between cells that are widely separated within an organism and controls how an entire organism behaves. These signals, which in this case are known as hormones, are formed in the endocrine cells that in turn make up the endocrine glands (such as the hypothalamus, the adrenal glands, the pancreas, the thyroid gland, the ovaries or the testicles) that are responsible for the secretion of these hormones into the bloodstream and that through long distances through the blood system, act in organs other than those of origin to produce a particular response (*Alberts et al., 2015*). An example of this type of signaling is the case of thyroid hormones produced by the thyroid gland, which produce a wide variety of effects in the organism, such as the control of fatty acid or glucose metabolism, the control of heartbeat or brain development in the first stages after birth (*Guyton and Hall, 2011*).

Paracrine

In the case of paracrine signaling, this consists in the secretion of a signal that is exocytosed into the extracellular space and this secreted molecule binds to or is uptaken by a receptor cell that is in the immediate vicinity of the cell that has sent this signal, thus acting locally (*Alberts et al., 2015*). Two of the best and most studied example of this type of communication are the cytokines and the synapses. Cytokines (such as interleukins like IL-2 or interferons like IFN-γ) are small molecules specialized in long-distance communication produced by many different types of cells and whose main function is to act as signaling molecules to produce a response in the acceptor cell. Their main role is within the immune system acting in the inflammatory response. Synapse is a specialized structure between neurons (or between a neuron and a muscle cell) allowing the transmission of a chemical message through neurotransmitters that are exocytosed from the axon of one neuron as a consequence of the change of membrane potential, and the endocytosis of these neurotransmitters through the dendrite of another neuron, thus transmitting a local message from cell to cell.

Autocrine

The latter group of distant signaling comprises that signal which is produced by a cell and which in turn is received by the receptors of that same cell. Examples of these are found in the regulation of the immune system, such as the stimulation of monocytes through the self-production of interleukin-1 (IL-1) and the use of cancer cells of this mechanism, by the production of the Wingless-related integration site (Wnt) ligand for the autoactivation of the Wnt-β-catenin signaling pathway, promoting the proliferation of these cells.

Contact-dependent communication

Contact-dependent communication or signaling it is defined as “cell–cell communication in which the signal molecule remains bound to the signaling cell and only influences cells that physically contact it” (*Alberts et al., 2015*). However, while this definition is correct, at present it is probably incomplete as will be seen below. One could perhaps complete this definition of contact-dependent communication as communication between cells involving physical contact between them with the signal molecule either interacting with both sender and receiver or this molecule being transferred between donor and acceptor. This type of communication can be found from prokaryotic cells to different eukaryotic

organisms such as: pili, plasmodesma, cytonemes, gap junctions or tunneling nanotubes (*Figure 2*).

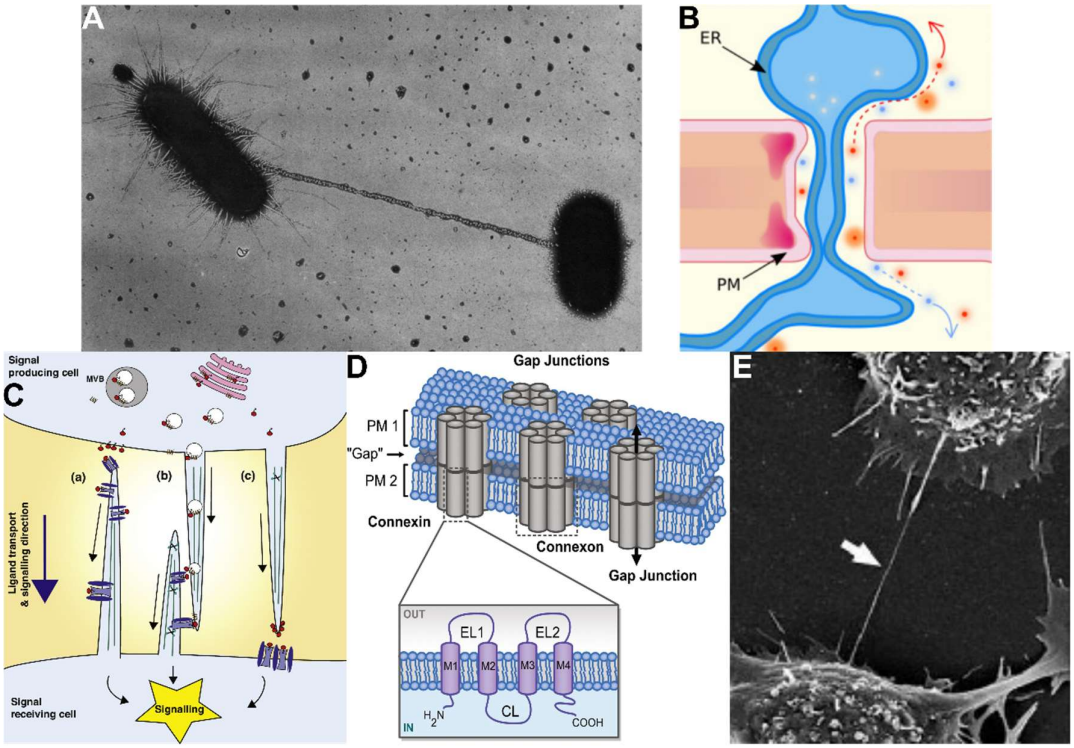

Figure 2. Types of contact dependent communication.

(A) Pili are connections between bacteria that allow them to transfer genetic material between each other. (B) Plasmodesmata are aqueous channels connecting the endoplasmic reticulum of two cell walls of plants cells. (C) Cytonemes are membrane extensions made of actin for the transport and exchange of morphogens. (D) Gap junctions form a soluble open channel between neighboring cells that allows the transfer of small molecules. (E) Tunneling nanotubes are F-actin membranous structures that connect the cytoplasms of two cells and serve as a route for the exchange of a wide variety of biological material. Obtained from Brinton, 1971; Li et al., 2020; Zhang and Scholpp, 2019; Stephan et al., 2021; Rustom et al., 2004.

Pili

Sex pili (or pilus in singular) are projection-like structures in a wide variety of bacteria (*Figure 2A*). These structures, formed by a protein called pilin, function as appendages that will connect one bacterium to another and bring them into close contact in such a way as to allow cell-to-cell exchange of material in a direct manner. The pili can grow up to 20 µm long, connecting two distanced bacterias (*Wang et al., 2009*). The pili are used as a mechanism of horizontal gene transfer between bacteria facilitating the exchange of plasmids from one bacterium to another (*Filloux., 2010*).

Plasmodesmata

Plasmodesmata (or plasmodesma in singular) are aqueous cylindrical-shaped channels (~ 40 nm diameter) formed in between the cell walls of plant cells, which in their center desmotubules that connect the endoplasmic reticulum of adjacent cells is found (*Tilney et al., 1991*) (*Figure 2B*). This structure is formed when the endoplasmic reticulum is confined between the cell walls of a dividing cells forming therefore a cytoplasmic connection between these two newly formed cells (*Lucas et al., 1993*). It is a type of very short contact communication, a few hundred nanometers, since this distance is due exclusively to the separation of the cells by their cell wall (*Peters et al., 2021*). This structure allows the direct transfer of proteins, genetic material or viruses between paired cells (*Roberts and Oparka, 2003*).

Cytonemes

Cytonemes are extensions made by actin that provide an efficient long distance-transport of morphogens, found in the wing disc of drosophila melanogaster, although were also observed in vertebrates (*Ramírez-Weber and Kornberg, 1999*) (*Figure 2C*). They can connect separated cells over dozens of μm, reaching 150 μm (*Daly et al., 2022*), and the diameter of these structures varies from repeating wide segments and thin segments (*Wood et al, 2021*). Morphogens are molecules that are used to give information about the position in the embryo. Moreover, similar structures were observed in other organism such as sea urchin, known as thin filopodia (0.2-0.4 micron in diameter), which are involved in gastrulation forming extensions from primary mesenchyme cells, ectodermal and secondary mesenchyme cells (*Miller et al., 1995*).

Gap junctions

Gap junctions are channels formed by proteins called connexins (integral membrane proteins), which are important in the transport of ions and biological molecules between cytoplasm of two neighboring cells (*Figure 2D*). Indeed, they have been shown to play a critical role in immune response, neural activity and development (*Maeda and Tsukihara, 2011*). These gap junctions channels connect two neighbouring cells forming a chanell of 2-4nm (*Meşe et al., 2007*) and they present an outer diameter of ~90 ángstrom, which contain “gap junction intercellular channels” formed by “connexons”, which in turn are formed by six connexin subunits that are around the central pore (with an entrance of ~40

ángstrom) (*Maeda and Tsukihara, 2011*) a cut-off of 1kDa allowing the transfer of small material such as salts or amino acids but not large molecules such as proteins or nucleic acids (*Weber et al., 2004*).

Tunneling nanotubes

Tunneling nanotubes are a recently discovered type of direct cell-to-cell communication that allows the exchange of a wide variety of cargoes between cells up to 100 µm (*Figure 2E*).

Chapter 2. Tunneling nanotubes

In 2004, in the group of Hans-Hermann Gerdes (*Rustom et al., 2004*), they identified a new biological process of cell communication. These new structures were called Tunneling nanotubes (or TNTs for short) as they were tubular structures connecting two cells allowing the passage through them of organelles from one cell to another.

They were first identified in the neural PC12 cells (rat pheochromocytoma cells), human embryonic kidney (HEK) and normal rat kidney (NRK) cells. By staining the cell membrane, Rustom and colleagues showed that extremely fine and normally straight structures were formed between the cells. These structures were in between 50 and 200 nm in diameter and they could be several times longer than the cell diameter. These TNTs were shown to be fragile structures as mechanical disruption, prolonged exposure to light and chemical fixation destroyed many of them, however, interestingly, trypsin treatment did not cause their destruction, suggesting that TNTs, unlike other membrane protrusions, are not attached to the substrate. When they performed ultrastructural studies of the TNTs by scanning electron microscopy (SEM) and transmission electron microscopy (TEM), they observed that these structures extended directly from one cell to another and in turn connected the membranes of these two connected cells in a continuous manner providing cytoplasmic continuity. Furthermore, treating the cells with latrunculin-B, a F-actin depolymerizer compound, destroyed all the TNTs, revealing that these structures are formed by F-actin (*Figure 3*).

Perhaps the most important feature of these TNTs was revealed when they studied the role of these structures in intercellular communication, as they observed how vesicular-like structures moved through the TNTs from one cell to another. They also showed how

synaptophysin (a marker of endosomes) and Myosin Va (a motor protein) were present in TNTs, suggesting that cargo transport was plausible through these structures and that this transport was probably through actin-associated motor proteins. Indeed, after labeling the intracellular membrane compartments with green fluorescent 1,1-dioctadecyl-3,3,3,3,3-tetramethylindocarbocyanine perchlorate (DiI) or red fluorescent 3,3-dioctadecyloxacarbocyanine perchlorate (DiO) in cells that would be used as donors to study the transfer of membranous material between cells, they observed that a large number of acceptor cells (marked in a different color to distinguish them from donor cells) had received fluorescent organelles. To corroborate that this transfer took place through TNTs, they repeated this same organelle exchange study but this time at 0°C to block both endo- and exocytosis and phagocytosis and found that there was still transfer of material in this condition. Furthermore, treatment of the cells with latrunculin-B blocked all transfer, thus suggesting that this organelle exchange was carried out through the TNTs (*Rustom et al., 2004*).

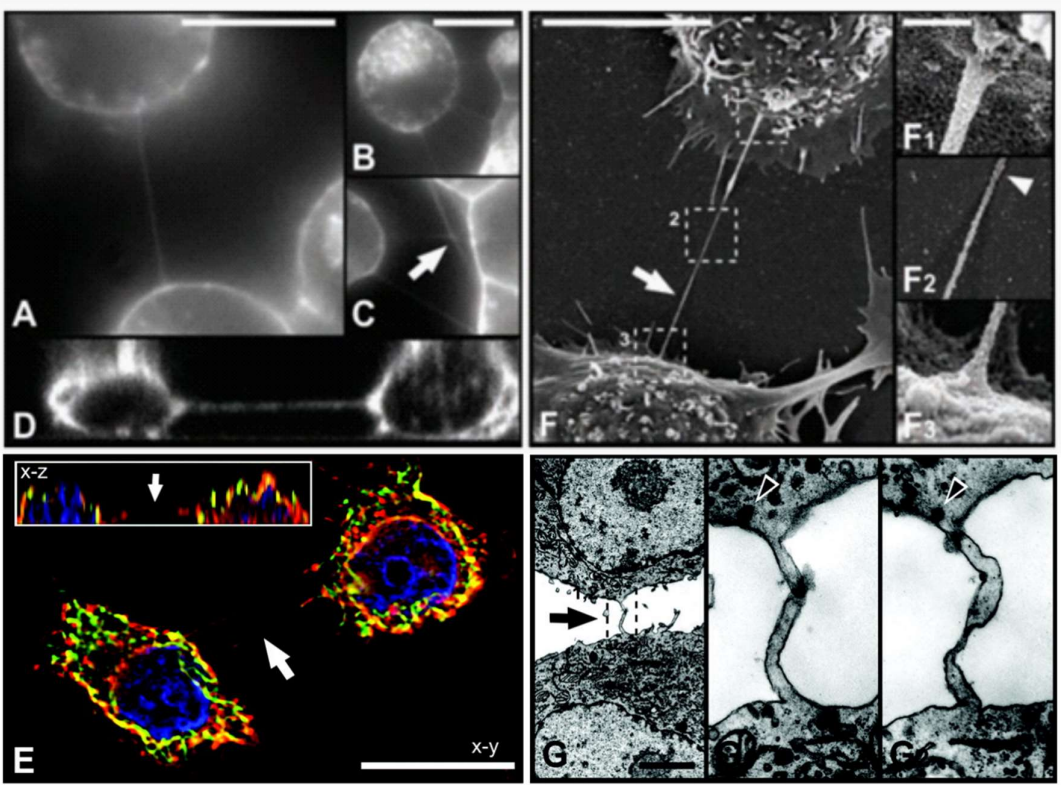

Figure 3. Original description of the Tunneling nanotubes.

(A-D) PC12 cells stained with wheat germ agglutinin (WGA) to label the membrane showed membranous protrusion between them and not attached to the substratum which they called as Tunneling nanotubes or TNTs. (E) TNTs contained actin (red) but they did not contain

microtubules (green). (F) and (G) shows the images obtained by SEM and TEM respectively revealing the ultrastructure of the TNTs. Annotated areas in (F) are shown as higher magnification images in F1-F3. Annotated areas in (G) are shown as higher magnification images in G1 and G2 Scale bars: (A to E), 15 µm; (F), 10 µm; (F1 to F3), 200 nm; (F), (G) 2 µm; (G1 and G2), 200 nm. Obtained from Rustom et al. 2004.

After this first description of TNTs, a definition of TNTs was established as thin membranous structures based on F-actin that connect distant cells over short and long distances and allow the direct transfer of cellular material. Although this definition is still valid, as we will see afterwards, almost 20 years of study of these structures have allowed us to qualify and add information to this first description.

Structure of the TNTs

In the first definition of the TNTs in *Rustom et al., 2004*, TNTs were described as individual structures in the form of thin, straight protrusions (although by electron microscopy - EM - they appeared more twisted and shorter, which may be an artifact of the preparation of the cells for EM). Subsequent studies observed that these structures are not always a single protrusion, but may be formed by two filopodia-like protrusions that meet each other and interact at the tips (*Sowinski et al, 2008*). In other studies, these TNTs were shown to connect two different cells, but they did not form the classic open TNT structure, but instead, appeared to contact the opposite membrane without fusing. They showed the presence of gap junctions between the end of the TNT and the other membrane, forming a sort of synapse between them, which enabled long-distance communication. (*Okafo et al., 2017*). These divergences in the structure of TNTs are also evident from a morphological point of view, since TNTs ranging from short and thin to relatively long and thick have been described (*Austefjord et al., 2014*).

However, despite all these structural and morphological differences of TNTs, all studies had shown that TNTs were single protrusions. It was not until 2019 when an ultrastructural study of TNTs in neuronal cells carried out by our laboratory changed this conception (*Sartori-Rupp et al., 2019*). Our laboratory was able to establish a new method for studying the ultrastructure of TNTs. Since traditional EM methods for studying cellular structures resulted in the breakdown of the thinnest TNTs, a pipeline was established consisting of chemical fixation of TNTs with preservative agents and the use of fluorescence microscopy (FM) to locate TNTs among cells (which were stained for membrane) that were seeded on EM grids. Once identified which cells were connected,

the position of these connections was noted and the grids were frozen for study by cryo-electron microscopy (cryo-EM) and cryo-electron tomography (cryo-ET) to better preserve the native form of the fragile TNTs. This correlative light and electron microscopy (CLEM) approach allowed an extensive study of the TNTs, giving rise to very interesting results about the ultrastructure of these connections. With this approach, in mouse neuronal CAD cells and in human neuronal SH-SY5Y cells, it was possible to observe how the TNTs that are visualized as the usual single TNTs by FM, are actually formed, when using Cryo-EM, by a bundle of individual tunneling nanotubes (iTNTs) each of them defined by its own cell membrane and containing actin inside them. As might be expected for structures that serve to transport material between cells, cellular organelles such as vesicles, multivesicular bodies and mitochondria were also detected inside iTNTs. The diameter of single TNTs was shown to be between 600 and 900 nm, while that of iTNTs was 120 nm, with bundles consisting of 2-11 iTNTs, with the whole structure having an average diameter of 145-700 nm.. The presence of a bundle of highly ordered and normally parallel iTNTs forming the basic structure of the TNTs of neuronal cells seemed to imply the presence of some cell adhesion molecule that could control this structure. They were able to identify N-cadherin, a cell adhesion molecule dependent of calcium (Ca^{2+}) member of the cadherin family of proteins, as the molecule that was found between one iTNT and another presumably maintaining the bundle structure of the iTNTs and promoting the stability of this structure. Finally, thanks to the application of correlative focus ion beam scanning electron microscopy (FIB-SEM) on TNTs, they were able to corroborate that TNTs and iTNTs in CAD cells could be open-ended at the contact sites of these structures with the cells (*Sartori-Rupp et al., 2019*). Therefore, this study opened a new frontier and questions on how the ultrastructure of the TNTs that had already been characterized in other cell types could actually be.

Characteristics of TNTs

According to the definition of TNTs, the main characteristics of TNTs are: cytoskeleton inside, cytoplasmic continuity between two cells and ability to transfer cargo.

Cytoskeletal composition of the TNTs

The first identification of TNTs (*Rustom et al., 2004*) characterized them as structures formed by F-actin. Thus, the treatment with F-actin-depolymerizing agents such as

latrunculin-B or cytochalasin B inhibited the formation of the TNTs (*Rustom et al., 2004; Wang and Gerdes, 2015*). Over the years, numerous studies demonstrated that this actin cytoskeleton-based composition of TNTs was true for numerous cell types such as kidney HEK (*Smith et al., 2011*), urothelial RT4 (*Kabaso et al., 2011*), urothelial T24 (*Kabaso et al., 2011*), endothelial HUVEC (*Wang et al., 2010*), epithelial HeLa (*Schiller et al., 2013*), neuronal CAD (*Gousset et al., 2009*), neuronal SH-SY5Y (*Satori-Rupp et al., 2019*) and many others.

However, over time it was discovered that TNTs not only contain actin, but in some cases also microtubules. Here we find cases such as A549, H28, HBEC-3 cells (*Dubois et al., 2018),* NK cells (*Chauveau et al., 2010*), macrophages (*Onfelt et al, 2006*; *Dupont et al, 2020*), astrocytes (*Wang et al., 2012*) or glioblastoma stem-like cells (*Pinto et al., 2021*) (*Figure 5B*). Intriguingly, TNTs that are natively made up of actin can, upon receiving certain stimuli, go on to form TNTs that also contain microtubules. This is the case, for example, of the αherpesvirus US3 protein kinase which is able to induce the formation of long TNTs containing stabilized microtubules in ST cells (*Jansens et al., 2017*), or even in the case of the cells in which TNTs were first described (PC12 cells) it has been shown that after receiving UV radiation damage and becoming apoptotic, TNTs that were previously positive for actin and negative for microtubules become positive for both components of the cytoskeleton and provide them with a rescue mechanism by receiving mitochondria from surrounding healthy cells (*Wang and Gerdes, 2015*). Interestingly, treatment with cytochalasin B abolished the formation of microtubule-containing TNTs, whereas drugs that disrupt microtubules such as nocodazole or drugs that stabilize microtubules as paclitaxel did not alter TNT formation (*Wang et al., 2010*), showing the central role of the actin cytoskeleton on the TNT's biogenesis.

Finally, TNTs whose composition includes elements of the intermediate filaments have also been identified. This is the case of Normal Porcine Urothelial (NPU) cells, in which connections were identified that were positive for actin, tubulin and cytokeratin-7, thus showing the presence of actin filaments, microtubules and intermediate filaments (*Resnik et al., 2019*).

All these studies show the complexity of these structures and raise the need to unify criteria when studying TNTs. Here I propose the terminology "TNTs" for those which fulfill the original description of these structures by *Rustom et al., 2004* (actin based

membranous connections, not attached, open ended and able to transfer cargo) and "TNT-like connections" for those structures that varies from this definition (connections composed by microtubules or intermediate filaments in addition to actin or close-ended connections).

Open-endedness?

As was the case for the composition of cytoskeleton elements in TNTs, the first description of TNTs was that of open-ended structures (*Rustom et al., 2004*). However, in this case the answer to the question of whether TNTs are open structures or not is more complex as it requires electron microscopy techniques that can therefore access the contact areas between TNTs and opposing cells. Thanks to the efforts of different groups, the answers started to come, however these answers did not clear the doubts about the cytoplasmic continuity of the TNTs since TNTs were found to be open or closed depending on the cell line in which they were studied highlighting again the diversity of structures.

Examples of TNTs that were open, apart from the original study by Rustom and colleagues, were found in A549 epithelial cells (*Kumar et al., 2017*), MDCK (*Kumar et al., 2017*), between T24 and RT4 bladder cells (*Lu et al., 2017*) or STHdh neuronal cells (*Sharma and Subramaniam, 2019*). In either case, the formation of TNTs that are open-ended is hypothesized to require the presence of cell adhesion molecules that would place the membranes facing each other in such a way that membrane fusion could occur (*Abounit and Zurzolo, 2012*). On the other hand, other cell types showed TNTs-like connections that were closed, as is the case in Jurkat cells (*Sowinski et al., 2008*), in macrophages (*Okafo et al., 2017*) or pericytes in the mouse retina (*Alarcon-Martinez et al., 2020*). In our case, the cells we mainly worked with in the laboratory for the study of TNTs, mouse neuronal CAD cells and human neuronal SH-SY5Y cells, both showed to have TNTs (or iTNTs in this case) that could be either open or closed, although, those closed iTNTs were found within the iTNT bundle in the middle of two cells, which presumably could be iTNTs in the process of extension or retraction (*Sartori-Rupp et al., 2019*) (*Figure 4*).

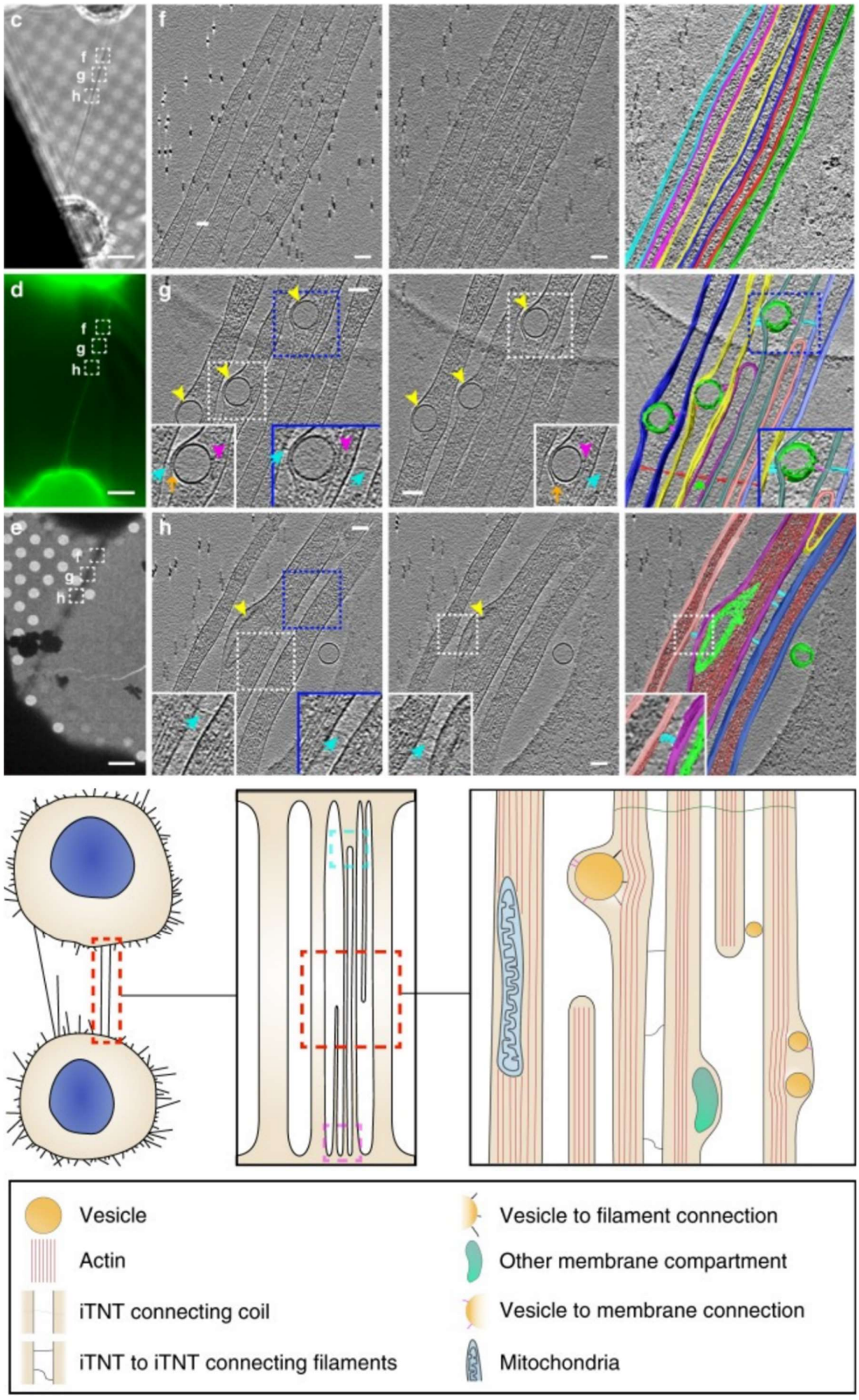
c
f
g
h
d
e
Vesicle
Actin
iTNT connecting coil
iTNT to iTNT connecting filaments
Vesicle to filament connection
Other membrane compartment
Vesicle to membrane connection
Mitochondria

Figure 4. Ultrastructure of the TNTs in CAD and SH-SY5Y neuronal cells.

Low magnification TEM images (c, d, e) shows how the TNTs look like a single tube but at a higher magnification cryo-ET images (f, g, h) this single tubes are in fact made of a multiple individual tubes (iTNTs), each one delimitated by its own membrane. iTNTs contain actin (colored in red in g) and vesicles in them (pointed by yellow arrowheads and colored in green in f) and are attached to each others by thin linkers (pointed by turquoise arrowheads and colored in turquoise in g and h). On the bottom, the schematic diagram of the ultrastructure of TNTs and iTNTs in neuronal cells. Obtained from Sartori-Rupp et al., 2019.

Why TNTs or TNT-like connections can be found to be open or closed is a question as yet unanswered, since those TNTs that were shown to be closed were also capable of transferring membrane-delimited compartments (in this case just movement of the compartments along the TNTs was detected but not the transfer of this material between cells, which would imply a supply of membrane or different molecules to the TNTs) or mitochondria (*Sowinski et al., 2008*; *Okafo et al., 2017*). Perhaps finding TNTs that are closed is due to limitations in the use of EM techniques (because just use of SEM it is not enough to visualize the open-endedness of these structures) or close-ended TNT is a transitionary step captured in the precise moment of the ultrastructural analysis due to the dynamic nature of these structures or simply the presence of open or closed TNTs is due to different mechanisms of formation and functionality of TNTs in different cell types. In either case, more ultrastructural studies are needed to better address the question of cytoplasmic continuity.

Cargo transfer as the fundamental indicator of the functionality of TNTs

As we have seen so far, the unique and differential property of TNTs with respect to other types of protrusions is their ability to transfer cargo across it. Over the years, the list of different cargoes that are capable of being transferred by TNTs has only grown, including Ca^{2+}, pathogens (such as viruses and bacteria), organelles, misfolded proteins or genetic material (*Figure 5B*).

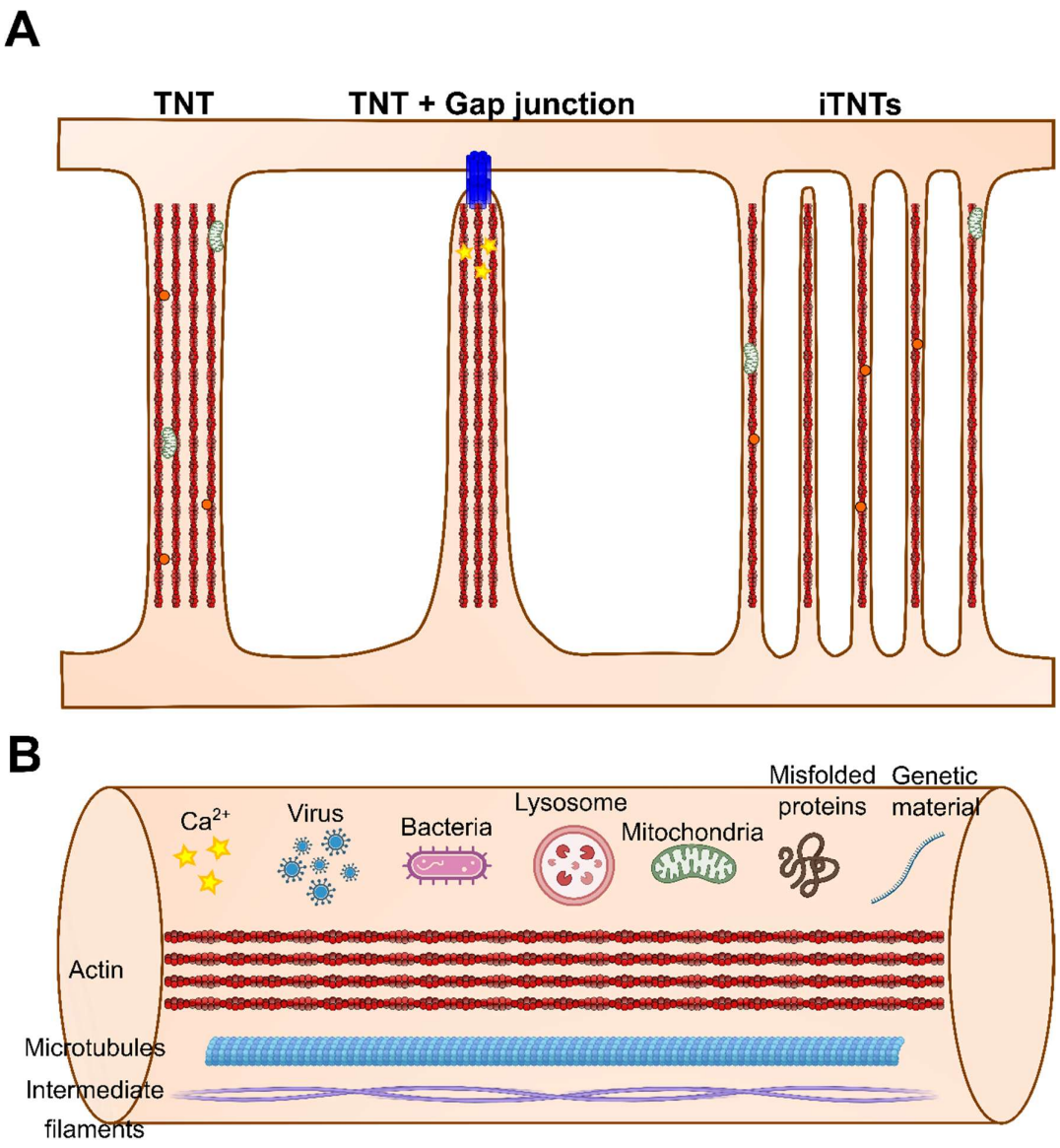

Figure 5. Architecture of the different types of TNTs and the cargo that can be transfer by these structures.

(A) TNTs can vary in architecture ranging from the first described single tube containing biological material in it, to TNTs that are close and ending in a gap junction specialized for the Ca^{2+} transfer, or multiple individual TNTs forming a bundle of thin parallel tubes. (B) TNTs are always based on the actin cytoskeleton but some TNTs or TNT-like connections can also contain microtubules of intermediate filaments. These structures can transfer a wide variety of cargo such as Ca^{2+}, viruses, bacteria, lysosomes, mitochondria, misfolded proteins or genetic material

Calcium signaling

While one might think that intercellular Ca^{2+} transport through these structures is carried out by TNTs connecting to opposing cells through gap junctions, this is not always the case, as it has been shown that Ca^{2+} transport can be through TNTs terminated in gap-

junctions (*Wittig et al., 2012*) (*Figure 5A*) or on the other hand that this Ca^{2+} transfer is dependent on inositol triphosphate receptors (IP3R) (*Smith et al., 2011*). Interestingly, this Ca^{2+} transfer through TNTs has been observed in vivo between TNTs connecting mouse retinal pericytes, allowing a coordination in the neurovascular tissue and responses to the light. (*Alarcon-Martinez et al., 2020*).

Pathogens and TNTs

Many viruses are capable of both inducing the formation of TNTs, and of "hijacking" these structures to spread from one cell to another (for a much more extensive review of TNTs and viruses see *Jansens et al., 2020*). As a result, shortly after the discovery of TNTs, they were recognized as mechanisms by which Human Immunodeficiency Virus (HIV) could be transmitted among T cells (*Sowinski et al., 2008*). Later, it was demonstrated that HIV induced the formation of TNTs in macrophages, and that this virus was found in TNTs formed between macrophages, suggesting that TNTs can also be used to propagate HIV in macrophages (*Eugenin et al., 2009*).. Likewise, very recently our group has demonstrated how SARS-CoV-2 not only induces the formation of TNTs but can also be transferred from permissive to the virus epithelial cells into non-permissive neuronal cells, providing a potential explanation for how this disease could spread to the brain (*Pepe et al., 2022*). These two cases represent only a couple of examples of a long list of viruses that can either induce or travel through TNTs (*Jansens et al., 2020*).

In the case of bacteria, examples are scarcer. For example, *Listeria monocytogenes* was described, years before the discovery of TNTs, as spreading from one macrophage to another through cellular protrusions of actin that were phagocytosed by another cell (*Tilney and Portnoy, 1989*). Although it is not clear that these protrusions are TNTs, it seems plausible that these bacteria could use TNTs as a route from one cell to another. Another clearer example is the case of *Mycobacterium bovis*, which showed how this bacterium could transfer from one macrophage to another by "surfing" on the surface of the TNTs connecting two cells until it reached the recipient cell (*Önfelt et al., 2006*).

Organelle transfer

Organelles best characterized as being transferred by TNTs are lysosomes and mitochondria.

Lysosomes

In the same study mentioned above, they not only described how bacteria could use TNTs to move from one cell to another but also observed for the first time how lysosomes could also be transferred by TNTs (*Önfelt et al., 2006*). As a clear example of the duality of TNTs in terms of their beneficial or detrimental effects on cells, we can find the lysosome transfer. TNTs can be used for the elimination of harmful substances from one cell to another (*Victoria and Zurzolo., 2017*), but they can also be used to propagate misfolded proteins that have escaped degradation in these lysosomes (*Dilsizoglu Senol et al., 2021*).

Mitochondria

TNTs have been shown to transfer mitochondria in a wide range of cell lines. Since mitochondria play multiple functions in the target cells, mitochondrial trafficking has notable and variable effects (*Vignais et al., 2017*). As in the case of lysosomes, the transfer of mitochondria by TNTs is also believed to be a beneficial or detrimental mechanism for the whole organism depending on the context, since the exchange of mitochondria can mean a supply of an additional energy source to a cell in need of it or (in the context of cancer) this transfer of mitochondria can favor tumor progression (*Pinto et al., 2020*). Some of the beneficial effects of mitochondria transfer by TNTs can be observed in the delivery of mitochondria from astrocytes to neurons which offers a protective effect and improves the recovery of the latter after a stroke (*Hayakawa et al., 2016*) or the transfer of mitochondria between pericytes and astrocytes, which allows the latter to be rescued after ischemia (*Pisani et al., 2022*). But as mentioned above, the transfer of mitochondria could also have a detrimental effect on the organism, and this is especially true in the context of cancer in which receiving mitochondria would be beneficial to these cancer cells but detrimental to the organism. Certain examples can be found in the transfer of mitochondria via TNTs between mesenchymal cells and breast cancer cells (*Pasquier et al., 2013*) or in squamous cell carcinoma (*Sáenz de Santa María, et al., 2017*), as well as a growing body of documentation regarding the relationship of mitochondrial transfer by TNTs and the acquisition of cancer cell drug resistance (*Hekmatshoar et al., 2018*).

Trafficking of misfolded proteins

Misfolded proteins, as we will see in the next section, play a fundamental role in the establishment and progression of different diseases. To date, there are a multitude of

studies that have been able to demonstrate the transfer of misfolded proteins between cells via TNTs.

The study of the transfer of misfolded proteins by TNTs began with the discovery that the pathogenic and infectious form of the prion protein (scrapie prion protein or PrP^{Sc}, that can cause the Creutzfeldt-Jakob disease) can use TNTs as a transfer route between neuronal cells (*Gousset et al., 2009*) and years later it was shown that PrP^{Sc} colocalized within the lumen of TNTs in endosomal compartments corresponding to early endosomes or lysosomes, and that this PrP^{Sc} increases both the formation of TNTs and their ability to transfer vesicles (*Zhu et al., 2015*).

After these discoveries, more attention was given to other misfolded protein transportation by TNTs. This led to greater knowledge of how α-synuclein (protein responsible for Parkinson's disease) travel from one cell to another. As seen in neuronal CAD cells, α-synuclein fibrils are transferred between cells via TNTs. When these proteins arrived at a new cell, they were able to seed soluble α-synuclein found in the cytosol of the recipient cell (*Abounit et al., 2016*). Years later, it was also discovered that α-synuclein was able to escape lysosomal degradation and spread across different cells. This led to the aggregation of other α-synuclein molecules in different cells (*Dilsizoglu Senol et al., 2021*). Primary neurons and human neuronal precursor cells have also shown this same trend with α-synuclein transport via TNTs (*Vargas et al., 2019*; *Grudina et al., 2019*).

As in the previous case, another misfolded protein that has been observed to be related to TNTs is huntingtin (Htt), which can lead to Huntington's disease. It was not even ten years ago when it was demonstrated in a neuronal cell line and in primary neurons that when these cells were treated with an Htt mutant, aggregates of these proteins were formed, causing the increase of TNTs and their transfer (*Costanzo et al., 2013*). A mechanism by which the formation of TNTs related to Htt is induced has recently been demonstrated. This is through Rhes (Ras Homolog Enriched in the Striatum) which not only promotes the formation of new TNTs, but in turn this protein is responsible for cell-to-cell transport of Htt in striatal cells (*Sharma and Subramaniam, 2019*).

Amyloid-β is another misfolded protein that is transferred through TNTs, and it is the major component of amyloid plaques in the brains of Alzheimer's patients. In this case

we have the first reports came from Wang and colleagues (*Wang et al., 2011*) who showed how this amyloid-β is transferred between neurons through TNTs producing an increase in cytotoxicity and much more recently other teams confirmed not only the transfer of β amyloid-β but also the bidirectional transfer of this protein (*Zhang et al., 2021*) and that the formation of TNTs by amyloid-β is probably due to the damage caused by this protein in the plasma membrane (*Dilna et al., 2021*).

Finally, it has been observed that both monomeric and fibrillar Tau (protein responsible for tauopathies and that together with amyloid-β, can cause Alzheimer's disease) can be transferred across TNTs (*Tardivel et al., 2016*), both synthetic and derived from Alzheimer's disease patients (*Chastagner et al., 2020*) and that both endogenous and exogenous Tau aggregates are found on TNTs in endosomal compartments that have escaped autophagy and can presumably travel through TNTs to cause new Tau aggregates in recipient cells (*Chastagner et a., 2020*).

Genetic material

In addition to all of the above-mentioned positions, one type that is particularly important for its possible implications in the alteration of recipient cells is the transfer of genetic material, especially RNA-based material. Thus, examples of microRNAs (miRNA) transfer between stromal cells and tumor cells and tumor to tumor cells (*Thayanithy et al., 2014*), miRNAs in breast cancer cell lines (*Connor et al., 2015*) or the transfer of messenger RNA (mRNA) (*Haimovich et al., 2017*) have been observed, although examples today of this type of transfer are numerous (*Haimovich et al., 2020*). While it has been characterized in some of these studies that the transfer of this genetic material appears to correlate with more aggressive or invasive tumor phenotypes, all the possible indications for genetic changes that potentially have the transfer of this type of cargo in both physiology and pathology have yet to be determined.

Existence of TNTs *in vivo*

TNTs or TNT-like structures have been shown to be present during the development of organisms such as sea urchin, zebrafish or chick embryos (*Miller et al., 1995*; *Caneparo et al., 2011; Teddy and Kulesa, 2004*) but were questioned at first because they could not show one of the main features of TNTs, namely the transfer of cargo, but today are considered as TNT-like connections (*Cordero Cervantes and Zurzolo, 2021*). The

identification of TNTs and their characterization in material transfer was a great challenge when observing these structures in an organism, however, over the years and with the advancement of techniques it has been possible to characterize *bona fide* TNTs *in vivo*. These efforts have culminated in an increasing number of studies demonstrating the existence of these TNTs, especially in the brain (for more extensive reviews in this field, see *Cordero Cervantes and Zurzolo, 2021*; *Khattar et al., 2022*). Relevant examples in this regard are found in the aforementioned study demonstrating the presence of TNT-like connections in the mouse retina that enable Ca^{2+} signaling transfer (*Alarcon-Martinez et al., 2020*), the correlation between material transfer and TNT-like connections between photoreceptor neurons formed by microtubules called photoreceptor nanotubes (*Ortin-Martinez et al., 2021*) or the identification of TNTs formed between astrocytes and neurons in the mouse cerebral cortex (*Chen and Cao, 2021*). In the cancer context, especially with material from patient, TNTs or TNT-like structures were firstly found in solid tumor cells ex vivo with this TNTs containing mitochondria in tissue sections of patients (*Lou et al., 2012*). These findings were corroborated by additional observations showing intercellular connections in squamous cell carcinoma (*Antanavičiūtė et al., 2014*; *Sáenz de Santa María et al., 2017*), ovarian (*Thayanithy et al., 2014*) and pancreatic cancer (*Desir et al., 2018*). Additionally, similar findings were seen when human glioblastoma cells were engrafted into mice models (*Osswald et al., 2015*).

While all these findings extend and solidify the existence of TNTs, more efforts are still needed to show and characterize TNTs *in vivo* without any doubt.

Roles of TNTs in physiology and pathology

As mentioned above, cargo transfer through TNTs can have both beneficial and detrimental effects at the recipient cell or at the level of the whole organism and this is commonly determined by the type of cargo being transported.

Linked to the previous section, it seems obvious to think that the transfer of pathogens such as viruses and bacteria can serve as a route of propagation and dissemination of these same pathogens. PrP^{Sc}, α-synuclein, Htt, amyloid-β and Tau proteins are the main causes of the establishment and development of Creutzfeldt-Jakob disease, Parkinson's disease, Huntington's disease and Alzheimer's disease. That all these proteins can promote the formation of TNTs, be transferred by these structures or seed new aggregates in recipient

cells, leads to think about the fundamental role that TNTs could have in vivo in the dissemination of these diseases in the brain (*Abounit et al., 2016*). In the context of cancer, TNTs and TNT-like connections have been found in numerous different types of cancer (*Pinto et al., 2020*). The microenvironment found in tumors has been shown to favor the formation of TNTs, such as hypoxia (*Desir et al., 2016*), acidic pH (*Kretschmer et al., 2019*) or low serum condition (*Lou et al., 2012*) and signaling cascades that are dysregulated in some cancer types favor the formation of these TNTs, such as PI3K/Akt/mTor (*Desir et al., 2016*) or p53 (*Wang et al., 2011*). Likewise, the transfer of cargo in the context of cancer can have a very important influence on the progression of this disease. Examples of this can be found in bladder cancer, where mitochondrial exchange favors the invasiveness of acceptor cells (*Lu et al., 2017*) or miRNA transfer promotes the acquisition of more aggressive phenotypes in less aggressive cells (*Lu et al., 2019*) and not only through a cellular co-culture but with a protocol to isolate mitochondria called MitoCeption, they were able to observe how mitochondria transfer from Mesenchymal Stromal Cells (MSC) to cancer cells favored cell invasion and proliferation (*Caicedo et al., 2015*).

But just as it is clear that TNTs play a fundamental role in the development and propagation of diseases, it is no less evident that these structures play a no less important role in different physiological and beneficial processes for cells. In this context it is believed that TNTs or TNT-like connections have a very important role during development such as in the sea urchin gastrula (*Miller et al., 1995*), zebrafish gastrulation *(Caneparo et al., 2011*) or chick embryo (*Teddy and Kulesa, 2004; McKinney and Kulesa, 2011*). Knowing that many of these structures have the ability to transfer material, it is possible that this transfer capacity is fundamental to supply different cells with the necessary material at the right time for their correct development (*Korenkova et al., 2020*). Apart from its possible role during development, the transfer of cargo through TNTs has been shown to have beneficial effects in turn. In this regard, it has been observed that TNTs can transfer cystinosin-containing lysosomes from macrophages to cystinosin-deficient fibroblasts (from a mouse model of cystinosis) via TNTs, thus correcting lysosomal defects in these acceptor cells (*Naphade et al., 2015*). As previously mentioned, mitochondrial transfer has beneficial effects also on stroke recovery (*Hayakawa et al., 2016*), on cell rescue after ischemia (*Pisani et al., 2022*) and Ca^{2+}

signaling on the coordination of pericytes by TNT-like connections (interpericyte TNTs or IP-TNTs) to respond to light stimuli (*Alarcon-Martinez et al., 2020*)

Therefore, and once again, we can see how TNTs have a dual functionality, in this case to be both beneficial and detrimental to an organism. Likewise, the mechanism of formation of TNTs in physiological or pathological contexts and their ability to transfer material gives us an idea of the importance of certain factors that condition these structures. ROS production in response to H_2O_2 treatment leaded to an increase in mitochondrial transfer via TNTs (*Liu et al., 2014*). Other stimuli such as serum deprivation, acidic enviroment or hyperglycemia enhance the formation of TNTs and their ability to share material (*Lou et al., 2012*). On the other hand, it has been shown that cellular stress, such as HIV infection or SARS-CoV-2, increases the production of TNTs (*Eugenin et al., 2009*; *Pepe et al., 2022*). Additionally, it has been discovered that chemotherapeutic drugs have an impact on the frequency of TNT production and cargo trafficking. Treatment with the DNA-intercalating Zeocin boosted the formation of TNTs (*Domhan et al., 2011*), as well as the use of the chemotherapeutic agent Cytarabine increased the physical contact between cells and mitochondrial incorporation (Moschoi et al., 2006). These studies can give us an idea of how the fine regulation of the formation and material transfer capacity of TNTs could contribute to the correct maintenance of homeostasis.

Differences between TNTs and other cellular protrusions

As we have seen so far, TNTs are unique protrusions in that they allow direct cell-to-cell transport of a multitude of cargoes. However, cells can form a variety of actin-based protrusions that, although similar to TNTs, can differ from the latter in structure, regulators or function (*Figure 6*).

Membrane protrusions such as cilia (*Figure 6A*) are both actin- and microtubule-based structures, and can be subdivided into motile cilia, primary cilia and nodal cilia (*Hua and Ferland, 2018*). In fact, these protrusions are derived from centrioles. Their main functions are to sense the environment and transduce mechanical and chemical signals from it (*Satir and Christensen, 2007*). Thus, they are different from TNTs both in composition (as TNTs formed by microtubules are the smallest) and function (as TNTs have not been described as environmental sensors to date).

The interaction between the extracellular matrix (ECM) and cells is a fundamental process for cell motility, migration and development and is carried out by focal adhesions. However, there are small F-actin-based protrusions whose role is also to interact with the ECM but which are slightly different from the focal adhesions in both composition and function, namely invadosomes (*Albiges-Rizo et al., 2009*) (*Figure 6B*). Within the framework of invadosomes are included podosomes and invadopodia which, although similar, have different characteristics, for example podosomes are extremely dynamic while invadopodia are much more persistent as well as invadopodia are typically found in cancer cells (*Stefan Linder, 2009*). In general, invadosomes are involved in functions such as degrading ECM and facilitating migration and invasion especially in the context of cancer (*Castro-Castro et al., 2016*; *Mrkonjic et al., 2017*, *Ferrari et al., 2019*). Therefore, the main differences with TNTs are precisely these two functions, because although it is believed that TNTs should generate some kind of metalloproteases to degrade the ECM between two cells *in vivo* to form these connections this is not yet proven, and furthermore, TNTs can also favor invasion in a cancer context but this on the contrary is not by promoting motility, but thanks to the transfer of different cargoes that will provoke a more invasive phenotype in the acceptor cells.

Perhaps the types of membrane protrusion most similar to TNTs are the filopodia (*Figure 6C*). Filopodia are actin-based membrane protrusions that typically reach short distances (less than 10 μm in length). Normally the generation of filopodia is based on the deformation of the plasma membrane through the push of the actin cytoskeleton by nucleation of F-actin through the Arp2/3 complex (*J L Gallop, 2019*). Filopodia have a role in many biological processes, including wound healing, neurite outgrowth, embryonic development, and others. They are used to explore the cell environment during processes like cell migration, for example (*Faix and Rottner, 2006*; *Gupton and Gertler, 2007*). As in the previous cases, the major difference between TNTs and filopodia is the cargo transfer capacity of TNTs and not on filopodia. Furthermore, previous work from our group has shown that although filopodia and TNTs share the same protein complexes regulating actin cytoskeleton, these complexes regulate the two types of actin-based protrusions in an opposite manner, with the network formed by CDC42/IRSp53/VASP promoting the formation of filopodia but inhibiting the formation of TNTs, suggesting that these two structures have predetermined different fates and specific functions (*Delage et al., 2016*).

The aforementioned cytonemes are also similar structures to TNTs, but as I have already discussed, cytonemes transmit morphogens that will produce a signal transduction in the recipient cell, thus varying in function to the TNTs (*Korenkova et al., 2020*) (*Figure 6D*).

Finally, protrusive structures between cells called mitotic bridges can also be observed (*Figure 6E*). When observing these structures at low resolution, their great similarity to TNTs may confuse these two structures, but mitotic bridges are reminiscent of two dividing cells, and although it has been observed that they can exchange material, a phenotype that differentiates them from TNTs is the presence of the midbody in a central position between the two dividing cells (*Fykerud et al., 2016*).

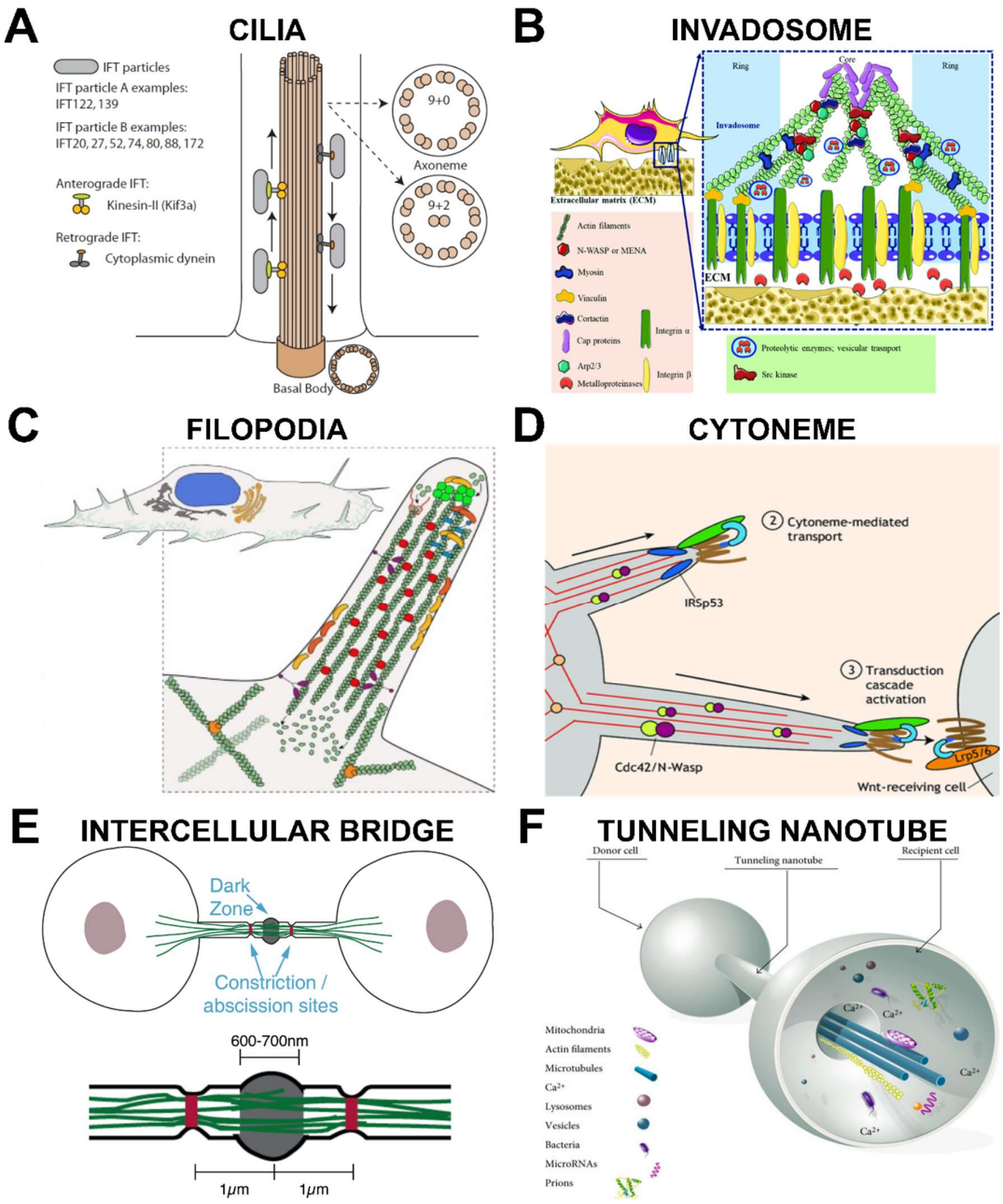

Figure 6. Cellular protrusions.

(A*) Cilia are actin- and microtubule-based protrusions which mainly serve as sensors of the environment. (B) Invadosomes form the interaction between the cells and the extracellular matrix involved in processes such as migration or invasion. (C) Filopodia are short and dynamic actin protrusions involved in a wide variety of cellular functions. (D) Cytonemes are actin membranous extensions that serve as a route of communication between cells by morphogens. (E) Intercellular bridges are reminiscent protrusions devoid from the division of two cells. (F) Tunneling nanotubes differ from all these other protrusion by their ability of transfer biological material by forming and open channel between the cytoplasm of neighboring cells.*

Process of formation of the TNTs

Mechanism of formation

Two mechanisms of TNT formation have been proposed: actin-driven mechanism and cell dislodgement mechanism (*Figure 7*). The two hypotheses for TNT generation presented here might both take place in the same cell type, therefore they are not mutually exclusive.

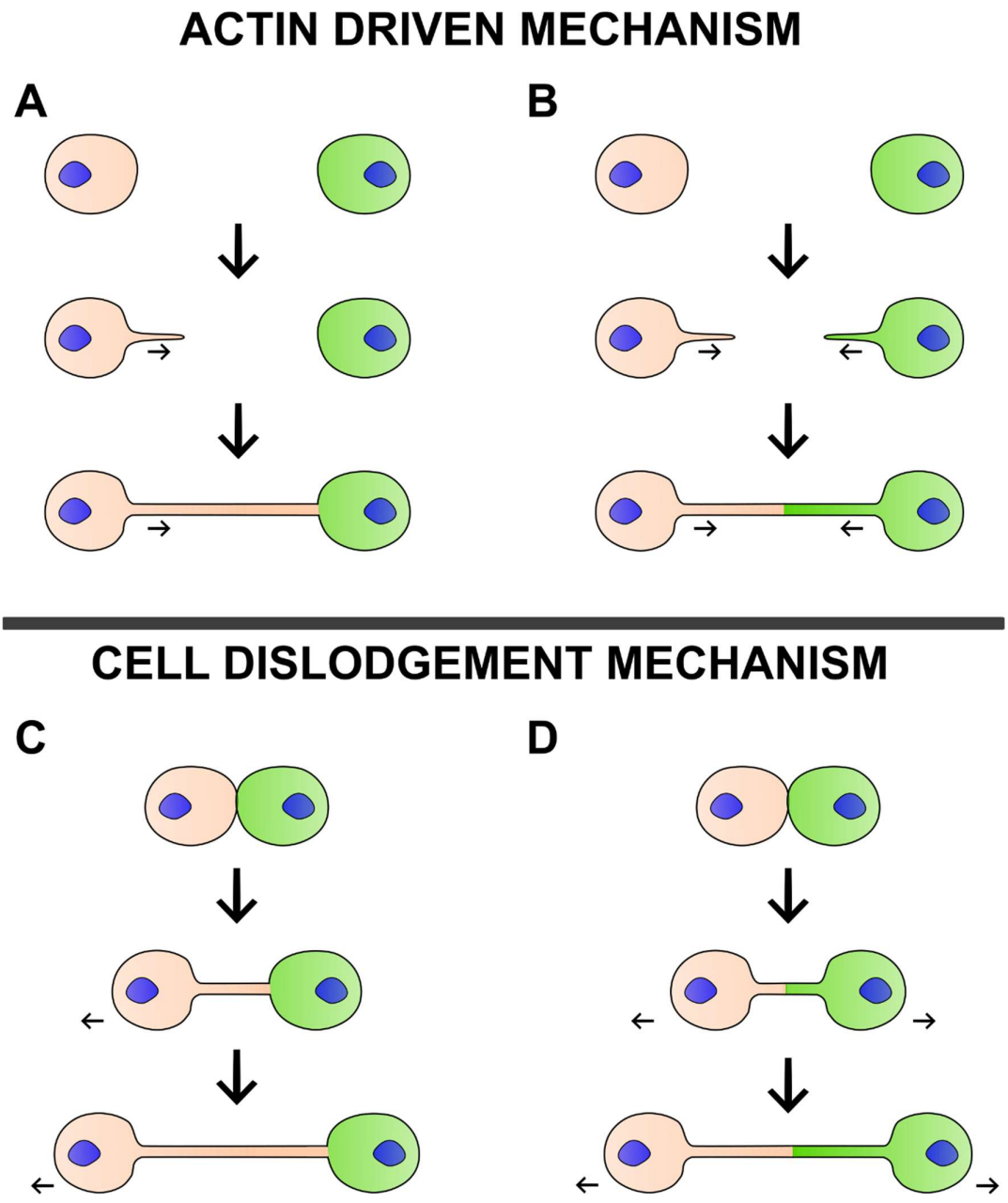

Figure 7. Mechanism of formation of the TNTs.

(A&B) The actin driven mechanism consists on the extension of a filopodia-like protrusion from one cell (A) or both cells (B) that will contact the other cell (A) or the other protrusion (B) and membranes attachment and fusion would occur to form an open channel. (C&D) The cell dislodgement mechanism occurs when two cells that are in close contact and they will separate forming between them a protrusion originated from one of the cells (C) or from both cells (D), which would be open-ended.

Actin-driven mechanism (or filopodia-like protrusion mechanism)

According to the earliest proposed model for TNT biogenesis (*Rustom et al., 2004*), one or both of the cells involved in the formation of this structures can cause the growth of a F-actin filopodia-like protrusions (*Figure 7A&B*). Actin polymerization might occur to provoke the protrusion to lengthen and grow toward the recipient cell which can occur through chemotaxis as in the case of cytonemes (*Ramirez-Weber and Kornberg, 1999*). Following elongation, the protrusion's tip establishes direct physical contact with the target cell, possibly involving adhesion molecules (*Abounit and Zurzolo., 2012*). Finally, membrane fusion must take place upon cell-cell contact in order to allow membrane continuation in order to establish an open TNT connection. To date, neuronal PC12 and mouse CAD cells and normal rat kidney (NRK) cells have shown that TNT production through actin-driven protrusion occurs (*Bukoreshtliev et al., 2009*; *Gousset et al., 2009*; *Rustom et al., 2004*).

Cell dislodgement mechanism

This second mechanism (*Figure 7C&D*) of the formation of the TNTs has been shown to be very common on TNTs that are formed in between immune cells (*Watkins and Salter, 2005*; *Onfelt et al, 2006; Sowinski et al., 2008*) but also in HEK293, HUVEC or neural crest cells (*Wang et al., 2010*). In this type of TNT biogenesis, TNTs would arise from two cells that are in very close contact and when these cells migrate in opposite directions, they would leave between them a TNT that can be formed by only one of the cells or by both cells. It is hypothesized, although there is no evidence as yet, that cell adhesion molecules would favor the initial stages of this type of TNT formation and that TNT-cell membrane fusion could occur either at the beginning of this process or at some point during the formation (*Abounit and Zurzolo., 2012*).

Actin related proteins in TNT formation

Although various actin regulators and vesicle trafficking components appear to supply the material needed for the elongation process, the molecular machinery at the core of

TNT production is yet unknown (for a more exhaustive review about actin related proteins and TNTs, refer to *Ljubojevic et al., 2020*). One of the most important positive regulators of TNT in many cell types is M-Sec (*Hanna et al., 2019*; *Hase et al., 2009*; *Ohno et al., 2010*). It can activate downstream proteins including the cell division control protein 42 homolog (CDC42) and the small GTPase Ral-A to rearrange the actin cytoskeleton or deliver membrane to the site of TNT production. Through direct binding to the neural Wiskott-Aldrich syndrome protein (N-WASP), the Ras superfamily member CDC42 regulates actin polymerization. This direct binding then activates the Arp2/3 protein complex, which encourages actin branching. As mentioned before, the CDC42/IRSp53/VASP network, which promotes the extension of filopodia, negatively regulates TNT formation in CAD cells while elevating Eps8, an actin regulatory protein, promotes TNT formation, indicating that these two actin modifiers may have opposing effects on the formation of filopodia and TNT (*Delage et al., 2016*).

Major steps of the formation

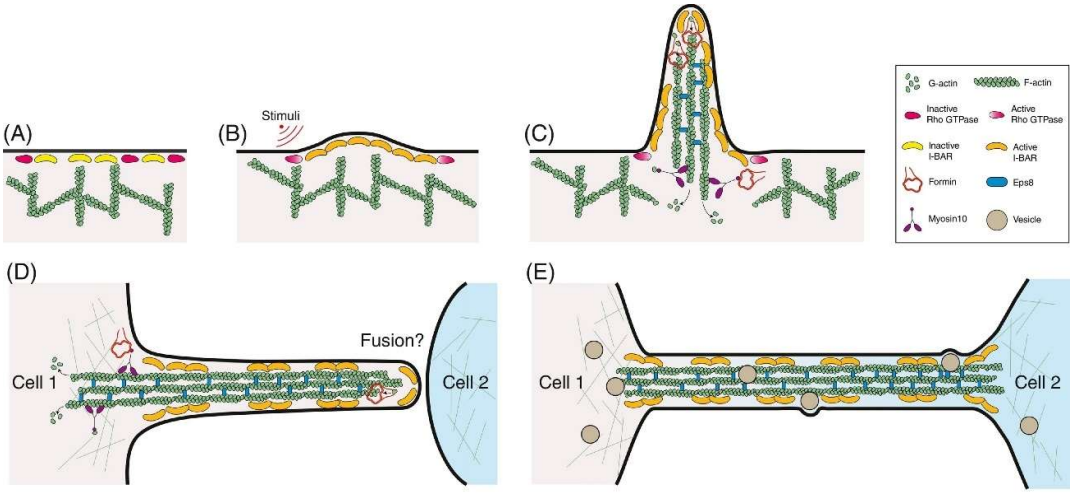

Figure 8. Model of the steps in the TNT's formation.

(A) Cells are in an inactive state. (B) Cells can be stimulated by various signals that would induce the negative membrane curvature required for TNT formation. (C) Actin polymerization is triggered to form initial actin bundles that can overcome membrane elasticity, allowing further TNT elongation. (D) TNT grown from cell 1 reaches opposite cell 2 and fuses with its membrane through an unknown fusion mechanism. (E) Functional TNTs formed between cell 1 and cell 2 containing direct actin filaments, can now exchange large cargoes. Obtained from Ljubojevic et al., 2021.

Membrane deformation and initiation of protrusion growth

For the formation of actin-based protrusions, two processes are necessary, although it is still unclear whether one precedes the other or whether they eventually occur at the same time.

One of these processes that could lead to the formation of a protrusion is the deformation of the membrane producing curvature of the membrane (*Ljubojevic et al., 2020*). This membrane deformation can be carried out by proteins such as the inverse Bin-Amphiphysin-Rvs domain proteins (I-BAR proteins) that can cause outward membrane curvature (*Chatzi and Westbrook, 2021*) and/or by proteins such as the tetraspanins CD9 or CD81 that can cause membrane curvature due to their molecular shape (*Zimmerman et al., 2016; Umeda et al., 2020*) (*Figure 8A-C*).

For the initiation of the growth of protrusions by the action of actin filaments pushing out the membrane or membrane proteins pulling actin filament polymerization (as it is the case for I-BAR proteins in filopodia biogenesis -*Zhao et al., 2011*-), different regulators have been discovered in recent years. In this respect we have Rho GTPases such as CDC42 which is a well-known regulator of filopodia formation (*Nobes and Hall, 1995*). However, this regulation is contrary in the case of TNTs, because as mentioned above, CDC42 together with IRSp53 and VASP negatively regulates the formation of TNTs (*Delage et al., 2016*). However, it is more likely that the regulation of the initiation of TNT formation by actin related proteins is rather cell type specific, since this same CDC42 which is a negative regulator of TNTs in neuronal cells, is a positive regulator in macrophages (*Hanna et al., 2017*).

Elongation

The longer distances than the filopodia that the TNTs reach suggest that these structures are under tight control of actin nucleators, suppliers and elongators (*Ljubojevic et al., 2020*) (*Figure 8D)*, whereas in the case on TNT-like connections containing microtubules (which these protrusions would be longer and more stable) this process would be also presumably under the control of microtubule targeting agents. However, little or nothing is known at this time about the elongation of TNTs and it should be is extrapolated from what happens with other protrusions such as filopodia. Regulators thought to act at this step could be the formin family of proteins for their ability to incorporate G-actin into a

growing filament (*Yu et al., 2017*) or the protein Epidermal growth factor receptor kinase substrate 8 (Eps8) that could function as a stabilizer of TNTs through its ability to form actin bundles (*Delage et al., 2016*) or Dephosphorylated β-Ca^{2+}-Calmodulin-dependent protein kinase II (βCaMKII) which increases the duration of TNTs presumably through its binding to G-actin and preventing their nucleation (*Vargas et al., 2019*; *Sanabria et al., 2009*).

Adhesion and fusion with the opposing cell

Interestingly, this step would be the last to occur in TNTs formed by actin-driven mechanism but the first step in TNTs formed by cell dislodgement.

In either case, prior to fusion, the membrane of the TNTs and the opposing cell should recognize each other and place themselves in a juxtaposed position and this is speculated to be accomplished through cell adhesion molecules (*Abounit and Zurzolo, 2012*). In fact, over the years there have been a few studies that have identified different cadherins to be present on TNTs or even at the tip of them (*Jansens et al., 2017*; *Lokar et al., 2010*; *Chang et al., 2022*) but the role of these cadherins in TNTs has not been investigated in depth (*Figure 8D&E)*.

Once the membranes are facing each other, molecules would be needed that could generate a membrane curvature between TNT and the opposing cell such that the space between the lipidic bilayers would be so small as to produce a mixing of these membranes and thus the fusion between TNT and the opposing cell (*Abounit and Zurzolo, 2012*). To date, no regulator of TNT fusion has been found, but it tends to be thought that molecules involved in other membrane fusion processes would also play a very important role in TNT fusion, such as the tetraspanins CD9 and CD81, molecules widely characterized in different membrane fusion processes (*Rubinstein et al., 2006*; *Ishii et al., 2009*; *Charrin et al., 2013*; *Takeda et al., 2003*) (*Figure 8D&E)*.

Since these last processes of adhesion and fusion of TNTs with the opposing cells have not been investigated, I considered that studying therefore candidates to have a very important role in these steps of the formation of TNTs such as cadherins and tetraspanins focusing on N-cadherin and on the tetraspanin CD9 and CD81, could broaden our knowledge about TNTs to be applied in the future to other fields beyond cell biology.

Chapter 3: Cadherins and the cadherin adhesome

As was the case for intercellular communication, the correct maintenance of cell-to-cell interactions is essential for processes such as homeostasis, development or cell-to-cell communication itself. Although today we have a vast knowledge in this field, we do not have to go back much more than 50 years to know that these functions, well established today, were no more than hypotheses at that time. 45 years ago, two independent groups not only discovered the first molecules involved in cell-to-cell interaction but also the two methods of cell interaction: Ca^{2+} independent cell adhesion with the protein that later became known as NCAM (Neural Cell Adhesion Molecule) (*Thiery et al., 1977*) and Ca^{2+} dependent cell adhesion with the protein that later became known as cadherin (*Takeichi, 1977*). In this section, I will focus on these proteins that act as Ca^{2+} dependent cell adhesion molecules known as cadherins.

The cadherin superfamily

Following this historical overview, and strongly recommending a nice review of the initial work in the field of cadherins by the discoverer of these molecules himself (*Takeichi, 2018*), it was not until a few years later that these proteins were truly identified. The first of these identified molecules was identified by an antibody called "ECCD1" and they named this Ca^{2+} dependent cell adhesion molecule as "cadherin" (*Yoshida-Noro et al., 1984*) and a year later by treating the cells with an antibody called "NCD1" they saw how cell adhesions were disrupted and also how these two antibodies did not recognize the same antigens since ECCD1 only recognized targets in epithelial cells while NCD1 only in neuronal cells, which led them to rename these two molecules as E-cadherin (Epithelial-Cadherin or ECAD) for the ECCD1 target and N-cadherin (Neural-Cadherin or NCAD) for the NCD1 target (*Hatta et al., 1985*). To date, these initial cadherins are grouped into a superfamily of proteins, divided into several subfamilies and with more than 100 members. Despite the vast number of members in this superfamily, it is accepted that the common function for all of them is to be a major cell-cell adhesion mechanism, while their structure, although sharing some homology (especially in the sequence of the extracellular domain know as cadherin motif), differs among the different subfamilies (*Suzuki and Hirano, 2016*).

Over the years, the classification of this superfamily that we know today was formed (*Figure 9)*. The classical cadherins are further subdivided into two groups, type I and type II cadherins classified according to differences in the amino acid sequence of the cytoplasmic region of these cadherins (*Suzuki et al., 1991*). While type I cadherins are more tissue-specific, type II cadherins are expressed together in many tissues (*Bekirov et al., 2002*), but both form what is known as "cadherin adhesome" forming the adherens junctions that are composed of these cadherins and molecules associated with their cytoplasmic tail known as catenins (in this case p120-catenin, β-catenin and α-catenin) bound to the actin cytoskeleton. Among the type I cadherins we can find ECAD, NCAD, P (Placental)-cadherin, R (Retinal)-cadherin or M (Muscle)-cadherin; and some examples of type II are VE (Vascular Endothelial)-cadherin, K (Kidney)-cadherin, CDH8, CDH9, CDH10, CDH11 or CDH12 (*Suzuki and Hirano, 2016*). Another subfamily of cadherins is those that form desmosomes, structures similar to adherens junctions but different from the latter in that desmosomes form punctate cell-to-cell junctions. Here we find desmogleins (*Koch et al., 1990*) and desmocollins (*Collins et al., 1991*). Unlike classical cadherins, desmosomal cadherins do not interact with catenins and actin through their cytoplasmic tail, but form complexes with plakoglobins, plakophilins, desmoplakin and the intermediate filament (*Angst et al., 2001*). The largest subfamily of cadherins are the so-called protocadherins, further subdivided into "clustered" and "non-clustered" protocadherins. Although they share the function of cell adhesion with the classical cadherins (*Obata et al., 1995*), they differ from the latter in that their extracellular domain is longer and they do not possess a catenin-binding region (*Hayashi and Takeichi, 2015*). Since they are widely expressed in the nervous system, their functions are related to the nervous system by controlling its proper functioning and development (*Hayashi and Takeichi, 2015*). We can also find a great variety of different cadherin-like proteins, such as 7D-cadherins, Fat and Dachsous, Flamingo... that differ in morphology with the classical cadherins and in functions since, apart from cell adhesion, they have more varied functions such as cell signaling (*Hirano and Takeichi, 2012*).

Within this superfamily, the classical type I cadherins (especially ECAD and NCAD) are by far the most studied and best known.

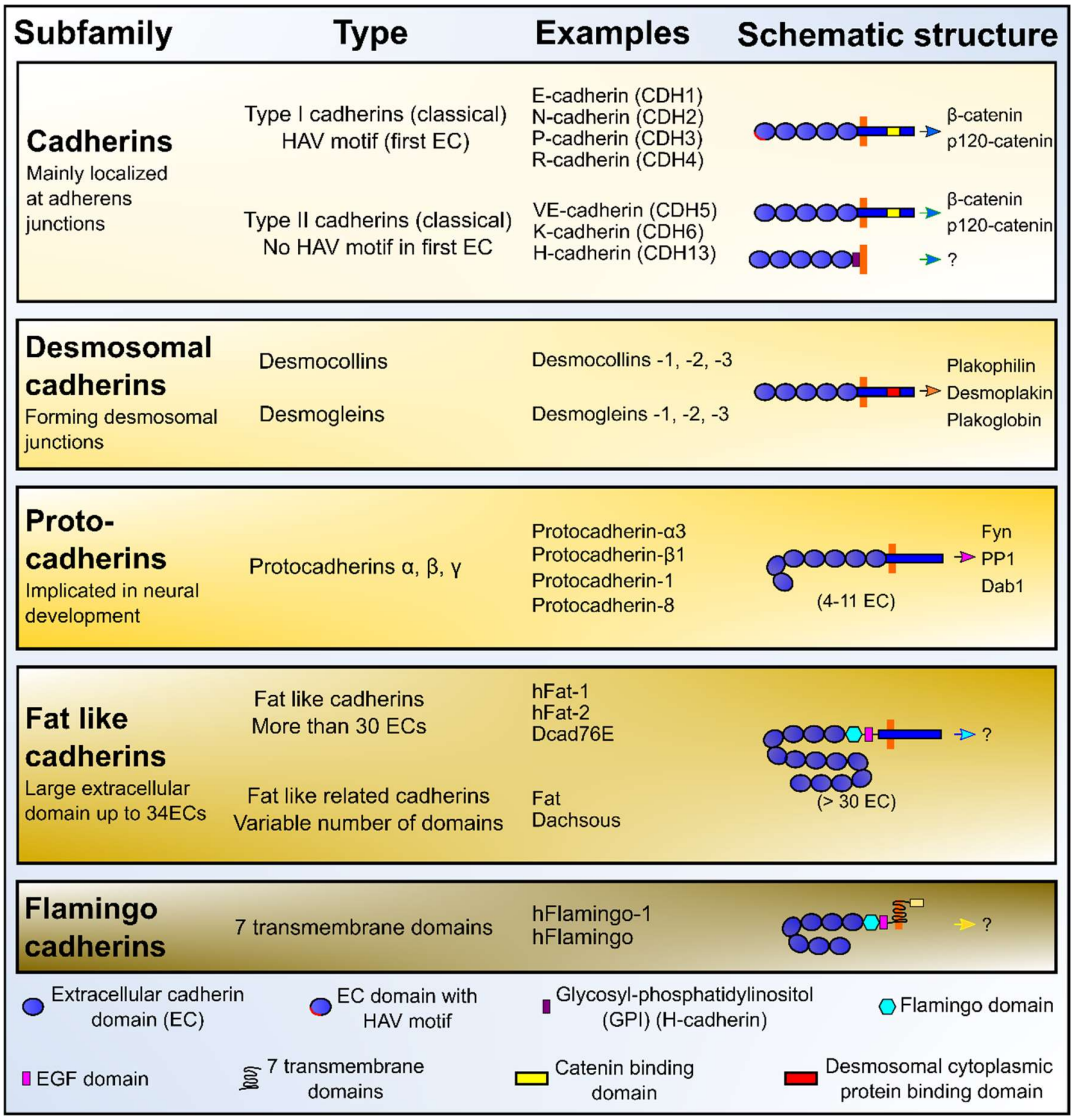

Figure 9. The cadherin superfamily.

The cadherin superfamily includes a wide variety of proteins, sharing the cadherin motif repeats at the extracellular domains and the general function as cell-to-cell adhesion molecules, but varying in the number of the repeats of the cadherin motifs and the associated molecules. This superfamily includes the classical cadherins (type I and II), desmosomal cadherins, protocadherins, or other cadherin-like proteins. Adapted from Peinado et al., 2004.

Classical cadherins and the cadherin adhesome

Classical cadherins are composed by an ectodomain formed by five highly conserved regions (EC1-5) each of them formed by 110 amino acids, being the first the most distant from the membrane and with 3 Ca^{2+} ions in between each EC domain rigidifying this structure (*Overduin et al., 1995*; *Boggon et al., 2002*), a single transmembrane pass and a cytoplasmic tail (*Takeichi, 1990*). The cadherin adhesion is made by the interaction of

two cadherins on two opposing cells in a trans conformation through their EC1 in a "strand-swap" interaction (*Shapiro and Weis, 2009*), but interactions between the EC1-EC2 of two different cadherins in cis on the same cell is needed for the strengthening of the adhesion (*Harrison et al., 2011*). Cadherin-associated molecules are coupled to the cytoplasmic tail of the cadherin: p120-catenin, β-catenin and α-catenin. Through α-catenin, this "cadherin adhesome" is linked to the actin cytoskeleton which finally gives integrity to the complex forming the adherens junction (*Mège and Ishiyama, 2017*) (*Figure 10)*.

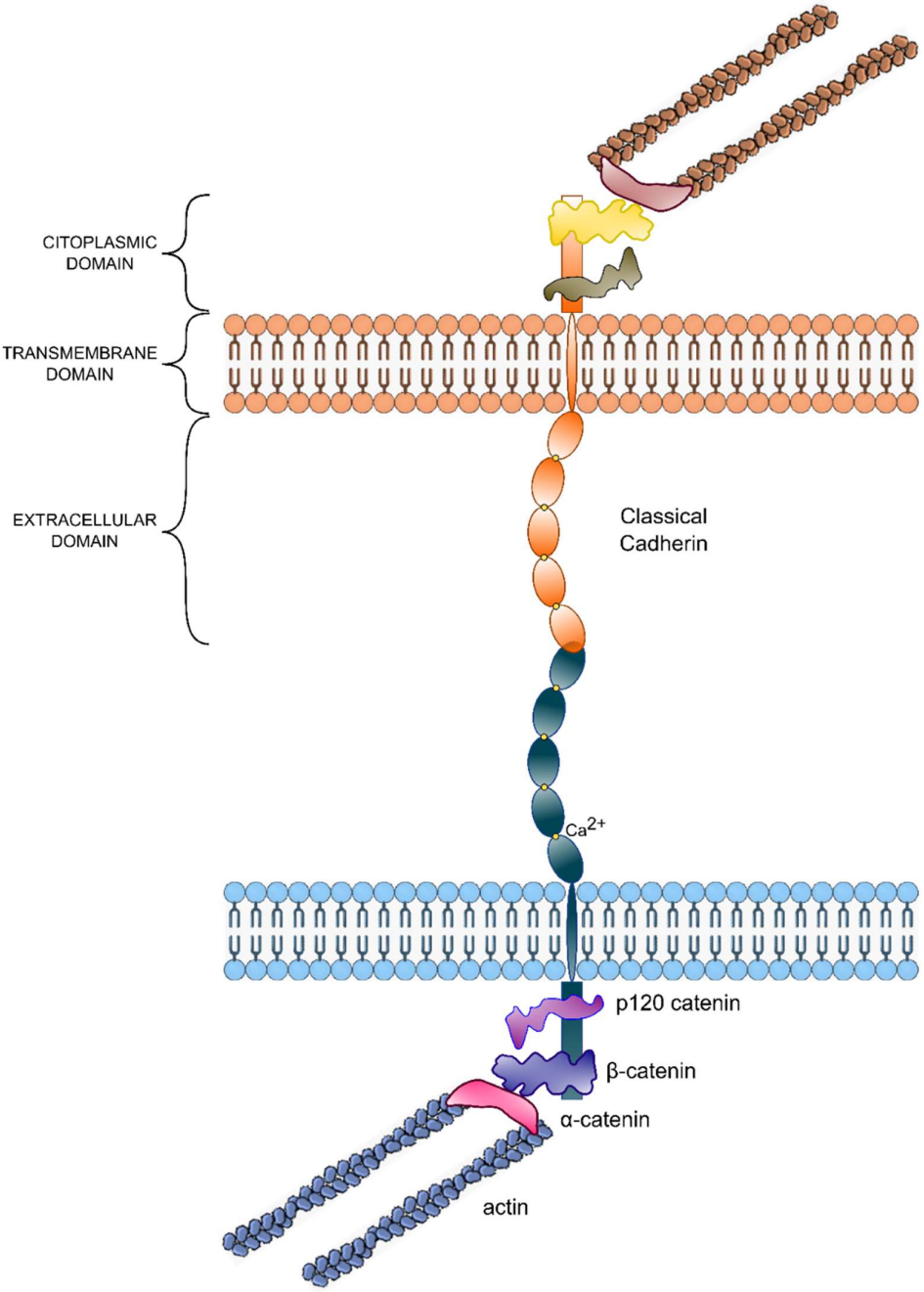

Figure 10. The classical cadherin adhesome.

The classical cadherin adhesome is form by the cadherin (e.g., ECAD or NCAD) from one cell that will bind in an homophilic manner to another cadherin of the opposing cell. Cadherin associated molecules, p120-catenin, β-catenin, are bound to the cytoplasmic tail of the cadherin with α-catenin interacting with β-catenin and actin linking the cadherins to the cytoskeleton.

Adherens junctions link the actin cytoskeleton of neighboring cells together, and provide the physical connection needed for morphogenetic processes like neurulation, cell migration, sheet sealing of epithelial cells, and growth and differentiation of cells (*Gumbiner, 2005*; *Halbleib and Nelson, 2006*; *Lien et al., 2006*; *Kardash et al., 2010*). Adherens junctions are also involved in signaling and controlling the growth (*Cavallaro and Dejana, 2011*), as ECAD with the Epidermal Growth Factor Receptor (EGFR) (*Qian et al., 2004*) or NCAD with the Fibroblast Growth Factor Receptor (FGFR) (*Suyama et al., 2002*), differentiation (*Halbleib and Nelson, 2006*), and fate of cells (*Lechler, 2012*), as well as maintaining the homeostasis of adult tissues (*Leckband et al., 2011*). In addition, cadherins are also involved in brain development and cell-cell communication processes, the best known being the role of NCAD in functions including the maturation of neural tissues, the construction of circuits, and the emergence and alteration of synapses (*Hirano and Takeichi, 2012*).

Nevertheless, all these functions of cadherins depend on the correct assembly of their associated molecules mentioned above: the catenins.

Catenins

Catenins were so named because at their discovery they were believed to be the link of cadherins to the actin cytoskeleton (which was later confirmed), and therefore their name was adapted from the Latin "*catena*" meaning chain (*Ozawa et al., 1989*). Catenin family is formed by: α-catenin, β-catenin, δ-1-catenin (or p120-catenin), δ-2-catenin (or Neural Plakophilin-Related ARM-repeat Protein -NPRAP-), γ-catenin (or plakoglobin) and plakophilin. Except for α-catenin, all catenins contain a central Armadillo domain of between 9 and 12 repeats that makes them form their interaction domains (*McCrea and Gu, 2010*). Of these, the cadherin adhesome of the classical type I cadherins is formed by the interaction of p120-catenin and β-catenin with the cytoplasmic tail of the cadherins and α-catenin interacting with β-catenin and the actin cytoskeleton and as we will see below, these catenins play many more roles than just being a complement to cadherins in cell adhesion.

p120-Catenin

Identified in 1994 as a substrate of Src kinase with direct interaction with ECAD (*Reynolds et al., 1994*), its main functions are to control the stability and recycling of cadherins and to control actin dynamics at the level of adherens junctions by interacting with Rho GTPases.

p120-Catenin can control the strengthening of cadherin-based adhesion (*Thoreson et al., 2000*), the clustering of these molecules (*Yap et al., 1998*), the presence of cadherins in the membrane preventing the recycling of the cadherins by blocking the ubiquitinylation of the cadherins (*Hartsock and Nelson, 2012*), or conditioning the correct development of the organism (*Davis and Reynolds, 2006*).

In addition to all these functions, p120-catenin can in turn control cellular architecture by controlling actin dynamics through its interaction with various Rho GTPases. Thus, this catenin favors the formation of filopodia and lamellipodia and increases the migratory capacity of cells presumably by increasing the activity of CDC42 and Rac (*Grosheva et al., 2001*). It may modulate actin dynamics by inhibiting RhoA activity by disrupting actin stress fibers (*Reynolds et al., 1996*) but this RhoA inhibition is mutually exclusive with interacting with cadherins (*Anastasiadis et al., 2000*).

Finally, p120-catenin has also been reported to interact with microtubules and enhance their stability by affecting the migratory capacity of cells (*Ichii and Takeichi, 2007*).

ß-Catenin

β-Catenin binds to the cytoplasmic tail of cadherins in a position lower than p120-catenin and also to α-catenin (*Huber et al., 1997*) and it is this binding to cadherins that presumably protects them from degradation (*Huber et al., 2001*).

But as was the case with p120-catenin, β-catenin is involved in other roles beyond its function in interacting with cadherins. However, the involvement of β-catenin in processes other than coupled to cadherins is thought to be mediated to mechanical stimuli such as constriction by an abundant density of cells or changes in cell morphology (*Desprat et al., 2008*; *Benham-Pyle et al., 2015*). Therefore, β-catenin can be found not associated with cadherins, participating in the Wnt pathways (Wnts are proteins secreted serving as signaling molecules when they bound to their receptor proteins called

Frizzled), but for this it has to be translocated to the nucleus where it is a cofactor with T cell factor/lymphoid enhancer factor (TCF/LEF) (*Nelson and Nusse, 2004*). Without the presence of Wnt, β-catenin accumulates in the cytoplasm and is subsequently degraded by a complex formed by Adenomatosis Polyposis Coli (APC) and Axin proteins among others (*Nelson and Nusse, 2004*). Therefore, when translocated to the nucleus, β-catenin together with TCF/LEF can activate a wide variety of genes that have a great impact on stem cells, metabolism or cancer development and establishment (*Ramakrishnan and Cadigan, 2017*).

α-Catenin

The last member of the adherens junction is interacting on the one hand with β-catenin and on the other hand with the actin cytoskeleton. Therefore, its main function is to anchor the cadherin-catenin complex to the cytoskeleton, but it is also able to control actin dynamics.

α-Catenin interacts with numerous actin binding proteins such as α-actinin (*Knudsen et al., 1995*), ZO-1 (*Itoh et al., 1997*), vinculin (*Hazan et al., 1997*), afadin (*Pokutta et al., 2002*), formin-1 (*Kobielak et al., 2004*) or eplin (*Abe and Takeichi, 2008*), which allows control of actin dynamics (*Kobielak et al. 2004*; *Tang and Brieher 2012*; *Abe and Takeichi, 2008*; *Drees et al., 2005*; *Benjamin et al., 2010*) and it is able to direct bundle actin filaments (*Rimm et al. 1995*). Although α-catenin has an undoubted actin-binding domain and it has been known for years that this α-catenin binds directly to actin (*Pokutta et al. 2002*; *Rimm et al. 1995*) and thus connects adherens junctions to the actin cytoskeleton giving it its functionality (*Mège et al., 2006*), in 2005 the ability of α-catenin to bind both β-catenin and actin was doubted (*Yamada et al., 2005*; *Drees et al., 2005*). It was not until an element that had not been considered was added, and that is that when tension was applied to this cadherin-catenin-actin complex, α-catenin went from weakly binding actin to having a strong binding with it (*Buckley et al., 2014*). Therefore, the most widely accepted today is that α-catenin binds to actin directly, but it is not until force and tension are applied allowing vinculin to bind to α-catenin and this last binds to the contractile cytoskeleton of actomyosin (*Mège and Ishiyama, 2017*).

Outside of adherens junctions, α-catenin can be found in the cytosol in the form of monomers or dimers (*Drees et al., 2005*) that are able to inhibit the Arp2/3 complex in

vitro, which could mean the regulation of actin dynamics away from cadherins in cells. Cytosolic α-catenin appears in complex with APC and β-catenin and may play an important role in the transcription of genes of the Wnt/β-catenin pathway (*Su et al., 1993*). α-catenin dimers can also be found in membranes that do not form adherens junction and in this case, it was observed to induce a clear increase in filopodia (*Wood et al., 2017*). Last and very interestingly, α-catenin has been recently identified at the margins of mesenchymal cells, where it interacts with F-actin and binds with vinculin within integrin adhesions, suggesting that α-catenin has a role not only in adherens junction but also in cell adhesion to the extracellular matrix (*Mukherjee et al., 2022*).

Cadherins, catenins and TNTs

Unfortunately, the role of cadherins and/or catenins in TNTs has hardly been studied. The first report of the presence of the cadherin-catenin complex in TNTs dates back to 2010, in which Lokar and colleges found in urothelial T24 cells both NCAD and β-catenin present along TNTs and hypothesized that the cadherin-catenin complex would serve as an anchoring pathway for TNTs with the opposing cell to subsequently form an open channel (*Lokar et al., 2010*) but no functional role other than the presence of these molecules was investigated (*Figure 11A*). Another cadherin, in this case ECAD also together with β-catenin were found in Swine Testicle (ST) cells being enriched in the adhesion zone of the TNTs with the opposing cell and could provide cytoplasmic continuity with the opposing cell (*Jansens et al., 2017*), again without asserting the role of these molecules in TNTs other than anchors (*Figure 11B*). ~~O~~ur lab has recently discovered that, at least in neuronal cells, TNTs are made of iTNTs that form a bundle and this structure appears to be held together by N-cadherins molecules, which by cryo correlative EM are localized at links between iTNTs and at the base of treads that appear to coil around the iTNTs bundle (*Sartori-Rupp et al., 2019*) (*Figure 11C*) Thus I started my thesis with the aim to study the role of N-cadherin in TNTs, a project directed by Professor Chiara Zurzolo in collaboration with Dr. Anna Pepe, a postdoc in the lab. Furthermore, a recent study (*Chang et al., 2022*) shows that TNT-like connections are formed by two filopodia coming from two different cells that interact with each other forming what they call "Double Filopodial Bridge" or "DFB". When one of these two filopodia separates from the other, a single TNT-like cell-cell connection called "Single Filopodial Bridge" or "SFB" remains (*Figure 11D*). The authors address how the

formation of these DFBs and their transition to SFP depends on NCAD (and presumably on catenins but they only investigated the presence of β-catenin) and that this transition is a consequence of the torsion exerted by myosin (*Chang et al., 2022*). While the localization of NCAD in this transition may support the presumed possible role of NCAD in the iTNTs bundle, the authors, contrary to all previous studies, suggest that the accumulation of NCAD in the TNT-opposing cell contact areas and the unidirectional Ca^{2+} transfer indicate the presence of close-ended TNTs. However, in this study the authors do not analyse the ultrastructure of these TNT-like connections, neither perform any transfer experiments showing anything other than calcium-mediated communication. Finally, our lab showed that the formation of TNTs in neuronal cells is through the Wnt/Ca^{2+} pathway and therefore Wnt/β-catenin pathway independent (*Vargas et al., 2019*), which does not exclude a possible role of β-catenin in the regulation of TNTs, but within the cadherin-catenin complex.

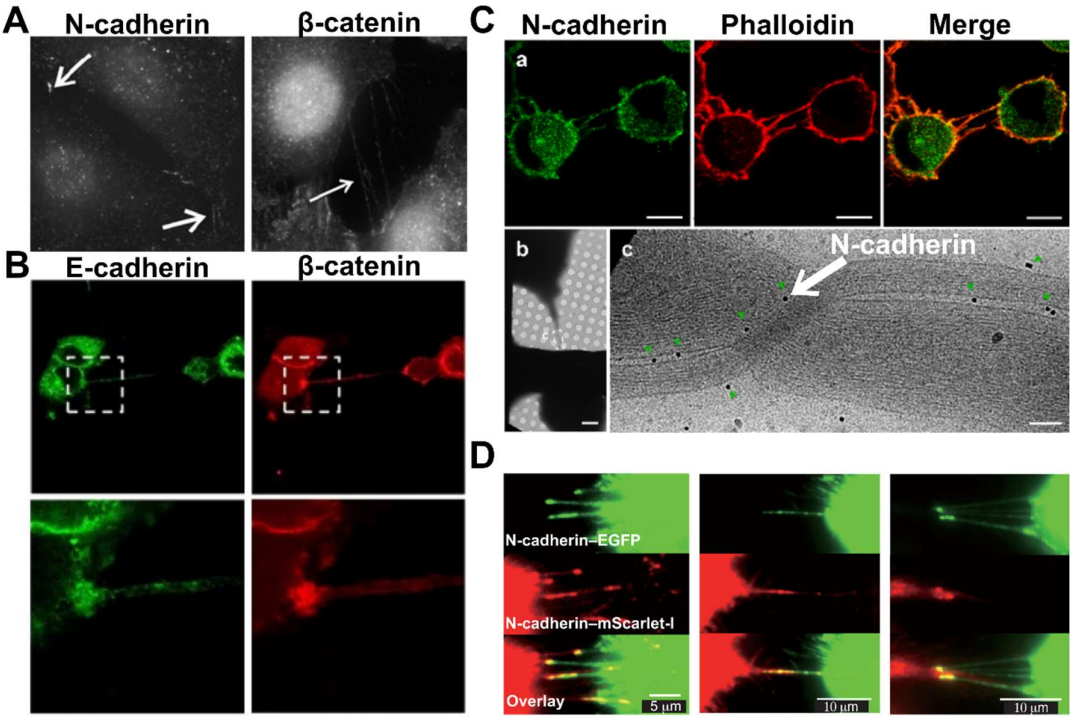

Figure 11. Presence of cadherins on TNTs.

(A*) Presence of NCAD and β-catenin (both in grey) on TNTs in urothelial T24 cells. (B) Presence of ECAD (green) and β-catenin (red) on TNTs in ST cells. (C) Presence of NCAD on TNTs in neuronal CAD cells by immunofluorescence (NCAD in green and actin in red) and by immunogold (black dots pointed by green arrowheads). (D) Presence of NCAD from both cells (in green NCAD from one cell and in red NCAD from the other) on DFB or SFB in HeLa cells. Obtained from Lokar et al., 2010; Jansens et al., 2017; Sartori-Rupp et al., 2019 and Chang et al., 2022.*

Therefore, the aim of my first thesis project is to provide a more comprehensive study on the role of NCAD in TNTs as well as of the cadherin-catenin complex in TNTs by studying the function of the linker of cadherins to the actin cytoskeleton, α-catenin.

Chapter 4: Tetraspanins

In 1990 with the immunoprecipitation of a previously unknown membrane antigen of 26 kiloDaltons (kDa) (*Oren et al., 1990*) what would later become known as the "tetraspanin" family of proteins was discovered. This protein was called TAPA-1 "Target of an Antiproliferative Antibody" and later became known as Cluster of Differentiation 81 or simply CD81. Subsequently, other membrane antigens similar to CD81 such as CD63 (*Metzelaar et al., 1991*) or CD9 (*Boucheix et al., 1991*) were discovered, that by sequence similarity suggested that they might be members of a new family of proteins (*Boucheix et al., 1991*) which would be called transmembrane 4 superfamily (TM4SF) or simply tetraspanins (*Figure 12*), including to date 33 members in mammals (among which are the most studied and known: CD9, CD63, CD81, CD82 or CD151) that although they differ slightly in sequence but are conserved both in structure and between species (*Hemler, 2003*; *Charrin et al., 2014*) with wide expression over cells and tissues for CD9, CD63, CD81 or CD151 (but restricted expressions for other tetraspanins such as uroplakins or peripherins) and a large number of different functions due to the formation of associations with a multitude of proteins forming specific membrane domains called tetraspanin-enriched microdomains (TEMs) (*Boucheix and Rubinstein, 2001*).

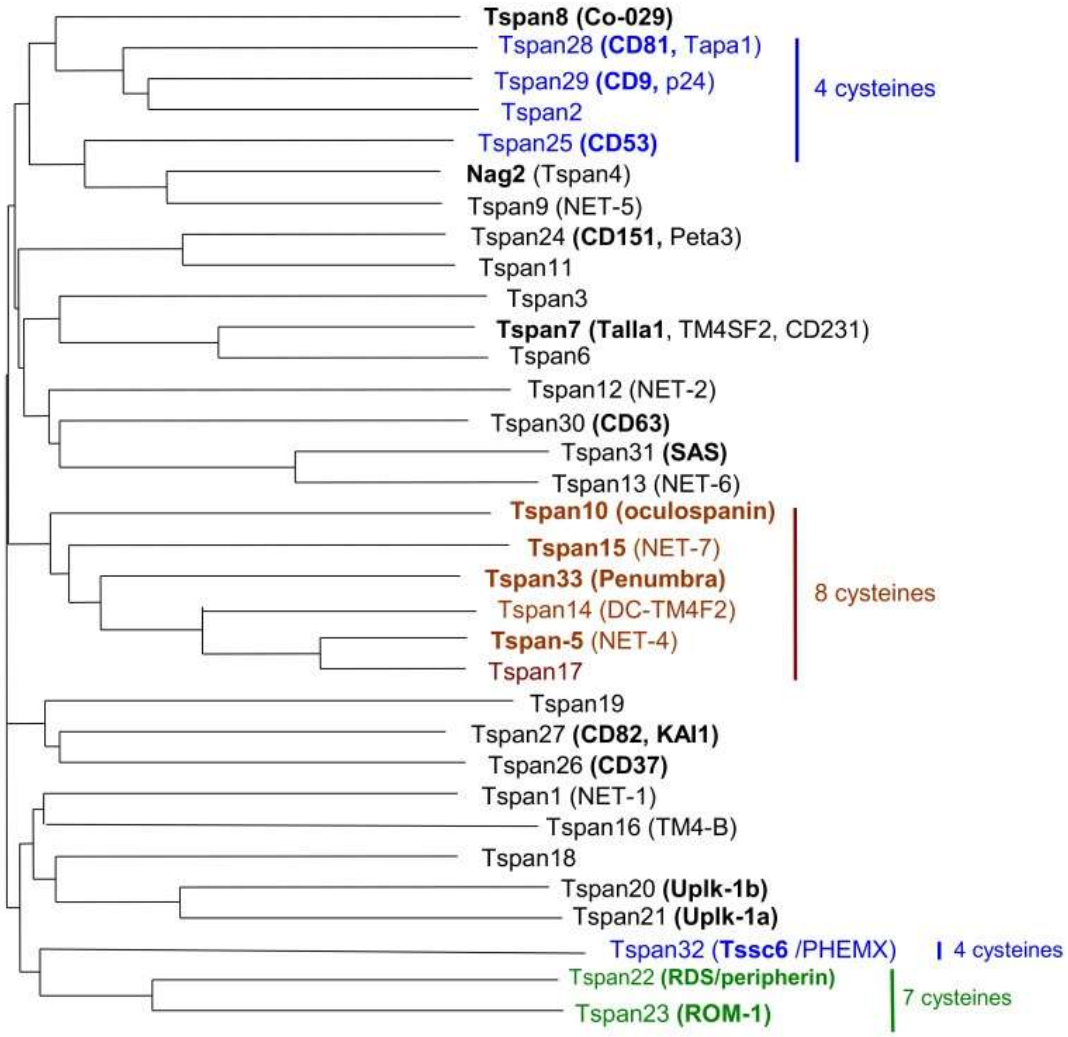

Figure 12. The tetraspanin superfamily.

Homology tree of human tetraspanins. Names in bold correspond to common names. It shows when the number of cysteines in the extracellular loop EC2 differs from six cysteines. Obtained from Bonnet et al., 2019.

In this section, I will explore the structure, membrane domains and general functions of tetraspanins, paying special attention to CD9 and CD81 tetraspanins since the second project of my thesis is focused on them.

Structure of tetraspanins

Tetraspanins are small integral membrane proteins that share a common structure consisting of two extracellular domains, one intracellular domain, four transmembrane domains and two short cytoplasmic tails (*Hemler et al., 2003*) (*Figure 13*). To be considered tetraspanins, they must possess several conserved amino acids, including a

CCG motif and two additional cysteine residues that contribute to two key disulfide bonds in the second extracellular domain fundamental for its correct folding (*Kitadokoro et al., 2001*; *Seigneuret et al., 2001*).

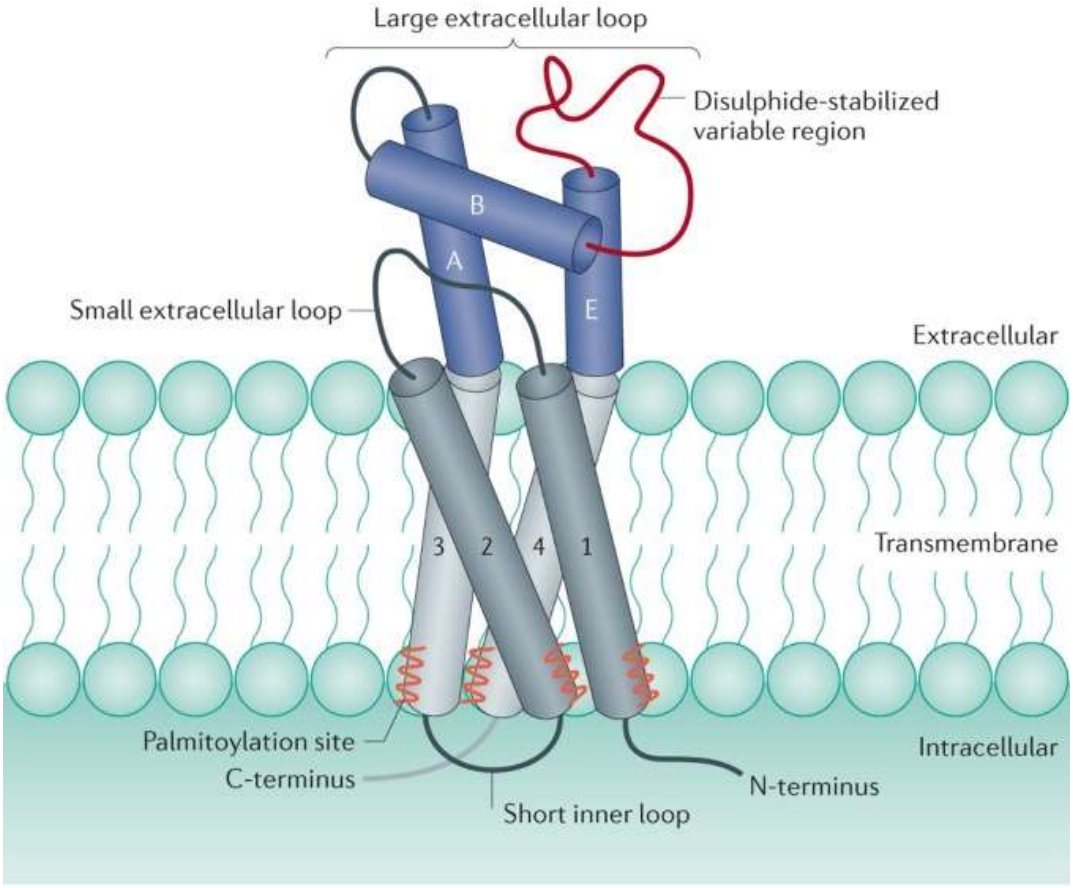

Figure 13. General tetraspanin structure.

Common features of the tetraspanin superfamily. These proteins are composed two short cytoplasmic tails, four transmembrane passes, one short intracellular loop and two extracellular loops, one short loop (SEL) and one large loop (LEL). Obtained from Hemler et al., 2014.

The two extracellular domains form loops that are distinct from each other, one of them being short, known as Short Extracellular Loop (SEL) or EC1, and the second long, called Large Extracellular Loop (LEL) or EC2. The SEL is relatively unknown in function, but is believed to be necessary for the correct expression of LEL but does not appear to allow tetraspanin interactions (*Masciopinto et al., 2001*). In contrast, the LEL is much better known. Practically all tetraspanins possess a constant and a variable domain in the LEL (*Seigneuret et al., 2001*) and it is believed that this variable region of the LEL is responsible for forming the interactions with other proteins typical of tetraspanins (*Stipp et al., 2003*). Notable examples of this are the failure of CD81 to interact with Hepatitis

C virus E2 protein when the variable region of the LEL corresponding to the C-D helix regions is mutated (*Higginbottom et al., 2000*), or certain amino acid residues in the variable region of the murine CD9 LEL that are critical for sperm-oocyte interaction (*Zhu et al., 2002*).

The transmembrane domains are highly conserved between tetraspanins and between species (*Stipp et al., 2003*). It is speculated that these transmembrane domains may play a fundamental role in tetraspanin-to-tetraspanin interactions at least for tetraspanin CD151 (*Berditchevski et al., 2001*) and the interactions between the various transmembrane domains are essential for the correct expression of CD82 in the membrane (*Cannon and Cresswell, 2001*).

Regarding the cytoplasmic domains of tetraspanins, their general functions are rather unknown and it is believed that they may vary from one tetraspanin to another (*Stipp et al., 2003*). Some examples of cytoplasmic tail rollovers can be found in tetraspanin CD63, which upon mutation of the C-terminal domain of CD63 this protein is mislocalized to the membrane rather than to the endoexosomal compartment (*Rous et al., 2002*). C-terminal changes in the intracellular tail of 3 amino acids for another 3 corresponding to CD82 cause CD9 not to fulfill its role in cell aggregation functions or adhesion to the extracellular matrix (*Wang et al., 2011*). In the case of CD81, it is believed that this tetraspanin could interact with the actin cytoskeleton through the interaction of its C-terminal tail with the ezrin-radixin-moesin (ERM) complex (*Sala-Valdés et al., 2006*).

Specific structure of CD9 and CD81

Although these two tetraspanins logically maintain the typical structure of these tetraspanins, in recent years the crystal structure of these two proteins has become known, offering new information about these two tetraspanins (*Figure 14*).

CD81 crystal structure was first published by *Zimmerman et al., 2016*. The structure of CD81 resembles a “waffle cone”, with the LEL domain covering the membrane lumen surrounded by four transmembrane helices. The overall folding of the four transmembrane helices is not similar to that of any other intact membrane protein of known structure. The transmembrane (TM) region consists of two pairs of essentially independent antiparallel helices: one pair includes TM1/TM2 and the other pair TM3/TM4. The two pairs of helices converge near the cytoplasmic side of the membrane

only through the contact between TM2 and TM3 (*Figure 14A*). In the large hydrophobic cavity between the TM domains, they founded an electro dense zone which was revealed as a binding site to the cholesterol. Interestingly, when they performed molecular dynamics simulations, they observed that when no lipids were added to the simulation, the LEL dissociated from TM 3 and 4 and an "open" CD81 conformation was observed, whereas when they added cholesterol, it bound to the central cavity causing the LEL to bind to the transmembrane domains in a “close” conformation (*Figure 14B*).

The crystal structure of human CD9 published by *Umeda et al., 2020* show CD9 folds into four transmembrane domains whose intracellular ends are in close proximity, while their extracellular ends are loosely packed to form a large central pocket within the intramembrane region. The SEL between TM1 and TM2 and the LEL between TM3 and TM4 span this central cavity. The LEL is stabilized by a pair of disulfide bonds between highly conserved cysteine residues. It is conceivable that there is a third disulfide bond at the intracellular ends of TM helices, which may originate from bound palmitoyl units, consistent with the heterogeneity in band detected by western blot of the purified CD9 protein (*Figure 14C*). Interestingly, the general structure of CD9 adopts an inverted cone-like molecular shape that when included in lipid membranes generated membrane curvature (*Figure 14E*). Finally, molecular dynamic simulations showed how the SEL and LEL are flexible and can switch between two conformations, closed with the LEL associated to the SEL, or open with the LEL in a position above the SEL. The inner pocket shows an electron dense zone that presumably serves to bind some lipids that would cause the change from open to closed when bound, although it is doubtful that it is cholesterol since CD9 lacks the amino acids to bind cholesterol in its cavity and this electron dense zone was observed when cholesterol was not added (*Figure 14D*).

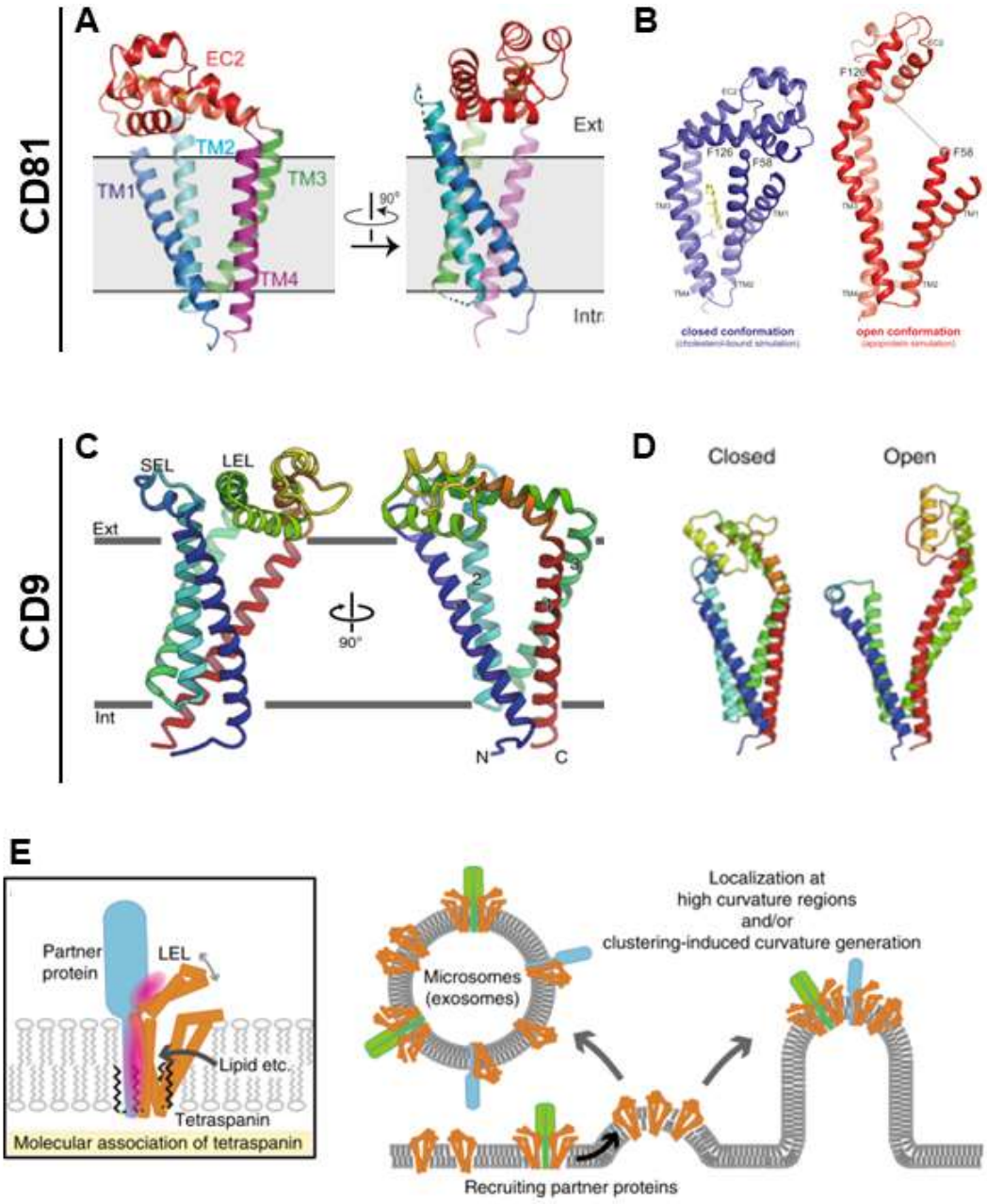

Figure 14. Specific structure of CD9 and CD81.

(A and B) Structure and conformation of CD81. (A) Crystal structure of human CD81. (B) Molecular dynamics simulation of CD81 showing a close conformation (with cholesterol) or open conformation (without cholesterol). (C and D) Structure and conformation of CD9. (C) Crystal structure of human CD9. (D) Molecular dynamics simulation of CD9 showing a close conformation (with lipid) or open conformation (without lipid). (D) Model of the membrane curvature induction by tetraspanins and formation of exosomes and membrane protrusions. Obtained from Zimmerman et al., 2016 and Umeda et al., 2020.

Therefore, the overall structure of CD9 and CD81 is very similar, in fact sharing 60% homology in the sequence (*Umeda et al., 2020*) but although the structures are similar, they have some specificities that could explain specific roles.

Tetraspanin-enriched microdomains (TEMs) or tetraspanin web

If anything characterizes this family of proteins, it is their ability to associate (directly or indirectly) with a vast number of different proteins. To mention just a small part of these associations, tetraspanins can interact with molecules such as a great variety of integrins, coreceptors like CD2 or CD4, MHC molecules, adhesion receptors, growth factors, other tetraspanins... (*Boucheix and Rubinstein, 2001*; *Hemler, 2003*; *Yáñez-Mó et al., 2009*; *Charrin et al., 2009*) (*Figure 15*). This is what is known as TEMs or tetraspanin webs and while they may be similar to other membrane domains such as lipid rafts, TEMs are different because of different characteristics from lipid rafts such as not containing GPI-anchored proteins or caveolin (*Yauch et al. 2000*; *Berditchevski et al. 2002*), being disaggregated when treated with Triton X-100 but resistant to cholesteryl ester depletion (*Class et al., 2001*). This therefore suggests that TEMs and lipid rafts are distinct membrane domains.

In TEMs, tetraspanins can interact directly with other proteins although it is speculated that the most common interactions of tetraspanins are with other tetraspanins or with the same class of tetraspanin (like CD9-CD9, CD9-CD81, CD81-CD151), being even more homophilic interaction than heterophilic (*Kovalenko et al., 2004*). Apart from interacting with other tetraspanins, these proteins can form direct interactions with other molecules, perhaps the most and best known being the interaction of tetraspanins with at least 11 different types of integrins, especially in the case of CD151 (*Hemler, 2003*), or the associations of CD9 and CD81 with their almost obligatory interacting proteins (they are known as tetraspanins partners) CD9P1 (also known as EWI-F) and EWI-2 (also known as IGSF8 or CD81P3) (*Charrin et al. , 2001*; *Stipp et al., 2001*).

But in turn, these primary complexes can interact with other molecules or complexes forming secondary indirect associations. Examples are the dependent association of EWI-2 tetraspanins with integrins (*Stipp et al., 2003*), complex formation with metalloproteases (*Arduise et al., 2008*), cadherins (*Chattopadhyay et al., 2003*),

complement proteins (*Saiz et al., 2018*) and a variety of other proteins (*Charrin et al., 2009*). Furthermore, through these interactions, the tetraspanins can be linked to the actin cytoskeleton, for example, in the case of the tetraspanins CD9 and CD81, their associated partner proteins (EWI-2 and CD9P-1) bind to the ezrin-radixin-moexin (ERM) complex that interacts with the actin cytoskeleton (*Sala-Valdés et al., 2006*).

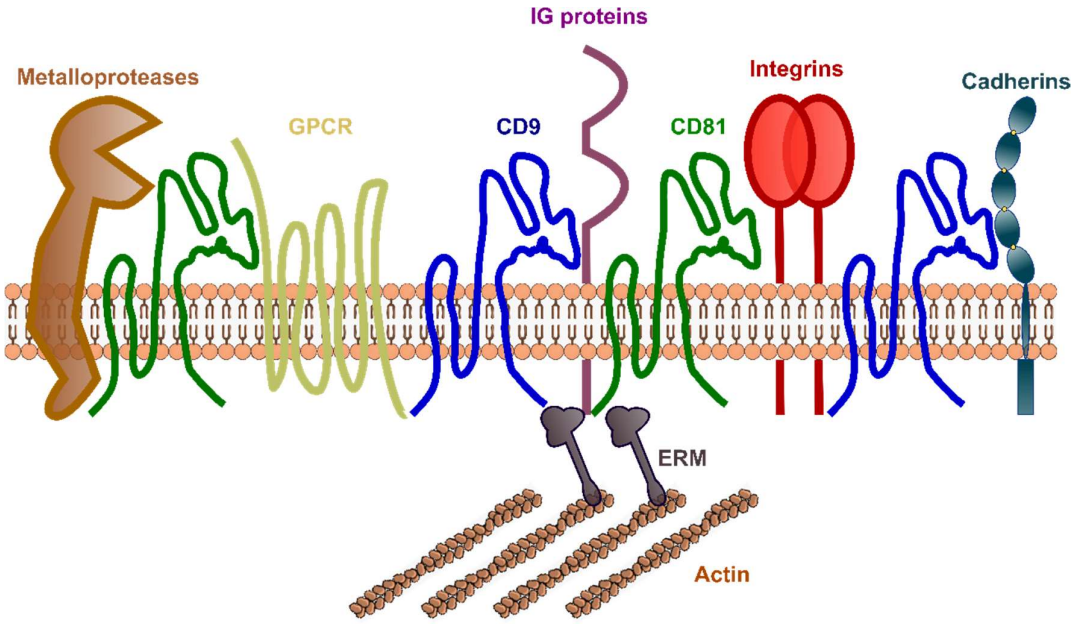

Figure 15. Tetraspanin-Enriched Microdomains (TEMs).

TEMs are functional unit of the plasma membrane characterized for containing tetraspanins that forms interaction (directly or directly) with a great variety of proteins including other tetraspanins, metalloproteases (e.g., ADAM10), GPCRs, immunoglobulin-like proteins (e.g., CD9P-1 or EWI-2), integrins, or cadherins.

General functions of the tetraspanins

Since tetraspanins presumably carry out functions in association with other proteins that they do not carry out on their own, they are known as "molecular facilitators" (*Maecker et al., 1887*). Thanks to the formation of these complexes by tetraspanins, these proteins can carry out a great variety of functions which are determined by the proteins forming the complex in which they are associated.

Role of tetraspanins in Extracellular Vesicles (EVs)

Extracellular vesicles are small membrane particles released from cells into the extracellular space. Tetraspanins, especially CD9, CD63, CD81 and CD82 are

exceptional markers of EVs (*Théry et al., 2018*), but as tetraspanins can be detected at the membrane, different tetraspanins are markers for the presence of different types of EVs. However, the term EVs comprises a large number of different particles that are subdivided into different sizes and origin, such as lipoproteins, exomeres, exosomes, microvesicles, ectosomes or apoptotic bodies (*Mathieu et al., 2019*). It has recently been shown that the composition of these tetraspanins can be different in exosomes (EVs formed in the endocytic compartment) and in ectosomes (EVs formed by plasma membrane budding) (*Mathieu et al., 2021*). In this study, although not exclusively, CD63 is the main marker of exosomoes together with LAMP1 or syntenin-1, whereas CD9 and CD81 are predominantly found in ectosomes together with other proteins such as BSG or SLC3A2 opening the framework for the interpretation of functions by discriminating the different EVs by their tetraspanin content (*Figure 16*). Indeed, it has already been demonstrated how these two populations of EVs can elicit different effects, exemplified by how treatment with Homosalate (a compound that increases the release of vesicles positive for SLC3A2/CD98 and CD9 and thus presumably ectosomes) but not Bafilomycin A1 (which would release vesicles corresponding to exosomes and positive for CD63), increases the migratory capacity in tumor cells (*Grisard et al., 2022*), thus demonstrating how these two populations of EVs have different functions.

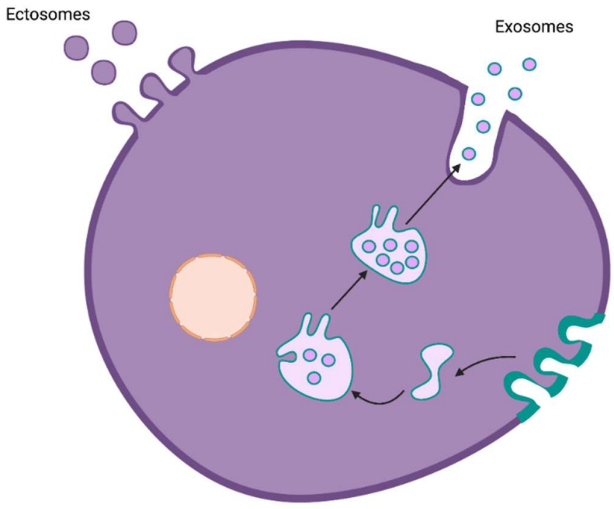

Figure 16. Biogenesis of exosomes and ectosomes.

Exosomes are released upon multivesicular bodies exocytosis, while exosomes are assembled and released from the plasma membrane. Regarding tetraspanins, CD63 is the main marker of exosomes while CD9 and CD81 are founded mainly in the ectosomes.

But tetraspanins are more than just markers of EVs. In fact, the aforementioned molecular structure of these two tetraspanins is believed to be responsible for the formation of these EVs (*Zimmerman et al., 2016*; *Umeda et al., 2020*). Different tetraspanins regulate the sorting and recycling of other molecules through the recycling pathway (*Andreu and Yáñez-Mó, 2014*). Finally, the content formed in the different compartments by different tetraspanins can have very varied functions such as in the immune system, progression and establishment of cancer, or the transfer of genetic material, encompassed in the fact that these vesicles serve as intercellular communicators (*Colombo et al., 2014*).

Integrin-dependent adhesion

As mentioned before, it has long been known that tetraspanins are associated with various integrins. Of these, laminin-binding integrins α3β1, α6β1, and α6β4 directly bind to CD151 (but other tetraspanins can also bind integrins) (*Serru et al., 1999*; *Yauch et al., 1998*). CD151 has minimal effect on the adhesion or diffusion of matrix proteins bound to these integrins. Instead, CD151 was shown to regulate the activation of several signaling molecules downstream of these integrins, including Akt, Src, focal adhesion kinase (FAK), p130CAS, paxillin, and Rho family GTPases (*Takeda et al., 2007*; *Yamada et al., 2008*; *Yang et al., 2008*; *Hong et al., 2012*). Importantly, the effect of CD151 on the activation of these molecules appears to depend on the cellular context, suggesting that CD151 does not act as an adaptor molecule for any particular signaling pathway. In contrast, several studies have suggested a role for CD151 in regulating adhesion enhancement, a dynamic process that follows integrin-mediated adhesion involving receptor aggregation and interactions with cytoskeleton, structural and signaling elements.

CD151 also regulates enhanced adhesion following platelet fibrinogen receptor binding, integrin αIIb/β3 (*Lau et al., 2004*) and the tetraspanins CD81 and CD37 regulate lymphoid B cell adhesion to integrin α4β1 ligands under flow (*Feigelson et al., 2003*; *van Spriel et al., 2012*). The impaired integrin α4β1 activity observed in CD37-null B cells is associated with altered cell membrane distribution of integrins and may be responsible for impaired Akt-dependent survival of long-lived antibody-secreting cells, which in turn leads to responses leading to impaired IgG1 production from T cell-dependent antigens (*van Spriel et al., 2012*).

Infectious diseases and tetraspanins

Tetraspanins are associated with multiple viral, bacterial or parasite infections especially in pathogen entry (*Monk and Partridge, 2012*). CD81 and TSPAN9 (do not mistake with CD9 which is TSPAN29) were identified in small interfering RNA screens as host factors regulating the early steps of influenza virus and αvirus infection, respectively (*Karlas et al., 2010*; *Ooi et al., 2013*) and both of the tetraspanins were speculated to regulate viral fusion in endosomes (*Ooi et al., 2013*; *He et al., 2013*). CD151 has been shown to contribute to the endocytosis of human papillomavirus (HPV) 16, the causative agent of cervical cancer (*Scheffer et al., 2013*). CD9 can regulate different viral induced processes such as fusion, budding or release of the virus (*Brousseau et al., 2018*) CD81 is essential for the entry of the malaria parasite into hepatocytes, and in the first stage of the mammalian malaria parasite *Plasmodium* life cycle, and is an important receptor for the hepatitis C virus envelope protein E2 (*Silvie et al., 2003*; *Dubuisson et al., 2008*).

Membrane protrusive activity by CD9 and/or CD81

Related with the protrusive activity of the membrane, the tetraspanins CD9 and CD81 have been shown to induce curvature formation (*Bari et al., 2011; Umeda et al., 2020*) probably because of their inverted cone-like structure (*Zimmerman et al., 2016*; *Umeda et al., 2020*) (*Figure 14*) and this is what is believed to initiate the formation of actin-based membrane protrusions (*Ljubojevic et al., 2021*). Such is the case that both CD9 and CD81 have been shown to be involved in the formation of certain protrusions.

In the case of CD9, it has been shown that the induction of clusters of these proteins causes the formation of microvilli in the cell-cell contact zone (*Singethan et al., 2008*). In digitation junctions, membrane microprotrusions between cells with a digit-like or finger-like structures, tetraspanin CD9 as well as CD81 and CD82 are present, in addition to other components of TEMs such as integrin α3β1, CD44 or EWI2 and different tetraspanins regulate the formation of digitation junctions differently, as CD9 promotes the formation of these structures while CD82 inhibits it. (*Huang et al., 2018*)

In the case of CD81, this tetraspanin increases the formation of microvilli, as well as the length and curvature of their tips and conversely, the ablation of this protein reduced the number of microvilli and their length (*Bari et al., 2011*). It has recently been demonstrated that the ability of CD81 to deform membranes also depends on the presence or absence

of cholesterol and its conformational state (*Caparotta and Masone, 2021*). The authors demonstrated that the interaction of CD81-CD81 molecules collectively promotes the transition to an open conformational state and in turn, CD81 has the ability to capture membrane cholesterol, rigidifying membranes and preventing membrane deformation.

Membrane fusion by CD9 and/or CD81

CD9 and CD81 tetraspanin proteins control several cell-to-cell fusion processes but not always in the same manner.

In mice, if CD9 is absent, the eggs are severely affected in their ability to merge with sperm (*Kaji et al., 2000*; *Le Naour et al., 2000*; *Miyado et al., 2000*). The shape of the egg's microvilli is also impacted (*Runge et al., 2007*). Interestingly, the expression of CD81 in eggs lacking CD9 buffered this infertility, presumably showing a cooperation of these two tetraspanins in egg-sperm fusion (*Kaji et al., 2002*; *Rubinstein et al., 2006*). Additionally, double CD9/CD81 knockout mice is completely infertile (*Rubinstein et al., 2006*). In contrast to the functions of these tetraspanins in the oocyte, and at least in the case of CD9, this tetraspanin does not seem to have any role in sperm, since CD9 null male mice are completely fertile (*Le Naour et al., 2000*).

In addition, both CD9 and CD81 work together as negative regulators of macrophage (*Takeda et al., 2003*) and muscle cell fusion (*Charrin et al., 2013*). Under fusogenic conditions, monocytes decreased the expression of CD9 and CD81 and treatment with antibodies against these proteins resulted in promoted fusion of monocytes and alveolar macrophages (*Takeda et al., 2003*). In muscle cells, lack of CD9 or CD81 provokes dystrophy of the myofibers which are formed quicklier. Tetraspanin-associated molecule CD9P-1 is important in muscle cell fusion since the lack of this protein recapitulates the lack of the tetraspanins. When there is no CD9 P-1 or CD9 and CD81 present in the cells, muscle cells fuse together at a higher rate (*Charrin et al., 2013*). Contrary to these two previous examples, inhibition of CD9 impairs the fusion the macrophages-like cells RAW264.7 to form osteoclast-like cells suggesting an important role during osteoclastogenesis (*Ishii et al., 2006*).

Thus, while the role of these tetraspanins in cell-to-cell fusion is clear, these tetraspanins can act as positive or negative regulators, perhaps showing that their role in fusion depends on cell type or on as yet unknown cellular responses.

Relationship with TNTs

If I mentioned earlier that there were few studies relating TNTs to cadherins, in the case of tetraspanins, to the best of my knowledge, there is only one study to date that relates TNTs to tetraspanins. In this study, only the presence of both CD9 and CD81 on TNTs in T-cells was demonstrated (*Lachambre et al., 2014*) (*Figure 17*).

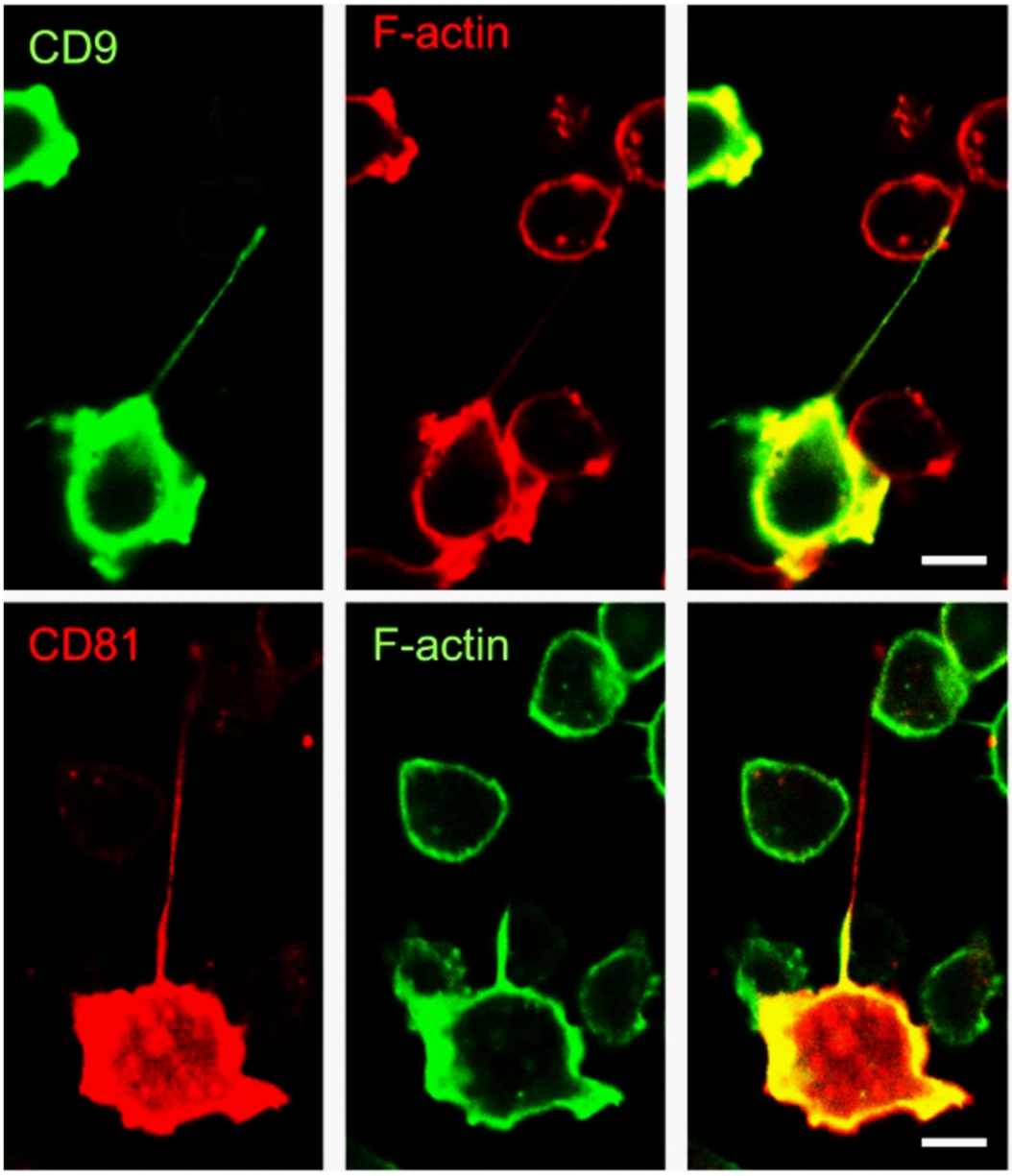

Figure 17. Presence of CD9 and CD81 on TNTs.

CD9 (green, top panel) and CD81 (red, bottom panel) was shown to be present on TNTs (distinguished by actin stained in red -top panel-, and green -bottom panel-) on T cells. Obtained from Lachambre et al., 2014

Therefore, to date, any role of tetraspanins in TNTs is completely unknown and by focusing on the two functions of tetraspanins mentioned above (membrane deformation and fusion), my second project was conceived with the speculation that CD9 and/or CD81 tetraspanins might have a very relevant role in different processes of TNT formation. Furthermore, results from our laboratory on mass spectrometry of TNTs performed by Dr. Christel Brou throughout my thesis showed that the tetraspanins CD9 and CD81 were among the most represented integral membrane proteins in the TNT fractions, further increasing interest in studying the role of these proteins in TNTs.

Section 3: Material and Methods

Since the results of my thesis are presented in the next section in two manuscripts that will be soon submitted, the complete and precise information of all the material and methods used during my PhD are presented in both manuscripts in their corresponding sections. However, here I have considered that given the importance and recurrence of the main assays to identify and characterize TNT formation and functionality, these methods should be explained in depth. Additionally, here there is also described the material and methods corresponding to the results annexes that don't belong to any of the manuscripts.

Identification and quantification of TNTs

Important note: this assay will be indifferently referred to as % of cells connected by TNTs, TNT-connected cells or TNT number throughout the following sections of my thesis.

Since TNTs are structures that connect distant cells, the first key step for the quantification of the TNTs is to seed the cells in sub-confluent conditions, so the cells would be at optimal distances allowing TNT formation and visualization. So, cells in culture are detached by trypsinization, counted and seeded. For SH-SY5Y cells, optimal conditions are 100000 cells in a 12 mm Ø coverslip or 400000 cells in a 35 mm Ø ibidi dish.

Once cells are seeded, they are kept in culture for around 24 hours, so SH-SY5Y cells (that need around 8 hours to adhere properly) can form the TNT connections between them. After these 24 hours of culture, samples are fixed with special fixatives to preserve TNT structure, called "Fixative 1" and "Fixative 2" (*Abounit et al., 2015*).

- Composition of Fixative 1: 2% paraformaldehyde (PFA), 0.05% glutaraldehyde, 0.2 M HEPES, quantity sufficient of 1X PBS, prepared fresh.
- Composition of Fixative 2: 4% PFA, 0.2 M HEPES, quantity sufficient of 1X PBS, prepared fresh.

This step consists in the fixation first with Fixation 1 for 15 minutes at 37°C, another 15 minutes at 37°C with Fixation 2 and finally 3 gentle rinses with 1X PBS. After this, cells are stained with fluorescent-conjugated Wheat Germ Agglutinin (WGA) at 1:300 and

DAPI at 1:1000 in 1X PBS for 15 minutes at room temperature to stain membrane and nucleus respectively (alternatively or additionally fluorescent-conjugated phalloidin could be use at 1:1000 in 1X PBS for 1 hour at room temperature to stain the actin), followed by 3 gentle washes with 1X PBS 5 minutes each. Finally, coverslips are mounted on glass slices with Aqua-Poly/Mount or this Aqua-Poly/Mount is added to the ibidi dishes and samples are kept at 4°C (*Figure 18A*). Using an inverted confocal microscope, several random Z-stacks of different places of the sample are acquired by using a 40X objective.

Analysis by microscopy

The acquired images are analyzed with the help of the Icy software (https://icy.bioimageanalysis.org/) using the "Manual TNT annotation" plugging (*Figure 18A*). First, cells are identified are marked thanks to the DAPI staining which will give the total number of cells (*Figure 18B, green circles*). Following the morphological criteria of the TNTs (structures that connect distance cells and not attached to the substratum), the first Z-slices of the images are discarded (*Figure 18C*) and thanks to the membrane staining, continuous protrusions that connects separated cells are identified and marked (*Figure 18D, green lines pointed by yellow arrowheads*). By knowing the total number of cells and the cells that are connected by this green line (which in fact marks the TNTs), the % of cells connected by TNTs is obtained.

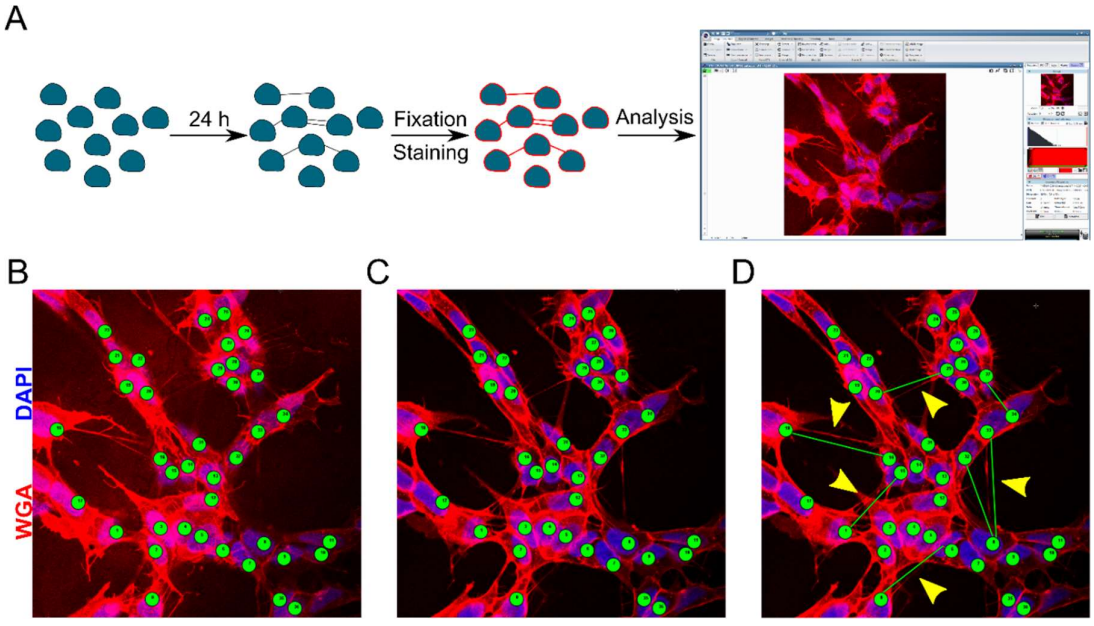

Figure 18. Identification and quantification of TNTs.

(A) Protocol of cell culture, fixation, staining and image acquisition for TNT identification. (B, C, D) Image analysis of the samples with the Icy software. (B) Identification of the cells by marking the nucleus with green circles. Each circle represents one cell. (C) First initial Z-slices are discarded not to quantify attached protrusion. (D) Protrusions that connect distant cells are marked by green lines. Each line represents two cells connected by TNTs, pointed by yellow arrowheads. Note that if two cells are connected by more than one TNT, just one line is drawn.

Characterization of the functionality of the TNTs by vesicle transfer

Important note: this assay will be referred to as % of acceptor cells receiving DiD-vesicles, % of acceptor cells receiving vesicles, vesicle transfer or coculture throughout the following sections of my thesis indifferently.

The key feature of TNTs is their ability to transfer a wide variety of cellular material. Therefore, just the identification of TNT-like structures in not enough to define *bona-fide* TNTs and functional assays regarding their ability to transfer material must be performed. This assay consists in a coculture of two different populations of cells: donor cells (that are those who will have the stained material to transfer) and acceptor cells (that are expressing rather soluble GFP or mCherry to distinguish them from the donor population). As it was the case for the TNT quantification, sub-confluent cell cocultures are required to allow the cells to proper form TNTs. For SH-SY5Y cells, optimal conditions are 50000 donor and 50000 acceptor cells in a 12 mm Ø coverslip, 200000 donor and 200000 acceptor cells in a 35 mm Ø ibidi dish (for microscopy analysis) or 300000 donor and 300000 acceptor cells in a well of a 6-well plate (for flow cytometry analysis).

First, the donor population is loaded with DiD (a lipophilic dye that is rapidly internalized and stains the vesicles) at 1:1000 in the corresponding medium (RPMI 1640) at 37°C for 30 minutes in the incubator. After this time, both donor and acceptor cells are detached and counted, and the desired number of cells of each population is plated in a ratio 1:1. Co-cultured cells are left in the incubator for around 24 hours and in the next day:

- For microcopy analysis, cells are fixed (with the protocol of Fixative 1 and Fixative 2 if samples are used for TNT counting or directly with 4% PFA for 20 minutes at room temperature if no TNT identification is going to be performed), stained with WGA and DAPI and mounted in the same way as for TNT identification. Samples are kept at 4°C until the image acquisition (which again it is performed in the same way as for TNT identification (*Figure 19A*).
- For flow cytometry analysis, cells are collected by trypsinization, pelleted and fixed with 4% PFA, then passed through a cell strainer to avoid the formation of clumps and resuspended in a flow cytometry tube with the same volume of 1X PBS as PFA contains the sample (so final volume of PFA is 2%). Samples are kept in the fridge until they are passed through a cytometer (*Figure 19A*).

Additionally, to exclude any transfer not involving a cell-contact mediated mechanism (and therefore presumably depending on TNTs), a secretion control is performed (*Figure 19B*). Donor cells loaded with DiD are cultured alone for 24 hours and after this time the supernatant of this cells is collected, centrifuged to eliminate any remaining cell or cell debris and added to the acceptor cells that are plated separately. This control is kept in culture for the same time as the coculture and analyzed in the same way (*Figure 19B*).

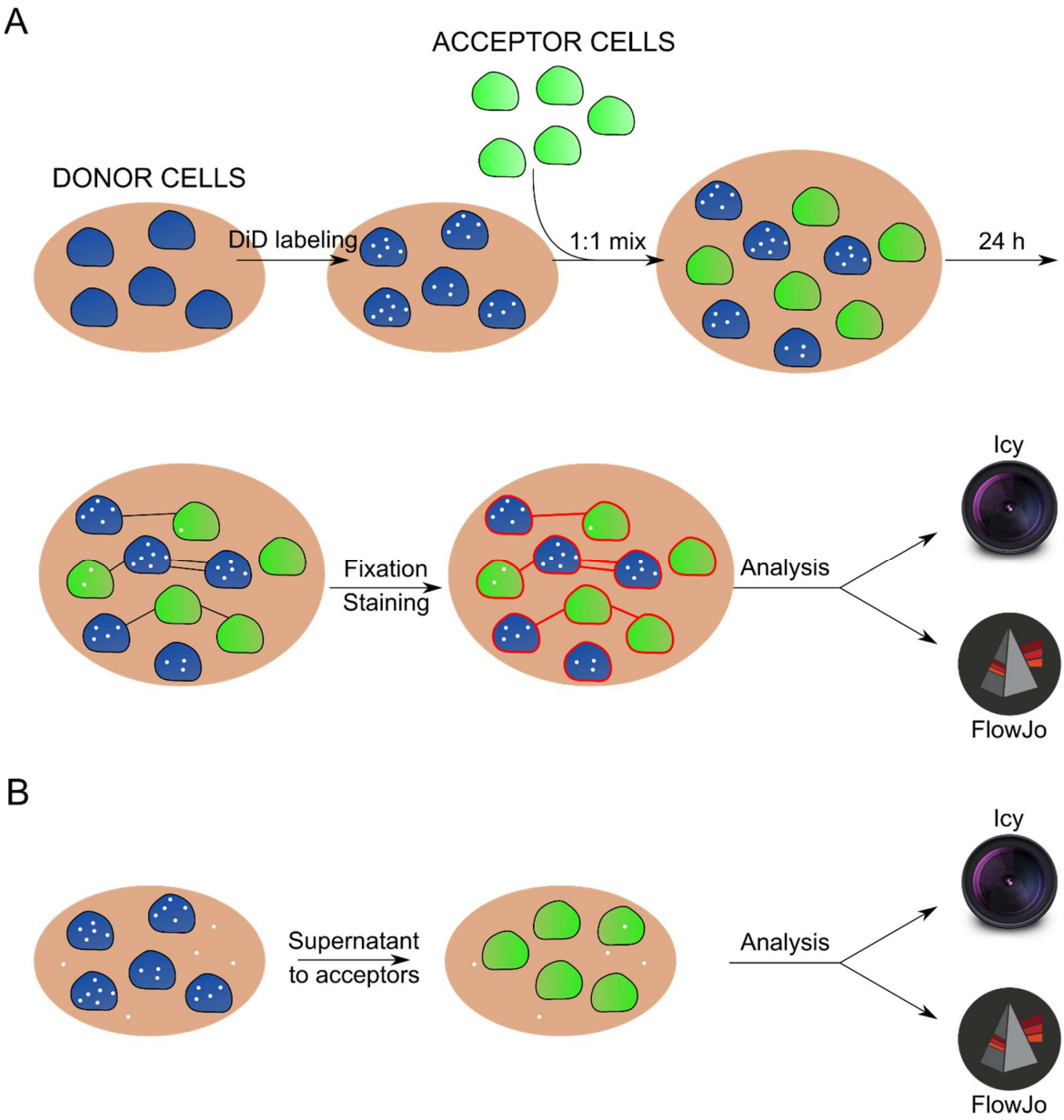

Figure 19. Characterization of the functionality of the TNTs by vesicle transfer.

(A) Schematic representation of the vesicle transfer assay steps including donor cells labelling, mix and coculture of donors and acceptors, fixation, staining (only in the case of microscopy analysis of the samples) and analysis. (B) Schema of the secretion control test showing the recollection of the supernatant, addition of this supernatant to the acceptor population and analysis. Donor cells are represented in blue, acceptor cells in green, DiD-vesicles in white dots and brown background represents the cell culture medium.

Quantification by microscopy

Z-stacks images are open with the Icy software (https://icy.bioimageanalysis.org/) and they will be analyzed by using specific protocols for this assay called "Protocol part 1"and "Protocol part 2" (*Figure 20A*). By running the Protocol part 1 and setting the color channel of your acceptor cells, the software will automatically detect your acceptor cells and it will create a grey mask of the cell shape on top of every cell (*Figure 20B*). This will require some manual correction to discard acceptor cells overlapping with donor cells or acceptor cells to close that the software will not detect the cell boundaries. After this step, and having previously set up the DiD channel and the threshold for DiD detection (with a negative control not stained with DiD), Protocol part 2 is run and the software will automatically detect the spot corresponding to DiD signal by marking them with green pixels (*Figure 20C, yellow arrowheads in the enlargement*). Knowing the number of acceptor cells containing DiD signal among the total number of acceptor cells, the % of acceptor cells with DiD-vesicle will be obtained.

This analysis is done exactly in the same way for both coculture or secretion samples.

A

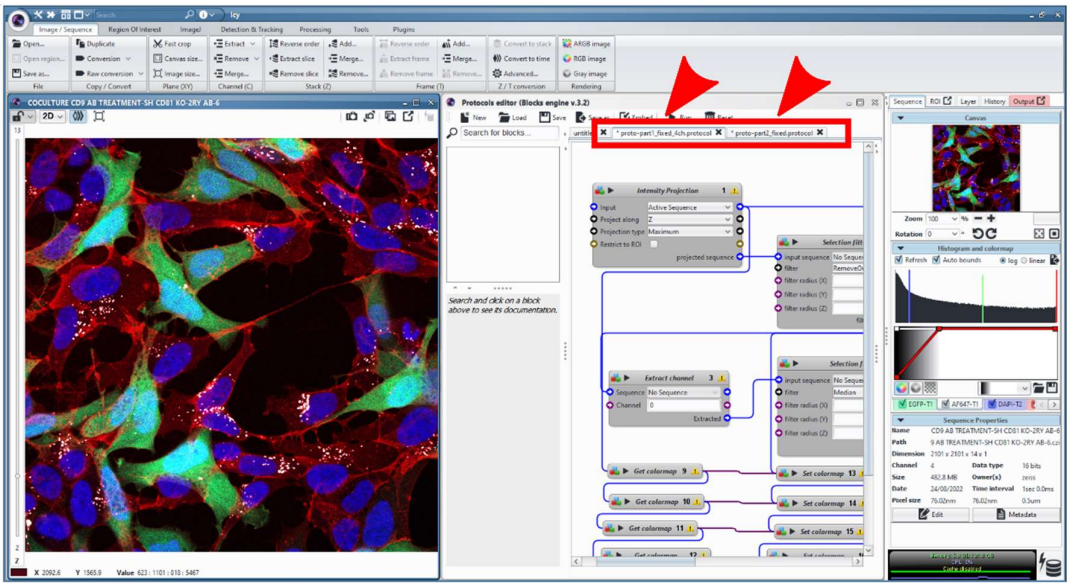

B

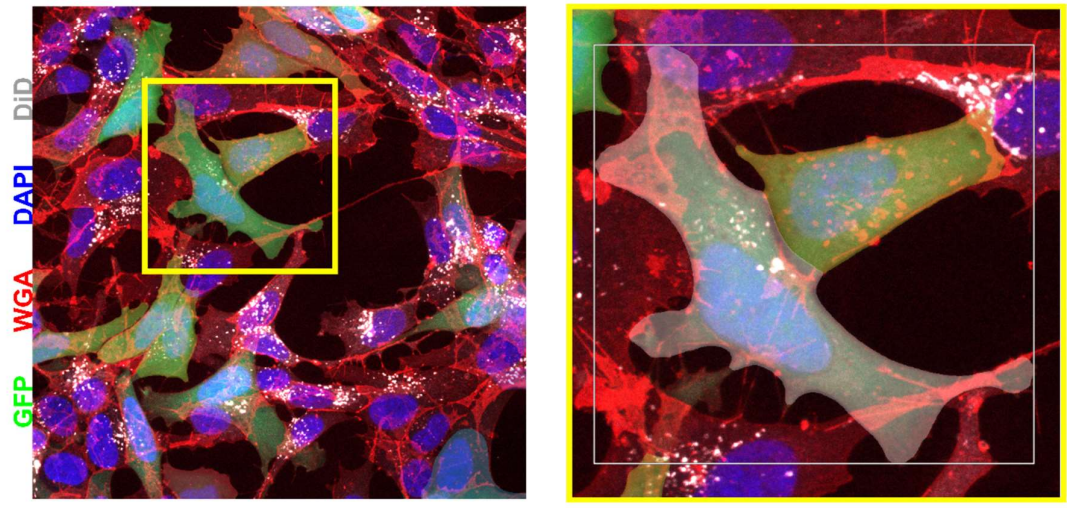

C

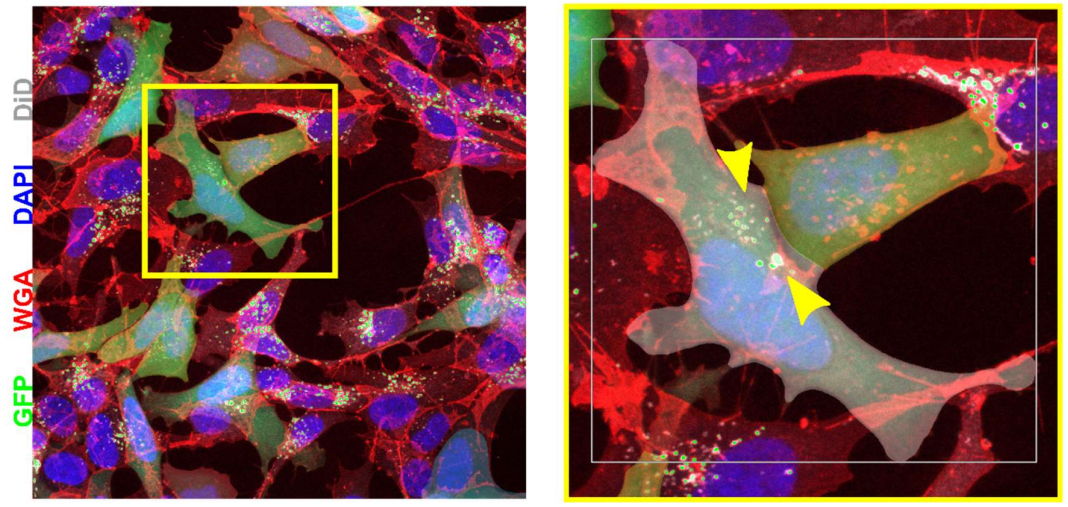

Figure 20. Quantification of the vesicle transfer by microscopy.

(A) Icy software view of the image analysis protocol by microscopy. Protocols part 1 & 2 are framed by a red rectangle and pointed by red arrowheads. (B) Example of an image after running the Protocol part 1. Green cells corresponding to acceptor cells are automatically detected and marked with a gray mask. The yellow square represents the enlarged image on the right. (C) Example of an image after running the Protocol part 2. Green pixel spots correspond to DiD-vesicles that are automatically detected and marked. The yellow square represents the enlarged image on the right and the yellow arrowheads point to the vesicles detected.

Quantification by flow cytometry

Files obtained after passing the samples for a cytometer (in this case a CytoFlex) and open and analyze with the FlowJo software (https://www.flowjo.com/). Samples are first gated with the area obtained by the side scatter (SSC) and the area obtained by the forward scatter (FSC) to discard cell debris and to keep all the cells in the sample. After this, samples are gated with the width of the SSC and the area of the FSC to exclude the cells in doublets and keep only singularized cells (*Figure 21A*). After this, cells are compensated (if necessary) and the gates for positive and negative of GFP and DiD are delimited according to the positive (GFP+ and DiD+ cells) and negative (Unstained cells) samples (*Figure 21B*). Finally, these gates are applied to the samples of interest.

This analysis it is done exactly in the same way for both coculture or secretion samples.

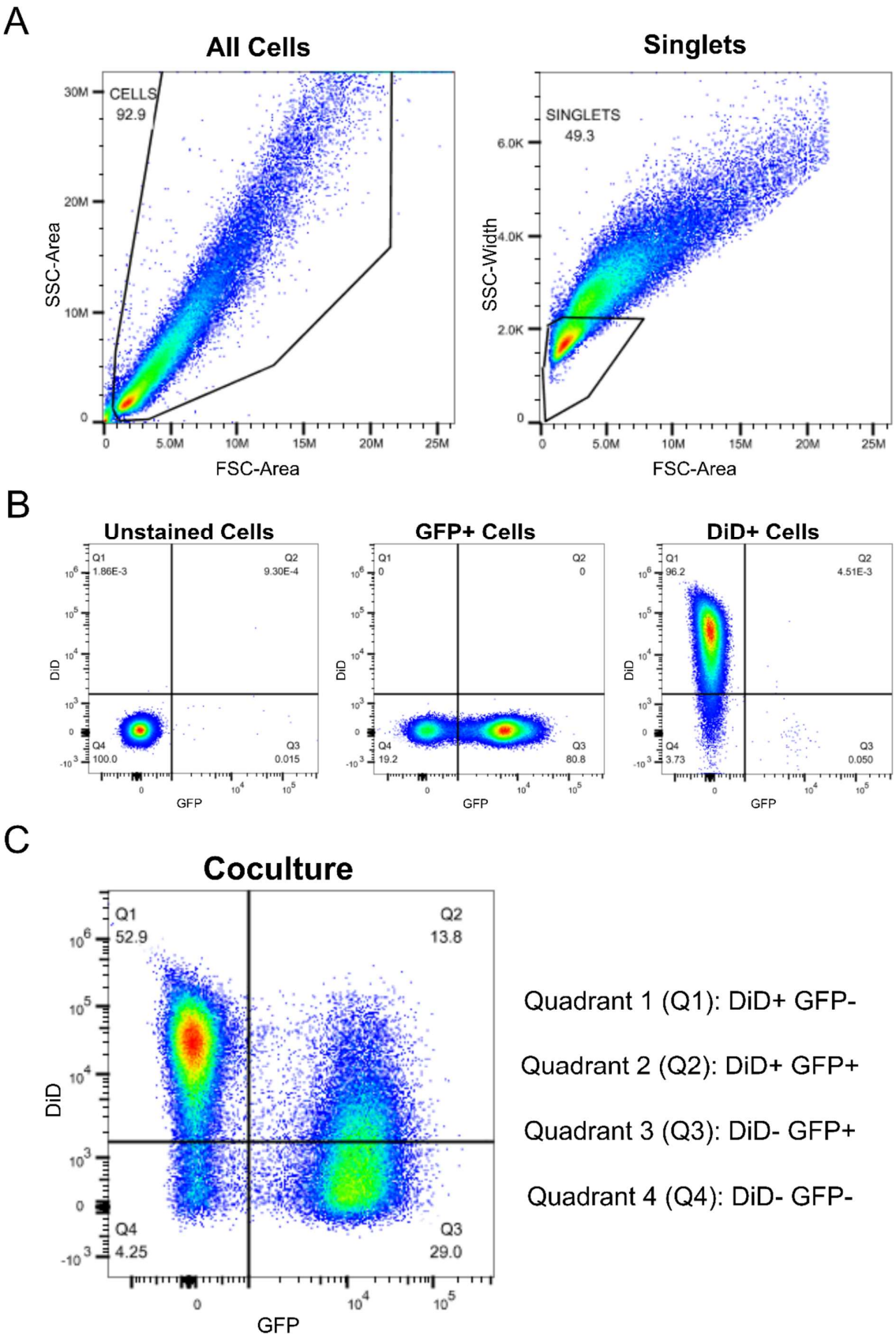
A
All Cells
CELLS
92.9
SSC-Area
FSC-Area
Singlets
SINGLETS
49.3
SSC-Width
FSC-Area
B
Unstained Cells
Q1
1.86E-3
Q2
9.30E-4
Q4
100.0
Q3
0.015
DiD
GFP
GFP+ Cells
Q1
0
Q2
0
Q4
19.2
Q3
80.8
DiD+ Cells
Q1
96.2
Q2
4.51E-3
Q4
3.73
Q3
0.050
C
Coculture
Q1
52.9
Q2
13.8
Q4
4.25
Q3
29.0
Quadrant 1 (Q1): DiD+ GFP-
Quadrant 2 (Q2): DiD+ GFP+
Quadrant 3 (Q3): DiD- GFP+
Quadrant 4 (Q4): DiD- GFP-

Figure 21. Quantification of the vesicle transfer by flow cytometry.

(A) Flow cytometry images of an example of the gates applied to select all cells subsequently singularized cells. (B) Examples of flow cytometry images of unstained, GFP positive and DiD positive samples to compensate and apply the gate strategy based on the positive or negative for each color. (C) Example of coculture flow cytometry images. Quadrant 1 (Q1) delimits DiD+ and GFP- cells, Quadrant 2 (Q2) delimits DiD+ and GFP+ cells, Quadrant 3 (Q3) delimits DiD- and GFP+ cells and Quadrant 4 (Q4) delimits DiD- and GFP- cells.

Immunoprecipitation (GFP-trap)

Cell lines

SH-SY5Y cells overexpressing NCAD tagged to GFP (NCADGFP cells) and SH-SY5Y cells expressing soluble GFP are described in the corresponding Material & Methods section of the first manuscript.

SH-SY5Y cells overexpressing CD9 tagged to GFP (CD9GFP cells) and SH-SY5Y cells overexpressing CD81 tagged to GFP (CD81GFP cells) were obtained by lentiviral infection with each corresponding plasmid (see lentiviral preparation on Material & Methods of the second manuscript). To overexpress CD9 or CD81 tagged to GFP, SH-SY5Y were plated the day before the infection at a confluency of around 70% and next day the lentiviruses were added to the cells. 24 hours later the medium with the lentiviruses were removed and replaced. After this, cells were splitted 1:5 and reinfected for 24 hours. After these 24 hours, medium was replaced every 2-3 days. These cells were tested for the expression of CD9 and/or CD81 by western blot (WB). The pool of cells was seeded in 96-well plates through a limiting dilution in such a way that 0.5 cells are seeded per well, and after allowing them to grow, they were analyzed and the clones overexpressing the protein of interest were selected and tested for expression of CD9 or CD81 by immunofluorescence and WB.

Protocol of the GFP-trap

Cells of interest were cultured in a T75 flask until confluency. When cells were ready, they were washed 3 times with ice cold 1X PBS and then added 2 mL of the lysis buffer and left the flask under agitation for 30 minutes at 4°C. The lysis buffer is made to preserve tetraspanin interaction with mild detergent. Its specific composition is: 150mM

NaCl, 30mM Tris, 1mM $MgCl_2.6H_2O$, 1mM $CaCl_2$, 1% Brij 97, pH 7.4 + protease inhibitors. After these 30 minutes, the cell lysate was collected and centrifuged at 10000g for 15 minutes at 4°C. The pellet was discarded and the protein concentration of the supernatant is measured (from here samples corresponding to "lysate" were prepared with 30 µg of proteins.

The agarose beads containing nanobodies anti-GFP bound to these agarose beads (ChromoTek GFP-Trap® Agarose) are prepared by 3 washes with PBS +/+, each wash followed by centrifugation at 2000g for 3 minutes, removing the supernatant. Immunoprecipitation (IP) samples were prepared with 20 µL of beads, 500 µg of proteins and dilution buffer until 500 µL (composition of the dilution buffer: 150mM NaCl, 30mM Tris, 1mM $MgCl_2.6H_2O$, 1mM $CaCl_2$, pH 7.4 and no detergent). The tubes with the mix were put in rotation at 4°C for in between 60-90 minutes. After that time, the tubes were centrifuged at 2000g for 3 minutes and supernatant was kept as control (sample called "supernatant"). Two additional washes with washing buffer are made (composition of the washing buffer: 150mM NaCl, 30mM Tris, 1mM $MgCl_2.6H_2O$, 1mM $CaCl_2$, 0.5% Brij 97, pH 7.4). 20 µL of Laemmli 2X is added to the final pellet and samples corresponding to this final pellet ("IP"), "lysate" and supernatant are used for WB analysis of the GFP-trap

Section 4: Results

Manuscript 1: Beyond cell adhesion: the role of N-cadherin and α-catenin in TNTs

Premises and summary

This project was conceived after the discoveries on the ultrastructure of the TNTs in neuronal cells (*Sartori-Rupp et al., 2019*). In this study performed in the lab, the authors were able to show that, although by confocal microscopy TNTs look like one single tube, at an ultrastructural level TNTs can be made of various thinner tubes, called individual TNTs (or iTNTs). These iTNTs form a bundle normally made of in between 2 and 6 tubes and, interestingly, they found in between these tubes the cell adhesion molecule NCAD. Therefore, the original idea of this project was to investigate a possible role of NCAD as a holder of the iTNT bundle. Furthermore, thanks to a couple of previous studies describing the presence and accumulation of NCAD (*Lokar et al., 2010*) or ECAD (*Jansens et al., 2017*) at the tips of the TNTs and a correlation with the formation of open-ended TNTs, we decided to expand the knowledge about NCAD regarding TNTs. Thus, we wondered whether this molecule could just be much more than a holder of the iTNTs in the bundle or a linker of TNT's tip with the opposing cells, and we investigated the role of NCAD in different TNT formation processes, such as TNT genesis, stabilization and even fusion of the TNTs, both at a micrometer resolution (by confocal studies) and at nanometer resolution (by Cryo-EM studies). Moreover, we didn't just stay in the study of the NCAD, but we decided to investigate a member of the adherens junctions formed by NCAD, α-catenin. Although there is another two catenins in this complex, we opted for α-catenin since it is the physical link of cadherins with the actin cytoskeleton (*Mège and Ishiyama, 2017*) and for its ability to bind and bundle actin (*Rimm et al. 1995*) and since TNTs are made up of actin we speculated that NCAD, thought α-catenin binding to the actin cytoskeleton could regulate TNT formation and functionality.

In the manuscript here presented, we have shown how NCAD and α-catenin inhibit the biogenesis of the TNTs but on the other hand they positively regulate TNT stability and transfer function, presumably through facilitating the fusion of the TNT with the opposing cell. In addition, we showed that these two proteins could facilitate the formation of highly organized and structured bundles of iTNTs. Furthermore, we have demonstrated

that the regulation of the TNTs by NCAD requires the presence of α-catenin, being this molecule downstream of NCAD.

Contribution

The original concept of the project was conceived by Professor Chiara Zurzolo and Dr. Anna Pepe before my arrival in the lab. The final conception of this project was made mainly by Dr. Anna Pepe, Professor Chiara Zurzolo and myself with contributions by Dr. Christel Brou. The project was done in collaboration with Dr. Anna Pepe.

The cell biology part was designed, performed and analyzed by me in collaboration with Dr. Anna Pepe and the ultrastructural studies was designed, performed and analyzed by Dr. Anna Pepe. Specifically in the manuscript, experiments corresponding to Figure 1 G-M, Figure 2 G-I, Figure 5, Supplementary Figure B & C and Supplementary Figure 3 were done by Dr. Anna Pepe, with the rest of the experiments corresponding to the rest of the figures and videos done by myself.

The manuscript presented here it is a collaborative work of Dr. Anna Pepe and myself, with some correction from Dr. Christel Brou and corrected and expanded by Professor Chiara Zurzolo.

Beyond cell adhesion: the role of N-cadherin and α-catenin in TNTs

Authors

Anna Pepe[1] *, Roberto Notario Manzano[1-2] *, Anna Sartori-Rupp[3], Christel Brou[1], Chiara Zurzolo[1].

[1] Membrane Traffic and Pathogenesis, Institut Pasteur, UMR3691 CNRS, 75015 Paris, France

[2] Sorbonne Université, ED394-Physiologie, Physiopathologie et Thérapeutique, 75005 Paris, France

[3] Plateforme Technologique Nanoimagerie, Institut Pasteur, 25 rue du Docteur Roux, 75015, 12 Paris, France.

*These authors contribute equally to this work

Correspondance: chiara.zurzolo@pasteur.fr

Abstract

Cell-to-cell communication it is a fundamental mechanism by which unicellular and multicellular organisms, maintain relevant functions as development or homeostasis. Tunneling nanotubes (TNTs) are a type of contact-mediated cell-to-cell communication defined by being membranous structures based on actin that allow the exchange of different cellular material. TNTs have been shown to have unique structural features compared with other cellular protrusions and to contain the cell adhesion molecule N-Cadherin. Here, we investigated the possible role of N-Cadherin and of its primary linker to the actin cytoskeleton, α-Catenin in regulating the formation and transfer function of TNTs. Our data indicate that N-Cadherin through its downstream effector α-Catenin is a major regulator of TNT formation, ultrastructure as well as of their ability to transfer material to other cells.

Introduction

Tunneling nanotubes (TNTs) are non-adherent F-actin based membranous structures that form continuous cytoplasmic bridges between cells over distances ranging from several hundred nm up to 100 μm (Cordero Cervantes and Zurzolo, 2021). These structures, firstly described in cell cultures (Rustom et al., 2004), allow cell-to-cell communication by facilitating the transfer of different cargoes between cells including ions (Lock et al., 2016), organelles such as lysosomes (Abounit et al., 2016) or mitochondria (Wang and Gerdes, 2015; Lu et al., 2017; Pinto et al., 2021) and genetic material (Lu et al., 2019). TNTs have also been described in pathological situations, allowing the spreading of pathogens (Ariazi et al., 2017) like viruses and bacteria (Sowinski et al., 2008; Onfelt et al., 2006; Dagar et al., 2021; Pepe et al. 2022) and misfolded proteins such as PolyQ Huntingtin, fibrillar tau and α-synuclein aggregates (Gousset et al., 2009; Costanzo et al., 2013; Abounit et al., 2016; Loria et al 2017; Vargas et al, 2019; Dilsizoglu Senol et al, 2021; Chastagner et al., 2020). Finally, TNTs can also be involved in the establishment and progression of different types of cancer, and in some cases, TNT could accelerate mitochondrial exchange in tumor cells (Thayanithy et al., 2014; Desir et al., 2018; Pinto et al., 2020; Pinto et al., 2021). This ability to transfer a wide variety of cargoes through an open channel connecting two cells is what defines the functionally these structures, being therefore unique compared to other cellular structures. Despite the large amount of

observations supporting the role of TNTs in intercellular communication, the mechanisms of TNT formation and the molecular components and regulators of their structure are still poorly investigated (Cordero Cervantes and Zurzolo, 2021). Previous work has shown that although filopodia and TNTs share the same protein complexes regulating actin cytoskeleton, these complexes appear to regulate the two types of actin-based protrusions in an opposite manner, suggesting that the two types of protrusions have predetermined fates and specific functions (Delage et al., 2016; Ljubojevic et al., 2021). Recently, by developing a correlative light and cryo-electron tomography (ET) workflow, we have shown that TNTs are a unique structure compared to filopodia (Sartori-Rupp, Cordero Cervantes, Pepe et al., 2019). This analysis performed in two different neuronal cell types showed that although TNTs appear as single connections by fluorescence microscopy (FM), most of them are comprised of a bundle of individual Tunneling Nanotubes (iTNTs) that can contain vesicles and organelles and can be open-ended, thus allowing direct transfer of cellular components. These data also showed long threads coiling around the iTNTs bundles as in the process of holding them together. Of interest, we found N-Cadherin localized at the attachment point of these threads on the iTNTs membrane, as well as decorating short connections (possibly linkers) between the single tubes (Sartori-Rupp, Cordero Cervantes, Pepe et al., 2019). These results were the first structural description of TNTs directly pointing to N-Cadherin as a possible player in the regulation of TNTs. Consistently, few studies in different cell types supported the ability of the TNTs to interact with the opposing cell through E-Cadherin (Jansens et al., 2017) or N-Cadherin (Lokar et al., 2010) and demonstrated the presence of N-Cadherin along the TNTs or at the end of these structures (Chang et al., 2022; Li et al., 2022). N-Cadherin (Hatta et al., 1985) is a transmembrane molecule that belongs to the cadherin superfamily that is responsible for cell-to-cell adhesion (Brasch et al., 2012). Specifically, N-Cadherin is one of the classical type I cadherins that mediate homophilic cell adhesion dependent on Ca2+. It is composed by an ectodomain formed by five highly conserved regions, a single transmembrane pass and a cytoplasmic tail. The cadherin adhesion is made by the interaction in trans of two cadherins placed on two opposing cells; in addition, interactions in cis on the same cell is needed for strengthening the adhesion (Harrison et al., 2011; Mège and Ishiyama, 2017). Cadherin-associated molecules are coupled to the cytoplasmic tail of the cadherin: p120-catenin, β-catenin and α-Catenin (Zaidel-Bar 2013; Huveneers and de Rooij, 2013). This “cadherin adhesome” is linked to the actin cytoskeleton through α-Catenin, which is required for the functionality of the complex

(Kwiatkowski et al., 2010; Yoneruma, 2011). α-Catenin is much more than just the link between cadherins and the actin cytoskeleton, since it is an actin-binding and bundler protein (Rimm et al., 1995) which can also interact with many other actin-binding proteins (Knudsen et al., 1995; Weiss et al., 1998) therefore controlling actin dynamics, as limiting the formation of branched actin filaments (Dress et al., 2005) or inducing the formation of filopodia by the recruitment of them to PIP3 membranes (Wood et al., 2017). Interestingly, our recent data suggest that a limitation of the branched actin pathway favors the linear actin organization that allows the formation of long protrusions such TNTs, in comparison with other, much shorter and dynamic, protrusions like filopodia (Henderson et al., 2022). Based on all these results, it is conceivable that the cadherin-catenin complex could have an important function on the regulation of the TNTs. Therefore, we decided to investigate the role of N-Cadherin and α-Catenin in the formation, functionality and ultrastructure of the TNTs. By combining quantitative assays in living cells with cryo-correlative fluorescent electron microscopy (cryo-CLEM) and tomography here we demonstrate that N-Cadherin is an organizer of the TNT structure and function since the lack of this protein results in disordered and nonfunctional iTNTs. On the other hand, N-Cadherin overexpression increases the stability of these structures and the transfer of vesicles within them. We further demonstrate that α-Catenin its required and is working downstream N-Cadherin in the regulation pathway of TNTs.

Results

1. N-cadherin interference affects both functionality and ultrastructure of the TNTs

N-Cadherin was previously shown to be present in TNTs in murine neuronal CAD cells (Sartori-Rupp, Cordero Cervantes, Pepe et al., 2019) as well as in Hela and in urothelial cells (Chang et al., 2022, Lokar et al., 2010). To address its role, in this study we used SH-SY5Y human neuronal cells, a more relevant model of study for different physiological and pathological neuronal conditions (Sartori-Rupp, Cordero Cervantes, Pepe et al., 2019; Dilsizoglu Senol et al., 2019, Chastagner et al., 2020; Pepe et al., 2022). Immunofluorescence using anti-N-Cadherin antibody analyzed by confocal microscopy revealed that the transmembrane protein decorated the TNTs formed between these cells (Fig EV1A). Furthermore, immunogold-labeling and cryo-ET showed N-Cadherin localization on the iTNTs membranes and in between iTNTs (Fig EV1B, C), confirming

our previous observations in murine CAD cells (Sartori-Rupp, Cordero Cervantes, Pepe et al., 2019). To investigate a possible role on TNT formation and functionality, N-Cadherin was knocked-down (KD) in an acute manner (average decrease of 82% compared to RNAi Control) in SH-SY5Y (Fig EV1D). TNTs hover above the substrate and even over other cells, and unlike dorsal filopodia, they directly connect two or more distant cells (Sartori-Rupp, Cordero Cervantes, Pepe et al., 2019; Delage et al., 2016; Abounit et al., 2015). Based on these criteria, by confocal microscopy we quantified the % of TNTs connected cells (see Material and Methods), and found an increase to 56% in RNAi N-Cadherin cells compared to 35% in RNAi Control cells (Fig 1A, B, C). To test if the increase in TNTs in RNAi N-Cadherin cells correlated to an increase in TNT-mediated vesicle transfer, we performed a transfer assay in a co-culture (Abounit et al., 2015) (Fig EV1E top). Donor cells, either RNAi Control cells or RNAi N-Cadherin cells loaded with DiD-vesicles were co-cultured with acceptor cells previously interfered for N-Cadherin and labelled with soluble GFP (in order to be distinguished from donors). After 16h of co-culture, cells were fixed and labelled with WGA to stain the membranes and DAPI to stain the nuclei (Fig 1D, E). By using confocal microscopy and the ICY software (icy.bioimageanalysis.org), we calculated the percentage of acceptor cells positive for DiD vesicles. We found that in down-regulated N-Cadherin co-cultures, the percentage of transferred DiD vesicles by a contact-dependent mechanism (17%) was significantly lower compared to the controls (32%) (Fig 1D-F). In order to rule out any contribution of secretion to the vesicle transfer observed in our co-culture conditions, we performed “secretion tests” in which supernatants from donor RNAi Control and RNAi N-Cadherin cells loaded with DiD-vesicles, were used to challenge acceptor SH-SY5Y cells (Fig EV1E bottom). We did not detect significant signal for DiD in the acceptor cells that received the supernatants from the donor cells compared to the contact-mediated transfer (Fig 1F, Fig EV1F), suggesting that the main mechanism of transfer is through contact-mediated transfer, likely TNT-mediated.

In order to understand the mechanisms by which N-Cadherin KD would increase the number of TNT connected cells but decrease TNT-mediated vesicle transfer, we adapted our established pipeline for cryo-TEM (Sartori-Rupp, Cordero Cervantes, Pepe et al., 2019, Pepe et al., 2022) to analyze the structure of TNTs in RNAi N-Cadherin cells. Consistent with our previous data (Sartori-Rupp, Cordero Cervantes, Pepe et al., 2019), TNTs between SH-SY5Y wild type cells are prevalently composed by a bundle of parallel

iTNTs (between 2 and 6) (Fig 1G, H). Strikingly, we observed that in down-regulated conditions iTNTs did not run parallel (Figure 1I-J) and braided over each other (Fig 1K). We also observed that compared with the controls, in KD cells there were more tips close-ended (Fig 1 K, L). These still images could represent iTNT (i) in the process of extending towards other cells, (ii) retracting from opposite cells or (iii) unable to fuse with the opposite cells. To understand whether there was a significative impact of N-Cadherin depletion on the iTNTs morphology, we performed a quantitative analysis of our cryo-EM data to calculate the percentage of close-ended iTNTs vs continuous iTNTs connecting two cells, both in RNAi Control and RNAi N-Cadherin cells. In control conditions we found that 75% of iTNTs (composed between 2-7 iTNTs per TNT) were extending fully between two distant cells, while 25% were interrupted and showed closed tips. In contrast, in RNAi N-Cadherin SH-SY5Y cells, we found a decrease (52%) in fully extended iTNTs (between 2-7 iTNTs per TNT) and an increase of tip-closed iTNTs (48%) (Fig 1M). It is important to precise that Cryo-ET cannot explore the connecting regions between iTNTs and cell bodies because samples are too thick (>500 nm in thickness), therefore we do not know whether the iTNTs connecting two cell bodies are closed or continuous. However, the images showing disconnected/disjointed and close-ended iTNTs, combined with the decreased in TNT mediated vesicle transfer suggested that in KD cells, TNTs are probably unable to engage and/or fuse with the cell body of the opposing cell, consequently preventing transfer of material.

2. Overexpression of N-cadherin promotes TNT-mediated transfer and impacts TNTs ultrastructure

In order to further investigate the effect of N-Cadherin on TNTs we produced an SH-SY5Y cell line stably overexpressing (OE) GFP N-Cadherin, where ectopically expressed GFP N-Cadherin showed a similar cellular distribution compared to the endogenous protein (Fig EV1G). By quantitative confocal microscopy we found that GFP-N-Cadherin cells had a decreased percentage of TNT-connected cells (10%) compared to control cells transfected only with GFP (33%) (Fig 2A-C). However, it is worth mentioning that compared to controls, these cells exhibited an epithelial-like morphology, where cells tended to stay close to each other in clusters (Fig EV1G), even when we seeded in low concentration to favor a sparse distribution, optimal for the study of TNTs. Therefore, one possibility is that the reduction in TNTs resulted from the fact that TNTs formed by

these cells were hidden by the cell bodies in the clusters. To investigate this possibility, we took advantage of a previously used approach consisting in adding a short pulse of trypsin to the culture so to separate the cell bodies and observe the TNTs formed between them (*Staufer et al., 2018*). In the Supplementary Movie 1 we can observe how immediately after the addition of trypsin, the cells retract their cell bodies "revealing" the TNT-like structures formed between them. As shown before (*Staufer et al., 2018*) after addition of trypsin, the % of TNT connected cells increases conspicuously compared to *wild-type* conditions (around 2.5 times more TNTs when we treat the cells with trypsin than in *wild-type* conditions) (Fig EV1H). However, also in this condition GFP N-Cadherin cells formed significantly less TNTs than control cells (respectively 70% compared to 85%) (Fig EV1H-J), confirming that N-Cadherin OE resulted in a reduction of TNT connected cells (Fig 2A-C). Next, to assess the functionality of the TNTs formed by the GFP N-Cadherin cells, we performed a co-culture where GFP N-Cadherin cells loaded with DiD were used as donors and SH-SY5Y mCherry cells as acceptors. Donor and acceptor cells were co-cultured for 24h and the percentage of acceptor cell that received DiD labelled vesicles were quantified in the different conditions (Fig EV1E). Contact-mediated DiD labelled vesicles transfer cells was significantly higher (40 %) compared to control co-cultures (25 %) when GFP N-Cadherin cells were used as donors (Fig 2D-F). Importantly, negligible transfer of DiD labelled vesicles transferred by secretion in control conditions and in GFP N-Cadherin overexpression was observed (Fig 2F). Thus, the decrease in TNT formation by ectopic expression of N-Cadherin was accompanied by an increase in their transfer function, opposite compared to N-Cadherin downregulation.

In order to understand these results in the light of possible effects on TNT ultrastructure, we analysed by cryo-TEM the TNTs formed between SH-SY5Y cells in which N-Cadherin was upregulated (Fig 2G-I). We found that in cells overexpressing N-Cadherin the percentage of TNTs formed by a single tube (65%) was much higher than the % of TNTs formed by an iTNTs bundle (35%) (Fig 2G-H). This was almost the opposite compared to control SH-SY5Y cells where 40% of TNTs were formed by a single tube while 60% cells were formed by 2 or more iTNTs (Fig 2I). Interestingly in RNAi N-Cadherin cells the % of single tube TNTs decreased even more (26,3%) and the majority of TNTs (73,7%) were formed by 2 or more iTNTs (Fig 2I). In addition, 3D Cryo-TEM images revealed that contrary to KD cells (Fig 1I-L, Fig EV2A-B) the iTNTs in GFP N-

Cadherin cells were straight and run mostly parallel towards the opposite cell (Fig EV2G-K). Quantitative analysis revealed a tendency to have more fully extended iTNTs (58%) and less close-ended tips (42%) (Fig EV2H) compared to the KD cells (52% and 48% respectively) (Fig 1M). Of interest in our tomograms, we could also discern thin structures connecting the plasma membrane of two iTNTs (Fig EV2G) consistent to our previous observations (*Sartori-Rupp, Cordero Cervantes, Pepe et al., 2019*). All these changes in the architecture of TNTs in cells overexpressing N-Cadherin could contribute to the increased transfer that we observed in these conditions (Fig 2F).

3. N-cadherin enhances the stability of the TNTs

One possible explanation for the decrease or increase in vesicle transfer, respectively in N-cadherin KD and OE conditions, is that N-cadherin would regulate formation of functional TNT for example, by favoring a stable attachment of the TNT tip with the opposing cell or by stabilizing the iTNT bundles. Because the *de novo* formation of TNTs is very difficult to image, thus it is challenging to get quantitative data, to test our hypothesis we measured by live imaging the lifetime of already formed TNTs in N-Cadherin KD and OE cells compared to respective control conditions (see Material and Methods) (see example on Fig 3A and Supplementary Movie 2). In RNAi N-Cadherin cells we observed a clear decrease tendency in the duration of TNTs compared to the respective RNAi Control (18.5 minutes vs 22.5 minutes) (Fig 3B and Supplementary Movies 3 & 4 respectively). On the other hand, the duration of TNTs in GFP N-Cadherin cells was significatively increased compared to its control (GFP expressing cell), (34.5 minutes vs 20 min) (Fig 3C and Supplementary Movie 5). Thus, although in N-Cadherin OE there are less TNTs, these are fully formed and more stable, explaining the higher vesicle transfer. On the contrary in N-Cadherin KD there are more TNTs, but these are more disorganized, have more close-ended tips and they are less stable, thus resulting in lower vesicle transfer.

4. N-cadherin and α-catenin cooperate in TNT regulation

One possible explanation of our data is that N-Cadherin may affect TNT stability and facilitate vesicle transfer by providing an adhesion complex to bridge connected cells. To this end we decided to investigate the possible role of α-Catenin, which forms a complex

with N-Cadherin mediating the interaction with the actin cytoskeleton, providing integrity of the complex and strengthening adhesion (*Mège and Ishiyama, 2017*).

We assessed first the presence of α-Catenin in our cell model (Fig EV3A). α-Catenin is endogenously expressed by SH-SY5Y cells and is localized at the plasma membrane, in the cytoplasm and on TNTs (Fig EV3A), where it largely co-localizes with N-Cadherin (Fig EV3A). To investigate the involvement in TNT regulation, α-Catenin was KD in an acute manner by RNA of interference (RNAi) (average decrease of 85% compared to RNAi Control) (Fig EV3B), and TNTs were imaged and quantified. Similar to N-Cadherin KD, the percentage of TNT-connected cells increased to 48% in the α-Catenin depleted cells compared to 29% in RNAi Control cells (Fig 4A-C). Furthermore, as for N-Cadherin KD, we found that in KD α-Catenin co-cultures the percentage of transferred DiD labelled vesicles (18%) was significantly lower compared to control cells (29%) with insignificant transfer by secretion in both conditions (Fig 4D-F).

On the other hand, upon α-Catenin OE (mEmerald α-Catenin), the percentage of cells connected by TNTs was significative reduced to around 14% compared to 29% in control conditions (Fig 4G-I). Despite this reduction, the contact-dependent vesicle transfer showed a significant increase, from 25% in control to 33% of acceptor cells containing transferred vesicles in mEmerald α-Catenin cells with a minimal contribution of the transfer being by secretion (Fig 4J-L). Once more, these results were in line with the results we obtained by overexpressing N-Cadherin (Fig. 2A&C).

To understand if the overlapping functional consequences of N-Cadherin and α-Catenin OE/KD corresponded to similar effects on the ultrastructure and organization of TNTs we analysed by cryo-TEM the morphology of TNTs in cells where α-Catenin was up or down-regulated. Similar to N-Cadherin, in SH-SY5Y cells down-regulated for α-Catenin, iTNTs did not run parallel (Fig 5A-F), were braided over each other (Fig 5A, C, D, F) and most of iTNTs were close-ended (Fig 5A-F), while in mEmerald α-Catenin cells were running mostly parallel (Fig 5 H-L). In addition, 34,4% of iTNTs of RNAi α-Catenin cells were fully extended, while 65% showed closed tip. In contrast, in mEmerald α-Catenin cells, we found a decrease (28%) of closed iTNTs and an increase of fully extended iTNTs (72%) (Fig 5M).

Because α-Catenin KD and OE results completely phenocopied the interference and overexpression of N-Cadherin respectively (Fig 1-5), we wondered whether affecting the level of one protein may in turn affect the level of the other protein. We were able to observe that knocking-down α-Catenin did not significantly change the levels and location of N-Cadherin (Fig. EV3C). On the other hand, α-Catenin levels were reduced upon KD of N-Cadherin and increased upon its overexpression (Fig EV3D, E). These data indicate the N-cadherin effects may be directly linked to the downstream role of α-Catenin, similar to what has been suggested before (*Shimoyama et al., 1992; Watabe-Uchida et al., 1998; Bajpai et al., 2009*).

5. N-cadherin regulation of TNTs requires α-catenin

Considering α-Catenin as linker of the N-Cadherin complex to the actin cytoskeleton, which is the main cytoskeletal component of TNTs in neuronal cells, we decided to KD α-Catenin in cells overexpressing N-Cadherin and look at the effects on TNTs.

RNAi mediated KD of α-Catenin in GFP N-Cadherin cells and in control cells transfected with mCherry lead to a significative reduction in the levels of this protein compared to the RNAi Control (74% of reduction in GFP N-Cadherin/RNAi α-Catenin cells and 80% in mCherry/RNAi α-Catenin cells) (Fig EV4A). Importantly, N-Cadherin levels and subcellular location were not significatively affected by the downregulation of α-Catenin in GFP N-Cadherin cells (Fig EV4B).

We found that α-Catenin KD in GFP N-Cadherin cells led to a significant increase in TNT connected cells compared to RNAi Control cells (from around 8% to almost 19%) (Fig 6A-C). Furthermore, DiD-vesicle transfer assay in coculture revealed that GFP N-Cadherin/RNAi α-Catenin cells transferred significantly less vesicles (24%) compared to RNAi Control conditions (44%) by a contact-mediated mechanism (Fig 6D-F), again with a low transfer by secretion compared to the total transfer. These data showed that KD of α-Catenin overcomes almost completely the effect of N-Cadherin overexpression, suggesting that α-Catenin acts downstream N-Cadherin in the regulation of TNTs.

Considering that cadherins are cell adhesion molecules that act in trans, affecting the downstream actin cytoskeleton through α-Catenin, we decided to investigate the effects of trans interaction between these two molecules on the establishment of functional

TNTs. To this aim we co-cultured one cell population overexpressing N-Cadherin with another cell population KD for α-Catenin and analyzed both the number of TNTs and their functionality. As for the previous experiments, KD of α-Catenin resulted in 71% of reduction in the levels of this protein compared to the RNAi Control (Fig EV4C), whilst α-Catenin levels in GFP N-Cadherin cells were almost 2 folds compared to the RNAi Control cells (Fig EV4C), confirming the observations made by IF (Figure EV3D, E). As expected, upon α-Catenin KD there was an increase in both the total percentage of TNT connected cells (Fig EV5A) and in the percentage of heterotypic connections (e.g., the connections between GFP N-Cadherin cells and α-Catenin KD cells) (Fig EV5B) without altering the % distribution of connections between the different cell types (Fig EV5C for the RNAi Control and Fig EV5D for the RNAi α-Catenin).

We then performed the DiD-vesicle transfer assay in two different conditions: 1) GFP N-Cadherin cells as donor cells cocultured with either RNAi Control (Fig 6G) or RNAi α-Catenin cells (Fig 6H) as acceptors; 2) RNAi Control (Fig 6I) or RNAi α-Catenin cells (Fig 6J) as donors cocultured with GFP N-Cadherin cells as acceptors. Contact-mediated transfer of DiD-vesicles was around 44% between GFP N-Cadherin cells as donor and RNAi Control cells as acceptors and 46% between RNAi Control cells as donors and GFP N-Cadherin cells as acceptors. Interestingly, KD of α-Catenin either in the donor or in the acceptor population resulted in around 50% of decrease of the contact mediated transfer compared to control conditions with a 22% and 24% of acceptor cells receiving DiD-vesicles respectively for the two aforementioned conditions (Fig 6K) suggesting that α-Catenin was necessary both in the donor and acceptor cells for a functional TNT to be established. Again, a minimal part of the total transfer corresponded to a secretion mechanism (Fig 6K).

To better understand these results, we analysed the structure of TNTs formed between one cell population overexpressing N-Cadherin and another cell population KD for α-Catenin by correlative cryo-TEM where we could recognize the two cell populations differently labeled in FM (Fig 7A). As shown in the example of Fig 7 we frequently observed that TNTs established between these two different cell populations corresponded to a bundle of 2 iTNTs (Fig 7A, Fig EV6). Interestingly, both the iTNT coming from the GFP N-Cadherin cells and the ones coming from the RNAi α-Catenin cells had close-ended tips (Fig 7D-G, Fig EV6). Quantitative analysis of these cryo-EM

data revealed that 90% of iTNT originating from GFP N-Cadherin cells and 90% of iTNT originating from RNAi α-Catenin cells were closed-tip iTNTs (Fig 7H) and only 10% were fully extended between the two cell populations (Fig 7H). These results strongly indicated α-Catenin working downstream N-Cadherin was needed both in the donor and acceptor cell to establish functional TNTs.

Discussion

Most of neuronal TNTs are composed of bundles of open-ended individual tunneling nanotubes (iTNTs) that are held together by threads and linkers labeled with anti-N-Cadherin antibodies (Sartori-Rupp, Cordero Cervantes, Pepe et al., 2019).

Here we show that N-Cadherin interference leads to an increase in TNT-connected cells and a decrease in TNT-mediated vesicle transfer. On the contrary, overexpression of N-Cadherin, results in a decrease in TNT-connected cells but an increase of vesicle transfer. These data uncover a role for N-Cadherin in the functional establishment of TNTs. However, the question arises as to why N-cadherin KD leads to an increase in TNT connected cells while N-Cadherin OE leads to a decrease? Why should there be less transfer in conditions when TNTs increase, and more transfer when TNTs are reduced?

Cryo-EM and tomography (Sartori-Rupp, Cordero Cervantes, Pepe et al., 2019) on RNAi N-Cadherin cells revealed that the canonic structure of the TNTs, i.e. the parallel bundle of iTNTs, was highly altered, with iTNTs crossing over each other and in many cases without specific direction. Conversely, N-Cadherin OE led to an opposite phenotype, with iTNTs highly ordered, running parallel to each other, and directed straight toward the opposing cell. This alteration of the bundle structure of the iTNTs is consistent with a role for N-Cadherin treads in facilitating the organization of the bundle of iTNTs into a highly ordered, parallel and more stable structure. Furthermore, we observed that cells forming TNTs use other pre-existing protrusions as guides to grow (Supplementary Movies 6&7), the lack of N-Cadherin would therefore cause the disappearance of these guides and therefore these iTNTs would have no reference for growth/retraction (Fig 8). Our data are supported by recent findings showing that double filopodial bridges (DFB, that the authors consider as precursors of close-ended TNTs in HeLa cells), were dissociated resulting into separation of paired cells by downregulating N-Cadherin (or inhibiting its function with EGTA) (Chang et al., 2022). In the same study, the authors show N-

Cadherin decorating the whole DFB/TNT-like structure and preferentially enriched in the areas of contact with opposite cells. They interpret these enrichments as an indication of close-ended TNTs formation, also supported by the fact that they only observe unidirectional transfer of Ca2+ (and not of different cellular material or organelles) in these structures. We found a similar enrichment of N-Cadherin at the TNTs ends (Supplementary Movies 8&9), however, when we overexpress N-Cadherin, in addition to these enrichments we observe a significant increase in vesicle transfer. This, together with our previous ultrastructural study of TNTs (Sartori-Rupp, Cordero Cervantes, Pepe et al., 2019), suggest that at least in our cellular model these TNTs should be open-ended and that the continuity between TNT and opposite cell seems to be facilitated by N-Cadherin (Fig 8).

Indeed, quantitative analysis of our cryo-EM data showed in RNAi N-Cadherin cells there was a substantial increase in the number of close-ended iTNTs in a bundle, thus, explaining the decrease in vesicle transfer. We can therefore speculate that N-Cadherin may also regulate the process of fusion of the TNT with the opposing cell. The involvement of cadherin proteins in cellular fusion has been described in myoblast (Mège et al., 1992), in trophoblastic cells fusion (Ishikawa et al., 2014) and in multinucleated osteoclasts formation (Mbalaviele et al., 1995). Nevertheless, N-Cadherin is not able to directly trigger fusion because the distance between two molecules of N-Cadherin on the opposite membranes is 37.8 nm (Harrison et al., 2011) is too big to lead to spontaneous fusion. However, N-Cadherin could facilitate a pre-fusion event -the adhesion between the opposite cell membranes prior to the fusion. Therefore, in N-Cadherin KD conditions, failure in the adhesion of the TNTs with the opposing cell would impair fusion resulting in close-ended TNTs and reduction of material transfer. Furthermore, in GFP N-Cadherin cells, TNTs were predominantly formed by a single-tube reaching a diameter of 600 nm, and very often containing organelles inside them (Fig 2H). The presence of larger tubes together with the increase in fully extended connections could further explain the higher transfer observed in conditions of OE of N-Cadherin (Fig 8). One interesting question raised from these data is whether the single larger tubes are derived from iTNTs and what is the role of N-Cadherin in this event. N-Cadherin is present on short linkers between iTNTs, (Sartori-Rupp, Cordero Cervantes, Pepe et al., 2019; Fig EV3G), it may be possible that the increased presence N-Cadherin could allow the fusion of iTNTs in single tubes (Fig 8). In conditions of N-Cadherin OE, TNTs were more stable (e.g., lasted

longer) compared to KD or control cells. One possible explanation is that the N-Cadherin linkers could stabilize the iTNTs bundles and therefore reduce TNT fragility, as well as, that the single tubes are more robust and last longer compared to the bundles. This is line with recent atomic force microscope (AFM) measurements demonstrating that TNTs are elastic structures and that N-Cadherin regulates flexural strength of the TNTs (Li et al., 2022). Further studies will be needed to understand the specificity and nature and origin of iTNTs and single tubes.

We observed that α-Catenin KD and OE phenocopied the effects on TNTs of N-Cadherin.Through the link with the actin cytoskeleton, the N-Cadherin and α-Catenin complex might regulate actin dynamics (Dress et al., 2005; Wood et al., 2017), interact with other actin-related proteins such as cortactin (Helwani et al., 2004), Arp2/3 complex (Dress et al., 2005) or formins (Kobielak et al., 2004) and other proteins involved in actin polymerization-depolymerization cycle which is a key step in TNT formation (Ljubojevic et al., 2021). It is well known that adherens junction formation is initiated with an interdigitation junction formation (Troyanovsky, 2018), clustering of the cadherin molecules (Mège and Ishiyama, 2017) and actin cytoskeleton reorganization with the formation of actin bundle cables, therefore maintaining the actin cytoskeleton "sequestered" in a very well-organized actin belt typical of these junctions (Cavey and Lecuit, 2009). Indeed, this actin belt would be the opposite to what has been thought to initiate TNT formation, which would rely on membrane deformation and new actin filament formation that would push the membrane outwards (Ljubojevic et al., 2021). We speculate that by affecting N-Cadherin we could affect cortical actin, such that by inhibiting N-Cadherin a gradient of actin could be formed which, not being anchored to the membrane by the cadherin-catenin complex, could form small protrusions that may be TNT precursors. Inversely, in OE condition N-Cadherin clusters could promote the formation of an actin belt resulting de facto in TNT inhibition. A similar phenotype was found in the case of dendritic spines, which changed their morphological features to a filopodia-like protrusions following N-cadherin inhibition (Togashi et al., 2002).

In addition, despite N-Cadherin OE, the lack of α-Catenin is sufficient to recapitulate the observed KD effects of N-Cadherin or α-Catenin in naive cells, showing that α-Catenin is a downstream effector of N-Cadherin in the regulation of TNTs. Finally, we have shown that α-Catenin is necessary in both cell population as KD in donors or acceptors

results in decrease in vesicles transfer and increase in closed-tips TNTs. We can speculate that these iTNTs are not functional and are not able to fuse with the opposite cells to share materials. We hypothesize that TNT fusion might resemble myoblast fusion (Kim and Chen, 2019). In Drosophila myoblast fusion, fusion-competent myoblast cells extend F-actin finger-like protrusion that invade the opposing founder cell (Sens et al., 2010). The membranes of these invasive protrusions and the receiving cell are engaged by cell adhesion molecules (Shilagardi et al., 2013) that would initiate a signaling cascade towards the cytoskeleton increasing cortical tension by the pushing forces of the protrusions and the pulling of the membrane of the receiving cells that will eventually lead to a pore formation and membrane fusion (Kim et al., 2015). In our case, we could think TNTs protrusions would invade the opposing cell and both membranes would adhere through N-Cadherin that might transmit the pushing/pulling forces to the cortical actin cytoskeleton through α-Catenin forming a fusion competent site, so an open-ended connection could be formed.

Overall, our study begins to shed some light on the mechanisms of formation of such peculiar structure, revealing the essential role and different functions of the N-Cadherin-α-Catenin complex in TNTs in neuronal cells. Although there is indication that this pathway could be relevant also in other cell types, further studies will be necessary to confirm this and to reveal the remaining molecular determinants and biophysical properties of functional, open-ended TNTs

Materials and Methods

Cell lines, plasmids and transfection procedures

Human neuroblastoma (SH-SY5Y) cells were cultured at 37 °C in 5% CO2 in RPMI-1640 (Euroclone), plus 10% fetal bovine serum and 1% penicillin/streptomycin (gift from Simona Paladino, Department of Molecular Medicine and Medical Biotechnology, University of Naples Federico II, Naples, Italy). N-cadherin GFP plasmid was available in the lab and was obtained from Sandrine Etienne-Manneville (Pasteur Institute, Paris, France) (*Gousset el al., 2013; Camand et al., 2012*), mEmerald-α-catenin plasmid was purchased from Addgene (#53982). To obtain clones that express N-cadherin GFP or mEmerald-α-catenin, cells were transfected with the corresponding plasmid using Lipofectamine 2000 (Invitrogen) following the manufacture recommendations and

selected with 300 ug/mL of geneticin for 10-14 days, changing the medium every 3-4 days. The pool of cells was seeded in 96-well plates through a limiting dilution in such a way that 0.5 cells are seeded per well, and after allowing them to grow, they were analyzed and the clone overexpressing the protein of interest were selected. Human siRNA Oligo Duplex for N-cadherin (SR300716) and α-catenin (SR301060) were purchased from Origene. siRNA was transiently transfected to the cells through Lipofectamine RNAimax (Invitrogen) following the manufacture recommendations and the experiments are carried out in between 48 and 72 hours after the transfection.

Sample preparation for visualization and quantification of the TNTs

SH-SY5Y cells were trypsinized and counted and 100.000 cells were plated overnight (O/N) in coverslips. Cells transfected with the corresponding siRNA were trypsinized and counted at 48 hours post-transfection and 100.000 cells were plated on coverslips O/N. 16 hours later cells were fixed with specific fixatives to preserve TNTs first with fixative solution 1 (2% PFA, 0.05% glutaraldehyde and 0.2 M HEPES in PBS) for 15 min at 37 °C followed by a second fixation for 15 min with fixative solution 2 (4% PFA and 0.2 M HEPES in PBS) at 37 °C (for more information, *Abounit et al., 2015*). After fixation cells were washed with PBS and membrane was stained with conjugated Wheat Germ Agglutinin (WGA)-Alexa Fluor (1:300 in PBS) (Invitrogen) and DAPI (1:1000) (Invitrogen) for 15 minutes at room temperature, followed by 3 gentle washes with PBS and finally samples were mounted on glass slides with Aqua PolyMount (Polysciences, Inc.).

Quantification of TNT-connected cells

Various Z-stacks images of different random points of the samples are acquired with an inverted laser scanning confocal microscope LSM700 (Zeiss) controlled by the Zen software (Zeiss). Images are analyzed following the morphological criteria of the TNTs: structures that connect distant cells and not adherent, so for, first slices are excluded and only connections present in the middle and upper stacks are counted. Cells containing TNTs between them are marked as TNT-connected cells and by counting the number of cells that have TNTs between them and the total number of cells, the percentage of cells connected by TNTs is obtained. Analysis of the TNT-connected cells was performed in ICY software (https://icy.bioimageanalysis.org/) using the “Manual TNT annotation

plugin". At least 200 cells per condition were counted in each experiment. Image were processed with the ImageJ software.

DiD transfer assay (co-culture assay)

DiD transfer assay is described elsewhere (Abounit et al., 2015) a co-culture is performed consisting of two populations of cells labeled differently: first, your cells of interest (donors) are treated with Vybrant DiD (dialkylcarbocyanines), a lipophilic dye that stains the vesicles, 1:1000 (Thermo Fisher Scientific) in complete medium for 30 minutes at 37 °C (Life Technologies) and second, these cells are co-cultured at a ratio of 1:1 with another population of cells (acceptors) marked in another color (normally cells expressing soluble GFP or soluble mCherry) and grown for about 16 hours. For SH-SY5Y 50.000 donor cells are cocultured with 50.000 acceptor cells on coverslips. The results are analyzed through microscopy as described above and the final results are obtained by semiquantitative analysis with the ICY software from calculating the percentage of acceptor cells with marked vesicles among the total number of acceptor cells. At least 100 acceptor cells per condition were counted in each experiment. Image montages were built afterward in ImageJ software

Trypsin treatment experiment

Cell singularization by trypsin in was adapted from (Staufer et al.). SH-SY5Y cells were plated the day before the experiment, seeding twice as many cells as under normal conditions, 800.000 cells per condition, since trypsin treatment would cause us to lose part of the cells that would detach in Ibidi μ-dishes (Biovalley, France) to favor cell adhesion with the substrate. 16 hours later the culture medium was replaced by 0.05% Trypsin/EDTA (Gibco), enough to cover the whole dish, for 3 minutes at room temperature. Immediately after these cells were fixed, stained, sealed and analyzed exactly in the same way as described in "sample preparation for visualization and quantification of the TNTs"

Immunofluorescence

For immunofluorescence, 100.000 cells were seeded on glass coverslips and after O/N culture they were fixed with 4% paraformaldehyde (PFA) for 15 minutes at °C, quenched with 50 mM NH_4Cl for 15 min, permeabilized with 0.1% Triton X-100 in PBS and

blocked in 2% BSA in PBS. Primary antibodies used are: rabbit anti-N-Cadherin (ABCAM ref: ab76057), rabbit anti-N-Cadherin (Genetex ref: GTX127345) mouse anti-N-Cadherin (BD Biosciences ref: 610920), and rabbit anti-α-catenin (Sigma ref: c2081) all of them at 1:1000 in 2% BSA in PBS during 1 hour. After 3 washes of 10 minutes each with PBS, cells were incubated with each corresponding AlexaFluor-conjugated secondary antibody (Invitrogen) at 1:1000 in 2% BSA in PBS during 1 hour. For those experiments showing the actin cytoskeleton, cells were labeled with Rhodamine Phalloidin (Invitrogen) at 1:1000 in the same mix and conditions as the secondary antibodies. Then, cells were washed 3 times of 10 minutes each with PBS, stained with DAPI and mounted on glass slides with Aqua PolyMount (Polysciences, Inc.). Images were acquired with a confocal microscope LSM700 (Zeiss) and processed with the ImageJ software.

Western blot

For Western blot cells were lysed with lysis buffer composed by 150 mM NaCl, 20 mM Tris, 5 mM EDTA, pH 8.0. Protein concentration was measured by a Bradford protein assay (Bio- Rad). Samples were boiled at 100 °C for 5 min and loaded in handcrafted 8% SDS-polyacrylamide gel or 4-12% Criterion™ XT Bis-Tris XT Precast Gels (Bio-Rad) and electrophoresed in 1X Tris/Glycine/SDS buffer (Bio-Rad) or 1X XT MOPS buffer (Bio-Rad) respectively for 1.5-2 hours at 90V. Proteins were transferred to 0.45 µm Nitrocellulose membranes (Bio-Rad) with 1X Tris/Glycine transfer buffer (Bio-Rad) for 1.5 hours at 90V in a cold chamber. Membranes were blocked in 5% non-fat milk in Tris-buffered saline with 0.1% Tween 20 (TBS-T) for 1 hour. Membranes were incubated O/N at 4 °C with the corresponding primary antibodies at 1:1000 in 5% non-fat milk TBS-T. Primary antibodies used for Western blot were: rabbit anti-N-Cadherin (ABCAM ref: ab76057), rabbit anti-N-Cadherin (Genetex ref: GTX127345) mouse anti-N-Cadherin (BD Biosciences ref: 610920), rabbit anti-α-catenin (Sigma ref: c2081) and mouse anti-α-tubulin (Sigma ref: T9026). Membranes were washed 3 times 10 minutes each with TBS-T and then incubated with the corresponding IgG secondary antibodies horseradish peroxidase-conjugated (GE Healthcare Life Sciences) at 1:1000 for 1 hour at room temperature. Membranes were washed 3 times 10 minutes each. Membrane protein bands were detected with Amersham™ ECL Prime Western Blotting Detection Reagent

(Cytiva). Membranes were imaged using Amersham™ Imager 680 (GE Healthcare Life Sciences).

Live Imaging

400.000 SH-SY5Y cells were plated the day before the experiment in Ibidi µ-dishes. After 16 hours of culture, live time series images were acquired with a 60 × 1.4NA CSU oil immersion objective lens on an inverted Elipse Ti microscope system (Nikon Instruments, Melville, NY, USA). Cells were labeled with 1:1000 dilution of conjugated WGA-Alexa Fluor in the corresponding media. Images were captured in immediate succession with one of two cameras, which enabled time intervals between 20 and 40 seconds per z-stack or between 50 and 70 seconds per z-stack when using two lasers. For live cell imaging, the 37 °C temperature was controlled with an Air Stream Stage Incubator, which also controlled humidity. Cells were incubated with 5% CO2 during image acquisition.

Cell preparation for cryo-EM

Carbon-coated gold TEM grids (Quantifoil NH2A R2/2) were glow-discharged at 2 mA and 1.5–1.8 × 10^{-1} m bar for 1 minute in an ELMO (Cordouan) glow discharge system. Grids were sterilized under UV three times for 30 minutes at R. T. and then incubated at 37 °C in complete culture medium for 2 hours. 300,000 SH-SY5Y cells (RNAi-N-Cadherin/ α-catenin, GFP-N-Cadherin/mEmerald catenin) were counted and seed on cryo-EM grids positioned in 35 mm Ibidi µ-Dish (Biovalley, France). After 24 hours of incubation, resulted in 3 to 4 cells per grid square. Prior to chemical and cryo-plunging freezing, cells were labeled with WGA-Alexa-488 (1:300 in PBS) for 5 min at 37 °C. For correlative light- and cryo-electron microscopy, cells were chemically fixed in 2% PFA + 0.05% GA in 0.2 M Hepes for 15 minutes followed by fixation in 4% PFA in 0.2 M Hepes for 15 minutes and kept hydrated in PBS-1X buffer prior to vitrification.

For cell vitrification, cells were blotted from the back side of the grid for 10 seconds and rapidly frozen in liquid ethane using a Leica EMGP system as we performed before (36).

Cryo-electron tomography data acquisition and tomogram reconstruction

The cryo-EM data was collected from different grids at the Nanoimaging core facility of the Institut Pasteur using a Thermo Scientific (TF) 300kV Titan Krios G3 cryo-

transmission electron microscopes (Cryo-TEM) equipped with a Gatan energy filter bioquantum/K3. Tomography software from Thermo Scientific was used to acquire the data. Tomograms were acquired using dose-symmetric tilt scheme (76), a +/-60 degree tilt range with a tilt step 2 was used to acquire the tilt series. Tilt images were acquired in counting mode with a calibrated physical pixel size of 3.2 Å and total dose over the full tilt series of 3.295 e- /Å2 and dose rate of 39,739 e-/px/s with an exposure time of 1s. The defocus applied was in a range of -3 to – 6 µm defocus.

Cryo-EM and tomography (Figure 1 and Supplementary 1) was performed on a Tecnai 20 equipped with a field emission gun and operated at 200 kV (Thermo Fisher company). Images were recorded using SerialEM software on a 4k x 4k camera (Ultrascan from Gatan) and a Falcon II (FEI, Thermo Fisher) direct electron detector, with a 14 µm pixel size. Tilt series of TNTs were acquired covering either an angular range of – 52° to + 52°. The defocuses used were −6 µm.

The tomograms were reconstructed using IMOD (eTomo). Final alignments were done by using 10 nm fiducial gold particles coated with BSA (BSA Gold Tracer, EMS). Gold beads were manually selected and automatically tracked. The fiducial model was corrected in all cases where the automatic tracking failed. Tomograms were binned 2x corresponding to a pixel size of 0.676 nm for the Titan and SIRT-like filter (15) option in eTomo was applied. For visualization purposes, the reconstructed volumes were processed by a Gaussian filter.

Cryo-EM N-Cadherin immuno-labeling

SH-SY5Y cells were plated on grids as described in above. After incubation O/N at 37 °C, cells were fixed with PFA 4% for 20 min at 37 °C, quenched with 50 mM NH4Cl for 15 min, and blocked with PBS containing 1% BSA (w/v) for 30 min at 37 °C. Cells were labeled with a rabbit anti-N-Cadherin ABCAM 76057 antibody (1:200), followed by Protein A-gold conjugated to 10 nm colloidal gold particles (CMC, Utrecht, Netherlands). SH-SY5Y cells were then rapidly frozen in liquid ethane as above.

Statistical analysis

The statistical analysis for the experiments concerning the percentage of TNT-connected cells and the DiD transfer assay are described elsewhere (Pinto et al., 2021). Briefly, the

statistical tests were computed using either a logistic regression model computed using the 'glm' function of R software (https://www.R-project.org/) or a mixed effect logistic regression model using the lmer and lmerTest R packages, applying a pairwise comparison test. For the rest of experiments, Student's t-test (for 2 groups) or One-Way ANOVA (for more than 2 groups) tests were applied. All column graphs, Student's t-test and One-Way ANOVA statistical analysis were performed using GraphPad Prism version 9 software.

Bibliography

Abounit, S., Bousset, L., Loria, F., Zhu, S., Chaumont, F., Pieri, L., Olivo-Marin, J., Melki, R., Zurzolo, C., 2016. Tunneling nanotubes spread fibrillar α-synuclein by intercellular trafficking of lysosomes. EMBO J 35, 2120–2138. https://doi.org/10.15252/embj.201593411

Abounit, S., Delage, E., Zurzolo, C., 2015. Identification and Characterization of Tunneling Nanotubes for Intercellular Trafficking. Curr Protoc Cell Biol 67, 12.10.1-12.10.21. https://doi.org/10.1002/0471143030.cb1210s67

Ariazi, J., Benowitz, A., De Biasi, V., Den Boer, M.L., Cherqui, S., Cui, H., Douillet, N., Eugenin, E.A., Favre, D., Goodman, S., Gousset, K., Hanein, D., Israel, D.I., Kimura, S., Kirkpatrick, R.B., Kuhn, N., Jeong, C., Lou, E., Mailliard, R., Maio, S., Okafo, G., Osswald, M., Pasquier, J., Polak, R., Pradel, G., de Rooij, B., Schaeffer, P., Skeberdis, V.A., Smith, I.F., Tanveer, A., Volkmann, N., Wu, Z., Zurzolo, C., 2017. Tunneling Nanotubes and Gap Junctions–Their Role in Long-Range Intercellular Communication during Development, Health, and Disease Conditions. Front. Mol. Neurosci. 10, 333. https://doi.org/10.3389/fnmol.2017.00333

Bajpai, S., Feng, Y., Krishnamurthy, R., Longmore, G.D., Wirtz, D., 2009. Loss of α-Catenin Decreases the Strength of Single E-cadherin Bonds between Human Cancer Cells. Journal of Biological Chemistry 284, 18252–18259. https://doi.org/10.1074/jbc.M109.000661

Brasch, J., Harrison, O.J., Honig, B., Shapiro, L., 2012. Thinking outside the cell: how cadherins drive adhesion. Trends in Cell Biology 22, 299–310. https://doi.org/10.1016/j.tcb.2012.03.004

Camand, E., Peglion, F., Osmani, N., Sanson, M., Etienne-Manneville, S., 2012. N-cadherin expression level modulates integrin-mediated polarity and strongly impacts on the speed and directionality of glial cell migration. Journal of Cell Science 125, 844–857. https://doi.org/10.1242/jcs.087668

Cavey, M., Lecuit, T., 2009. Molecular Bases of Cell-Cell Junctions Stability and Dynamics. Cold Spring Harbor Perspectives in Biology 1, a002998–a002998. https://doi.org/10.1101/cshperspect.a002998

Chang, M., Lee, O., Bu, G., Oh, J., Yunn, N.-O., Ryu, S.H., Kwon, H.-B., Kolomeisky, A.B., Shim, S.-H., Doh, J., Jeon, J.-H., Lee, J.-B., 2022. Formation of cellular close-ended tunneling nanotubes through mechanical deformation. Sci. Adv. 8, eabj3995. https://doi.org/10.1126/sciadv.abj3995

Chastagner, P., Loria, F., Vargas, J.Y., Tois, J., I Diamond, M., Okafo, G., Brou, C., Zurzolo, C., 2020. Fate and propagation of endogenously formed Tau aggregates in neuronal cells. EMBO Mol Med 12. https://doi.org/10.15252/emmm.202012025

Cordero Cervantes, D., Zurzolo, C., 2021. Peering into tunneling nanotubes—The path forward. EMBO J 40. https://doi.org/10.15252/embj.2020105789

Costanzo, M., Abounit, S., Marzo, L., Danckaert, A., Chamoun, Z., Roux, P., Zurzolo, C., 2013. Transfer of polyglutamine aggregates in neuronal cells occurs in tunneling nanotubes. Journal of Cell Science jcs.126086. https://doi.org/10.1242/jcs.126086

Dagar, S., Pathak, D., Oza, H.V., Mylavarapu, S.V.S., 2021. Tunneling nanotubes and related structures: molecular mechanisms of formation and function. Biochemical Journal 478, 3977–3998. https://doi.org/10.1042/BCJ20210077

Delage, E., Cervantes, D.C., Pénard, E., Schmitt, C., Syan, S., Disanza, A., Scita, G., Zurzolo, C., 2016. Differential identity of Filopodia and Tunneling Nanotubes revealed

by the opposite functions of actin regulatory complexes. Sci Rep 6, 39632. https://doi.org/10.1038/srep39632

Desir, S., O'Hare, P., Vogel, R.I., Sperduto, W., Sarkari, A., Dickson, E.L., Wong, P., Nelson, A.C., Fong, Y., Steer, C.J., Subramanian, S., Lou, E., 2018. Chemotherapy-Induced Tunneling Nanotubes Mediate Intercellular Drug Efflux in Pancreatic Cancer. Sci Rep 8, 9484. https://doi.org/10.1038/s41598-018-27649-x

Dilsizoglu Senol, A., Samarani, M., Syan, S., Guardia, C.M., Nonaka, T., Liv, N., Latour-Lambert, P., Hasegawa, M., Klumperman, J., Bonifacino, J.S., Zurzolo, C., 2021. α-Synuclein fibrils subvert lysosome structure and function for the propagation of protein misfolding between cells through tunneling nanotubes. PLoS Biol 19, e3001287. https://doi.org/10.1371/journal.pbio.3001287

Drees, F., Pokutta, S., Yamada, S., Nelson, W.J., Weis, W.I., 2005. α-Catenin Is a Molecular Switch that Binds E-Cadherin-β-Catenin and Regulates Actin-Filament Assembly. Cell 123, 903–915. https://doi.org/10.1016/j.cell.2005.09.021

Gousset, K., Marzo, L., Commere, P.-H., Zurzolo, C., 2013. Myo10 is a key regulator of TNT formation in neuronal cells. Journal of Cell Science 126, 4424–4435. https://doi.org/10.1242/jcs.129239

Gousset, K., Schiff, E., Langevin, C., Marijanovic, Z., Caputo, A., Browman, D.T., Chenouard, N., de Chaumont, F., Martino, A., Enninga, J., Olivo-Marin, J.-C., Männel, D., Zurzolo, C., 2009. Prions hijack tunnelling nanotubes for intercellular spread. Nat Cell Biol 11, 328–336. https://doi.org/10.1038/ncb1841

Harrison, O.J., Jin, X., Hong, S., Bahna, F., Ahlsen, G., Brasch, J., Wu, Y., Vendome, J., Felsovalyi, K., Hampton, C.M., Troyanovsky, R.B., Ben-Shaul, A., Frank, J., Troyanovsky, S.M., Shapiro, L., Honig, B., 2011. The Extracellular Architecture of Adherens Junctions Revealed by Crystal Structures of Type I Cadherins. Structure 19, 244–256. https://doi.org/10.1016/j.str.2010.11.016

Hatta, K., Okada, T.S., Takeichi, M., 1985. A monoclonal antibody disrupting calcium-dependent cell-cell adhesion of brain tissues: possible role of its target antigen in animal

pattern formation. Proceedings of the National Academy of Sciences 82, 2789–2793. https://doi.org/10.1073/pnas.82.9.2789

Helwani, F.M., Kovacs, E.M., Paterson, A.D., Verma, S., Ali, R.G., Fanning, A.S., Weed, S.A., Yap, A.S., 2004. Cortactin is necessary for E-cadherin–mediated contact formation and actin reorganization. Journal of Cell Biology 164, 899–910. https://doi.org/10.1083/jcb.200309034

Hirano, S., Kimoto, N., Shimoyama, Y., Hirohashi, S., Takeichi, M., 1992. Identification of a neural α-catenin as a key regulator of cadherin function and multicellular organization. Cell 70, 293–301. https://doi.org/10.1016/0092-8674(92)90103-J

Huveneers, S., de Rooij, J., 2013. Mechanosensitive systems at the cadherin–F-actin interface. Journal of Cell Science 126, 403–413. https://doi.org/10.1242/jcs.109447

Ishikawa, A., Omata, W., Ackerman, W.E., Takeshita, T., Vandré, D.D., Robinson, J.M., 2014. Cell fusion mediates dramatic alterations in the actin cytoskeleton, focal adhesions, and E-cadherin in trophoblastic cells: Trophoblast Fusion and Cellular Alterations. Cytoskeleton 71, 241–256. https://doi.org/10.1002/cm.21165

Jansens, R.J.J., Van den Broeck, W., De Pelsmaeker, S., Lamote, J.A.S., Van Waesberghe, C., Couck, L., Favoreel, H.W., 2017. Pseudorabies Virus US3-Induced Tunneling Nanotubes Contain Stabilized Microtubules, Interact with Neighboring Cells via Cadherins, and Allow Intercellular Molecular Communication. J Virol 91. https://doi.org/10.1128/JVI.00749-17

Knudsen, K.A., Soler, A.P., Johnson, K.R., Wheelock, M.J., 1995. Interaction of alpha-actinin with the cadherin/catenin cell-cell adhesion complex via alpha-catenin. Journal of Cell Biology 130, 67–77. https://doi.org/10.1083/jcb.130.1.67

Kobielak, A., Pasolli, H.A., Fuchs, E., 2004. Mammalian formin-1 participates in adherens junctions and polymerization of linear actin cables. Nat Cell Biol 6, 21–30. https://doi.org/10.1038/ncb1075

Kumar, A., Kim, J.H., Ranjan, P., Metcalfe, M.G., Cao, W., Mishina, M., Gangappa, S., Guo, Z., Boyden, E.S., Zaki, S., York, I., García-Sastre, A., Shaw, M., Sambhara, S.,

2017. Influenza virus exploits tunneling nanotubes for cell-to-cell spread. Sci Rep 7, 40360. https://doi.org/10.1038/srep40360

Kwiatkowski, A.V., Maiden, S.L., Pokutta, S., Choi, H.-J., Benjamin, J.M., Lynch, A.M., Nelson, W.J., Weis, W.I., Hardin, J., 2010. In vitro and in vivo reconstitution of the cadherin-catenin-actin complex from Caenorhabditis elegans. Proceedings of the National Academy of Sciences 107, 14591–14596. https://doi.org/10.1073/pnas.1007349107

Ladoux, B., Nelson, W.J., Yan, J., Mège, R.M., 2015. The mechanotransduction machinery at work at *adherens* junctions. Integrative Biology 7, 1109–1119. https://doi.org/10.1039/c5ib00070j

Ljubojevic, N., Henderson, J.M., Zurzolo, C., 2021. The Ways of Actin: Why Tunneling Nanotubes Are Unique Cell Protrusions. Trends Cell Biol 31, 130–142. https://doi.org/10.1016/j.tcb.2020.11.008

Lock, J.T., Parker, I., Smith, I.F., 2016. Communication of Ca2+ signals via tunneling membrane nanotubes is mediated by transmission of inositol trisphosphate through gap junctions. Cell Calcium 60, 266–272. https://doi.org/10.1016/j.ceca.2016.06.004

Lokar, M., Iglič, A., Veranič, P., 2010. Protruding membrane nanotubes: attachment of tubular protrusions to adjacent cells by several anchoring junctions. Protoplasma 246, 81–87. https://doi.org/10.1007/s00709-010-0143-7

Loria, F., Vargas, J.Y., Bousset, L., Syan, S., Salles, A., Melki, R., Zurzolo, C., 2017. α-Synuclein transfer between neurons and astrocytes indicates that astrocytes play a role in degradation rather than in spreading. Acta Neuropathol 134, 789–808. https://doi.org/10.1007/s00401-017-1746-2

Lu, J., Zheng, X., Li, F., Yu, Y., Chen, Z., Liu, Z., Wang, Z., Xu, H., Yang, W., 2017. Tunneling nanotubes promote intercellular mitochondria transfer followed by increased invasiveness in bladder cancer cells. Oncotarget 8, 15539–15552. https://doi.org/10.18632/oncotarget.14695

Lu, J.J., Yang, W.M., Li, F., Zhu, W., Chen, Z., 2019. Tunneling Nanotubes Mediated microRNA-155 Intercellular Transportation Promotes Bladder Cancer Cells' Invasive and Proliferative Capacity. IJN Volume 14, 9731–9743. https://doi.org/10.2147/IJN.S217277

Mbalaviele, G., Chen, H., Boyce, B.F., Mundy, G.R., Yoneda, T., 1995. The role of cadherin in the generation of multinucleated osteoclasts from mononuclear precursors in murine marrow. J. Clin. Invest. 95, 2757–2765. https://doi.org/10.1172/JCI117979

Mege, R.M., Goudou, D., Diaz, C., Nicolet, M., Garcia, L., Geraud, G., Rieger, F., 1992. N-cadherin and N-CAM in myoblast fusion: compared localisation and effect of blockade by peptides and antibodies. Journal of Cell Science 103, 897–906. https://doi.org/10.1242/jcs.103.4.897

Mège, R.M., Ishiyama, N., 2017. Integration of Cadherin Adhesion and Cytoskeleton at *Adherens* Junctions. Cold Spring Harb Perspect Biol 9, a028738. https://doi.org/10.1101/cshperspect.a028738

Okafo, G., Prevedel, L., Eugenin, E., 2017. Tunneling nanotubes (TNT) mediate long-range gap junctional communication: Implications for HIV cell to cell spread. Sci Rep 7, 16660. https://doi.org/10.1038/s41598-017-16600-1

Önfelt, B., Nedvetzki, S., Benninger, R.K.P., Purbhoo, M.A., Sowinski, S., Hume, A.N., Seabra, M.C., Neil, M.A.A., French, P.M.W., Davis, D.M., 2006. Structurally Distinct Membrane Nanotubes between Human Macrophages Support Long-Distance Vesicular Traffic or Surfing of Bacteria. J Immunol 177, 8476–8483. https://doi.org/10.4049/jimmunol.177.12.8476

Pepe, A., Pietropaoli, S., Vos, M., Barba-Spaeth, G., Zurzolo, C., 2021. Tunneling nanotubes provide a novel route for SARS-CoV-2 spreading between permissive cells and to non-permissive neuronal cells (preprint). Cell Biology. https://doi.org/10.1101/2021.11.15.468633

Pinto, G., Brou, C., Zurzolo, C., 2020. Tunneling Nanotubes: The Fuel of Tumor Progression? Trends in Cancer 6, 874–888. https://doi.org/10.1016/j.trecan.2020.04.012

Pinto, G., Saenz-de-Santa-Maria, I., Chastagner, P., Perthame, E., Delmas, C., Toulas, C., Moyal-Jonathan-Cohen, E., Brou, C., Zurzolo, C., 2021. Patient-derived glioblastoma stem cells transfer mitochondria through tunneling nanotubes in tumor organoids. Biochemical Journal 478, 21–39. https://doi.org/10.1042/BCJ20200710

Rimm, D.L., Koslov, E.R., Kebriaei, P., Cianci, C.D., Morrow, J.S., 1995. Alpha 1(E)-catenin is an actin-binding and -bundling protein mediating the attachment of F-actin to the membrane adhesion complex. Proceedings of the National Academy of Sciences 92, 8813–8817. https://doi.org/10.1073/pnas.92.19.8813

Rustom, A., Saffrich, R., Markovic, I., Walther, P., Gerdes, H.-H., 2004. Nanotubular Highways for Intercellular Organelle Transport. Science 303, 1007–1010. https://doi.org/10.1126/science.1093133

Sartori-Rupp, A., Cordero Cervantes, D., Pepe, A., Gousset, K., Delage, E., Corroyer-Dulmont, S., Schmitt, C., Krijnse-Locker, J., Zurzolo, C., 2019. Correlative cryo-electron microscopy reveals the structure of TNTs in neuronal cells. Nat Commun 10, 342. https://doi.org/10.1038/s41467-018-08178-7

Shimoyama, Y., Nagafuchi, A., Fujita, S., Gotoh, M., Takeichi, M., Tsukita, S., Hirohashi, S., 1992. Cadherin dysfunction in a human cancer cell line: possible involvement of loss of alpha-catenin expression in reduced cell-cell adhesiveness. Cancer Res 52, 5770–5774.

Sowinski, S., Jolly, C., Berninghausen, O., Purbhoo, M.A., Chauveau, A., Köhler, K., Oddos, S., Eissmann, P., Brodsky, F.M., Hopkins, C., Önfelt, B., Sattentau, Q., Davis, D.M., 2008. Membrane nanotubes physically connect T cells over long distances presenting a novel route for HIV-1 transmission. Nat Cell Biol 10, 211–219. https://doi.org/10.1038/ncb1682

Staufer, O., Hernandez B., J.E., Rustom, A., 2018. Protease-resistant cell meshworks: An indication of membrane nanotube-based syncytia formation. Experimental Cell Research 372, 85–91. https://doi.org/10.1016/j.yexcr.2018.09.012

Thayanithy, V., Dickson, E.L., Steer, C., Subramanian, S., Lou, E., 2014. Tumor-stromal cross talk: direct cell-to-cell transfer of oncogenic microRNAs via tunneling nanotubes. Translational Research 164, 359–365. https://doi.org/10.1016/j.trsl.2014.05.011

Togashi, H., Abe, K., Mizoguchi, A., Takaoka, K., Chisaka, O., Takeichi, M., 2002. Cadherin Regulates Dendritic Spine Morphogenesis. Neuron 35, 77–89. https://doi.org/10.1016/S0896-6273(02)00748-1

Troyanovsky, S., 2012. Adherens Junction Assembly, in: Harris, T. (Ed.), Adherens Junctions: From Molecular Mechanisms to Tissue Development and Disease, Subcellular Biochemistry. Springer Netherlands, Dordrecht, pp. 89–108. https://doi.org/10.1007/978-94-007-4186-7_5

Vargas, J.Y., Loria, F., Wu, Y., Córdova, G., Nonaka, T., Bellow, S., Syan, S., Hasegawa, M., van Woerden, G.M., Trollet, C., Zurzolo, C., 2019. The Wnt/Ca $^{2+}$ pathway is involved in interneuronal communication mediated by tunneling nanotubes. EMBO J 38. https://doi.org/10.15252/embj.2018101230

Wang, X., Gerdes, H.-H., 2015. Transfer of mitochondria via tunneling nanotubes rescues apoptotic PC12 cells. Cell Death Differ 22, 1181–1191. https://doi.org/10.1038/cdd.2014.211

Watabe, M., Nagafuchi, A., Tsukita, S., Takeichi, M., 1994. Induction of polarized cell-cell association and retardation of growth by activation of the E-cadherin-catenin adhesion system in a dispersed carcinoma line. Journal of Cell Biology 127, 247–256. https://doi.org/10.1083/jcb.127.1.247

Watabe-Uchida, M., Uchida, N., Imamura, Y., Nagafuchi, A., Fujimoto, K., Uemura, T., Vermeulen, S., van Roy, F., Adamson, E.D., Takeichi, M., 1998. α-Catenin-Vinculin Interaction Functions to Organize the Apical Junctional Complex in Epithelial Cells. Journal of Cell Biology 142, 847–857. https://doi.org/10.1083/jcb.142.3.847

Weiss, E.E., Kroemker, M., Rüdiger, A.-H., Jockusch, B.M., Rüdiger, M., 1998. Vinculin Is Part of the Cadherin–Catenin Junctional Complex: Complex Formation between α-Catenin and Vinculin. Journal of Cell Biology 141, 755–764. https://doi.org/10.1083/jcb.141.3.755

Wood, M.N., Ishiyama, N., Singaram, I., Chung, C.M., Flozak, A.S., Yemelyanov, A., Ikura, M., Cho, W., Gottardi, C.J., 2017. α-Catenin homodimers are recruited to phosphoinositide-activated membranes to promote adhesion. Journal of Cell Biology 216, 3767–3783. https://doi.org/10.1083/jcb.201612006

Yonemura, S., 2011. Cadherin–actin interactions at adherens junctions. Current Opinion in Cell Biology 23, 515–522. https://doi.org/10.1016/j.ceb.2011.07.001

Zaidel-Bar, R., 2013. Cadherin adhesome at a glance. Journal of Cell Science 126, 373–378. https://doi.org/10.1242/jcs.111559

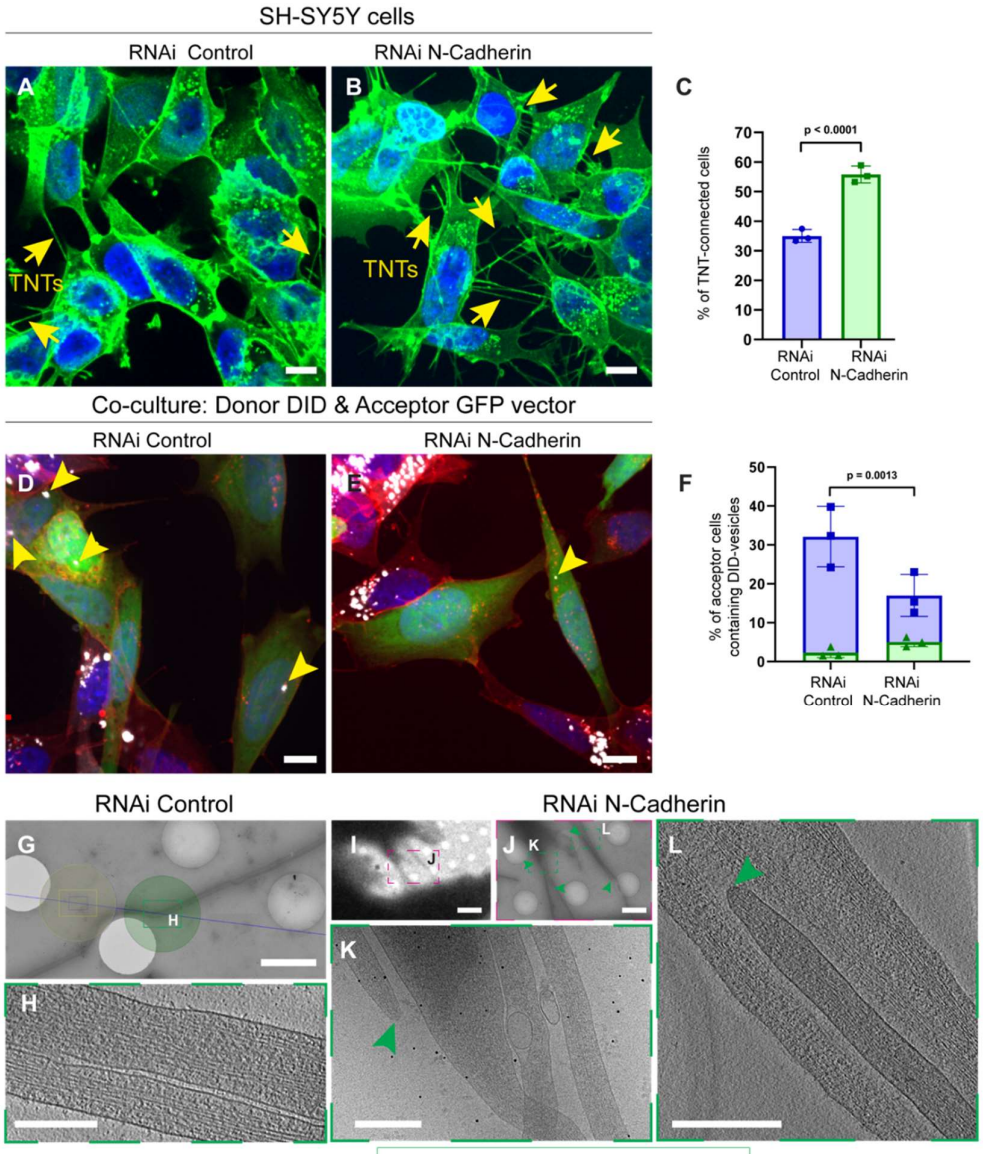

M

	Ultrastructure	
	% iTNTs full extended	% iTNTs tip closed
Control cells	75%	25%
RNAi N-Cadherin cells	52%	48%

Figure 1. N-Cadherin interference impacts the functionality and ultrastructure of the TNTs between SH-SY5Y cells.

A, B. Confocal micrograph showing (A) TNTs between RNAi Control and (B) TNTs between RNAi N-Cadherin cells. Cells stained with WGA-488 (green) and DAPI (blue) for the nuclei. The yellow arrows indicate the TNTs connected cells.

C. Graph showing the percentage of TNT-connected cells transfected with RNAi Control non-targeting (35% ± 2.17) and RNAi N-Cadherin (55.8% ± 2.85), (***p<0.0001 for RNAi Control versus RNAi N-Cadherin for N=3).

D, E. Representative confocal images showing 24h co-culture between (D) RNAi Control with DiD-labelled vesicles (donor) and GFP vector cells (acceptor), (E) RNAi N-Cadherin challenged with DiD-labelled vesicles (donor) and GFP vector cells (acceptor). Cellular membranes were labelled with WGA-546 (red), nuclei were stained with DAPI (blue). The yellow arrowheads indicate DiD-labelled vesicles detected in the cytoplasm of acceptor cells.

F. Graph showing the percentage of acceptor cells containing DiD-labelled vesicles from the co-cultures in cells transfected with RNAi Control (32.12%± 7.77 for contact-mediated transfer in blue; 2.31%± 1.31 for transfer by secretion in green) or RNAi N-Cadherin (17%± 5.4 for contact-mediated transfer in blue; 5.03%± 1.18 for transfer by secretion in green).

G. Cryo-EM intermedia micrograph showing TNT-connected RNAi Control cells.

H. High-magnification cryo-tomography slices corresponding to the green dashed squares in (G) showing full extended iTNTs. TNT-connected RNAi N-Cadherin cells acquired by cryo-EM (I) low (J) and intermediate magnification.

K. High-magnification cryo-EM slices showing the iTNT in the green dashed square in (J).

L. High-magnification cryo-tomography slices corresponding to the green dashed squares in (J).

M. Table showing the percentage of full extended iTNTs and tip-closed in RNAi Control cells and RNAi N-Cadherin cells.

Scale bars in (A, B, D, E) 20 μm, (G, J) 2 μm, (I) 10 μm, (H, K, L) 200nm.

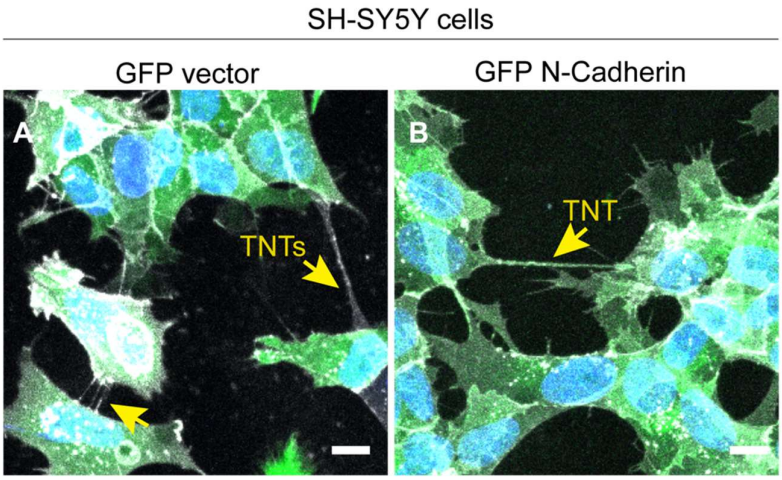

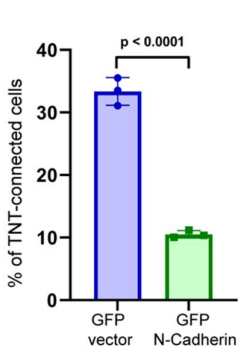

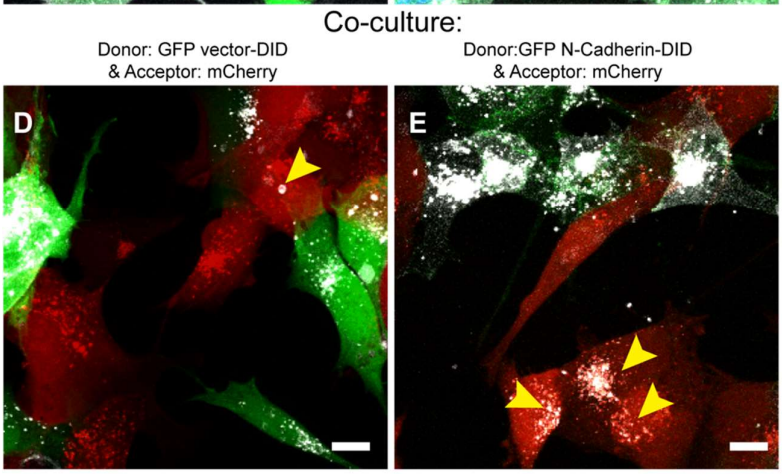

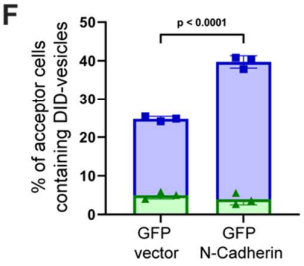

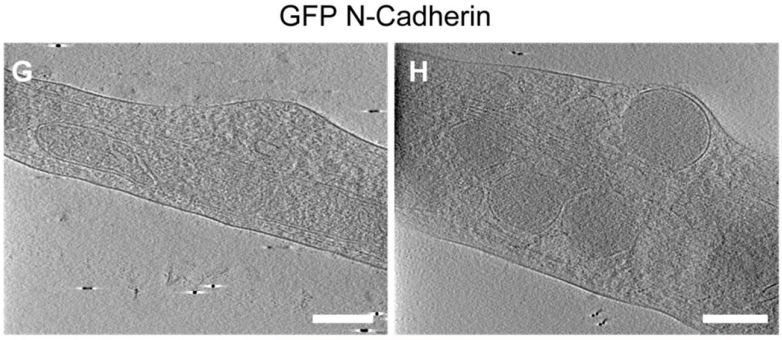

I

	Ultrastructure	
	% single TNT	% iTNTs
Control cells	40%	60%
RNAi N-Cadherin cells	26.3%	73.7%
GFP N-Cadherin cells	65%	35%

Figure 2. N-Cadherin overexpression impacts the functionality and ultrastructure of the TNTs between SH-SY5Y cells.

A, B. Confocal micrograph showing (A) TNTs between GFP vector expressing cells, (B) TNTs between GFP N-Cadherin cells. Cells stained with WGA-647 (gray) and DAPI (blue) for the nuclei. The yellow arrows indicate the TNTs connected cells.

C. Graph showing the percentage of TNT-connected cells in GFP expressing cells (33.4% ± 2.22) and GFP N-Cadherin (10.5%± 0.60), (***$p<0.0001$ for GFP vector versus GFP N-Cadherin for N=3).

D, E. Representative confocal images showing 24h co-culture between (D) GFP vector with DiD-labelled vesicles (donor) and mCherry cells (acceptor), (E) GFP N-Cadherin challenged with DiD-labelled vesicles (donor) and mCherry cells (acceptor). The yellow arrowheads indicate DiD-labelled vesicles detected in the cytoplasm of acceptor cells.

F. Graph showing the percentage of acceptor cells containing DiD-labelled vesicles from the co-cultures in GFP vector control cells (24.78%± 0.63 for contact-mediated transfer in blue; 4.97%± 0.93 for transfer by secretion in green) against GFP N-Cadherin cells (39.71%± 1.62 for contact-mediated transfer in blue; 3.95%± 1.48 for transfer by secretion in green). (***$p<0.0001$ for GFP vector versus GFP N-Cadherin for N=3).

G, H. High-magnification cryo-tomography slices showing single TNT-connected GFP N-Cadherin cells.

L. Table showing the percentage of single TNTs and iTNTs in Control, RNAi N-Cadherin and GFP N-Cadherin cells. Scale bars in (A, B, D, E) 10 μm, (G, H) 100nm.

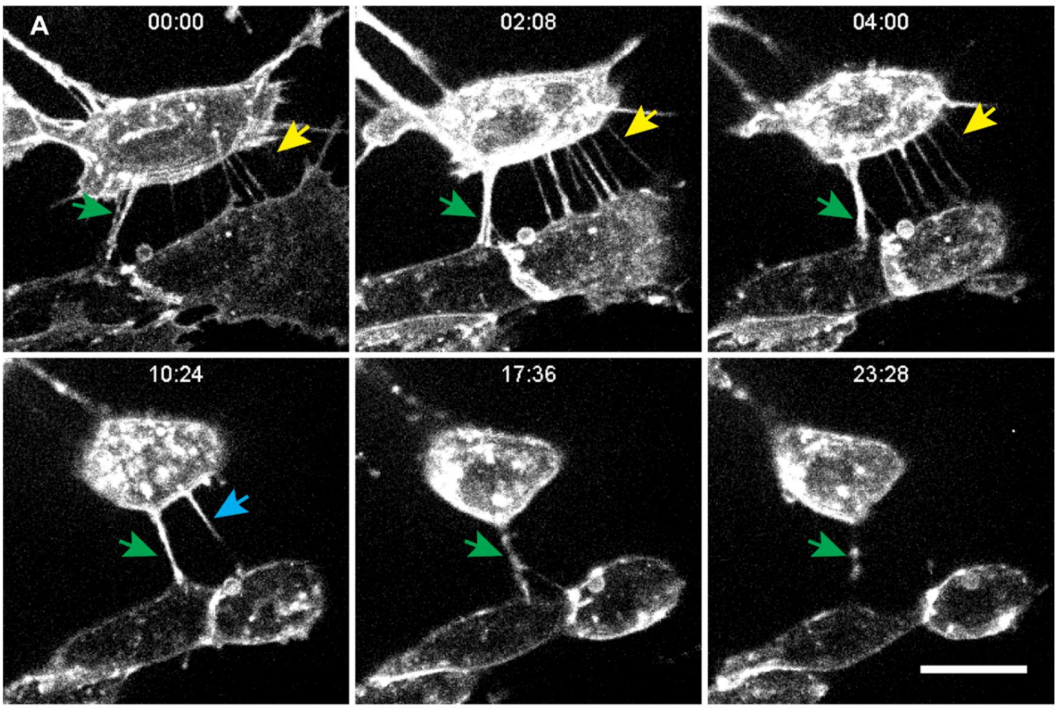
A
00:00
02:08
04:00
10:24
17:36
23:28

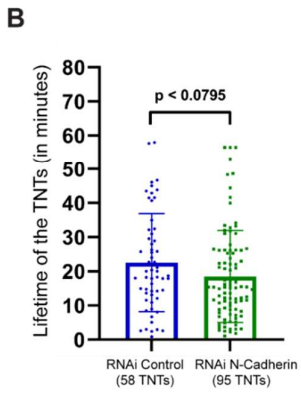
B
Lifetime of the TNTs (in minutes)
p < 0.0795
RNAi Control (58 TNTs)
RNAi N-Cadherin (95 TNTs)

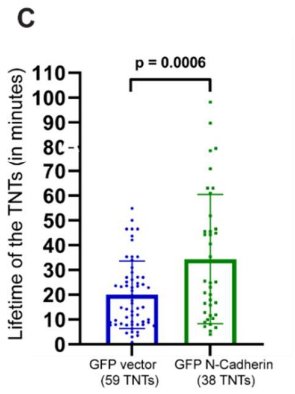
C
Lifetime of the TNTs (in minutes)
p = 0.0006
GFP vector (59 TNTs)
GFP N-Cadherin (38 TNTs)

Figure 3. N-Cadherin modulates the stability of the TNTs.

A. Representative snapshots of TNTs over time from Supplementary Movie 2. Arrowheads are pointing to the TNTs.

B. TNT's average duration in RNAi Control cells or RNAi N-Cadherin. Cells were stained with WGA-488 to visualize the cell membrane and TNTs. The graph represents the average lifetime ± SD of 58 TNTs in RNAi Control (22.5 minutes ± 14.33) and 95 TNTs in RNAi N-Cadherin (18.5 minutes ± 13.44).

C. TNT's average duration in control GFP vector cells or overexpressing N-cadherin. Cells were stained with WGA-647 to visualize the cell membrane and TNTs. Graph represents the average lifetime ± SD of 59 TNTs in GFP vector control cells (20 minutes ± 13.63) and 38 TNTs in GFP N-Cadherin cells (34.3 minutes ± 26.06).

Scale bars in (A) correspond to 10 μm.

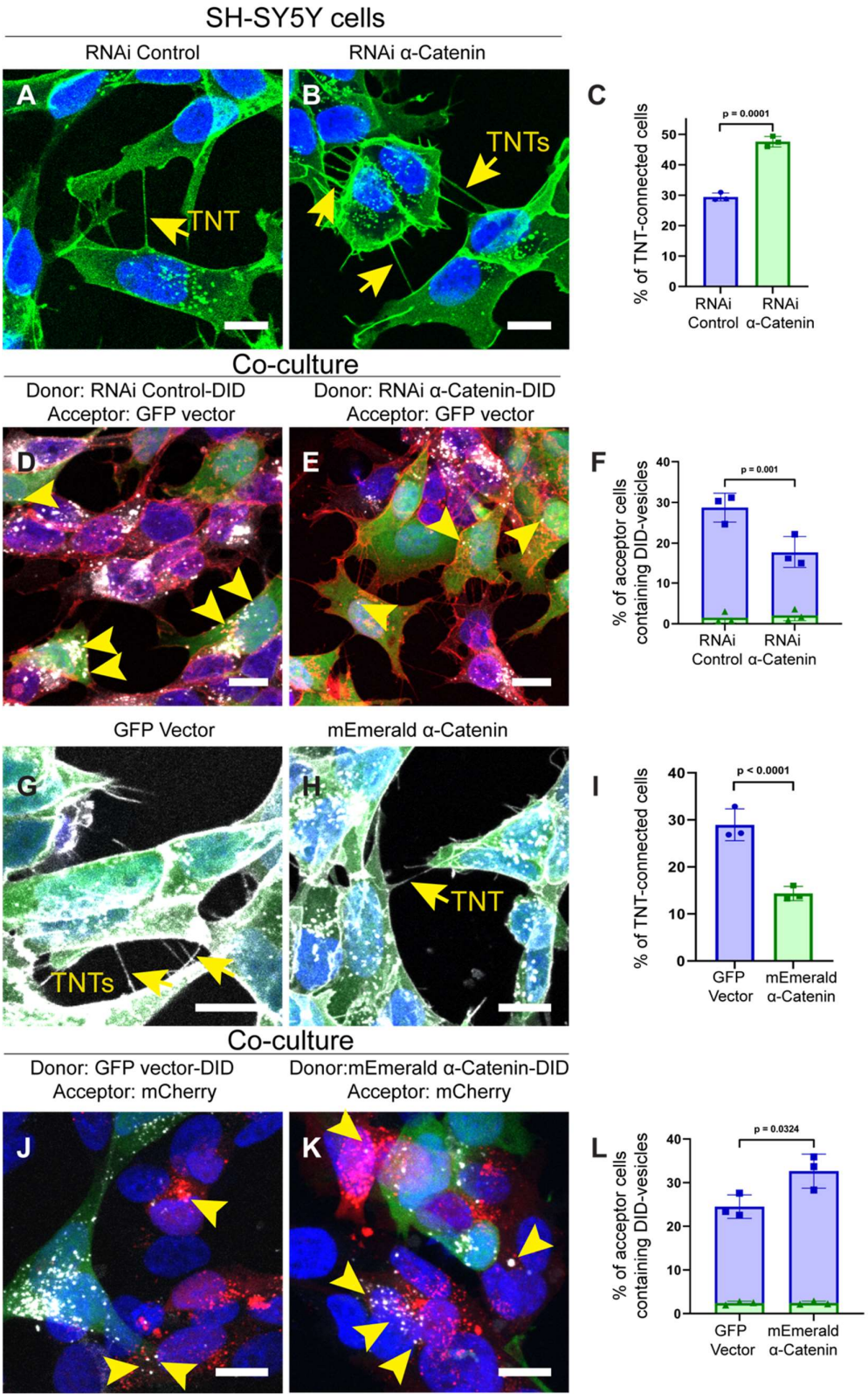
SH-SY5Y cells
RNAi Control
RNAi α-Catenin
A
TNT
B
TNTs
C
p = 0.0001
% of TNT-connected cells
RNAi Control
RNAi α-Catenin
Co-culture
Donor: RNAi Control-DID
Acceptor: GFP vector
Donor: RNAi α-Catenin-DID
Acceptor: GFP vector
D
E
F
p = 0.001
% of acceptor cells containing DID-vesicles
RNAi Control
RNAi α-Catenin
GFP Vector
mEmerald α-Catenin
G
TNTs
H
TNT
I
p < 0.0001
% of TNT-connected cells
GFP Vector
mEmerald α-Catenin
Co-culture
Donor: GFP vector-DID
Acceptor: mCherry
Donor:mEmerald α-Catenin-DID
Acceptor: mCherry
J
K
L
p = 0.0324
% of acceptor cells containing DID-vesicles
GFP Vector
mEmerald α-Catenin

Figure 4. α-Catenin interference and overexpression impact the formation and functionality of the TNTs between SH-SY5Y cells.

A, B. Confocal micrograph showing TNTs between (A) RNAi Control cells, (B) RNAi α-Catenin cells. Cells stained with WGA-488 (green) and DAPI (blue) for the nuclei. The yellow arrows indicate the TNTs connected cells.

C. Graph showing the percentage of TNT-connected cells transfected with RNAi Control non-targeting (29.4% ± 1.31) and RNAi α-Catenin (47.6% ± 1.71), (***p=0.0001 for RNAi Control versus RNAi α-Catenin for N=3).

D, E. Representative confocal images showing 24h co-culture between (D) RNAi Control challenged with DiD-labelled vesicles (donor) and GFP vector cells (acceptor), (E) RNAi α-Catenin with DiD-labelled vesicles (donor) and GFP vector cells (acceptor). Cellular membranes were labelled with WGA-546 (red), nuclei were stained with DAPI (blue). The yellow arrowheads indicate DiD-labelled vesicles detected in the cytoplasm of acceptor cells.

F. Graph showing the percentage of acceptor cells containing DiD-labelled vesicles from the co-cultures in cells transfected with RNAi Control (28.74%± 3.55 for contact-mediated transfer in blue; 1.5%± 1.33 for transfer by secretion in green) or RNAi α-Catenin (17.75%± 3.91 for contact-mediated transfer in blue; 2.08%± 1.35 for transfer by secretion in green). (**p=0.001 for RNAi Control versus RNAi α-Catenin for N=3).

G, H. Confocal micrograph showing TNTs between (G) GFP vector cells, (H) mEmerald α-Catenin cells. Cells stained with WGA-647 (grey) and DAPI (blue) for the nuclei. Yellow arrows indicate TNTs connecting two cells.

I. Graph showing the percentage of TNT-connected cells transfected with GFP vector (29% ± 3.38) and mEmerald α-Catenin (14.3%± 1.49), (***p<0.0001 for GFP vector versus mEmerald α-Catenin for N=3). Cells stained with WGA-647 (gray) and DAPI (blue) for the nuclei.

J, K. Representative confocal images showing 24h co-culture between (J) GFP vector with DiD-labelled vesicles (donor) and mCherry cells (acceptor), (K) mEmerald α-Catenin challenged with DiD-labelled vesicles (donor) and Cherry cells (acceptor). The

yellow arrowheads indicate DiD-labelled vesicles detected in the cytoplasm of acceptor cells.

L. Graph showing the percentage of acceptor cells containing DiD-labelled vesicles from the co-cultures in GFP vector control cells (24.52%± 2.70 for contact-mediated transfer in blue; 2.42%± 0.42 for transfer by secretion in green) against mEmerald α-Catenin cells (32.64%± 3.90 for contact-mediated transfer in blue; 2.45%± 0.39 for transfer by secretion in green). (*p=0.0324 for GFP vector versus mEmerald α-Catenin for N=3).

Scale bars, 10 μm.

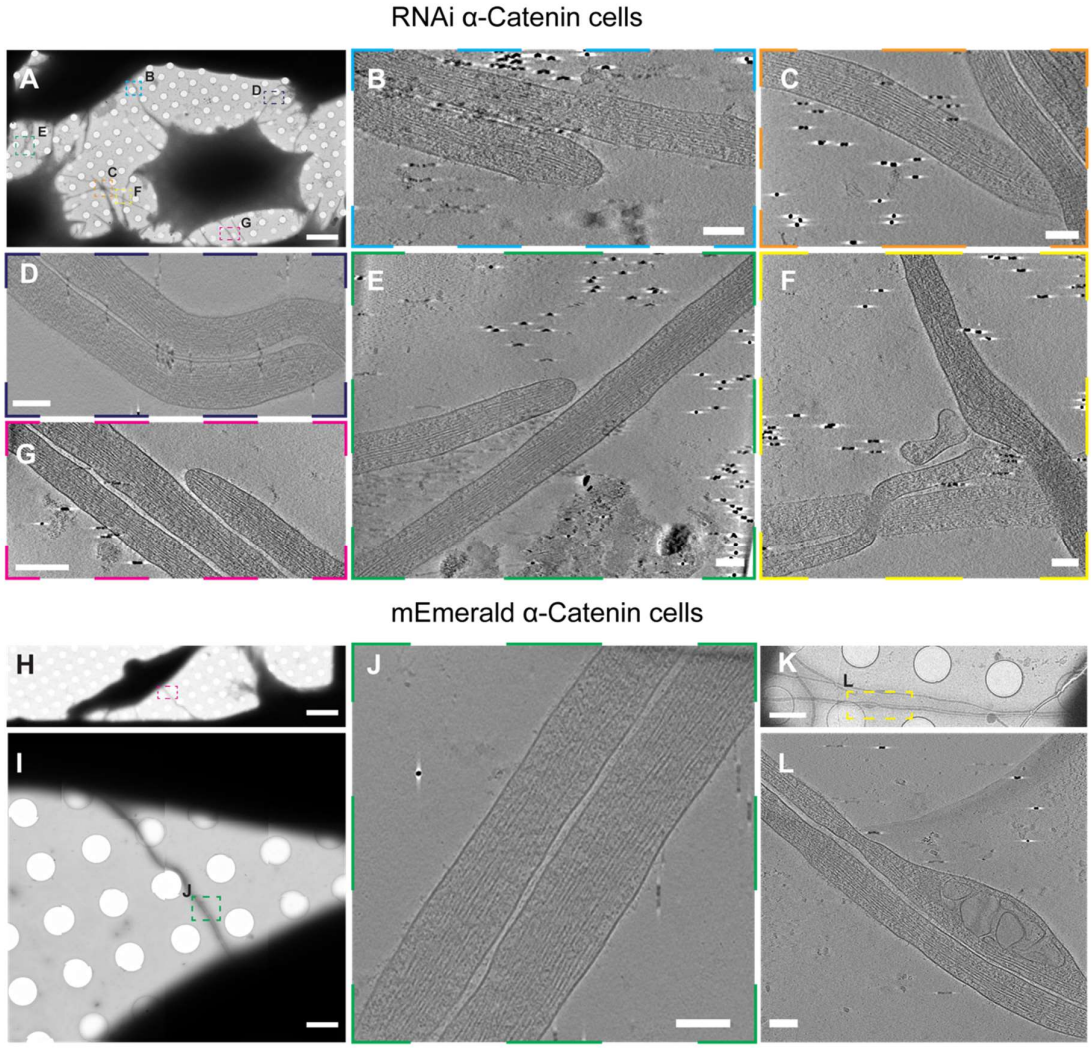

M

	Ultrastructure	
	% iTNTs full extended	% iTNTs tip closed
RNAi α-Catenin cells	34,4%	85,1%
mEmerald α-Catenin cells	72%	28%

Figure 5. Cryo-EM on TNTs formed between SH-SY5Y in which α-Catenin was up or down-regulated.

A-F. Cryo-EM grids were prepared using RNAi α-Catenin cells (A) Low magnification of cryo-EM micrograph showing TNTs connecting RNAi α-Catenin cells. (B-F) High-magnification cryo-tomography slices of the dashed square in (A) showing iTNTs with tip-closed (B, E, G) and iTNTs did not run parallel and braided over each other (C, D, E, F).

H-L. Cryo-EM grids were prepared using mEmerald α-Catenin cells. Low (H) and intermedia (I) magnification of cryo-EM micrograph showing TNT connecting mEmerald α-Catenin cells. (J) High-magnification cryo-tomography slices of the green dashed square in (I) showing parallel and continuous iTNTs. (K) Intermediate magnification of cryo-EM micrograph showing TNT connecting mEmerald α-Catenin SH-SY5Y cells. (L) High-magnification cryo-tomography slices of the yellow dashed square in (K) showing parallel and continuous iTNTs with vesicles inside.

Scale bars (A, H) 10 μm; (I, K) 2μm; (B-F, J, L) 100nm.

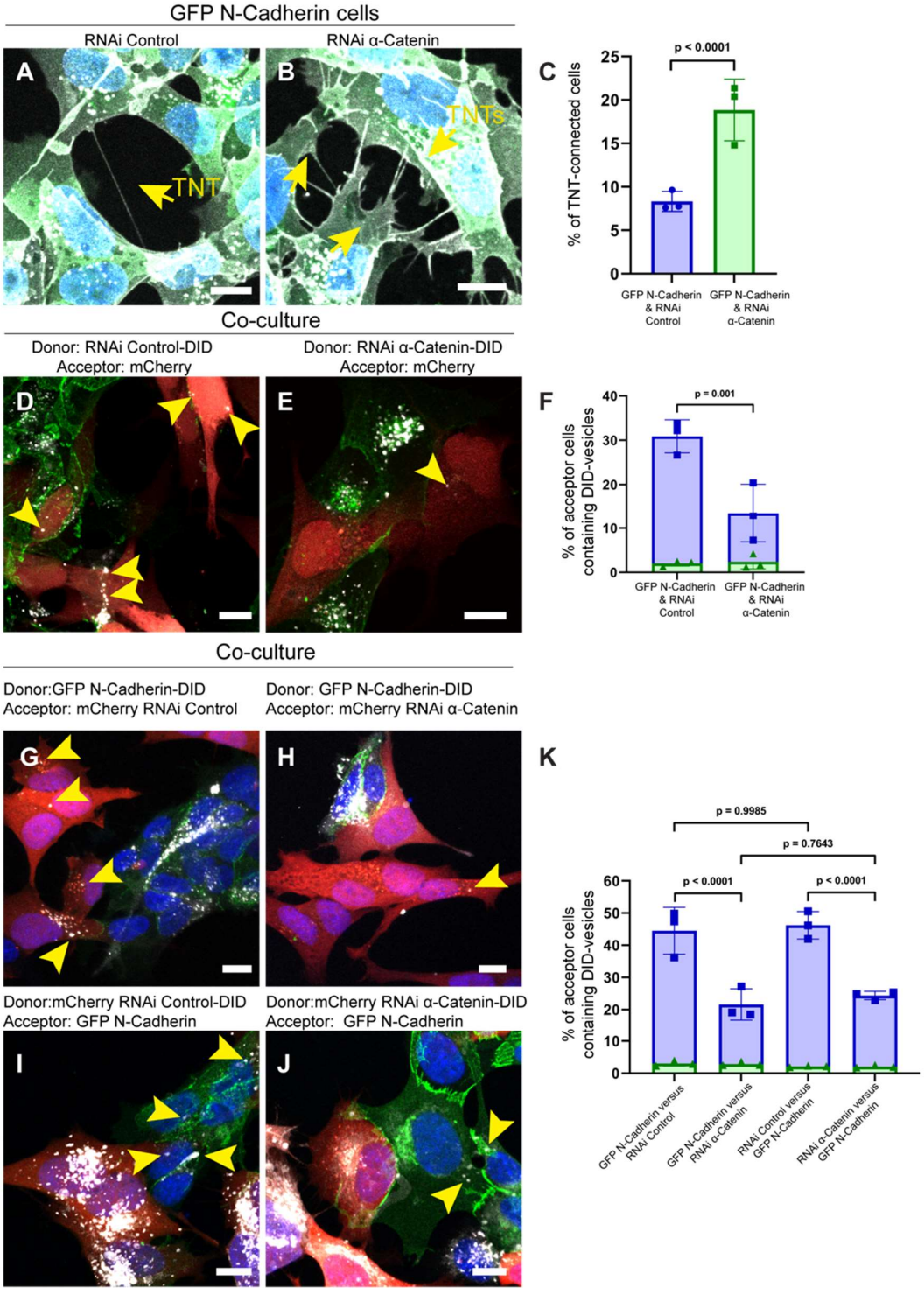
GFP N-Cadherin cells
RNAi Control
RNAi α-Catenin
A
TNT
B
TNTs
C
p < 0.0001
% of TNT-connected cells
25
20
15
10
5
0
GFP N-Cadherin & RNAi Control
GFP N-Cadherin & RNAi α-Catenin
Co-culture
Donor: RNAi Control-DID
Acceptor: mCherry
Donor: RNAi α-Catenin-DID
Acceptor: mCherry
D
E
F
p = 0.001
% of acceptor cells containing DID-vesicles
40
30
20
10
0
GFP N-Cadherin & RNAi Control
GFP N-Cadherin & RNAi α-Catenin
Co-culture
Donor:GFP N-Cadherin-DID
Acceptor: mCherry RNAi Control
Donor: GFP N-Cadherin-DID
Acceptor: mCherry RNAi α-Catenin
G
H
K
p = 0.9985
p = 0.7643
p < 0.0001
p < 0.0001
% of acceptor cells containing DID-vesicles
60
50
40
30
20
10
0
GFP N-Cadherin versus RNAi Control
GFP N-Cadherin versus RNAi α-Catenin
RNAi Control versus GFP N-Cadherin
RNAi α-Catenin versus GFP N-Cadherin
Donor:mCherry RNAi Control-DID
Acceptor: GFP N-Cadherin
Donor:mCherry RNAi α-Catenin-DID
Acceptor: GFP N-Cadherin
I
J

Figure 6. N-Cadherin regulation of the TNTs requires α-Catenin.

A, B. Confocal micrograph showing (A) TNTs between GFP N-Cadherin cells with RNAi Control and (B) TNTs between GFP N-Cadherin cells with RNAi α-Catenin. Cells stained with WGA-647 (gray) and DAPI (blue) for the nuclei. The yellow arrows indicate the TNTs connected cells.

C. Graph showing the percentage of TNT-connected GFP N-Cadherin cells transfected with RNAi Control (8.32% ± 1.15) and RNAi α-Catenin (18.8% ± 3.54), (***p<0.0001 for RNAi Control versus RNAi α-Catenin for N=3).

D, E. Representative confocal images showing 24h co-culture between (D) GFP N-Cadherin RNAi Control with DiD-labelled vesicles (donor) and mCherry cells (acceptor), (E) co-culture GFP N-Cadherin RNAi α-Catenin with DiD-labelled vesicles (donor) and mCherry cells (acceptor). The yellow arrowheads indicate DiD-labelled vesicles detected in the cytoplasm of acceptor cells.

F. Graph showing the percentage of acceptor cells containing DiD-labelled vesicles from the co-cultures in GFP N-Cadherin cells transfected with RNAi Control (43.93%± 2.59 for contact-mediated transfer in blue; 2.24%± 0.22 for transfer by secretion in green) or RNAi α-Catenin (23.53%± 5.23 for contact-mediated transfer in blue; 2.36%± 1.78 for transfer by secretion in green). (**p=0.001 for RNAi Control versus RNAi α-Catenin for N=3).

G, H. Representative confocal images showing 24h co-culture between (G) GFP N-Cadherin SH-SY5Y with DiD-labelled vesicles (donor) and SH-SY5YmCherry cells transfected with RNAi Control (acceptor), (H) co-culture between GFP N-Cadherin challenged with DiD-labelled vesicles (donor) and mCherry cells transfected with RNAi α-Catenin (acceptor).

I, J. Representative confocal images showing 24h co-culture between (I) mCherry cells transfected with RNAi Control with DiD-labelled vesicles (donor) and GFP N-Cadherin cells (acceptor). (J) 24h co-culture between mCherry cells transfected with RNAi α-Catenin challenged with DiD-labelled vesicles (donor) and GFP N-Cadherin cells (acceptor). The yellow arrowheads indicate DiD-labelled vesicles detected in the cytoplasm of acceptor cells.

K. Graph showing the percentage of acceptor cells containing DiD-labelled vesicles from the co-cultures in the conditions described in (G) (44.5%± 7.25 for contact-mediated transfer in blue; 3.04%± 0.80 for transfer by secretion in green), (H) (21.6%± 4.87 for contact-mediated transfer in blue; 2.89%± 0.60 for transfer by secretion in green), (I) (46.21%± 4.29 for contact-mediated transfer in blue; 2.12%± 0.21 for transfer by secretion in green) and (J) (24.37%± 1.29 for contact-mediated transfer in blue; 2.09%± 0.40 for transfer by secretion in green). (***$p<0.0001$ for (G) versus (H) for N=3; ***$p<0.0001$ for (I) versus (J) for N=3; ***$p<0.0001$ for RNAi Control versus RNAi α-Catenin as acceptors for N=3; ns $p=0.9985$ for (G) versus (I) for N=3; ns $p=0.7643$ for (I) versus (J) for N=3)

Scale bars: 10 μm.

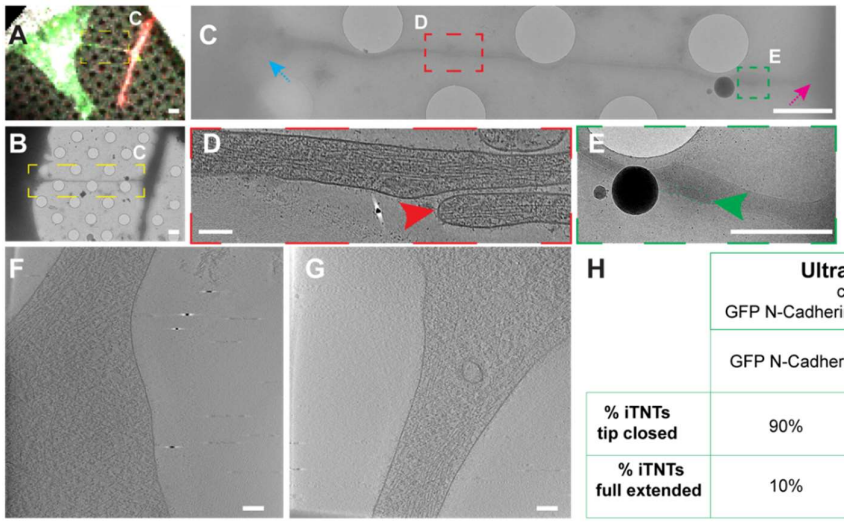

H

	Ultrastructure co-culture: GFP N-Cadherin *versus* RNAi α-catenin	
	GFP N-Cadherin	RNAi α-catenin
% iTNTs tip closed	90%	90%
% iTNTs full extended	10%	10%

Figure 7. Ultrastructure of TNTs between N-Cadherin and α-Catenin KD cells in co-culture.

A. Confocal micrograph showing TNTs between RNAi α-Catenin (mCherry) and N-Cadherin (GFP) cells.

B. Low cryo-EM micrograph showing TNT-connected cells in in the dashed yellow square in (A).

C. Intermedia cryo-EM micrograph of (B).

D. High-magnification cryo-tomography slices corresponding to the red dashed square in (C). E. Intermedia cryo-EM micrograph corresponding to the green dashed square in (C).

F. High-magnification cryo-tomography slices corresponding to the blue arrow in (C).

G. High-magnification cryo-tomography slices corresponding to the pink arrow in (C).

H. Table showing the percentage of TNTs full extended and tip-closed in between RNAi α-Catenin (mCherry) and N-Cadherin (GFP).

Scale bars in (A) 10 μm, (B, C, E) 2 μm, (D, F, G) 100nm.

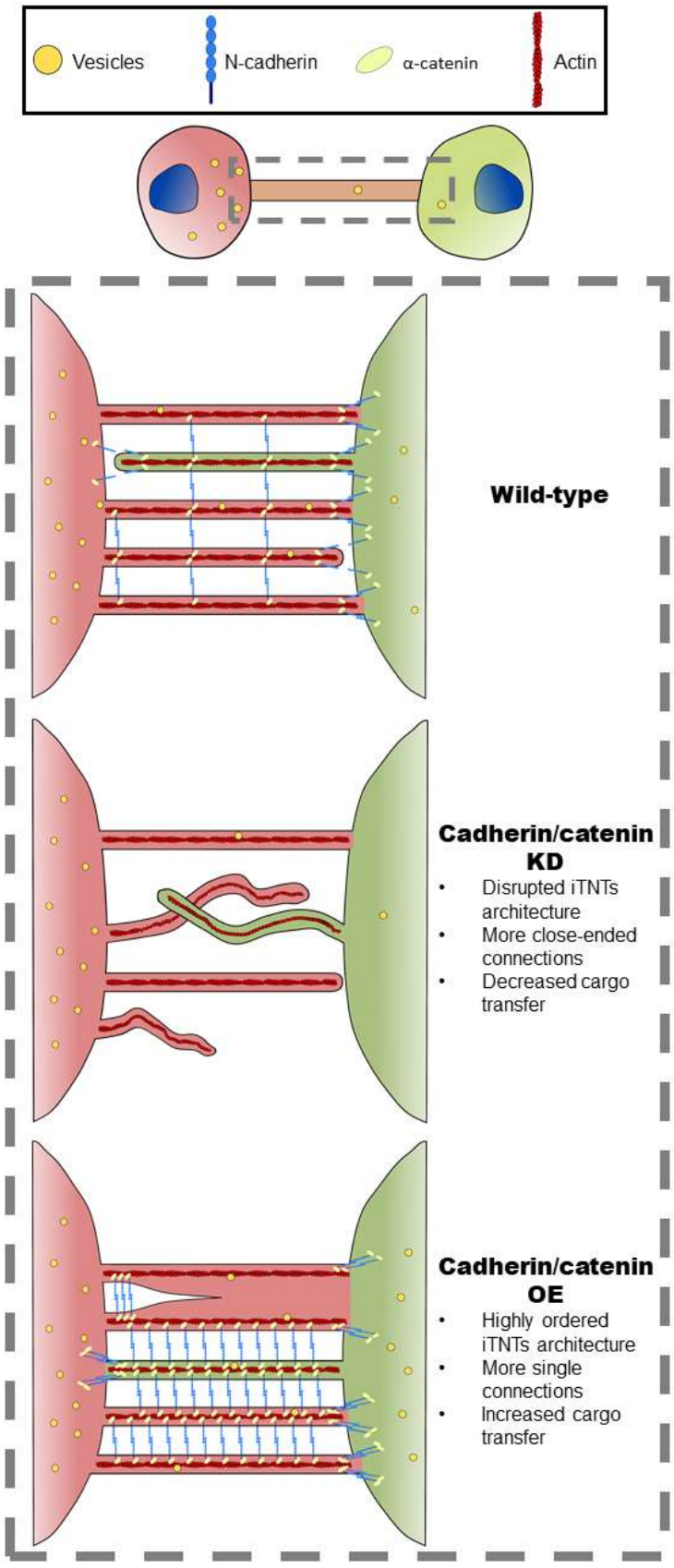
Vesicles
N-cadherin
α-catenin
Actin
Wild-type
Cadherin/catenin KD
• Disrupted iTNTs architecture
• More close-ended connections
• Decreased cargo transfer
Cadherin/catenin OE
• Highly ordered iTNTs architecture
• More single connections
• Increased cargo transfer

Figure 8. Scheme showing the role of the cadherin-Catenin complex in TNTs.

TNTs in wild type cells are formed by individual TNTs (iTNTs) that are held together and ordered by the adhesion complex formed by N-Cadherin and α-Catenin. When N-Cadherin or α-Catenin is downregulated, this structure of iTNTs is no longer ordered and TNT fusion defects occur. On the contrary, overexpressing either of these two molecules will order the iTNT bundle and increase the cargo transfer capacity of TNTs.

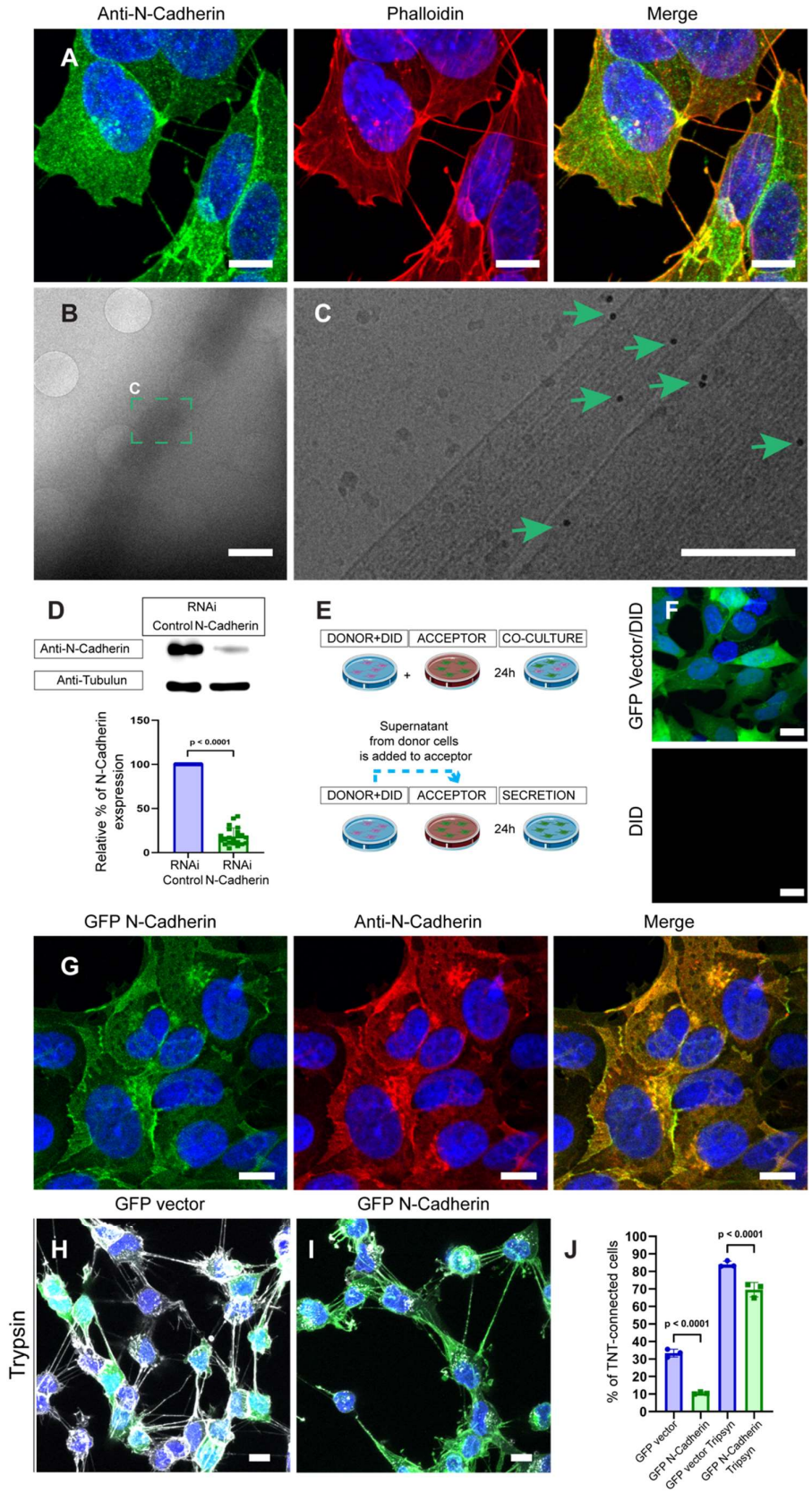
Anti-N-Cadherin
Phalloidin
Merge
A
B
C
D
RNAi
Control N-Cadherin
Anti-N-Cadherin
Anti-Tubulun
Relative % of N-Cadherin exspression
p < 0.0001
RNAi Control N-Cadherin
E
DONOR+DID
ACCEPTOR
CO-CULTURE
24h
Supernatant from donor cells is added to acceptor
SECRETION
F
GFP Vector/DID
DID
GFP N-Cadherin
G
GFP vector
H
I
Trypsin
J
% of TNT-connected cells
GFP vector
GFP N-Cadherin
GFP vector Tripsyn
GFP N-Cadherin Tripsyn

Figure EV1. Confocal and ultrastructure analysis of N-Cadherin in TNTs connected SH-SY5Ycells and co-culture and secretion pipeline.

A. Confocal micrograph of the IF of N-Cadherin showing TNTs connected SH-SY5Y cells. N-Cadherin (green) and actin (red). Cells stained and DAPI (blue) for the nuclei.

B, C. Immunogold EM anti-N-Cadherin (B) low magnification micrograph showing a TNT connecting SH-SY5Y cells, (C) high magnification of green dashed squares in (B) showing the presence of N-Cadherin (green arrows) on iTNTs.

D. Western blot of RNAi Control cells and RNAi N-Cadherin. Membrane was blotted with antibodies anti N-Cadherin and α-tubulin as loading control (top). Graph showing the relative expression of N-Cadherin in RNAi Control cells (100%) and RNAi N-Cadherin (18.1% ± 9.81) (***$p<0.0001$ for RNAi Control versus RNAi N-Cadherin for N=22) (bottom).

E. (top) Description of co-culture experiments: Donor cells stained with DiD label vesicles cells were co-cultured with the acceptor and incubate for additional 24h before to be fixed. (bottom) Description of secretion experiments: the medium from donor cells stained with DID were added on acceptor cells for 24h.

F. Representative confocal micrograph showing acceptor cells (GFP-labeled) that have received supernatant from DiD-labeled donor cells. Cells stained with DAPI (blue) for the nuclei.

G. Immunofluorescence of N-Cadherin (red) in GFP N-Cadherin cells. Cells stained with DAPI (blue) for the nuclei.

H, I. Confocal micrograph showing (E) TNTs between GFP vector cells treated with Trypsin-EDTA, (F) TNTs between GFP N-Cadherin cells treated with Trypsin-EDTA.

J. Graph showing the percentage of TNT-connected cells in GFP vector cells (84.1% ± 1.80) and GFP N-Cadherin cells (69.6% ± 4.13) treated with Trypsin-EDTA (***$p<0.0001$ for GFP vector versus GFP N-Cadherin for N=3). Cells stained with WGA-647 (gray) and DAPI (blue) for the nuclei.

Scale bars in (A, G, H, I) 10 μm, (B) 2 μm, (C) 100nm, (F) 20 μm.

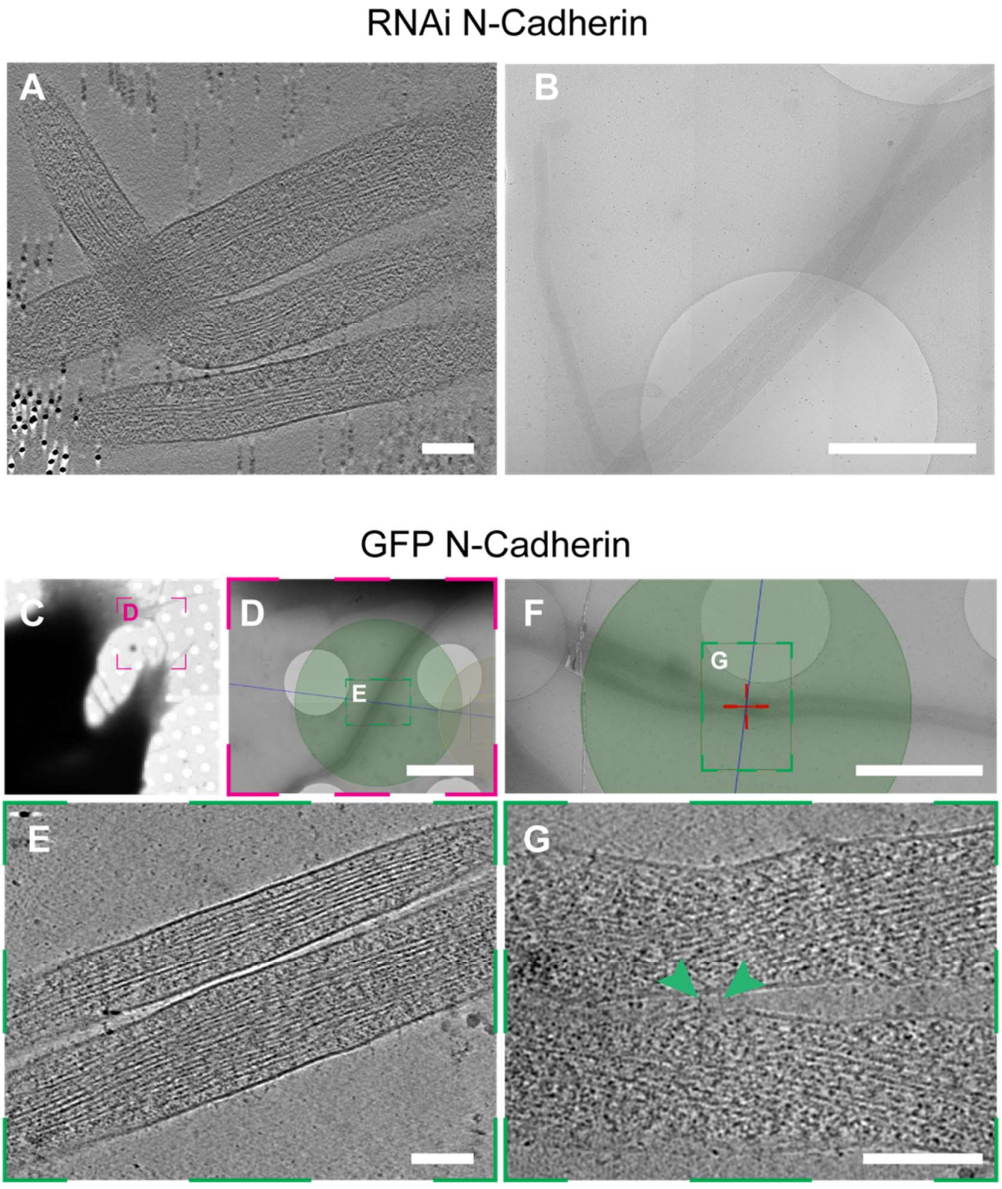

H

	Ultrastructure	
	% iTNTs full extended	% iTNTs tip closed
GFP N-Cadherin cells	58%	42%

Figure EV2. Cryo-EM on TNTs formed between SH-SY5Y in which N-Cadherin was up or down-regulated.

A, B. Cryo-EM grids were prepared using RNAi N-Cadherin cells (A) High-magnification cryo-tomography slices showing iTNTs with tip-closed (B) intermedia magnification of cryo-EM micrograph showing iTNTs connecting RNAi N-Cadherin cells with tip-closed and iTNTs did not run parallel and braided over each other.

C-G. Cryo-EM grids were prepared using GFP N-Cadherin cells. (C) Low (D) and intermedia (E) magnification of cryo-EM micrograph showing TNT GFP N-Cadherin cells. (F) Intermediate magnification of cryo-EM micrograph showing TNT connecting GFP N-Cadherin cells. (G) High-magnification cryo-tomography slices of the green dashed square in (F).

H. Table showing the percentage of TNTs full extended and tip-closed in GFP N-Cadherin cells.

Scale bars (A, E, G) 100nm, (B, F) 2μm.

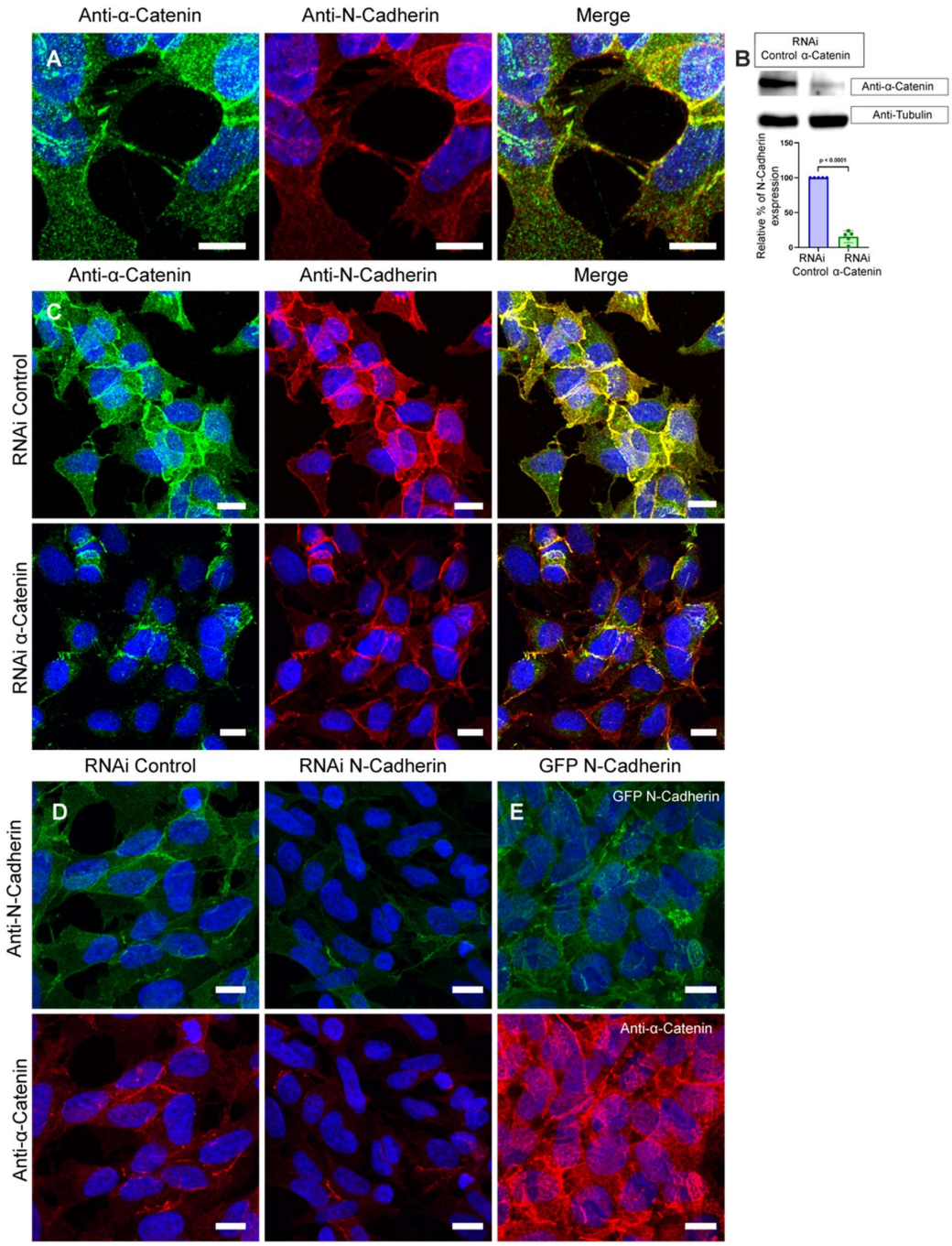
Anti-α-Catenin
Anti-N-Cadherin
Merge
A
B
RNAi
Control α-Catenin
Anti-α-Catenin
Anti-Tubulin
Relative % of N-Cadherin exspression
150
100
50
0
p < 0.0001
RNAi Control
RNAi α-Catenin
C
RNAi Control
RNAi N-Cadherin
GFP N-Cadherin
Anti-N-Cadherin
Anti-α-Catenin
D
E
GFP N-Cadherin
Anti-α-Catenin

Figure EV3. Expression of α-Catenin in RNAi α-Catenin and RNAi N-Cadherin cells.

A. Confocal micrograph showing α-Catenin (green) and N-Cadherin (red) IF in cells connected through TNTs. DAPI (blue) for the nuclei.

B. Western blot of RNAi Control and RNAi α-Catenin cells. Membrane was blotted with antibodies anti α-Catenin and α-tubulin. Graph shows the relative expression of α-Catenin in RNAi Control cells (100%) and RNAi α-Catenin (15.3% ± 8.49) of all the experiments concerning the knock-down of α-Catenin (***$p<0.0001$ for RNAi Control versus RNAi α-Catenin for N=5).

C, D, E. Confocal micrograph of (C) α-Catenin (green) and N-Cadherin (red) IF in RNAi Control and RNAi α-Catenin cells, (D) IF of α-Catenin (red) and N-Cadherin (green) in RNAi Control, RNAi N-Cadherin and (E) GFP N-Cadherin cells. Cells stained with DAPI (blue) for the nuclei.

Scale bars correspond to 10 μm.

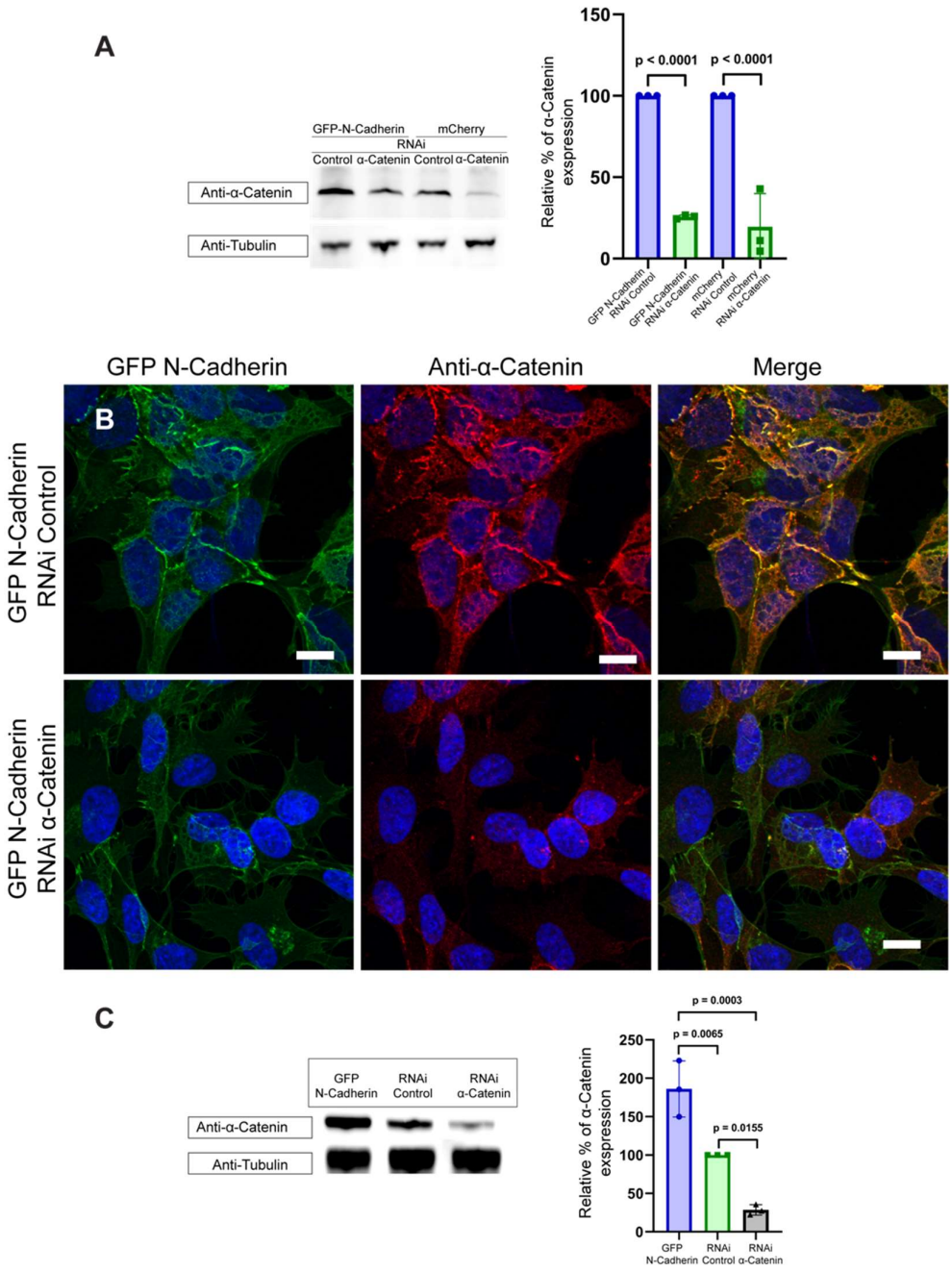
A
GFP-N-Cadherin
mCherry
RNAi
Control
α-Catenin
Control
α-Catenin
Anti-α-Catenin
Anti-Tubulin
Relative % of α-Catenin exspression
150
100
50
0
p < 0.0001
p < 0.0001
GFP N-Cadherin RNAi Control
GFP N-Cadherin RNAi α-Catenin
mCherry RNAi Control
mCherry RNAi α-Catenin
GFP N-Cadherin
Anti-α-Catenin
Merge
B
GFP N-Cadherin RNAi Control
GFP N-Cadherin RNAi α-Catenin
C
GFP N-Cadherin
RNAi Control
RNAi α-Catenin
Anti-α-Catenin
Anti-Tubulin
Relative % of α-Catenin exspression
250
200
150
100
50
0
p = 0.0003
p = 0.0065
p = 0.0155
GFP N-Cadherin
RNAi Control
RNAi α-Catenin

Figure EV4. N-Cadherin OE and α-Catenin KD.

A. Western blot of RNAi Control and RNAi α-Catenin cells in GFP N-Cadherin cells and mCherry cells. Membrane was blotted with anti α-Catenin and α-tubulin antibodies. Graph shows the relative expression of α-Catenin in GFP N-Cadherin RNAi Control cells (100%) and GFP N-Cadherin RNAi α-Catenin (25.65% ± 1.16), and mCherry RNAi Control cells (100%) and mCherry RNAi α-Catenin (19.51% ± 20.47) (***p<0.0001 for RNAi Control versus RNAi α-Catenin for N=3 in GFP N-Cadherin an mCherry cells).

B. Confocal micrograph of α-Catenin (red) IF in GFP N-Cadherin RNAi Control cells and GFP N-Cadherin RNAi α-Catenin cells. Cells stained with DAPI (blue) for the nuclei.

C. Western blot of RNAi Control, RNAi α-Catenin and GFP N-Cadherin cells. Membrane was blotted with antibodies anti α-Catenin and α-tubulin. Graph shows the relative expression of α-Catenin in RNAi Control cells (100%), RNAi α-Catenin (28.6% ± 6.75) and GFP N-Cadherin cells (186.1% ± 36.62) (*p=0.0155 for RNAi Control versus RNAi α-Catenin for N=3, **p=0.0065 for RNAi Control versus GFP N-Cadherin for N=3, **p=0.0003 for RNAi α-Catenin GFP N-Cadherin versus for N=3).

Scale bar (B) 10 μm.

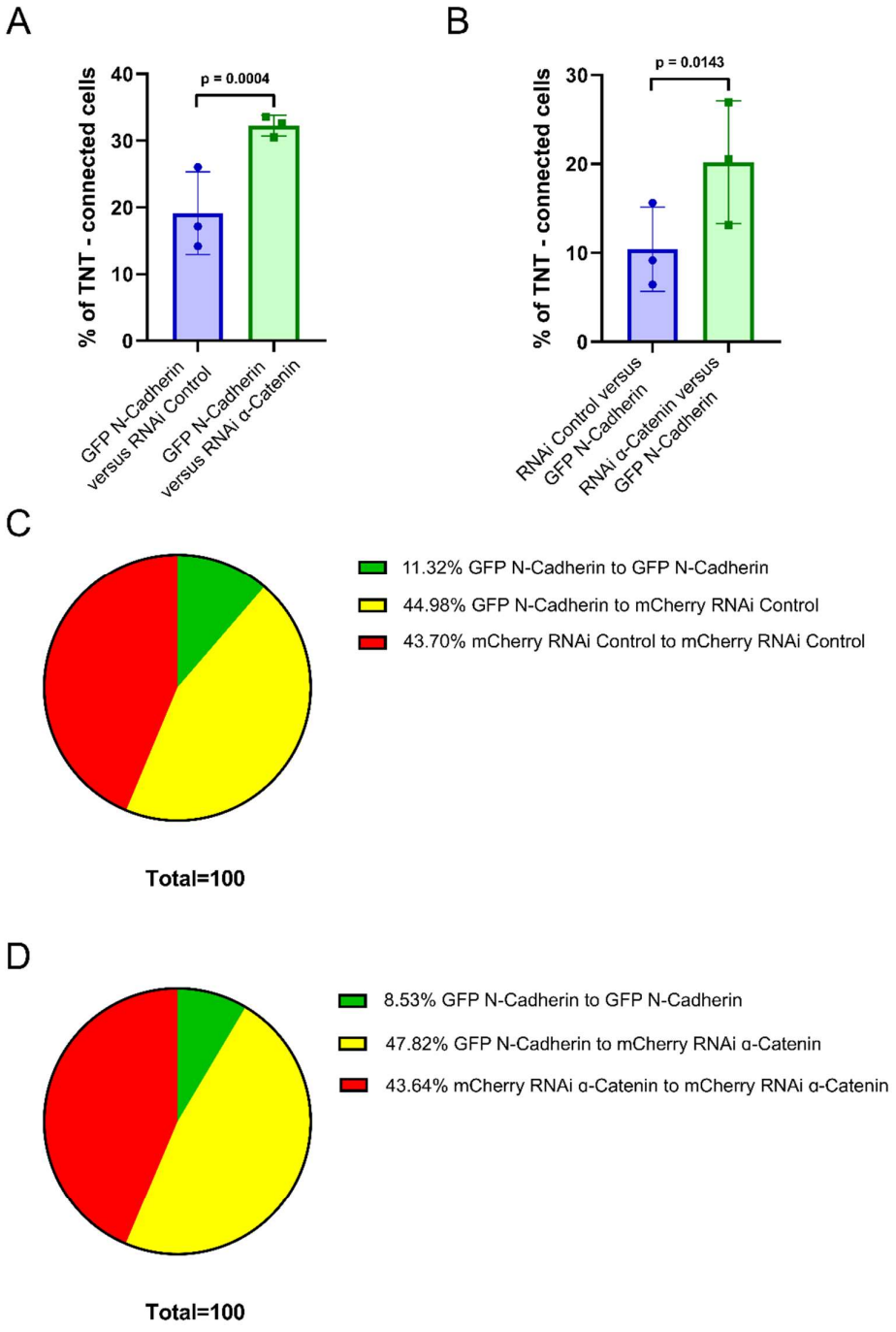
A
% of TNT - connected cells
40
30
20
10
0
p = 0.0004
GFP N-Cadherin versus RNAi Control
GFP N-Cadherin versus RNAi α-Catenin
B
% of TNT - connected cells
30
20
10
0
p = 0.0143
RNAi Control versus GFP N-Cadherin
RNAi α-Catenin versus GFP N-Cadherin
C
11.32% GFP N-Cadherin to GFP N-Cadherin
44.98% GFP N-Cadherin to mCherry RNAi Control
43.70% mCherry RNAi Control to mCherry RNAi Control
Total=100
D
8.53% GFP N-Cadherin to GFP N-Cadherin
47.82% GFP N-Cadherin to mCherry RNAi α-Catenin
43.64% mCherry RNAi α-Catenin to mCherry RNAi α-Catenin
Total=100

Figure EV5. % and distribution of TNT connections in the co-culture of cells OE N-Cadherin versus cells interfered for α-Catenin.

A. Graph showing the total percentage of TNT-connected cells between any kind of cells from the co-cultures in GFP N-Cadherin cells versus cells transfected with RNAi Control (19.1%± 6.19) or RNAi α-Catenin (32.2%± 1.58). (***p=0.0004 for RNAi Control versus RNAi α-Catenin for N=3).

B. Graph showing the percentage of TNT-connected cells by heterotypic connections (connections made by GFP N-Cadherin cells with RNAi Control or RNAi α-Catenin) from the co-cultures in GFP N-Cadherin cells versus cells transfected with RNAi Control (10.4%± 4.73) or RNAi α-Catenin (20.2%± 6.91). (*p=0.0143 for RNAi Control versus RNAi α-Catenin for N=3).

C. Graph showing the distribution of the cells connected in the co-culture of GFP N-Cadherin cells versus cells transfected with RNAi Control. Out of the 100% of the total cells connected, 8.53% corresponds to GFP N-Cadherin cells connected to GFP N-Cadherin cells, 47.82% corresponds to GFP N-Cadherin cells connected to mCherry RNAi Control cells and 43.64% corresponds to mCherry RNAi Control cells connected to mCherry RNAi Control cells.

D. Graph showing the distribution of the cells connected in the co-culture of GFP N-Cadherin cells versus cells transfected with RNAi α-Catenin. Out of the 100% of the total cells connected, 11.32% corresponds to GFP N-Cadherin cells connected to GFP N-Cadherin cells, 44.98% corresponds to GFP N-Cadherin cells connected to mCherry RNAi α-Catenin cells and 43.70% corresponds to mCherry RNAi α-Catenin cells connected to mCherry RNAi α-Catenin cells.

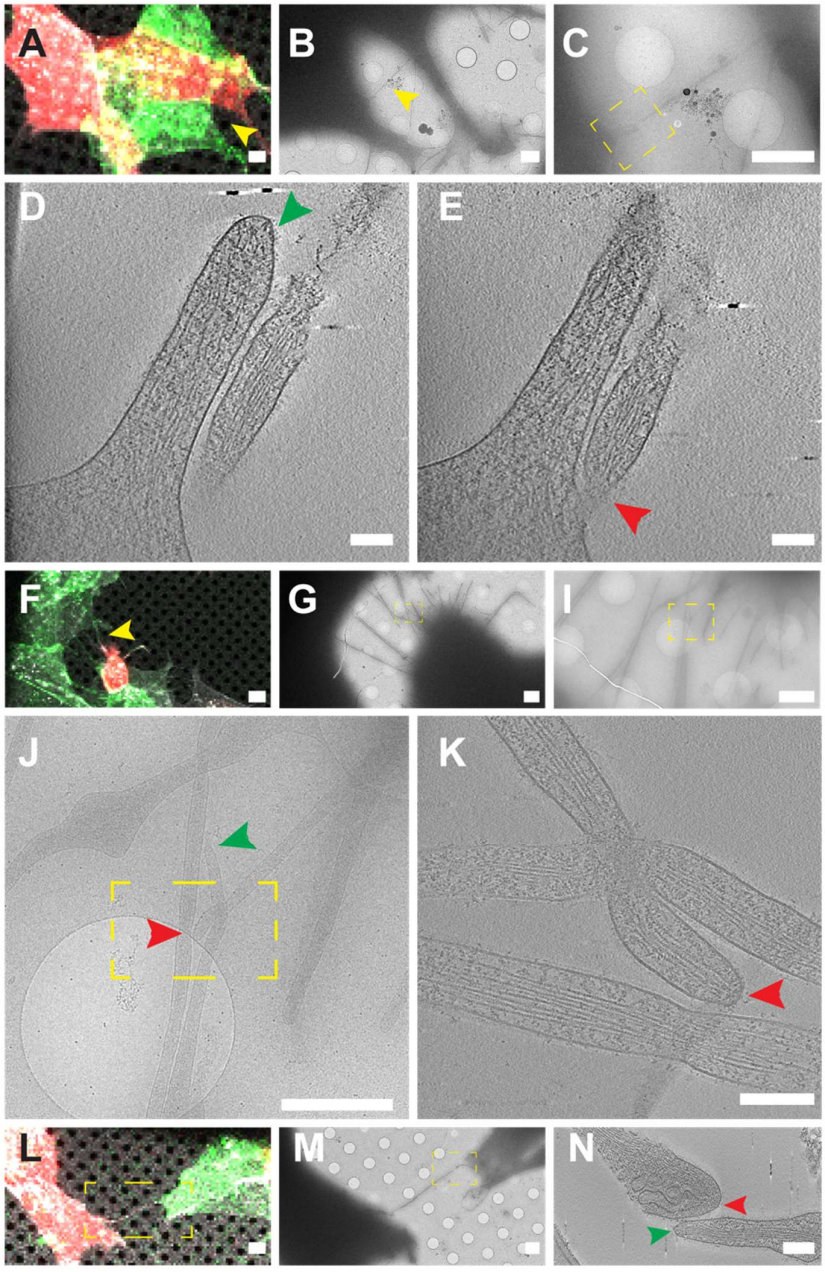
A
B
C
D
E
F
G
I
J
K
L
M
N

Figure EV6. Gallery of ultrastructure of TNTs between GFP N-Cadherin and α-Catenin RNAi. cells in co-culture.

A, F, L. Confocal micrograph showing TNTs between RNAi α-Catenin (mCherry) and N-Cadherin (GFP) cells.

B, G. Low cryo-EM micrograph showing TNT-connected cells in (A), (F), indicated by the yellow arrowhead and TNT in the dashed yellow square in (L).

C, I, M. Intermedia cryo-EM micrograph of (B), (G), (L) respectively.

J. Intermedia cryo-EM micrograph of the yellow dashed square in (I).

D, E. High-magnification cryo-tomography slices corresponding to the yellow dashed square in (C), red arrowhead indicates TNT coming from KD α-Catenin cells and green arrowhead indicates TNT coming from GFP N-Cadherin.

K, N. High-magnification cryo-tomography slices corresponding to the yellow dashed square in (J) and (M) respectively, red arrowhead indicates TNT coming from KD α-Catenin cells and green arrowhead indicates TNT coming from GFP N-Cadherin.

Scale bars in (A, F, L) 10 μm, (B, C, G, I, J, M) 2 μm, (D, E, K, N) 100nm.

Supplementary Movie 1. Trypsin treatment in GFP N-Cadherin cells. Time lapse video of the Trypsin/EDTA treatment in GFP N-Cadherin cells. Grey signal corresponds to GFP N-Cadherin. Time between steps: 16 seconds. Scale bar 10 μm.

Supplementary Movie 2. Stability measurements in already formed TNTs. Example of a time lapse video of already formed TNTs in which their persistency was measured. Cells were stained with WGA to visualize the membrane (grey). Time between steps: 16 seconds. Scale bar 10 μm.

Supplementary Movie 3. Measurement of the stability of the TNTs in RNAi Control cells. Example of a time lapse video of TNT duration in RNAi Control cells. Cells were stained with WGA to visualize the membrane (grey). Time between steps: 19 seconds. Scale bar 10 μm.

Supplementary Movie 4. Measurement of the stability of the TNTs in RNAi N-Cadherin cells. Example of a time lapse video of TNT duration in RNAi N-Cadherin cells. Cells were stained with WGA to visualize the membrane (grey). Time between steps: 15 seconds. Scale bar 10 μm.

Supplementary Movie 5. Measurement of the stability of the TNTs in GFP N-Cadherin cells. Example of a time lapse video of TNT duration in GFP N-Cadherin cells. Cells were stained with WGA to visualize the membrane. WGA signal it is shown on the left panel and GFP N-Cadherin signal it is shown on the right (both in grey). Time between steps: 52 seconds. Scale bar 10 μm.

Supplementary Movie 6. TNT formed *de novo* on top of another TNT in WT cells. Example of a time lapse video of a TNT using a preexisting TNT as a guide to grow

towards an opposite cell. Cells were stained with WGA to visualize the membrane (grey). Time between steps: 16 seconds. Scale bar 10 μm.

Supplementary Movie 7. TNT formed *de novo* by two dorsal filopodia in WT cells. Example of a time lapse video of a TNT formed by the interaction on two dorsal filopodia similar to the formation of "Double Filopodial Bridges". Cells were stained with WGA to visualize the membrane (grey). Time between steps: 20 seconds. Scale bar 10 μm.

Supplementary Movie 8. TNT formed *de novo* by cell dislodgement mechanism in GFP N-Cadherin cells. Example of a time lapse video of TNTs formed by the separation of the cell bodies of two cells in GFP N-Cadherin cells and showing accumulation of GFP N-Cadherin signal at the end of these TNTs. Grey signal corresponds to GFP N-Cadherin. Time between steps: 19 seconds. Scale bar 10 μm.

Supplementary Movie 9. Formation of TNTs and accumulation of N-Cadherin at the end of these structures in GFP N-Cadherin cells. Another example of a time lapse video of TNTs formed by cell dislodgement mechanism in GFP N-Cadherin cells and accumulation of GFP N-Cadherin signal at the tips of these TNTs. Grey signal corresponds to GFP N-Cadherin. Time between steps: 48 seconds. Scale bar 10 μm.

Manuscript 2: Tunneling nanotube composition and regulation by the tetraspanins CD9 and CD81

Premises and summary

Based on the initial results of my other project regarding a possible involvement of NCAD in TNT fusion, this project was conceived under the idea that tetraspanins could be major players on these events. To date, studies focused on the study of molecules that could be positive or negative regulators of TNT biogenesis are very numerous, however and to the best of my knowledge, there are no studies focused on molecules that could work on TNT fusion. As mentioned in the introduction, tetraspanins CD9 and CD81 are involved on in interesting cellular processes that are shared in the participate to TNT formation, such as membrane protrusive activity and membrane fusion. However, there is only one study (*Lachambre et al., 2014*) that has investigated the presence of tetraspanins CD9 and CD81 in TNTs, in which no functional role was assessed. Thanks to the work done by Dr. Christel Brou, using mass spectrometry analysis we discovered that these two tetraspanins were abundantly represented in the TNT fraction. Therefore, we we decided to investigate for the first time the possible role that CD9 and CD81 could have on the formation of new TNTs and on the functionality of these structures. Our hypothesis was that these tetraspanins could have a major role in different processes of TNT formation, such as protrusion initiation by membrane deformation and actin polymerization and/or in the process of fusion.

In the preliminary manuscript presented here, we were able to demonstrate that the composition of the TNTs it is different from other cellular structures such as extracellular vesicles, filopodia or the integrin adhesion complex. The speculated role of CD9 and CD81 on TNTs was confirmed when we showed that CD9, potentially by the clustering of these molecules, could have a role on the initiation of the formation of these protrusions, whereas CD81 could in turn control the fusion of the TNTs to form an open channel with the connected cell. Finally, we have shown that although both tetraspanins have a role in TNT formation, CD9 would intervene in the early steps while CD81 would act later on in the process.

However, in order to fully understand the role of both CD9 and CD81 in the regulation of TNTs, and especially their potential different role in the cell sending or receiving the

TNTs or the specific order in which these proteins act in TNTs, we are currently completing this manuscript with further experiments that will be presented in the perspectives where I will discuss both the results of the experiments and the rationale of the ongoing work.

Contribution

The original idea of investigating the tetraspanins CD9 and CD81 was conceived by Dr. Christel Brou. The final conception of this project was made by Dr. Christel Brou and myself with contributions from our collaborator Dr. Eric Rubinstein and Professor Chiara Zurzolo. The tetraspanins tools (plasmids, antibodies and protocols) were provided by Dr. Eric Rubinstein, who shared his large expertise in the tetraspanin field.

The cell biology regarding the role of CD9 and CD81 in the formation and functionality of the TNTs part was designed, performed and analyzed by myself and the mass spectrometry studies was designed, performed and analyzed by Dr. Christel Brou. Specifically, the experiments corresponding to Figure 1, Figure 2, Figure 8, Supplementary Figure 1, Supplementary Figure 2 and tables 1 to 7 were performed by Dr. Christel Brou, with the rest of the experiments corresponding to the rest of the figures done by me.

The manuscript presented here is a collaborative work of Dr. Christel Brou and myself, corrected and expanded by Dr. Eric Rubinstein and Professor Chiara Zurzolo.

The tetraspanins CD9 and CD81 are major components and regulators of tunneling nanotubes

Authors

Roberto Notario Manzano[1-2], Thibault Chaze[3], Eric Rubinstein[4], Mariette Matondo[3], Chiara Zurzolo[1] & Christel Brou[1]

[1] Membrane Traffic and Pathogenesis, Institut Pasteur, UMR3691 CNRS, 75015 Paris, France
[2] Sorbonne Université, ED394-Physiologie, Physiopathologie et Thérapeutique, 75005 Paris, France
[3] Proteomics Platform Mass Spectrometry for Biology UTechS, C2RT, Institut Pasteur, USR2000 CNRS, 75015 Paris, France
[4] Sorbonne Université, INSERM, CNRS, Centre d'Immunologie et des Maladies Infectieuses, CIMI-Paris, 75013 Paris, France.

Correspondance: chiara.zurzolo@pasteur.fr ; christel.brou@pasteur.fr

Summary

Tunneling nanotubes (TNTs) are open actin- and membrane-based channels, connecting remote cells and allowing direct transfer of cellular material (eg, vesicles, mRNAs, protein aggregates) from cytoplasm to cytoplasm. Although they are important especially in pathological conditions (e.g., cancers, neurodegenerative diseases), their precise composition and their regulation were still poorly described. Here, using a biochemical approach allowing to separate TNTs from cell bodies and from extracellular vesicles and particles (EVPs), we obtained the full composition of TNTs compared to EVPs. We then focused to two major components of our proteomic data, the CD9 and CD81 tetraspanins, and further investigated their specific roles in TNT formation and function. We show that these two tetraspanins have distinct functions: CD9 participates in the initiation of TNTs, whereas CD81 expression is required to allow the functional transfer of vesicle in the newly formed TNTs, possibly by regulating fusion with the opposing cell.

Introduction

Tunneling nanotubes (TNTs) are thin membranous conduits , supported by F-actin that form continuous cytoplasmic between cells over distances ranging from several hundred nm up to 100 µm (Rustom et al., 2004; Sartori-Rupp et al., 2019). They allow cell-to-cell communication by facilitating the transfer of different cargoes directly from cytoplasm to cytoplasm of the connected cells, including organelles (e.g., lysosomes, mitochondria - Abounit et al., 2016; Pinto et al., 2021 -), micro- or mRNAs, pathogens, and misfolded/aggregated proteins (e.g., prion proteins, tau or α-synuclein aggregates) (Vargas et al, 2019; Dilsizoglu Senol et al, 2021; Chastagner et al., 2020). TNTs could play major roles in various diseases, including neurodegenerative diseases or cancers of different types. In addition to cell cultures and tumors explants (Pinto et al 2020), TNT-like connections have been shown to exist in the retina and facilitate cellular material transfer between photoreceptors (Kalargyrou et al., 2021; Ortin-Martinez et al., 2021) or pericytes (Alarcon-Martinez et al., 2020), highlighting the importance of understanding of the biology of these protrusions in order to unravel their possible role(s) in vivo. TNT formation is highly dynamic and appears to be regulated on cellular stresses and actin regulators (Ljubojevic et al., 2020). Two models have been proposed for TNT formation: an actin driven mechanism allowing the growth of a protrusion from one cell into the

other following actin polymerization, and a cell dislodgement mechanism based on the separation of two cells in close contact, that when moving apart leave between them one or multiple TNTs, (Abounit and Zurzolo, 2012). TNTs formed by actin-driven mechanism would be produced by membrane deformation and elongation of the protrusion supported by actin polymerization followed by adhesion and fusion of this protrusion with the opposing cell in order to form a functional TNT. In the case of TNTs formed by cell dislodgement it is conceivable that adhesion and membrane fusion would be the first step and subsequently, with the separation of the cell bodies, the elongation of the protrusion by actin polymerization would take place (Abounit and Zurzolo, 2012; Ljubojevic et al., 2020). However, the mechanism(s) and specific pathways governing TNT formation as well as the molecular components of TNTs are still not known.

In addition to TNTs, one of the major pathways used by cells to transfer of materials over distances is the one mediated by membrane-enclosed vesicles, collectively called Extracellular Vesicles (EVs). EVs are released by all cells, and supposedly up taken by distant recipient cells (Charreau et al., 2021; van Niel et al., 2022) . They can be formed either by direct budding from the plasma membrane, or by secretion of intraluminal vesicles of multivesicular compartments (in which case they are called exosomes). Because of their common functions, their similar diameters, and because TNTs are fragile and easily broken and therefore can be released in cell culture supernatants (where EVs are also found), it has been challenging to distinguish them from EVs in terms of their composition (Gousset et al., 2019). Interestingly two of the common components between EVs and TNTs are members of the tetraspanin family, CD9 and CD81. These are a well-known and widely used markers for EVs (Théry et al., 2018), but a single paper describes their presence in TNTs when overexpressed in T cells (Lachambre et al., 2014).

The tetraspanin family (gathering 33 members) includes small four membrane-spanning domain proteins with two extracellular domains, a large loop harboring a tetraspanin-specific folding and two short cytoplasmic tails. Tetraspanins are involved in various cellular processes like migration, adhesion, signaling, pathogen infection, membrane damage reparation, membrane protrusive activity and cell-cell fusion (Boucheix and Rubinstein, 2001; Monk and Partridge, 2012; Termini and Gillete, 2017; Jouannet et al., 2016; Huang et al., 2022; Bari et al., 2011; Huang et al., 2018; Le Naour et al., 2000). Their function is linked at least in part to their ability to interact with other transmembrane

proteins, forming a dynamic network or molecular interactions referred to as the tetraspanin web or Tetraspanin-enriched microdomains (TEM). Inside this "web", the tetraspanins CD9 and CD81 directly interact with the Ig domain proteins CD9P1 (aka EWI-F, encoded by the PTGFRN gene) and EWI-2 (encoded by the IGSF8 gene), which have an impact on several fusion processes (Charrin et al., 2013; Cohen et al., 2022; Whitaker et al., 2019) and that may connect the tetraspanin web with the actin cytoskeleton through the Ezrin-Radixin-Moesin (ERM) complex (Sala-Valdés et al., 2006). However, despite their localization in TNTs and these intriguing properties, CD9 and CD81 specific roles in the formation or function of TNTs has not been investigated.

With the goal of identifying structural components of TNTs, and possibly specific markers and regulators of these structures, we established a protocol of TNT isolation from U2OS cultured cells, allowing to separate TNTs from extracellular vesicles and particles (EVPs) and from cell bodies. We obtained the full composition of TNTs, compared to EVPs. As CD9 and CD81 were major components of TNTs, based on the previous data outlined above, we further studied their specific roles in TNT formation and ability to transfer cellular material using human neuronal SH-SY5Y, a well-known cell model to study functional TNTs. Our data indicate that they have different functions and are respectively regulating two successive steps of the formation of TNTs, initiation of protrusion and membrane fusion.

Results

Purification of TNTs and EVPs

In order to isolate TNTs, we used U2OS cells because they are robustly adherent cells exhibiting few long protrusions, but are able to grow TNTs and transfer cellular material through these bridges (Figure S1A, B and Pergu et al., 2019). Additionally, we took advantage of the fact that TNTs are very sensitive to mechanical stress as they are not attached to substrate (Pontes et al., 2008; Rustom et al., 2004). We made use of cells stably expressing either H2B-GFP (labeling nuclei), actin chromobody-GFP (a live actin-detecting probe that does not affect actin dynamics (Melak et al., 2017)), GFP-CD9 or no fluorescent protein (Wild-Type; WT cells), actin-chromobody and CD9 both labeling TNTs (Figure S1A and B). First, extracellular vesicles and particles (EVPs) were directly collected from the cell culture supernatant and enriched following a standardized

procedure (Théry et al., 2018, Cocozza et al., 2020, Théry et al., 2006, Alvarez et al., 2012 and see Figure 1A). Next, after adding a small volume of PBS to the remaining cells, the cell flasks were heavily shacken in order to break the TNTs that were then isolated from the supernatant by ultracentrifugation after elimination of floating cells by low-speed centrifugations and filtration (see workflow on Figure 1A).

Four independent preparations of TNTs and EVPs from the same cell cultures (Figure 1B), were analyzed. To validate whether our protocol for preparing TNTs and TNTs vs. EVPs was accurate, we first tested if the crude preparations (before ultracentrifugation, Figure 1A) contained particles of expected sizes, and if they were fluorescent accordingly to the expected localization of the fusion proteins that were expressed by using NanoFCM technology, which allows to measure simultaneously a nanoparticle population for size, size distribution, concentration and fluorescent content on a single nano-flow cytometer. As shown in Figure 1C and S1C-E, both types of preparations (EVPs and TNTs) contained particles, which were differently labeled depending on the fluorescent protein expressed. The mean diameter of both types of structures was very similar (around 60 nm, Figure S1C, D), ranging from 40 to more than 100nm. The sizes of the particles as well as their concentrations were the same in all cell lines Figure S1D, E), showing that the expression of the various constructs did not significantly affect cell behaviors regarding TNTs or EVPs. However, when looking at the relative percentage of GFP-positive particles, depending on cell type and on TNT vs. EVP purifications, we observed that TNTs and EVPs both expressed GFP-CD9, as expected, to a significant amount (28 and 12 % of positive particles respectively, Figure 1C), showing that these particles were membrane-enclosed. Actin-chromobody-GFP was mostly present in TNT fraction (38%), in accordance with actin being detected in TNT fraction by WB (Figure S1E). In contrast, Actin-chromobody-GFP was barely detected in EVPs (0.2%), suggesting that both fractions are different and exhibit actin content in accordance with their identity. Finally, H2B-GFP was present in a very minor part of the particles (4.8 % for EVPs, 1.75% of TNTs), showing that contaminations with cell debris or nuclei were limited, and therefore validating our protocol. To further document the relative enrichment of some organelle markers throughout the isolation procedure, as compared to whole cell extracts (WCE), we performed Western blots (Figure 1D). TNTs and EVPs both expressed CD9 and CD63, and not the Golgi protein GM130, whereas tubulin (shown to partially label TNTs

on Figure S1A) was only detected in TNT fraction, further confirming that the procedure could differentially enrich the fractions in TNT and EVP content.

Analysis of TNTome

To obtain a full and accurate picture of U2OS TNT content (called TNTome), we made 12 independent preparations of TNT fractions (in red in Figure 1A), each starting from about 20x106 cells, and analyzed by LC-MS/MS. 1177 proteins were identified in at least 9 preparations (table S1). We first observed that proteins expected to be in TNTs, based on previous studies (and Figure S1A), like actin, Myosin10 (Gousset et al., 2013), ERp29 (Pergu et al., 2019), tetraspanins CD9 and CD81 (Lachambre et al., 2014) or N-cadherin (Sartori-Rupp et al., 2019, Chang et al., 2022) were indeed present in TNTome.

Less than 100 nuclear proteins, i.e. less than 8% were found (according to GO Cellular component analysis), which could result from partial contamination with cellular debris or dead cells. This is in accordance with nanoFCM results, were H2B-GFP positive particles were 4% of actin-chromobody-GFP positive ones.

The 1177 proteins have been ranked in 4 quartiles depending on their relative abundancy (average iBAQ), highlighting the enrichment of specific factors when considering gene ontology (table S1, Figure 2A). These factors could be components not only of TNTs (membrane factors, cytoskeleton), but also of the material that was circulating or in the process of being transferred at the time when TNTs were broken and purified. It could be why mitochondrial (8% of the total), lysosomal/endosomal or other vesicle proteins are listed. As highlighted by Proteomap analysis (Figure 2A), TNTome is rich in RNA-associated proteins (ribosomes, translation factors, Ribonucleoproteins), in accordance with TNTs being able to transfer micro and mRNAs (Haimovitch et al., 2021, Kolba et al., 2019).

A major group of proteins of interest were related to cytoskeleton (15%, i.e. 172 proteins, see table S2, analysis of GO terms, cellular components), As shown by STRING functional network representation, actin-related proteins were majority (Figure 2B, orange nodes) compared to microtubule-related (green nodes) or intermediate filament-related proteins (blue nodes). This was in accordance with the definition of TNTs, mainly supported by actin cytoskeleton (Rustom et al., 2004). However, recent work has shown

that TNT cytoskeletal composition could vary as in addition to actin they could contain microtubules as in some cancers (Figure S1A and Pinto et al., 2020; Lou, 2020), and also cytokeratins like in the case of urothelial cells (Resnik et al., 2018; Resnik et al., 2019).

When looking at membrane proteins, analysis of the GO terms (cellular components) of the TNTome classified around 500 proteins as membrane-related, 64 of which being strictly integral plasma membrane (see table S3 and Figure 2C). Among the latter, N-cadherin and other cadherin-related proteins (green nodes), as well as known N-cadherin interactors like□□-catenin, were found. We also noticed the presence of various integrin subunits, including ITGB1 and various alpha subunits (orange nodes). Possibly some focal adhesion membrane domains could have been disrupted by mechanical dissociation of TNTs. However, TNTome had only a partial overlap with integrin adhesion complexes (Horton et al., 2015, Figure S2A and tab1 of table S4) and with the consensus adhesome (Figure S2B, tab2 of table S4). In addition very important proteins of the focal adhesions, like Paxillin, GIT2, Parvins and PINCH1 were not in the TNTome, making unprobable focal adhesion being isolated in TNT preparations. Together with immunofluorescence confirming integrin labeling of TNTs (Figure S2C), it suggested that some integrin complexes could play specific roles in TNTs. We also analyzed whether TNT preparation could be containing filopodia, since they are similar protrusions grown by the cells. Despite common proteins described as core filopodia proteins in U2OS cells (like MyosinX, ITGA5, TLN1, FERMT2, MSN, LIMA1), TNTome was devoid of others (Myo15A, TLN2, PARVA, ITGB1BP1, see Jacquemet et al., 2019), making less probable an important contamination of TNTs with filopodia during the preparation. Together, these results suggested that the proteins identified in TNTome represent a specific composition of these protrusions, and not a pool of other types of protrusions which could have contaminated the preparation. As a further proof that TNTome was not a small proportion of cell extract or cell membranes, we observed that the integrin subunits in TNTome were not a perfect match of integrin U2OS content, since U2OS cells express ITGB5, B2, B4 and A9, A4 according to Beck et al., 2011 and we could detect ITGB4 and A4 by WB (Figure S2D). We also looked whether the TM proteins of the TNTome were the most abundant TM proteins of U2OS cells. We compared the rank in TNTome to the protein concentration (Beck et al., 2011) or to the level of RNA (Lundberg et al., 2010). Whether some factors are indeed very well expressed in U2OS cells (for instance ITGB1, SLC3A2, basigin, CLIC channels) and ranked in the first quartile of TNTome,

others are weakly expressed in U2OS cells (N-cadherin for instance). In addition, some cell surface proteins are highly expressed in U2OS cells (according to their corresponding RNA level Lundberg et al., 2010), but not detected in the TNTome, like SLC2A11 (Glucose transporter), APP, ITM2C, TNFR. As shown by WB in Figure S2D, we could detect membrane or membrane-associated proteins in U2OS cell extracts that were not listed in TNTome, like ITGB4, A4, EGFR, Cx43, and APP (Jouannet et al.,2016). Likewise, some proteins of very low abundancy in cells were found in TNTome (CALML5 for example), maybe reflecting a specific role in TNT formation. We also observed that the relative abundance of some proteins in TNT fractions compared to WCE (Figure S2E) was variable. As examples, CD9 and especially ADAM10 seemed to be relatively abundant in TNTs compared to WCE, whereas ITGB1 or ANXA2 TNT/WCE ratios were much lower. Altogether, these data suggested that TNT membrane composition was not just a fraction of cell surface membrane proteins, but rather that some proteins were excluded, other more present. This first consolidated our TNT purification procedure, and second highlighted that specific mechanisms and factors should be at stake to grow and maintain TNTs.

Comparison of the content of TNTs and EVPs

Because both EVs and TNTs have similar characteristics (membrane-formed, diameter, ability to transfer material to remote cells), we wanted to analyze their respective composition when prepared from the same cell cultures, following the full protocol schematized in Figure 1A. 4 independent and parallel preparations of TNT vs EVPs (providing from the same cell cultures) were compared. 961 proteins in total were identified at least in 3 of the 4 TNT and EVP preparations. When keeping TNT proteins that were also present in the 1177 list of TNTome (in 9 TNT preparations over the total of 12), a total of 801 proteins were finally differentially analyzed. Our results showed a different composition of TNTs and EVPs, although common factors represent 75% of them (see volcano plot in Figure 2D). Interestingly, 174 proteins were specific for TNTs when compared to EVPs (see tab1 of table S5), the ER chaperone ERp29, previously shown to be required for the formation of TNTs (Pergu et al., 2019), being among the most abundant. When discarding organelle-associated or translation linked proteins, 89 proteins remained in this TNT-only list (table S5, tab2, constitutive). 20% of them were involved in cytoskeleton, including the positive regulator of TNTs Myosin10 (Gousset et

al., 2013). When analyzing the proteins differentially abundant in TNT vs. EVPs (Figure 2D and table S6), we noticed the enrichment of TNTs in cytoskeleton-related proteins, especially actin, compared to EVPs. The EVP>TNT group included CD9, in perfect accordance with nanoFCM results (Figure 1C), as well as CD63, whereas CD81 was in the one described just above (TNT=EVP). Of note, CD9 and CD81 were among the more abundant transmembrane proteins of TNTs. Their interacting partners CD9P1 and EWI2 (respectively PTGFRN and IGSF8 in Figure 2C) as well as CD151 (a tetraspanin that directly associates with the integrins A3B1 and A6B1) and the two metalloproteases ADAM9 and ADAM10 were also identified (table S1 and yellow nodes in String representation of Figure 2C). The presence of some of the factors (CD9, CD81, ITGB1, CD151) described above in TNTs was confirmed by immunofluorescence in U2OS and SH-SY5Y cells (Figures S1A and S2C, Figure 3A).

Regulation of TNT formation by CD9 and CD81

To study the role of CD9 and CD81 in the formation of TNTs, we decided to use a cellular model in which TNT structure function has already been largely investigated, SH-SY5Y cells. These human neuronal cells form many TNTs (about 30 % of WT cells are connected by TNTs), which are easily visualized and distinguished from other protrusions by fluorescent imaging (Sartori-Rupp et al., 2019, Chastagner et al., 2020, Pepe et al., 2022).

First, we assessed the presence of CD9 and CD81 in TNTs by immunofluorescence (IF) of non-permeabilized cells using monoclonal antibodies against the large extracellular loop. CD9 and CD81 were overlapping throughout the plasma membrane and on TNTs, which were defined morphologically as protrusions containing actin, connecting two cells and not attached to the substrate (Figure 3A, CD9 in green and CD81 in red, yellow arrowheads indicate TNTs). We then knocked-out (KO) CD9 and/or CD81 by infecting SH-SY5Y cells with lentiviral CRISPR vectors targeting the corresponding genes. Western-blot analysis confirmed the lack of CD9 and/or CD81 expression in these cells (Figure S3A). CD9 KO cells, but not CD81 KO cells, showed a significant reduction of the percentage of TNT-connected cells compared to WT cells (Figure 3B&C). The % of TNT-connected cells was even lower in the double KO cells (named CD9&CD81 KO hereafter). The role of CD9 in TNT formation was confirmed by the finding that CD9 stable overexpression (OE) resulted in a significant increase in the % of TNT-connected

cells (Figure 3 D&E). Consistently with KO result, CD81 stable OE did not change the % of TNT-connected cells.

CD9 and CD81 in TNT function

The next and complementary step was to evaluate the possible influence of CD9 and CD81 on the functionality of TNTs. TNT functionality is understood as the intrinsic capacity to allow the transfer of different types of cellular material through the open channel formed between the cytoplasm of different cells. This was monitored by quantifying by flow cytometry the transfer of labeled vesicles between two different cell populations (¨donors¨ for the cells where vesicles were first labeled and ¨acceptors¨ for the cells that received the vesicles) (Abounit et al., 2015). A similar gating strategy was applied to all experiments (see panels corresponding to each experiment in Figures S4, S5), and the vesicle transfer through any mechanism other than cell contact-dependent was ruled out in all experiments by analyzing secretion controls, where the two cell populations were cultured separately (Figures S6, S7). Therefore, the amount of transferred vesicles occurring mainly through cell-contact-dependent mechanisms is an indirect way of monitoring TNT functionality that has to be analyzed with regard to TNT apparent number.

First, we co-cultured WT, CD9 KO, CD81 KO or CD9&CD81 KO donor cells versus WT acceptor cells expressing GFP (as schematized in Figure 4A). Consistently with the decrease of the % of cells connected by TNTs, CD9 KO cells showed a significantly decreased % of acceptor cells containing donor's vesicles compared to WT cells (Figures 4A and S4 to S7 panels A). On the other hand, despite having no effect on the number of TNTs, CD81 KO caused a significant reduction in vesicle transfer between cells. CD9&CD81 KO cells showed a dramatic decrease of vesicle transfer, consistent with the high decrease in the % of TNT-connected cells. Next, we performed a co-culture using tetraspanin OE cells as donor cells (Figure 4B). CD9 OE as well as CD81 OE significantly increased vesicle transfer compared to WT cells (Figures 4B and S4 to S7, B panels). Together with TNT countings above, these results suggested that CD9 might play a role in the formation or maintenance of TNT and that CD81 might play a complementary and/ or partially redundant role. To further investigate the effect of the two tetrasapanins on TNT function we analyzed the impact of the KO of CD9 or CD81 in acceptor cells. To this aim, we placed WT cells with stained vesicles as donors in co-culture with acceptor

cells expressing GFP that were either WT, CD9 KO or CD81 KO (Figure 4C). Surprisingly and contrary to the KO in donor cells, CD9 KO and CD81 KO cells as acceptors greatly increased the vesicle transfer (Figures 4C and S4 to S7, panels C). Altogether these results showed a positive effect of these two tetraspanins on formation and functionality of TNTs in the sending cell, but a negative effect in the receiving cell.

CD9 clustering and TNT formation

Knowing that the molecular conformation of CD9 molecules can induce membrane curvature (Bari et al., 2011; Umeda et al., 2020) and that induced clustering of CD9 can be achieved by treating cells with specific antibodies against this protein (Nydegger et al., 2006; Khurana et al., 2007) that could lead to the formation of protrusions such as microvilli (Singethan et al., 2008), we postulated that CD9 could be involved in the initial steps of formation and asked whether promoting CD9 clustering could affect TNT number and function. Incubation for 2 hours of WT SH-SY5Y cells with anti-CD9 antibody (CD9 AB), but not a control antibody (CTR AB), caused the presence of CD9 in patches on the plasma membrane suggesting that CD9 molecules (and CD81) were incorporated in multimolecular complexes that were clustered together by the antibodies. Furthermore, this antibody treatment for 2 hours in 24 hours cocultures (Figure 5B) lead to an increase in the % of TNT-connected cells (Figure 5C) that correlated with an increase on the vesicle transfer (Figure 5D). These data may suggest that CD9-enriched sites could serve as initiation platforms for TNTs or participate in the stability of these structures.

When repeated these set of experiments on CD81 KO cells, neither CD9 clustering (Figure 5E) nor the increase in the number of TNTs (Figure 5F&G) was affected by the lack of CD81. However, this increase in TNTs was not accompanied by an increase in vesicle transfer (Figure 5F&H) suggesting that CD9 does not require CD81 to form/stabilize TNTs, but that if CD81 is not present, TNT functionality is compromised.

Pathway of CD9 and CD81 in the regulation of TNTs

All the above results pointed out that both CD9 and CD81 participate in the regulation of the TNTs, however maybe not acting at the same steps of TNT formation. To further address which of these two proteins acts first we decided to KO one of them in cells that

stably overexpressed the other (Figure S3B). Whereas CD9 OE + CD81 KO cells exhibited the same % of cells connected by TNTs as CD9 OE cells (Figure 6A&B), we found a significant decrease when comparing CD81 OE + CD9 KO cells to CD81 OE cells. Consistently with the number of TNTs, the KO of CD81 on CD9 OE cells did not affect vesicle transfer compared to CD9 OE cells (Figures 7C and S4 to S7, panels D), but the KO of CD9 on CD81 OE cells significantly decreased the transfer compared to CD81 OE cells. These results were in accordance with CD9 acting first in the regulation of TNTs, and partially compensating the lack of CD81 when overexpressed. Instead CD81 OE could be counteracted by CD9KO, which would impair a step upstream CD81 action.

Discussion

Composition of TNTs is unique

Thanks to a newly established procedure in U2OS cells, we were able to reproducibly isolate a cellular fraction from cell bodies and from EVPs, and analyze their content by mass spectrometry. The physical characteristics as well as the proteome analysis of this fraction (called TNTome) suggested that it could be enriched in TNTs with minor contaminations with other cell protrusions material. Therefore, analysis of the TNTome could give valuable information on core components, traveling material or regulatory factors of TNTs. Our results regarding the unique composition of TNTs were in accordance with those obtained by Gousset et al., 2019, who used a laser captured microdissection approach combined with mass spectrometry to reveal the composition of various types of cellular protrusions in mouse CAD cells, including growth cones, filopodia and TNTs. Interestingly, among the 190 proteins identified in Gousset et al., 2019 in 2 samples from hCAD samples (enriched in TNTs), 101 were also found in TNTome (listed in table S7), mostly corresponding to the more abundant cellular proteins. It is possible that laser microdissection allowed a limited amount of material to be purified, and therefore few membrane proteins were identified (Gousset et al., 2019).

TNTome is rich in membrane-associated proteins, as well as in proteins participating to the cytoskeleton, in particular related to actin, as it was expected for these structures. TNTome is also abundant in ribonucleoproteins and translation-related factors (220 proteins, 19%). Some of them (as well as the proteins identified as nuclear in the

databases) could be contaminants coming from cellular debris, however this fraction should not be more than 10% of the total, based on nanoFCM results. Together with the fact that TNTs transfer mitochondria and lysosomes, it is possible that TNTs are used as a route to transfer RNAs alone or tethered to organelles by Annexins (several members in TNTome, including A11), G3BP1 or CAPRIN1 (both in the first quartile of TNTome, Liao et al., 2019, Lesnik et al., 2015, Cioni et al., 2019) or that local translation happens along the TNT to fuel it with required material. Transfer of mRNAs and microRNAs through TNTs has been described (Haimovitch et al., 2021, Kolba et al., 2019) and could be one of the major functions of this kind of communication. Whether specific RNAs travel through TNTs (for example associated to and encoding for specific organelles proteins) remains to be demonstrated and constitutes a new avenue of research.

Regarding membrane, beside tetraspanins, cadherins and integrins, some other plasma membrane TM proteins are of interest. Several amino acids (SLC3A2, SLC1A5 in the first quartile, SLC1A4 and SLC7A1 in the fourth) and monocarboxylate transporters (SLC16A1 in the second quartile) were found, suggesting together with the presence of mitochondria and of many metabolic enzymes that active metabolism takes place in TNTs and may be necessary to generate local ATP to power TNT growth (Garde et al., 2022). Of note SLC1A5 (Gln transporter ASCT2) and the lactate transporter MCT1 (SLC16A1) have been shown to interact with CD9 in pancreatic cancer stem cells (Wang et al., 2019) were it promoted their membrane localization and function. This hypothesis will need further investigation. Also, of great interest are SLC1A4 (neutral amino acid transporter) and STX7, which are the only TM proteins uniquely found in TNTs and not EVP fraction. As a matter of fact, our results suggested that TNTs are different in composition and maybe regulation from EVPs, although they share numerous factors. Further studying TNT proteins not being present in EVPs will possibly allow to identify TNT specific markers.

We focused our attention on tetraspanins CD9 and CD81 to further validate our proteomic approach. Among the structures described to comprise at least one of these factors and that could potentially be contaminants of our TNT preparations, are midbodies. Midbodies have been shown to contain CD9 and its partners CD9-P1 and EWI-2 (Addi nat et al., 2020), and these structures could be copurified with TNTs, although in minor amount given the fact that the cells were maintained in serum-free medium for 24 hours

before TNTs were harvested. However, no other specific markers of midbodies were detected in our MS data, including CRIK, CEP55, PLK1, PRC1, MKLP1 and 2, although they are expressed in U2OS cells (see Beck et al., 2011; Lundberg et al., 2010). Of note, only 13 TM proteins are common between TNTome and flemingsome (which has 29), including CD9, CD9P1, EWI2, but also CADH1 and 4, CD44, INTA3. Some of these proteins could have a specific role in both TNTs and midbodies, like CD9 and its associated factors. Alternatively, some of these proteins, relatively abundant on plasma membranes, could be randomly present, independently of the specific structure that is analyzed. In any case, TNT and midbodies have different composition.

Among the cellular structures that depend on tetraspanin-enriched microdomains are also the recently described migrasomes, which are substrate-attached membrane elongated organelles formed on the branch points or the tips of retraction fibers of migrating cells which allow the release and transfer of cellular material in other cells (Ma et al., 2015). Although migrasomes have been described to be enriched in and dependent on tetraspanins-enriched microdomains (Huang et al., 2019; Huang and Yu, 2021), they are fundamentally different from TNTs since they are attached to the substratum (and probably not collected during the procedure of TNT purification), and exhibit specific markers, identified by MS analysis, which are absent from TNTome (TSPAN 4 and 9, NDST1, PIGK, CPQ, EOGT for example, see Zhao et al., 2019). Altogether, our TNT purification protocol and proteomic analysis have revealed that TNTs have specific composition, and these data open new avenues to understand how TNTs are formed and regulated.

CD9 and CD81 regulate directional formation of TNTs

TNTome in U2OS revealed that CD9 and CD81 are among the most abundant integral membrane proteins in TNTs (see table S3, tab2), and previous results of overexpression (Lachambre et al., 2014) and our data showed that they are also present on TNTs in other cell lines, especially SH-SY5Y cells, making them probable obligate proteins of TNTs. In addition, given the distance between cells connected by TNTs, one can speculate that, under specific signal, one or several membrane proteins would drive growth of TNTs and stimulate actin polymerization, and/or subsequent membrane fusion with the opposing cell. CD9 and CD81, as part of TEMs, able to bring together additional proteins, were interesting candidates to fulfill these functions. That is why we have analyzed the ability

of the tetraspanins CD9 and CD81 to influence the number of TNTs and their functionality understood as the capacity for cargo transfer between cells in a strict cell contact-dependent manner.

Related with the protrusive activity of the membrane and its deformation, which is one mandatory step in the formation of TNTs, the tetraspanins CD9 and CD81 have been shown to induce curvature formation (Bari et al., 2011; Umeda et al., 2020) probably because of their inverted cone-like structure. CD9 promotes the formation of digitation junctions (Huang et al., 2018) and CD81 promotes microvilli formation and membrane bending (Bari et al., 2011). Our results showed that CD9 is able to increase the % of cells connected by TNTs, showing that CD9 is a positive regulator of TNT biogenesis or of TNT stability. Clustering of CD9 by antibody treatment for a short period of time (2 hours) was more than enough to produce a significant increase in the % of cells connected by TNTs and in the % of acceptor cells that had received vesicles, thus showing that functional TNTs were induced. One can speculate that signals promoting TNT growth would somehow induce CD9 clustering and conformational change, directing membrane curvature and eventually TNT growth initiation.

In contrast, OE or KO of CD81 did not affect the % of TNT-connected cells at all, indicating that CD81 does not seem to be involved in the origin of new TNTs. These different roles in the biogenesis of TNTs could be surprising since one of the characteristics of these tetraspanins is that they are associated with each other, with a very similar structure and shared functions (Boucheix and Rubinstein, 2001; Umeda et al., 2020). Recent results suggested that although both CD9 and CD81 undergo changes of conformation affecting their interaction with partner proteins, it happens spontaneously for CD9 (Umeda et al., 2020) but only in the presence of cholesterol in an internal pocket between their four membrane passages for CD81 (Zimmerman et al., 2016). Therefore, it is possible that a cascade of events could lead to changes in the composition of TEM through CD9 and CD81 involvement. However, although we can see how the single KO of CD9 and CD81 showed different results on the number of TNTs, when we did the double KO of CD9 and CD81, we could observe how the % of TNT-connected cells was dramatically decreased to even lower levels than with the CD9 KO alone. Therefore, this would indicate that CD9 and CD81 may have partially redundant roles in the biogenesis of TNTs, in accordance also with the partial compensation of CD81 KO by CD9 OE. This

is reminiscent of their role in oocyte fertilization, with both a complementary effect as CD9-/- CD81-/- mouse oocytes are completely sterile (Rubinstein et al., 2006), and also partial redundancy as CD81 expression on CD9-/- mouse oocytes restores fertilization to 50% of cases (Kaji et al., 2002).

Another fundamental process for the formation of functional TNTs is the fusion of the TNT membrane with the opposing cell to form these open channels (Sartori-Rupp et al., 2019). CD9 and CD81 have been shown to be positive regulators of sperm-egg fusion (Rubinstein et al., 2006) and bone marrow macrophage fusion-mediated osteoclast formation in the case of CD9 (Ishii et al., 2006), but negative regulators of cell muscle fusion (Charrin et al., 2013) and multinucleated giant cells formation (Takeda et al., 2003). Therefore, one possibility is that these tetraspanins participate in the fusion of the TNTs with the opposing cell. The co-cultures allowing to quantify the cell contact-dependent transfer of vesicles and therefore the functionality of the TNTs (which is an indirect way of checking whether these structures are in fact open or closed) showed a positive correlation between transfer capacity and number of TNTs when acting on CD9 in donor cells, implying that CD9 is a positive regulator of the whole set of processes of TNT formation. In contrast, CD81 in donor cells positively regulated the functionality of TNTs but not the apparent number of TNTs. Therefore CD81 probably does not play a role in attachment of TNTs to the opposing cell or in TNT stability (in which cases one would expect less TNTs on CD81 KO cells), or in stabilizing active CD9 (we would not see increased TNT number and transfer in CD9 OE + CD81 KO conditions) but rather favors the fusion of TNTs with the opposing cells. However, the results from these same KOs but in this case used as acceptor cells brought new insights to this model, since KO of CD9 or CD81 increased vesicle transfer from WT cells. Therefore, we can see a difference in function or asymmetry depending on the expression and localization of these proteins. The increased vesicle transfer when CD9 or CD81 are KO in acceptor cells could be explained by the peculiarity of the membrane domains around tetraspanins (TEMs). In this case, one could speculate that the absence of CD9/CD81 could affect these TEMs by affecting their lipid composition or certain tetraspanin partners, resulting in a change in the responsiveness of the acceptor cell to adhere and fuse with TNTs. Alternatively, CD9 and/or CD81 could be not needed in acceptor cell at all.

Importantly, these results showed that TNT formation and function is directional and leaded by tetraspanins. Since TNTs have been described in several cell lines, including SH-SY5Y, to be actually composed of bundles of iTNTs (Sartori-Rupp et al., 2019), one can speculate that each iTNT has a directionality imposed by CD9 surrounded by a specific TEM, the bundle of iTNTs forming the apparent TNT containing iTNTs with both orientations.

CD9 and CD81 act successively in the formation of TNTs

All these results together show that although CD9 and CD81 regulate the formation of TNTs, their respective role could be at different steps of the whole TNT formation process. CD81 KO in CD9 OE cells had no significant effect on both the % of TNT-connected cells and vesicle transfer compared to CD9 OE cells. In contrast, KO of CD9 on CD81 OE cells resulted in a significant decrease in the % of TNT-connected cells and vesicle transfer compared to CD81 OE alone. These results suggested that CD9 could act early in initiating the formation and allowing CD81 to subsequently participate in the fusion of TNTs with the opposing cell. Furthermore, when we treated CD81 KO cells with anti-CD9 antibodies, we observed the same increase in TNT number that was seen in WT cells, indicating that the TNT-forming capacity of CD9 is independent of CD81 and was induced by antibody treatment. However, vesicle transfer induction was completely blocked in CD81 KO cells, showing that the first steps of TNT formation were not impaired and that it is instead a late step, probably fusion, that is controlled by CD81. Recent work by *Huang et al., 2022* proposed a role for TEM in facilitating membrane repair by forming a rigid ring impairing membrane damage to spread. In a similar way, specific CD9/CD81 TEM could somehow protect membrane around the TNT site where fusion with opposing cell will occur. More work in identifying specific TEM composition in TNTs would be needed to address this hypothesis.

In summary, in this study we have shown that TNTs and EVPs are two cellular structures with partially overlapping composition, and that despite being part of both TNTs and EVPs, the tetraspanins CD9 and CD81 are fundamental regulators of TNT formation with complementary roles in the whole process of biogenesis of these structures. As schematized in the model of Figure 7, CD9 is required to grow TNTs, but not enough for their functionality, whereas CD81 is required for fully functional TNTs. In addition, the requirement of these tetraspanins is different in the emitting and receiving cells. TNTome

further analysis will be of great help to identify additional protein, as part of the TEM or not, that could participate in TNT formation and regulation.

Acknowledgements: We acknowledge the Center for Translational Science (CRT)-Cytometry and Biomarkers Unit of Technology and Service (CB UTechS), in particular P.H. Commère. Thanks to Dr. S. Charrin for helpful discussion, Dr. S. Lebreton for critical reading of the manuscript, all the members of the UTRAF unit for their support. We are grateful for financial support to C.Z. from Institut National du Cancer (PLBIO18-103) and Equipe Fondation Recherche Médicale (FRM EQU202103012692).

Author contributions: Conceptualization: RNM, CB, CZ; methodology: RNM, TC, ER, MM, CB; formal analysis: RNM, TC, CB; writing—original draft: RNM, CB.; writing—review and editing: RNM, CB, CZ, ER, TC, MM; funding acquisition: CZ, MM; supervision: CB.

Materials and Methods

Cell lines, lentiviral preparations, plasmids and transfection procedures

U2OS cells were cultured at 37 °C in 5% CO2 in Dulbecco's Modified Eagle's Medium (DMEM + Glutamax, + 4.5 g/l Glucose, + Pyruvate, Gibco), plus 10% fetal calf serum (FCS) and 1% penicillin/streptomycin (P/S). U2OS stably expressing H2B-GFP (Addgene 11680) and actin chromobody GFP (pAC-TagGFP from Chromotek) were obtained by transfection with Fugene HD according to manufacturer's instructions, followed by sorting of GFP-positive cells. GFP-CD9 expressing U2OS cells were obtained by lentiviral transduction as below, followed by limiting dilution to obtain a clone. SH-SY5Y human neuroblastoma cells were cultured at 37 °C in 5% CO2 in RPMI-1640 (Euroclone), plus 10% FCS and 1% P/S.

For the lentiviral preparations, human HEK 293T cells were cultured at 37 °C in 5% CO2 in DMEM (ThermoFisher), with 10% FCS and 1% P/S. Cells were plated one day before

transfection at a confluency around 70%. Transfection of the different plasmids was made in a ratio 4:1:4 using lentiviral components pCMVR8,74 (Gag-Pol-Hiv1) and pMDG2 (VSV-G) vectors and the plasmid of interest respectively using FuGENE HD (Promega) according to manufacturer's protocol. CRISPR lentiviral plasmid for CD9 and CD81 were a gift from Dr. Eric Rubinstein. The viral particules were collected and concentrated using LentiX-Concentrator (TakaraBio) after 48 h. To KO CD9 and/or CD81, SH-SY5Y were plated the day before the infection at a confluency of around 70% and next day the lentivirus was added to the cells. 24 hours later the medium with the lentiviruses was removed and cells were selected with RPMI + 1 µg/mL of puromycin for 2 days. After this, cells were splitted 1:5 and reinfected for 24 hours. After these 24 hours, medium was replaced with RPMI + 1 µg/mL of puromycin for 10 days changing the medium every 2-3 days. Finally, cells were tested for the absence of expression of CD9 and/or CD81 by western blot (WB).

CD9 and CD81 plasmids utilized to OE these proteins were a gift from Dr. Eric Rubinstein. To obtain clones that overexpress CD9 or CD81, SH-SY5Y were plated the day before at a confluency of around 70% and next day cells were transfected with the corresponding plasmid using Lipofectamine 2000 (Invitrogen) following the manufacture recommendations and 72 hours post-transfection cells selected with 350 µg/mL of Hygromicin B (Gibco) for 5 days, changing the medium every 2 days and then with 50 µg/mL of Hygromicin B for 10 days more. The pool of cells was seeded in 96-well plates through a limiting dilution in such a way that 0.5 cells are seeded per well, and after allowing them to grow, they were analyzed and the clones overexpressing the protein of interest were selected and tested for expression of CD9 or CD81 by immunofluorescence and WB.

TNT and EVP preparation

Two million of U2OS cells were plated in 75 cm2 flasks for 24 hours, next complete medium was replaced by medium without FCS for an additional 24 hours. For EVP preparation, conditioned medium was collected, centrifugated twice at 2000g to remove cells, concentrated 10-fold on Vivaspin 20 (MWCO 10kD, Cytiva), and next submitted to ultracentrifugation in a Beckman MLS50 rotor at 10,000g for 30 minutes at 4°C. Supernatant was collected and centrifugated at 100,000g for 70 minutes at 4°C, resulting

pellet was resuspended in PBS and centrifugated again at 100,000g for 70 minutes at 4°C. Pellets were used for Mass Spectrometry.

For TNT preparation, cell cultures after removing conditioned medium were washed carefully with PBS, next 2 ml of PBS was added in each flask, which was left on an oscillating shaker for 5 minutes before being shaked (30 sec horizontally, and 4 times 30 sec by banging them vigorously). PBS from all flasks was drained, collected and centrifugated twice at 2,000g, and filtered on 0.45 □M syringe filter (Corning) to remove detached cells, next submitted to ultracentrifugation at 100,000g for 70 minutes at 4°C. Pellets were used for Mass Spectrometry. After collecting EVPs and TNTs from cell cultures, cells were harvested in PBS, and cell extracts were prepared in Tris 50 mM pH 7.4, NaCl 300 mM, MgCl2 5 mM, Triton 1% with protease inhibitors (complete mini, Roche).

Nano-Flow Cytometry

The size and number of exosomes and TNT particles were identified by Nano-Flow Cytometry (NanoFCM). NanoFCM is applicable when the refractive index of input samples are the same or similar to that of silica particles. The standard working curve of scattering light intensity was established using silica standard sphere. EVPs and TNT particles were isolated from 1 flask of culture following the protocol above except the ultracentrifugation steps. The particle size distribution of samples was measured based on the scattering intensity.

Mass spectrometry

Digestion of TNT and EVPs samples

Protein pellets were dissolved in urea 8M, Tris 50mM pH 8.0, TCEP (tris(2-carboxyethyl)phosphine) 5mM and SDS (Sodium Dodecyl Sulfate) 2%. SDS was removed using a methanol/ chloroform/ water extraction. Briefly, 3V of ice-cold Methanol was added to the sample then mixed. 2 V of ice-cold chloroform was added and mixed. Then 3Vof ice cold water was added and mix. Sample were spinned for 3 min at 5000g at 4°C. Proteins at the organic/inorganic interface were kept and washed 3 times in ice cold methanol. Protein pellet were dissolved in Guanidine 1M, TCEP 5mM, Chloroacetamide 20mM, Tris 50mM pH8.0 and samples were heated 5 min at 90°C

before digestion in a mix of 500 ng of LysC (Promega) at 37°C for 2h. Dilution with tris 50mM was done before the addition of trypsin 500 ng (Promega) and digestion at 37°C for 8h. Digestion was stopped by adding 1% final of formic acid. Peptides were purified using a C18 based clean up standard protocol done using Bravo AssayMap device

LC-MS/MS analysis of TNT and EVPs.

LC-MS/SM analysis of digested peptides was performed on an Orbitrap Q Exactive Plus mass spectrometer (Thermo Fisher Scientific, Bremen) coupled to an EASY-nLC 1200 (Thermo Fisher Scientific). A home-made column was used for peptide separation (C_{18} 50 cm capillary column picotip silica emitter tip (75 µm diameter filled with 1.9 µm Reprosil-Pur Basic C_{18}-HD resin, (Dr. Maisch GmbH, Ammerbuch-Entringen, Germany)). It was equilibrated and peptide were loaded in solvent A (0.1 % FA) at 900 bars. Peptides were separated at 250 $nl.min^{-1}$. Peptides were eluted using a gradient of solvent B (ACN, 0.1 % FA) from 3% to 22% in 140 min, 22% to 42% in 61 min, 42% to 60% in 15 min (total length of the chromatographic run was 240 min including high ACN level step and column regeneration). Mass spectra were acquired in data-dependent acquisition mode with the XCalibur 2.2 software (Thermo Fisher Scientific, Bremen) with automatic switching between MS and MS/MS scans using a top 10 method. MS spectra were acquired at a resolution of 70000 (at *m/z* 400) with a target value of 3×10^6 ions. The scan range was limited from 400 to 1700 *m/z*. Peptide fragmentation was performed using higher-energy collision dissociation (HCD) with the energy set at 26 NCE. Intensity threshold for ions selection was set at 1×10^6 ions with charge exclusion of z = 1 and z > 7. The MS/MS spectra were acquired at a resolution of 17500 (at *m/z* 400). Isolation window was set at 2.0 Th. Dynamic exclusion was employed within 35 s.

All Data were searched using MaxQuant (version 1.6.6.0) using the Andromeda search engine (*Tyanova et al., 2016*) against a human reference proteome (75088 entries, downloaded from Uniprot the 29th of October 2020).

The following search parameters were applied: carbamidomethylation of cysteines was set as a fixed modification, oxidation of methionine and protein N-terminal acetylation were set as variable modifications. The mass tolerances in MS and MS/MS were set to 5 ppm and 20 ppm respectively. Maximum peptide charge was set to 7 and 5 amino acids were required as minimum peptide length. At least 2 peptides (including 1 unique

peptides) were asked to report a protein identification. A false discovery rate of 1% was set up for both protein and peptide levels. iBAQ value was calculated. The match between runs features was allowed for biological replicate only.

Data analysis

Quantitative analysis was based on pairwise comparison of protein intensities. Values were log-transformed (log2). Reverse hits and potential contaminant were removed from the analysis. Proteins with at least 2 peptides were kept for further statistics. Intensity values were normalized by median centering within conditions (normalizeD function of the R package DAPAR, *Wieczorek et al., 2017*). Remaining proteins without any iBAQ value in one of both conditions have been considered as proteins quantitatively present in a condition and absent in the other. They have therefore been set aside and considered as differentially abundant proteins. Next, missing values were imputed using the impute.MLE function of the R package imp4p (https://rdrr.io/cran/imp4p/man/imp4p-package.html). Statistical testing was conducted using a limma t-test thanks to the R package limma (*Pounds et al., 2006*). An adaptive Benjamini-Hochberg procedure was applied on the resulting p-values thanks to the function adjust.p of R package cp4p (*Smyth, 2004*) using the robust method described in (*Giai Gianetto et al., 2016* to estimate the proportion of true null hypotheses among the set of statistical tests. The proteins associated to an adjusted p-value inferior to a FDR level of 1% have been considered as significantly differentially abundant proteins.

Bioinformatic analysis and data mining

Twelve replicates were done for the discovery of TNT proteins. Nine over 12 were kept as being part of the TNT. The 1177 resulting proteins were sorting by quartiles according to their iBAQ value. For each of the 4 lists, proteins composition was depicted using ProteoMap tool (*Liebermeister et al., 2014*) to visualize their weighted GO organization and protein contribution for each GO term. Also, a DAVID analysis (*Sherman et al., 2022*) was done for each quartile of proteins. Functional charts and cluster were used to describe the dataset. Protein networks were visualized using STRING (*Szklarczyk et al., 2021*) and Cytoscape.

Sample preparation for TNT imaging

SH-SY5Y cells were trypsinized and counted, and 100,000 cells were plated on coverslips overnight (O/N). After O/N culture, cells were fixed with specific fixatives to preserve TNT, first with Fixative 1 (2% PFA, 0.05% glutaraldehyde and 0.2 M HEPES in PBS) for 15 min at 37 °C, then a second Fix for 15 min at 37 °C using fixative solution 2 (4% PFA and 0.2 M HEPES in PBS) (for further information, *Abounit et al., 2015*). After fixation, cells were washed with PBS and membranes were stained with conjugated wheat germ agglutinin (WGA)-Alexa Fluor (1:300 in PBS) (Invitrogen) and DAPI (1:1000) (Invitrogen) at room temperature 15 minutes. After gently washing 3 times with PBS, samples were mounted on glass slides with Aqua PolyMount (Polysciences, Inc.). Every different SH-SY5Y cell type (WT, tetraspanin KO or tetraspanin OE) was prepared in the exact same conditions.

Counting or quantification of the % TNT-connected cells (also term as TNT counting or TNT number)

With the use of an inverted laser scanning confocal microscope LSM 700 (Zeiss) controlled by the Zen software (Zeiss) multiple random Z-stack images of different points on the samples were acquired. The images were analyzed according to the morphological criteria of TNTs: structures that connect two distant cells and that are not attached to the substratum. First slices were excluded from the analysis, and only connections in the middle and upper stacks are considered. Cells that have TNTs between them were marked as cells connected by TNTs, and the number of these cells was compared to the total number of cells in the sample. This gives the percentage of cells connected by TNTs. The analysis was performed using ICY software (https://icy.bioimageanalysis.org/), by using the "Manual TNT annotation" plugin. In each experiment, at least 200 or more cells were analyzed in every condition. The images were adjusted and processed with the ImageJ software (https://imagej.nih.gov/ij/).

Co-culture assay (DiD transfer assay) and flow cytometry analysis

DiD transfer assays have been described elsewhere (*Abounit et al., 2015*). Briefly, the co-culture consists of two distinctly labeled cell populations: a first population of cells (donors) was treated with Vybrant DiD (dialkylcarbocyanine), a lipophilic dye that stains vesicles, at 1:1000 (Thermo Fisher Scientific) in complete medium for 30 min at 37 °C (Life Technologies), the cells were then trypsinized and mixed in a 1:1 ratio with a

different cell population (acceptors) of different color to distinguish them from donors (usually expressing GFP) and the co-culture was incubated O/N.

In the case of the co-cultures with KO, OE or OE + KO of CD9 and CD81, 400,000 donor cells were mixed with 400,000 acceptor cells on 6-well plates for analysis by flow cytometry. After O/N culture, cells were trypsinized, passed through a cell strainer to dissociate cellular aggregates and fixed with 2% PFA in PBS. Finally, these cells were passed through the CytoFLEX S Flow Cytometer (Beckman Coulter) under the control of the CytoExpert Acquisition software. The data were analyzed with FlowJo software following a similar strategy for all experiments: first the samples were gated to exclude cellular debris by plotting the area obtained with the side scatter (SSC-A) and the area obtained with the forward scatter (FSC-A) obtaining all the cells in the sample. Second, within this previous gate, the sample was gated to exclude cell doublets, plotting the width obtained with side scatter (SSC-W) and the area obtained with forward scatter (FSC-A) thus obtaining the singlets. Finally, within the singlet gate, the co-culture was gated using GFP and DiD expression, resulting in four quadrants delimiting double-negative, GFP-positive, DiD-positive and double-positive populations. The % of acceptor cells receiving DiD-vesicles it is obtained by calculating the percentage of acceptor cells with labeled vesicles out of the total number of acceptor cells.

In the case of the co-culture of the CD9 AB treatment, 50.000 donor cells were co-cultured with 50.000 acceptor cells on coverslips. Results were analyzed by microscopy as described above, and results were obtained by semi-quantitative analysis using ICY software (http://icy.bioimageanalysis.org/) by calculating the percentage of acceptor cells with labeled vesicles out of the total number of acceptor cells. In each experiment, count at least 100 recipient cells per condition. Image montages were built afterward in ImageJ software.

In all co-cultures a control of the transfer by secretion was performed, to determine whether the vesicle transfer we see is mainly through a contact-dependent mechanism or through secretory transfer. For this, DiD-loaded donor cells were seeded alone (800,000 cells for flow cytometry and 100,000 cells for microscopy) and cultured for 24 hours. After this, the supernatant from these cells was centrifuged and added to the acceptor cells that had been seeded on the previous day under the same conditions as the donors, and these acceptor cells were cultured with the supernatant from the donor cells for the same

time as in the co-cultures (24 hours) and next fixed and analyzed in the same way as above mentioned depending on whether it was analyzed by flow cytometry or microscopy.

CD9 antibody (AB) treatment

The experiments concerning the CD9 AB treatment were based on a previously used approach (*Singethan et al., 2008*). Both the TNT counting and vesicle transfer in the CD9 AB treatment were done in the same way as described above in the section corresponding to the TNT counting and coculture assay, with the only exception that after the 24 hours of coculture we added an additional step consisting in the incubation of these cells with either secondary antibodies as a control (Goat anti-rabbit Alexa Fluor 305 - Thermofisher ref: A21068-) or anti-CD9 (TS9, gifted from Dr. Eric Rubinstein) antibodies at a concentration of 10 μg/μL in RPMI medium without serum or P/S for 2 hours. Subsequently, as mentioned above, the cells were fixed, submitted to immunofluorescence. For cells treated with secondary antibodies, after fixation the cells were incubated with anti-CD9 and anti-CD81 antibodies (as described in the next section). For cells treated with CD9 AB, these cells were only incubated with anti-CD81 antibodies. Results were acquired by confocal microscopy.

Immunofluorescence of CD9 and CD81

For immunofluorescence, 100.000 cells were seeded on glass coverslips and after O/N culture they were fixed with 4% paraformaldehyde (PFA) for 15 minutes, quenched with 50 mM NH_4Cl for 10 minutes and blocked in 2% BSA in PBS for 20 minutes. Primary antibodies used were: mouse anti-CD9 IgG1 (TS9) and mouse anti-CD81 IgG2a (TS81) that were a gift from Dr. Eric Rubinstein, and all of them were used at 1:1000 in 2% BSA in PBS during 1 hour. After 3 washes of 10 minutes each with PBS, cells were incubated with each corresponding Alexa Fluor-conjugated secondary antibody (Invitrogen) at 1:1000 in 2% BSA in PBS during 1 hour. Specifically, the secondary antibodies used were: goat anti-mouse with epitope IgG1 Alexa Fluor 488 for CD9 (Invitrogen ref: A21121) and goat anti-mouse with epitope IgG2a Alexa Fluor 633 for CD81 (Invitrogen ref: A21136). For the experiments showing the actin cytoskeleton, cells were labeled with Phalloidin- Rhodamine (Invitrogen) at 1:1000 in the same mix and conditions as the secondary antibodies. Then, cells were washed 3 times of 10 minutes each with PBS, stained with DAPI and mounted on glass slides with Aqua PolyMount (Polysciences,

Inc.). Images were acquired with a confocal microscope LSM700 (Zeiss) and processed with the ImageJ software.

Western blot

For Western blot SH-SY5Y cells were lysed with lysis buffer composed by 150 mM NaCl, 20 mM Tris, 5 mM EDTA, pH 8.0. Protein concentration was measured by a Bradford protein assay (Bio-Rad). 20 µg of protein were submitted to western blot analysis. Primary antibodies used for Western blot were: mouse anti-CD9 IgG1 (TS9, 1:1000), mouse anti-CD81 IgG2a (TS81, 1:1000), mouse anti CD63 (1:1000), mouse anti ADAM10 (11G2, 1:1000) were gifts from Dr. Eric Rubinstein, rabbit anti-α-GAPDH (Sigma ref: G9545, 1:1000), rabbit anti-β-actin (Cell Signaling ref: 4967, 1:1000), mouse anti-α-tubulin (Sigma ref: T9026, 1:2000), mouse anti-GM130 (BD transduction Laboratories, ref:610822, 1:1000, rabbit ITGB1, ITGB4, ITGA4 (from integrin Ab Sampler kit, Cell signaling ref: 4749, 1:1000), rabbit anti-EGFR (Cell Signaling ref: 4267, 1:1000), rabbit anti-CX43 (Sigma ref: C6219, 1:3000), mouse anti-ANXA2 (Proteintech ref: 66035,1:2000).

Statistical analysis

Statistical analysis of experiments concerning the TNT counting and the DiD transfer assay are described elsewhere (*Pinto et al., 2021*). Briefly, the statistical tests were applied using either a logistic regression model computed using the 'glm' function of R software (https://www.R-project.org/) or a mixed effect logistic regression model using the lmer and lmerTest R packages, applying a pairwise comparison test between groups.

All graphs shown in this study have been made with GraphPad Prism version 9.

Bibliography

Abounit, S., Bousset, L., Loria, F., Zhu, S., de Chaumont, F., Pieri, L., Olivo-Marin, J.-C., Melki, R., Zurzolo, C., 2016. Tunneling nanotubes spread fibrillar α-synuclein by intercellular trafficking of lysosomes. EMBO J 35, 2120–2138. https://doi.org/10.15252/embj.201593411

Abounit, S., Delage, E., Zurzolo, C., 2015. Identification and Characterization of Tunneling Nanotubes for Intercellular Trafficking. Curr Protoc Cell Biol 67, 12.10.1-12.10.21. https://doi.org/10.1002/0471143030.cb1210s67

Abounit, S., Zurzolo, C., 2012. Wiring through tunneling nanotubes – from electrical signals to organelle transfer. Journal of Cell Science 125, 1089–1098. https://doi.org/10.1242/jcs.083279

Addi, C., Presle, A., Frémont, S., Cuvelier, F., Rocancourt, M., Milin, F., Schmutz, S., Chamot-Rooke, J., Douché, T., Duchateau, M., Giai Gianetto, Q., Salles, A., Ménager, H., Matondo, M., Zimmermann, P., Gupta-Rossi, N., Echard, A., 2020. The Flemmingsome reveals an ESCRT-to-membrane coupling via ALIX/syntenin/syndecan-4 required for completion of cytokinesis. Nat Commun 11, 1941. https://doi.org/10.1038/s41467-020-15205-z

Alarcon-Martinez, L., Villafranca-Baughman, D., Quintero, H., Kacerovsky, J.B., Dotigny, F., Murai, K.K., Prat, A., Drapeau, P., Di Polo, A., 2020. Interpericyte tunnelling nanotubes regulate neurovascular coupling. Nature 585, 91–95. https://doi.org/10.1038/s41586-020-2589-x

Alvarez, M.L., Khosroheidari, M., Kanchi Ravi, R., DiStefano, J.K., 2012. Comparison of protein, microRNA, and mRNA yields using different methods of urinary exosome isolation for the discovery of kidney disease biomarkers. Kidney Int 82, 1024–1032. https://doi.org/10.1038/ki.2012.256

Bari, R., Guo, Q., Xia, B., Zhang, Y.H., Giesert, E.E., Levy, S., Zheng, J.J., Zhang, X.A., 2011. Tetraspanins regulate the protrusive activities of cell membrane. Biochemical and Biophysical Research Communications 415, 619–626. https://doi.org/10.1016/j.bbrc.2011.10.121

Beck, M., Schmidt, A., Malmstroem, J., Claassen, M., Ori, A., Szymborska, A., Herzog, F., Rinner, O., Ellenberg, J., Aebersold, R., 2011. The quantitative proteome of a human cell line. Mol Syst Biol 7, 549. https://doi.org/10.1038/msb.2011.82

Boucheix, C., Rubinstein, E., 2001. Tetraspanins. Cell Mol Life Sci 58, 1189–1205. https://doi.org/10.1007/PL00000933

Chang, M., Lee, O.-C., Bu, G., Oh, J., Yunn, N.-O., Ryu, S.H., Kwon, H.-B., Kolomeisky, A.B., Shim, S.-H., Doh, J., Jeon, J.-H., Lee, J.-B., 2022. Formation of cellular close-ended tunneling nanotubes through mechanical deformation. Sci Adv 8, eabj3995. https://doi.org/10.1126/sciadv.abj3995

Charreau, B., 2021. Secretome and Tunneling Nanotubes: A Multilevel Network for Long Range Intercellular Communication between Endothelial Cells and Distant Cells. International Journal of Molecular Sciences 22, 7971. https://doi.org/10.3390/ijms22157971

Charrin, S., Jouannet, S., Boucheix, C., Rubinstein, E., 2014. Tetraspanins at a glance. J Cell Sci 127, 3641–3648. https://doi.org/10.1242/jcs.154906

Charrin, S., Latil, M., Soave, S., Polesskaya, A., Chrétien, F., Boucheix, C., Rubinstein, E., 2013. Normal muscle regeneration requires tight control of muscle cell fusion by tetraspanins CD9 and CD81. Nat Commun 4, 1674. https://doi.org/10.1038/ncomms2675

Chastagner, P., Loria, F., Vargas, J.Y., Tois, J., I Diamond, M., Okafo, G., Brou, C., Zurzolo, C., 2020. Fate and propagation of endogenously formed Tau aggregates in neuronal cells. EMBO Mol Med 12, e12025. https://doi.org/10.15252/emmm.202012025

Chastney, M.R., Conway, J.R.W., Ivaska, J., 2021. Integrin adhesion complexes. Curr Biol 31, R536–R542. https://doi.org/10.1016/j.cub.2021.01.038

Cioni, J.-M., Lin, J.Q., Holtermann, A.V., Koppers, M., Jakobs, M.A.H., Azizi, A., Turner-Bridger, B., Shigeoka, T., Franze, K., Harris, W.A., Holt, C.E., 2019. Late Endosomes Act as mRNA Translation Platforms and Sustain Mitochondria in Axons. Cell 176, 56-72.e15. https://doi.org/10.1016/j.cell.2018.11.030

Cocozza, F., Grisard, E., Martin-Jaular, L., Mathieu, M., Théry, C., 2020. SnapShot: Extracellular Vesicles. Cell 182, 262-262.e1. https://doi.org/10.1016/j.cell.2020.04.054

Cohen, J., Wang, L., Marques, S., Ialy-Radio, C., Barbaux, S., Lefèvre, B., Gourier, C., Ziyyat, A., 2022. Oocyte ERM and EWI Proteins Are Involved in Mouse Fertilization. Front Cell Dev Biol 10, 863729. https://doi.org/10.3389/fcell.2022.863729

Dilsizoglu Senol, A., Samarani, M., Syan, S., Guardia, C.M., Nonaka, T., Liv, N., Latour-Lambert, P., Hasegawa, M., Klumperman, J., Bonifacino, J.S., Zurzolo, C., 2021. α-Synuclein fibrils subvert lysosome structure and function for the propagation of protein misfolding between cells through tunneling nanotubes. PLoS Biol 19, e3001287. https://doi.org/10.1371/journal.pbio.3001287

Garde, A., Kenny, I.W., Kelley, L.C., Chi, Q., Mutlu, A.S., Wang, M.C., Sherwood, D.R., 2022. Localized glucose import, glycolytic processing, and mitochondria generate a focused ATP burst to power basement-membrane invasion. Dev Cell 57, 732-749.e7. https://doi.org/10.1016/j.devcel.2022.02.019

Giai Gianetto, Q., Combes, F., Ramus, C., Bruley, C., Couté, Y., Burger, T., 2016. Calibration plot for proteomics: A graphical tool to visually check the assumptions underlying FDR control in quantitative experiments. Proteomics 16, 29–32. https://doi.org/10.1002/pmic.201500189

Gousset, K., Gordon, A., Kumar Kannan, S., Tovar, J., 2019. A novel Microproteomic Approach Using Laser Capture Microdissection to Study Cellular Protrusions. Int J Mol Sci 20, 1172. https://doi.org/10.3390/ijms20051172

Gousset, K., Marzo, L., Commere, P.-H., Zurzolo, C., 2013. Myo10 is a key regulator of TNT formation in neuronal cells. J Cell Sci 126, 4424–4435. https://doi.org/10.1242/jcs.129239

Haimovich, G., Dasgupta, S., Gerst, J.E., 2021. RNA transfer through tunneling nanotubes. Biochem Soc Trans 49, 145–160. https://doi.org/10.1042/BST20200113

Horton, E.R., Byron, A., Askari, J.A., Ng, D.H.J., Millon-Frémillon, A., Robertson, J., Koper, E.J., Paul, N.R., Warwood, S., Knight, D., Humphries, J.D., Humphries, M.J., 2015. Definition of a consensus integrin adhesome and its dynamics during adhesion complex assembly and disassembly. Nat Cell Biol 17, 1577–1587. https://doi.org/10.1038/ncb3257

Huang, C., Fu, C., Wren, J.D., Wang, X., Zhang, F., Zhang, Y.H., Connel, S.A., Chen, T., Zhang, X.A., 2018. Tetraspanin-enriched Microdomains Regulate Digitation Junctions. Cell Mol Life Sci 75, 3423–3439. https://doi.org/10.1007/s00018-018-2803-2

Huang, Y., Yu, L., 2022. Tetraspanin-enriched microdomains: The building blocks of migrasomes. Cell Insight 1, 100003. https://doi.org/10.1016/j.cellin.2021.100003

Huang, Y., Zhang, X., Wang, H.-W., Yu, L., 2022. Assembly of Tetraspanin-enriched macrodomains contains membrane damage to facilitate repair. Nat Cell Biol 24, 825–832. https://doi.org/10.1038/s41556-022-00920-0

Huang, Y., Zucker, B., Zhang, S., Elias, S., Zhu, Y., Chen, H., Ding, T., Li, Y., Sun, Y., Lou, J., Kozlov, M.M., Yu, L., 2019. Migrasome formation is mediated by assembly of micron-scale tetraspanin macrodomains. Nat Cell Biol 21, 991–1002. https://doi.org/10.1038/s41556-019-0367-5

Ishii, M., Iwai, K., Koike, M., Ohshima, S., Kudo-Tanaka, E., Ishii, T., Mima, T., Katada, Y., Miyatake, K., Uchiyama, Y., Saeki, Y., 2006. RANKL-Induced Expression of Tetraspanin CD9 in Lipid Raft Membrane Microdomain Is Essential for Cell Fusion During Osteoclastogenesis. Journal of Bone and Mineral Research 21, 965–976. https://doi.org/10.1359/jbmr.060308

Jacquemet, G., Stubb, A., Saup, R., Miihkinen, M., Kremneva, E., Hamidi, H., Ivaska, J., 2019. Filopodome Mapping Identifies p130Cas as a Mechanosensitive Regulator of Filopodia Stability. Curr Biol 29, 202-216.e7. https://doi.org/10.1016/j.cub.2018.11.053

Jouannet, S., Saint-Pol, J., Fernandez, L., Nguyen, V., Charrin, S., Boucheix, C., Brou, C., Milhiet, P.-E., Rubinstein, E., 2016. TspanC8 tetraspanins differentially regulate the cleavage of ADAM10 substrates, Notch activation and ADAM10 membrane compartmentalization. Cell Mol Life Sci 73, 1895–1915. https://doi.org/10.1007/s00018-015-2111-z

Kaji, K., Oda, S., Miyazaki, S., Kudo, A., 2002. Infertility of CD9-deficient mouse eggs is reversed by mouse CD9, human CD9, or mouse CD81; polyadenylated mRNA injection developed for molecular analysis of sperm-egg fusion. Dev Biol 247, 327–334. https://doi.org/10.1006/dbio.2002.0694

Kalargyrou, A.A., Basche, M., Hare, A., West, E.L., Smith, A.J., Ali, R.R., Pearson, R.A., 2021. Nanotube-like processes facilitate material transfer between photoreceptors. EMBO Rep 22, e53732. https://doi.org/10.15252/embr.202153732

Khurana, S., Krementsov, D.N., de Parseval, A., Elder, J.H., Foti, M., Thali, M., 2007. Human Immunodeficiency Virus Type 1 and Influenza Virus Exit via Different Membrane Microdomains. J Virol 81, 12630–12640. https://doi.org/10.1128/JVI.01255-07

Kolba, M.D., Dudka, W., Zaręba-Kozioł, M., Kominek, A., Ronchi, P., Turos, L., Chroscicki, P., Wlodarczyk, J., Schwab, Y., Klejman, A., Cysewski, D., Srpan, K., Davis, D.M., Piwocka, K., 2019. Tunneling nanotube-mediated intercellular vesicle and protein transfer in the stroma-provided imatinib resistance in chronic myeloid leukemia cells. Cell Death Dis 10, 1–16. https://doi.org/10.1038/s41419-019-2045-8

Lachambre, S., Chopard, C., Beaumelle, B., 2014. Preliminary characterisation of nanotubes connecting T-cells and their use by HIV-1. Biology of the Cell 106, 394–404. https://doi.org/10.1111/boc.201400037

Lesnik, C., Golani-Armon, A., Arava, Y., 2015. Localized translation near the mitochondrial outer membrane: An update. RNA Biol 12, 801–809. https://doi.org/10.1080/15476286.2015.1058686

Liao, Y.-C., Fernandopulle, M.S., Wang, G., Choi, H., Hao, L., Drerup, C.M., Patel, R., Qamar, S., Nixon-Abell, J., Shen, Y., Meadows, W., Vendruscolo, M., Knowles, T.P.J., Nelson, M., Czekalska, M.A., Musteikyte, G., Gachechiladze, M.A., Stephens, C.A., Pasolli, H.A., Forrest, L.R., St George-Hyslop, P., Lippincott-Schwartz, J., Ward, M.E., 2019. RNA Granules Hitchhike on Lysosomes for Long-Distance Transport, Using Annexin A11 as a Molecular Tether. Cell 179, 147-164.e20. https://doi.org/10.1016/j.cell.2019.08.050

Liebermeister, W., Noor, E., Flamholz, A., Davidi, D., Bernhardt, J., Milo, R., 2014. Visual account of protein investment in cellular functions. Proc Natl Acad Sci U S A 111, 8488–8493. https://doi.org/10.1073/pnas.1314810111

Ljubojevic, N., Henderson, J.M., Zurzolo, C., 2021. The Ways of Actin: Why Tunneling Nanotubes Are Unique Cell Protrusions. Trends in Cell Biology 31, 130–142. https://doi.org/10.1016/j.tcb.2020.11.008

Lou, E., 2020. A Ticket to Ride: The Implications of Direct Intercellular Communication via Tunneling Nanotubes in Peritoneal and Other Invasive Malignancies. Frontiers in Oncology 10.

Lundberg, E., Fagerberg, L., Klevebring, D., Matic, I., Geiger, T., Cox, J., Älgenäs, C., Lundeberg, J., Mann, M., Uhlen, M., 2010. Defining the transcriptome and proteome in three functionally different human cell lines. Mol Syst Biol 6, 450. https://doi.org/10.1038/msb.2010.106

Ma, L., Li, Y., Peng, J., Wu, D., Zhao, X., Cui, Y., Chen, L., Yan, X., Du, Y., Yu, L., 2015. Discovery of the migrasome, an organelle mediating release of cytoplasmic contents during cell migration. Cell Res 25, 24–38. https://doi.org/10.1038/cr.2014.135

Melak, M., Plessner, M., Grosse, R., 2017. Actin visualization at a glance. J Cell Sci 130, 525–530. https://doi.org/10.1242/jcs.189068

Monk, P.N., Partridge, L.J., 2012. Tetraspanins: gateways for infection. Infect Disord Drug Targets 12, 4–17. https://doi.org/10.2174/187152612798994957

Nydegger, S., Khurana, S., Krementsov, D.N., Foti, M., Thali, M., 2006. Mapping of tetraspanin-enriched microdomains that can function as gateways for HIV-1. Journal of Cell Biology 173, 795–807. https://doi.org/10.1083/jcb.200508165

Ortin-Martinez, A., Yan, N.E., Tsai, E.L.S., Comanita, L., Gurdita, A., Tachibana, N., Liu, Z.C., Lu, S., Dolati, P., Pokrajac, N.T., El-Sehemy, A., Nickerson, P.E.B., Schuurmans, C., Bremner, R., Wallace, V.A., 2021. Photoreceptor nanotubes mediate the in vivo exchange of intracellular material. EMBO J 40, e107264. https://doi.org/10.15252/embj.2020107264

Pepe, A., Pietropaoli, S., Vos, M., Barba-Spaeth, G., Zurzolo, C., n.d. Tunneling nanotubes provide a route for SARS-CoV-2 spreading. Sci Adv 8, eabo0171. https://doi.org/10.1126/sciadv.abo0171

Pergu, R., Dagar, S., Kumar, H., Kumar, R., Bhattacharya, J., Mylavarapu, S.V.S., 2019. The chaperone ERp29 is required for tunneling nanotube formation by stabilizing MSec. J Biol Chem 294, 7177–7193. https://doi.org/10.1074/jbc.RA118.005659

Pinto, G., Brou, C., Zurzolo, C., 2020. Tunneling Nanotubes: The Fuel of Tumor Progression? Trends Cancer 6, 874–888. https://doi.org/10.1016/j.trecan.2020.04.012

Pinto, G., Saenz-de-Santa-Maria, I., Chastagner, P., Perthame, E., Delmas, C., Toulas, C., Moyal-Jonathan-Cohen, E., Brou, C., Zurzolo, C., 2021. Patient-derived glioblastoma stem cells transfer mitochondria through tunneling nanotubes in tumor organoids. Biochem J 478, 21–39. https://doi.org/10.1042/BCJ20200710

Pontes, B., Viana, N.B., Campanati, L., Farina, M., Neto, V.M., Nussenzveig, H.M., 2008. Structure and elastic properties of tunneling nanotubes. Eur Biophys J 37, 121–129. https://doi.org/10.1007/s00249-007-0184-9

Pounds, S., Cheng, C., 2006. Robust estimation of the false discovery rate. Bioinformatics 22, 1979–1987. https://doi.org/10.1093/bioinformatics/btl328

Resnik, N., Prezelj, T., De Luca, G.M.R., Manders, E., Polishchuk, R., Veranič, P., Kreft, M.E., 2018. Helical organization of microtubules occurs in a minority of tunneling membrane nanotubes in normal and cancer urothelial cells. Sci Rep 8, 17133. https://doi.org/10.1038/s41598-018-35370-y

Rubinstein, E., Ziyyat, A., Prenant, M., Wrobel, E., Wolf, J.-P., Levy, S., Le Naour, F., Boucheix, C., 2006a. Reduced fertility of female mice lacking CD81. Dev Biol 290, 351–358. https://doi.org/10.1016/j.ydbio.2005.11.031

Rubinstein, E., Ziyyat, A., Wolf, J.-P., Le Naour, F., Boucheix, C., 2006b. The molecular players of sperm-egg fusion in mammals. Semin Cell Dev Biol 17, 254–263. https://doi.org/10.1016/j.semcdb.2006.02.012

Rustom, A., Saffrich, R., Markovic, I., Walther, P., Gerdes, H.-H., 2004. Nanotubular highways for intercellular organelle transport. Science 303, 1007–1010. https://doi.org/10.1126/science.1093133

Sala-Valdés, M., Ursa, A., Charrin, S., Rubinstein, E., Hemler, M.E., Sánchez-Madrid, F., Yáñez-Mó, M., 2006. EWI-2 and EWI-F link the tetraspanin web to the actin cytoskeleton through their direct association with ezrin-radixin-moesin proteins. J Biol Chem 281, 19665–19675. https://doi.org/10.1074/jbc.M602116200

Sartori-Rupp, A., Cordero Cervantes, D., Pepe, A., Gousset, K., Delage, E., Corroyer-Dulmont, S., Schmitt, C., Krijnse-Locker, J., Zurzolo, C., 2019. Correlative cryo-electron microscopy reveals the structure of TNTs in neuronal cells. Nat Commun 10, 342. https://doi.org/10.1038/s41467-018-08178-7

Sherman, B.T., Hao, M., Qiu, J., Jiao, X., Baseler, M.W., Lane, H.C., Imamichi, T., Chang, W., 2022. DAVID: a web server for functional enrichment analysis and functional annotation of gene lists (2021 update). Nucleic Acids Research 50, W216–W221. https://doi.org/10.1093/nar/gkac194

Smyth, G.K., 2004. Linear models and empirical bayes methods for assessing differential expression in microarray experiments. Stat Appl Genet Mol Biol 3, Article3. https://doi.org/10.2202/1544-6115.1027

Szklarczyk, D., Gable, A.L., Nastou, K.C., Lyon, D., Kirsch, R., Pyysalo, S., Doncheva, N.T., Legeay, M., Fang, T., Bork, P., Jensen, L.J., von Mering, C., 2021. The STRING database in 2021: customizable protein-protein networks, and functional characterization of user-uploaded gene/measurement sets. Nucleic Acids Res 49, D605–D612. https://doi.org/10.1093/nar/gkaa1074

Takeda, Y., Tachibana, I., Miyado, K., Kobayashi, M., Miyazaki, T., Funakoshi, T., Kimura, H., Yamane, H., Saito, Y., Goto, H., Yoneda, T., Yoshida, M., Kumagai, T., Osaki, T., Hayashi, S., Kawase, I., Mekada, E., 2003. Tetraspanins CD9 and CD81 function to prevent the fusion of mononuclear phagocytes. J Cell Biol 161, 945–956. https://doi.org/10.1083/jcb.200212031

Termini, C.M., Gillette, J.M., 2017. Tetraspanins Function as Regulators of Cellular Signaling. Front Cell Dev Biol 5, 34. https://doi.org/10.3389/fcell.2017.00034

Théry, C., Amigorena, S., Raposo, G., Clayton, A., 2006. Isolation and Characterization of Exosomes from Cell Culture Supernatants and Biological Fluids. Current Protocols in Cell Biology 30, 3.22.1-3.22.29. https://doi.org/10.1002/0471143030.cb0322s30

Théry, C., Witwer, K.W., Aikawa, E., Alcaraz, M.J., Anderson, J.D., Andriantsitohaina, R., Antoniou, A., Arab, T., Archer, F., Atkin-Smith, G.K., Ayre, D.C., Bach, J.-M., Bachurski, D., Baharvand, H., Balaj, L., Baldacchino, S., Bauer, N.N., Baxter, A.A.,

Bebawy, M., Beckham, C., Bedina Zavec, A., Benmoussa, A., Berardi, A.C., Bergese, P., Bielska, E., Blenkiron, C., Bobis-Wozowicz, S., Boilard, E., Boireau, W., Bongiovanni, A., Borràs, F.E., Bosch, S., Boulanger, C.M., Breakefield, X., Breglio, A.M., Brennan, M.Á., Brigstock, D.R., Brisson, A., Broekman, M.L., Bromberg, J.F., Bryl-Górecka, P., Buch, S., Buck, A.H., Burger, D., Busatto, S., Buschmann, D., Bussolati, B., Buzás, E.I., Byrd, J.B., Camussi, G., Carter, D.R., Caruso, S., Chamley, L.W., Chang, Y.-T., Chen, C., Chen, S., Cheng, L., Chin, A.R., Clayton, A., Clerici, S.P., Cocks, A., Cocucci, E., Coffey, R.J., Cordeiro-da-Silva, A., Couch, Y., Coumans, F.A., Coyle, B., Crescitelli, R., Criado, M.F., D'Souza-Schorey, C., Das, S., Datta Chaudhuri, A., de Candia, P., De Santana, E.F., De Wever, O., Del Portillo, H.A., Demaret, T., Deville, S., Devitt, A., Dhondt, B., Di Vizio, D., Dieterich, L.C., Dolo, V., Dominguez Rubio, A.P., Dominici, M., Dourado, M.R., Driedonks, T.A., Duarte, F.V., Duncan, H.M., Eichenberger, R.M., Ekström, K., El Andaloussi, S., Elie-Caille, C., Erdbrügger, U., Falcón-Pérez, J.M., Fatima, F., Fish, J.E., Flores-Bellver, M., Försönits, A., Frelet-Barrand, A., Fricke, F., Fuhrmann, G., Gabrielsson, S., Gámez-Valero, A., Gardiner, C., Gärtner, K., Gaudin, R., Gho, Y.S., Giebel, B., Gilbert, C., Gimona, M., Giusti, I., Goberdhan, D.C., Görgens, A., Gorski, S.M., Greening, D.W., Gross, J.C., Gualerzi, A., Gupta, G.N., Gustafson, D., Handberg, A., Haraszti, R.A., Harrison, P., Hegyesi, H., Hendrix, A., Hill, A.F., Hochberg, F.H., Hoffmann, K.F., Holder, B., Holthofer, H., Hosseinkhani, B., Hu, G., Huang, Y., Huber, V., Hunt, S., Ibrahim, A.G.-E., Ikezu, T., Inal, J.M., Isin, M., Ivanova, A., Jackson, H.K., Jacobsen, S., Jay, S.M., Jayachandran, M., Jenster, G., Jiang, L., Johnson, S.M., Jones, J.C., Jong, A., Jovanovic-Talisman, T., Jung, S., Kalluri, R., Kano, S.-I., Kaur, S., Kawamura, Y., Keller, E.T., Khamari, D., Khomyakova, E., Khvorova, A., Kierulf, P., Kim, K.P., Kislinger, T., Klingeborn, M., Klinke, D.J., Kornek, M., Kosanović, M.M., Kovács, Á.F., Krämer-Albers, E.-M., Krasemann, S., Krause, M., Kurochkin, I.V., Kusuma, G.D., Kuypers, S., Laitinen, S., Langevin, S.M., Languino, L.R., Lannigan, J., Lässer, C., Laurent, L.C., Lavieu, G., Lázaro-Ibáñez, E., Le Lay, S., Lee, M.-S., Lee, Y.X.F., Lemos, D.S., Lenassi, M., Leszczynska, A., Li, I.T., Liao, K., Libregts, S.F., Ligeti, E., Lim, R., Lim, S.K., Linē, A., Linnemannstöns, K., Llorente, A., Lombard, C.A., Lorenowicz, M.J., Lörincz, Á.M., Lötvall, J., Lovett, J., Lowry, M.C., Loyer, X., Lu, Q., Lukomska, B., Lunavat, T.R., Maas, S.L., Malhi, H., Marcilla, A., Mariani, J., Mariscal, J., Martens-Uzunova, E.S., Martin-Jaular, L., Martinez, M.C., Martins, V.R., Mathieu, M., Mathivanan, S., Maugeri, M., McGinnis, L.K., McVey, M.J., Meckes, D.G., Meehan, K.L., Mertens, I., Minciacchi, V.R., Möller, A., Møller

Jørgensen, M., Morales-Kastresana, A., Morhayim, J., Mullier, F., Muraca, M., Musante, L., Mussack, V., Muth, D.C., Myburgh, K.H., Najrana, T., Nawaz, M., Nazarenko, I., Nejsum, P., Neri, C., Neri, T., Nieuwland, R., Nimrichter, L., Nolan, J.P., Nolte-'t Hoen, E.N., Noren Hooten, N., O'Driscoll, L., O'Grady, T., O'Loghlen, A., Ochiya, T., Olivier, M., Ortiz, A., Ortiz, L.A., Osteikoetxea, X., Østergaard, O., Ostrowski, M., Park, J., Pegtel, D.M., Peinado, H., Perut, F., Pfaffl, M.W., Phinney, D.G., Pieters, B.C., Pink, R.C., Pisetsky, D.S., Pogge von Strandmann, E., Polakovicova, I., Poon, I.K., Powell, B.H., Prada, I., Pulliam, L., Quesenberry, P., Radeghieri, A., Raffai, R.L., Raimondo, S., Rak, J., Ramirez, M.I., Raposo, G., Rayyan, M.S., Regev-Rudzki, N., Ricklefs, F.L., Robbins, P.D., Roberts, D.D., Rodrigues, S.C., Rohde, E., Rome, S., Rouschop, K.M., Rughetti, A., Russell, A.E., Saá, P., Sahoo, S., Salas-Huenuleo, E., Sánchez, C., Saugstad, J.A., Saul, M.J., Schiffelers, R.M., Schneider, R., Schøyen, T.H., Scott, A., Shahaj, E., Sharma, S., Shatnyeva, O., Shekari, F., Shelke, G.V., Shetty, A.K., Shiba, K., Siljander, P.R.-M., Silva, A.M., Skowronek, A., Snyder, O.L., Soares, R.P., Sódar, B.W., Soekmadji, C., Sotillo, J., Stahl, P.D., Stoorvogel, W., Stott, S.L., Strasser, E.F., Swift, S., Tahara, H., Tewari, M., Timms, K., Tiwari, S., Tixeira, R., Tkach, M., Toh, W.S., Tomasini, R., Torrecilhas, A.C., Tosar, J.P., Toxavidis, V., Urbanelli, L., Vader, P., van Balkom, B.W., van der Grein, S.G., Van Deun, J., van Herwijnen, M.J., Van Keuren-Jensen, K., van Niel, G., van Royen, M.E., van Wijnen, A.J., Vasconcelos, M.H., Vechetti, I.J., Veit, T.D., Vella, L.J., Velot, É., Verweij, F.J., Vestad, B., Viñas, J.L., Visnovitz, T., Vukman, K.V., Wahlgren, J., Watson, D.C., Wauben, M.H., Weaver, A., Webber, J.P., Weber, V., Wehman, A.M., Weiss, D.J., Welsh, J.A., Wendt, S., Wheelock, A.M., Wiener, Z., Witte, L., Wolfram, J., Xagorari, A., Xander, P., Xu, J., Yan, X., Yáñez-Mó, M., Yin, H., Yuana, Y., Zappulli, V., Zarubova, J., Žėkas, V., Zhang, J.-Y., Zhao, Z., Zheng, L., Zheutlin, A.R., Zickler, A.M., Zimmermann, P., Zivkovic, A.M., Zocco, D., Zuba-Surma, E.K., 2018. Minimal information for studies of extracellular vesicles 2018 (MISEV2018): a position statement of the International Society for Extracellular Vesicles and update of the MISEV2014 guidelines. J Extracell Vesicles 7, 1535750. https://doi.org/10.1080/20013078.2018.1535750

Tyanova, S., Temu, T., Cox, J., 2016. The MaxQuant computational platform for mass spectrometry-based shotgun proteomics. Nat Protoc 11, 2301–2319. https://doi.org/10.1038/nprot.2016.136

Umeda, R., Satouh, Y., Takemoto, M., Nakada-Nakura, Y., Liu, K., Yokoyama, T., Shirouzu, M., Iwata, S., Nomura, N., Sato, K., Ikawa, M., Nishizawa, T., Nureki, O., 2020. Structural insights into tetraspanin CD9 function. Nat Commun 11, 1606. https://doi.org/10.1038/s41467-020-15459-7

van Niel, G., Carter, D.R.F., Clayton, A., Lambert, D.W., Raposo, G., Vader, P., 2022. Challenges and directions in studying cell-cell communication by extracellular vesicles. Nat Rev Mol Cell Biol 23, 369–382. https://doi.org/10.1038/s41580-022-00460-3

Vargas, J.Y., Loria, F., Wu, Y.-J., Córdova, G., Nonaka, T., Bellow, S., Syan, S., Hasegawa, M., van Woerden, G.M., Trollet, C., Zurzolo, C., 2019. The Wnt/Ca2+ pathway is involved in interneuronal communication mediated by tunneling nanotubes. EMBO J 38, e101230. https://doi.org/10.15252/embj.2018101230

Wang, V.M.-Y., Ferreira, R.M.M., Almagro, J., Evan, T., Legrave, N., Zaw Thin, M., Frith, D., Carvalho, J., Barry, D.J., Snijders, A.P., Herbert, E., Nye, E.L., MacRae, J.I., Behrens, A., 2019. CD9 identifies pancreatic cancer stem cells and modulates glutamine metabolism to fuel tumour growth. Nat Cell Biol 21, 1425–1435. https://doi.org/10.1038/s41556-019-0407-1

Whitaker, E.E., Matheson, N.J., Perlee, S., Munson, P.B., Symeonides, M., Thali, M., 2019. EWI-2 Inhibits Cell–Cell Fusion at the HIV-1 Virological Presynapse. Viruses 11, 1082. https://doi.org/10.3390/v11121082

Wieczorek, S., Combes, F., Lazar, C., Giai Gianetto, Q., Gatto, L., Dorffer, A., Hesse, A.-M., Couté, Y., Ferro, M., Bruley, C., Burger, T., 2017. DAPAR & ProStaR: software to perform statistical analyses in quantitative discovery proteomics. Bioinformatics 33, 135–136. https://doi.org/10.1093/bioinformatics/btw580

Yáñez-Mó, M., Barreiro, O., Gordon-Alonso, M., Sala-Valdés, M., Sánchez-Madrid, F., 2009. Tetraspanin-enriched microdomains: a functional unit in cell plasma membranes. Trends Cell Biol 19, 434–446. https://doi.org/10.1016/j.tcb.2009.06.004

Zhao, X., Lei, Y., Zheng, J., Peng, J., Li, Y., Yu, L., Chen, Y., 2019. Identification of markers for migrasome detection. Cell Discov 5, 1–4. https://doi.org/10.1038/s41421-019-0093-y

Zimmerman, B., Kelly, B., McMillan, B.J., Seegar, T.C.M., Dror, R.O., Kruse, A.C., Blacklow, S.C., 2016. Crystal Structure of a Full-Length Human Tetraspanin Reveals a Cholesterol-Binding Pocket. Cell 167, 1041-1051.e11. https://doi.org/10.1016/j.cell.2016.09.056

Figure 1

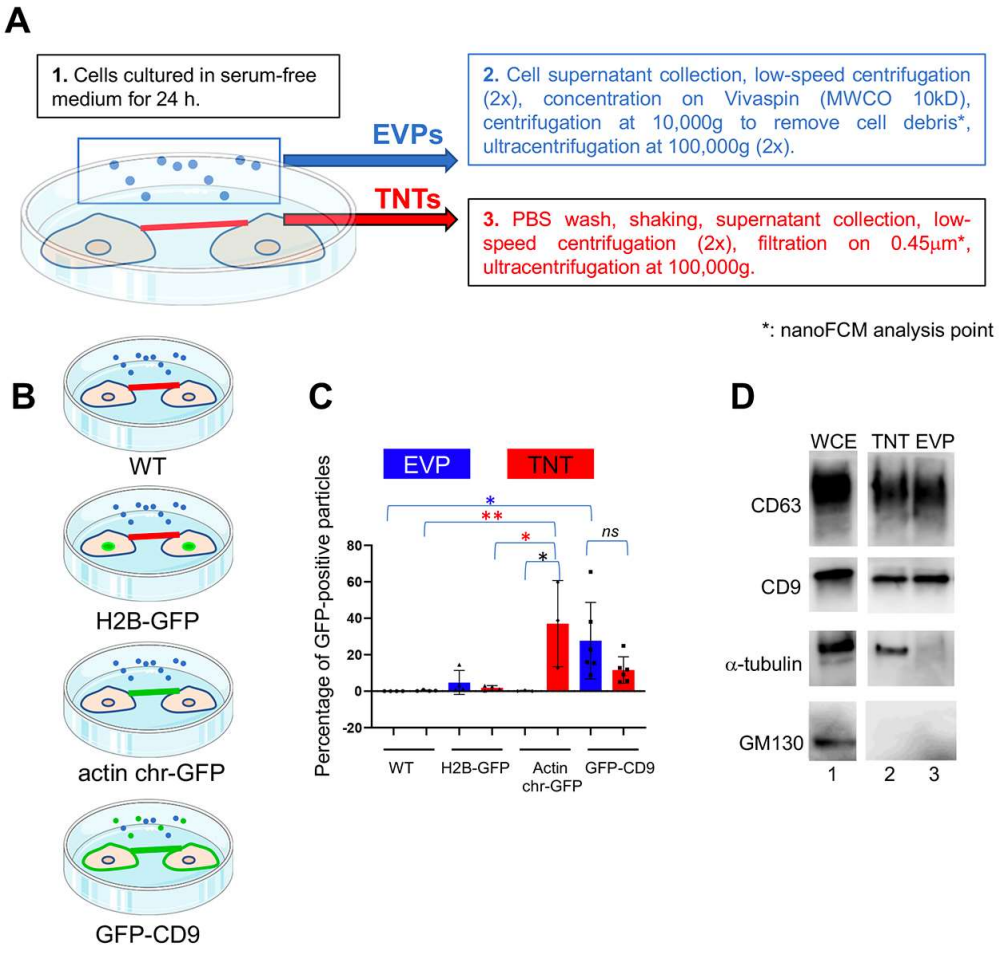
A
1. Cells cultured in serum-free medium for 24 h.
EVPs
TNTs
2. Cell supernatant collection, low-speed centrifugation (2x), concentration on Vivaspin (MWCO 10kD), centrifugation at 10,000g to remove cell debris*, ultracentrifugation at 100,000g (2x).
3. PBS wash, shaking, supernatant collection, low-speed centrifugation (2x), filtration on 0.45µm*, ultracentrifugation at 100,000g.
*: nanoFCM analysis point
B
WT
H2B-GFP
actin chr-GFP
GFP-CD9
C
EVP
TNT
Percentage of GFP-positive particles
80
60
40
20
0
-20
*
**
*
*
ns
WT
H2B-GFP
Actin chr-GFP
GFP-CD9
D
WCE
TNT EVP
CD63
CD9
α-tubulin
GM130
1
2
3

Figure 1: Validation of the purification procedures

A. Workflow for TNTs vs. EVPs purification. EVPs were purified from cell culture supernatant, TNTs from remaining attached cell supernatant after shaking. *indicates the fraction used for nanoFCM analysis.

B. Schematic representation of stably cell lines where green color indicates the location of GFP-tagged protein: H2B-GFP (nuclear), actin chromobody-GFP (actin cytoskeleton including TNTs) and GFP-CD9 (cell surface, TNTs, EVPs).

C. Scatter dot plot representing the mean percentage (with SD) of GFP-positive particles analyzed by nanoFCM. Statistical analysis of 4 independent experiments (6 for GFP-CD9, oneway Anova with Tukey post hoc correction) show the following respective p-values (from top): blue*: 0.0252, red**: 0.0089, red*: 0.0131, black*: 0.0161. Means values are (from left to right): 0.01, 0.3, 4.8, 1.75, 0.17, 37.07, 27.7 and 11.6.

D. Western blot of WCE (20□g, corresponding to around 0.1x106 cells), TNT and EVP (both from 10 106 cells) prepared from the same cells, blotted with CD9, □-tubulin and GM130 specific antibodies. White lane indicates that intervening lanes of the same gel (and same exposure) have been spliced out.

Figure 2

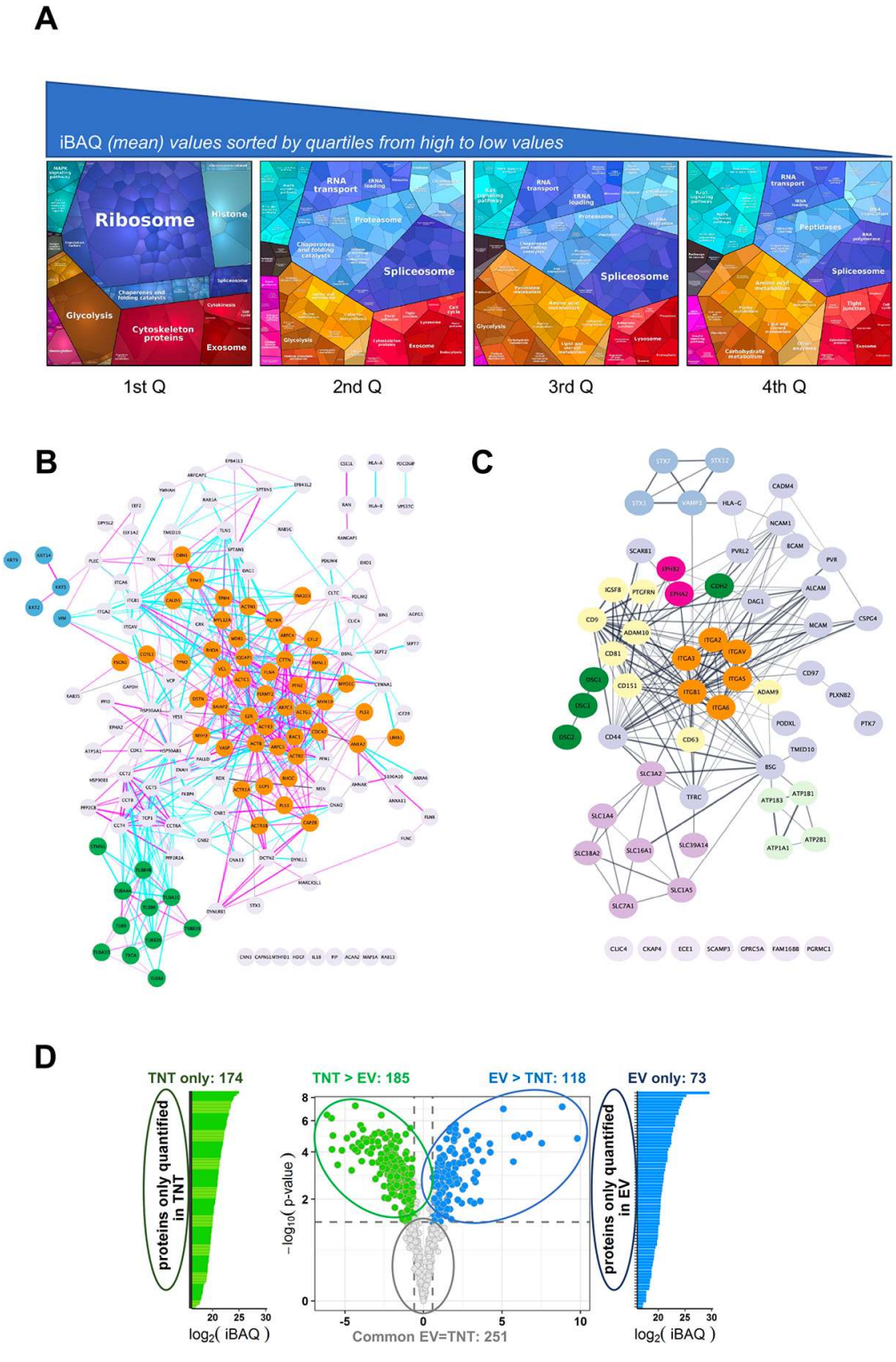
A
iBAQ (mean) values sorted by quartiles from high to low values
Ribosome
Histone
Glycolysis
Cytoskeleton proteins
Exosome
RNA transport
Proteasome
Spliceosome
Peptidases
1st Q
2nd Q
3rd Q
4th Q
B
C
D
TNT only: 174
TNT > EV: 185
EV > TNT: 118
EV only: 73
proteins only quantified in TNT
proteins only quantified in EV
−log10(p-value)
log2(iBAQ)
Common EV=TNT: 251

Figure 2: Analysis of the TNTome

A. Proteomap of the 1177 proteins of the TNTome, sorted in 4 quartiles depending on their mean iBAQ. Protein accession and mean iBAQ was used to create ProteoMap, analyzed according to Gene Ontology.

B. STRING physical association network for the cytoskeleton-related proteins listed in table S2. Color groups were created using Cytoscape. Green are microtubule-related proteins, blue are intermediate filaments, orange are actin-interacting proteins. Blue and pink edges show physical interactions based on databases and experiments respectively.

C. Full STRING functional association network for integral surface membrane proteins of TNTome, based on table S3. Orange are Integrin proteins, red are Ephrin receptors, dark green are Cadherins, light green are Sodium/potassium transporting ATPase ions channels, purple are monocarboxylate and amino acids transporters, and yellow are tetraspanin-related proteins.

D. Volcano plot of the mass spectrometry analysis based on the 4 EVP and TNT preparations, showing the maximum log2(Fold-change) in x-axis measured between TNT and EVP fractions and the corresponding -log10 (p-value) in y-axis. Dashed lines indicate differential analysis quadrants with log2 (Fold-change) =0.58 and false discovery rate FDR = 1%. Common EVP=TNT are non-significantly different (FDR >0.05) with FC>1.5, and FC<1.5. Each quadrant is named above and the number of identified proteins is indicated. Left and right are proteins non overlapping in both fractions: TNT-only and EVP only. Note that in EVP-only fraction, 10 proteins were found in TNTome (based on 12 experiments) and should therefore be removed. For the TNT proteins, only the proteins also present in TNTome have been counted.

Figure 3

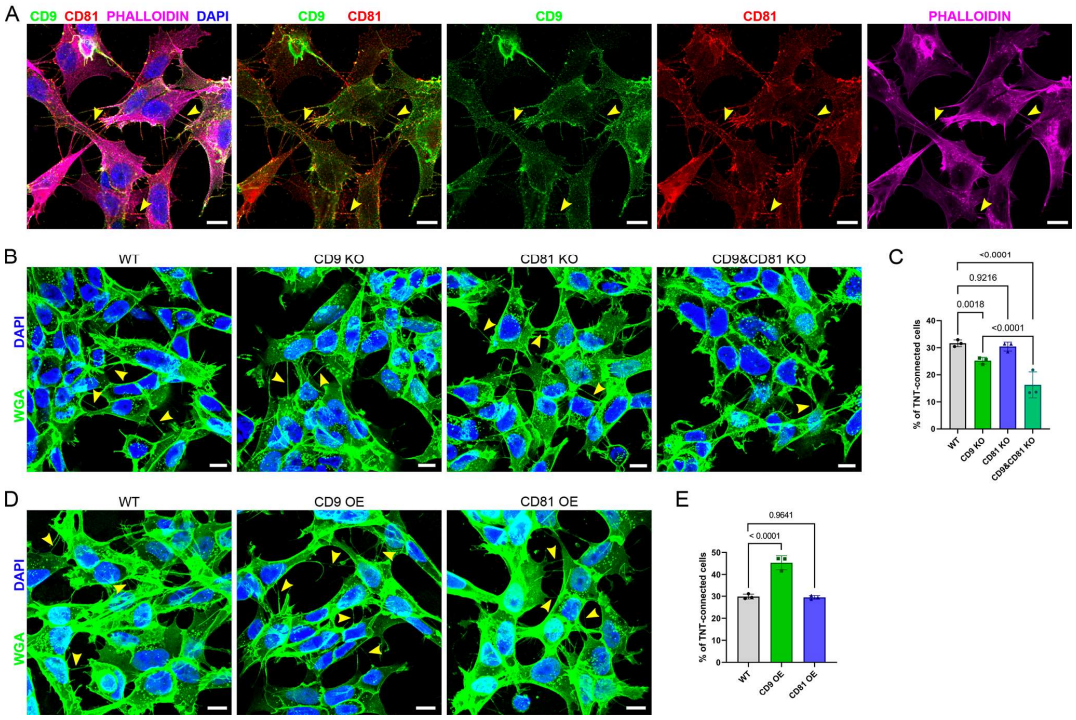
A
CD9 CD81 PHALLOIDIN DAPI
CD9 CD81
CD9
CD81
PHALLOIDIN
B
WT
CD9 KO
CD81 KO
CD9&CD81 KO
DAPI
WGA
C
<0.0001
0.9216
0.0018
<0.0001
% of TNT-connected cells
WT
CD9 KO
CD81 KO
CD9&CD81 KO
D
WT
CD9 OE
CD81 OE
DAPI
WGA
E
0.9641
< 0.0001
% of TNT-connected cells
WT
CD9 OE
CD81 OE

Figure 3: Expression of CD9/CD81 in TNTs and effects of their overexpression or invalidation

A. Immunofluorescence of CD9 (green) and CD81 (red) in SH-SY5Y cells. Cells were also stained with phalloidin (magenta) and DAPI (blue) to visualize actin and nuclei. This representative image corresponds to the 4th to 5th slices of a stack comprising 11 slices (1 being at the bottom). The yellow arrowheads point to TNTs, connecting two cells and not attached to the substrate. The scale bars are 10 µm.

B. Representative images of TNT-connected cells in WT, CD9 KO, CD81 KO and CD9&CD81 KO cells, stained with WGA-488 (green) to label the membrane and DAPI (blue) to label the nuclei. Yellow arrowheads point to TNTs. Scale bars correspond to 10 µm.

C. Graph of the % of TNT-connected cells in the different cells, from 3 independent experiments. Mean and standard deviation of the % of TNT-connected cells: WT = 31.6 ± 1.25; CD9 KO = 25.2 ± 1.24; CD81 KO = 30.4 ± 1.65; CD9 & CD81 KO = 16.3 ± 4.81. ** p=0.0018 for WT versus CD9 KO, ns p=0.9216 for WT versus CD81 KO, **** p<0.0001 for WT versus CD9 & CD81 KO, **** p<0.0001 for CD9 & CD81 KO versus CD9 KO.

D. Representative images of TNT-connected cells in WT, CD9 OE and CD81 OE cells, stained as in B. Yellow arrowheads show TNTs. Scale bars correspond to 10 µm.

E. Graph of the % of TNT-connected cells in the indicated cells from 3 independent experiments. Mean and standard deviation of the % of TNT-connected cells: WT = 29.8 ± 1.11; CD9 OE = 45.3 ± 3.17; CD81 OE = 29.5 ± 0.84. **** p<0.0001 for WT versus CD9 OE, ns p=0.9641 for WT versus CD81 OE.

Figure 4

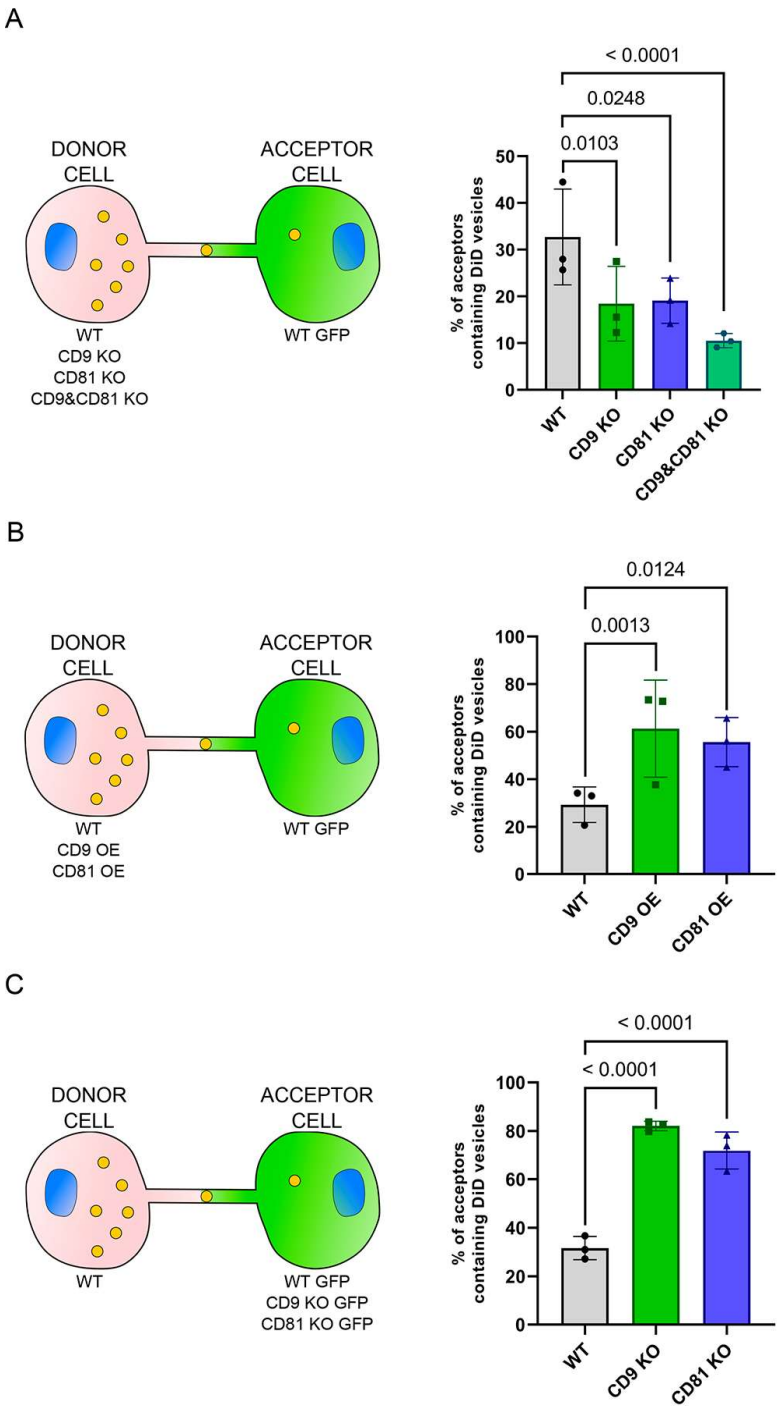
A
DONOR CELL
ACCEPTOR CELL
WT
CD9 KO
CD81 KO
CD9&CD81 KO
WT GFP
< 0.0001
0.0248
0.0103
% of acceptors containing DiD vesicles
50
40
30
20
10
0
WT
CD9 KO
CD81 KO
CD9&CD81 KO
B
DONOR CELL
ACCEPTOR CELL
WT
CD9 OE
CD81 OE
WT GFP
0.0124
0.0013
% of acceptors containing DiD vesicles
100
80
60
40
20
0
WT
CD9 OE
CD81 OE
C
DONOR CELL
ACCEPTOR CELL
WT
WT GFP
CD9 KO GFP
CD81 KO GFP
< 0.0001
< 0.0001
% of acceptors containing DiD vesicles
100
80
60
40
20
0
WT
CD9 KO
CD81 KO

Figure 4: Vesicle transfer assay in cells KO and OE of CD9 and CD81

Donor cells, loaded with DiD to stain the vesicles were cocultured with GFP cells as acceptors, as schematized on the left of each panel. Graphs are % of acceptor cells containing DiD vesicles from 3 independent experiments. Mean and standard deviation of the % of acceptor cells containing DiD vesicles are:

A. WT = 32.7 ± 10.25; CD9 KO = 18.4 ± 8; CD81 KO = 19.1 ± 4.86; CD9 & CD81 KO = 10.5 ± 1.52. * p=0.0103 for WT versus CD9 KO, * p=0.0248 for WT versus CD81 KO, **** p<0.0001 for WT versus CD9 & CD81 KO.

B. WT = 29.3 ± 7.45; CD9 OE = 61.3 ± 20.44; CD81 OE = 55.6 ± 10.31. ** p=0.0013 for WT versus CD9 OE, * p=0.0124 for WT versus CD81 OE.

C. WT = 31.7 ± 4.81; CD9 KO = 82.1 ± 1.98; CD81 KO = 71.9 ± 7.71. **** p<0.0001 for WT versus CD9 KO, **** p<0.0001 for WT versus CD81 KO.

Figure 5

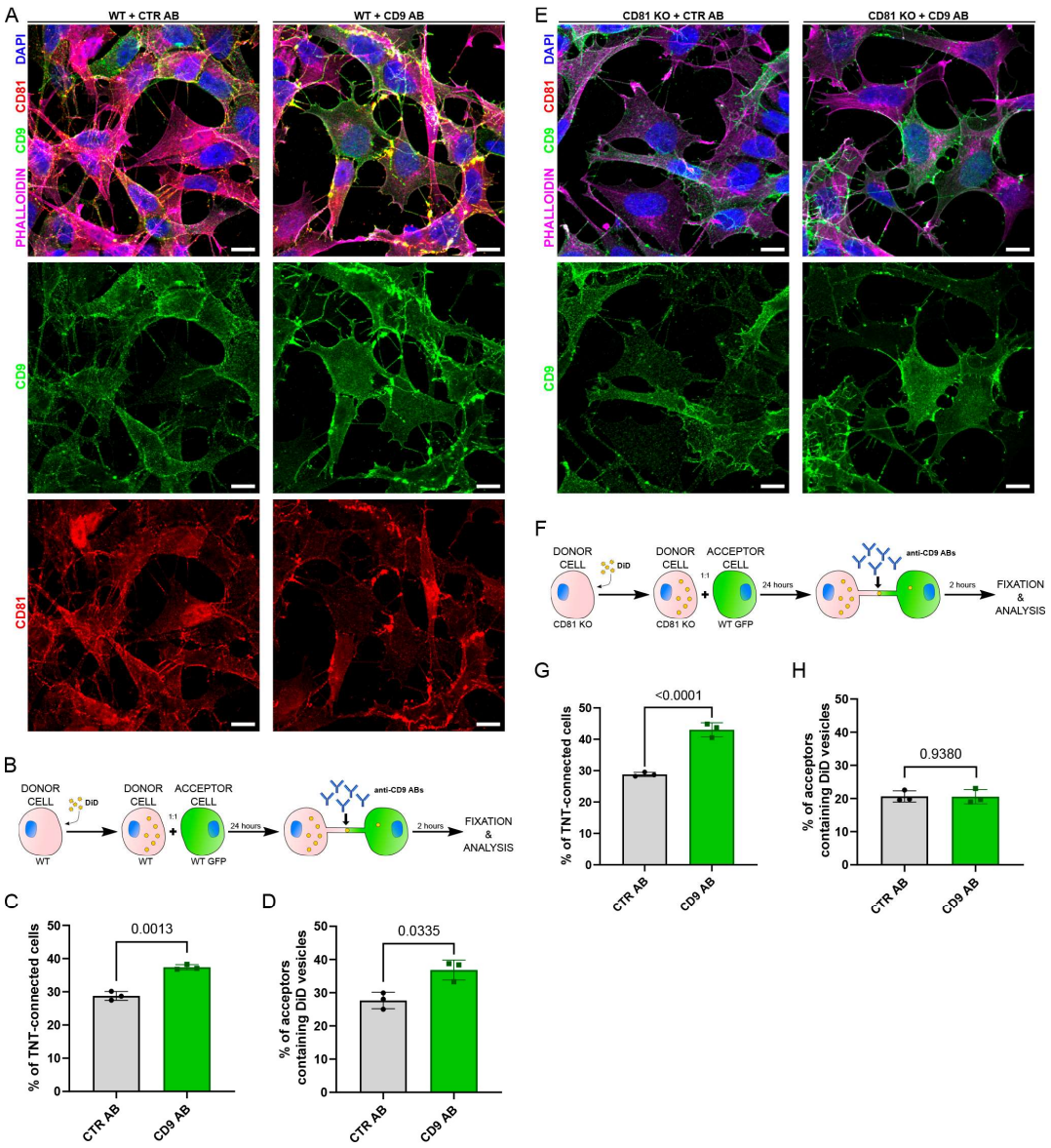
A
WT + CTR AB
WT + CD9 AB
DAPI
CD81
CD9
PHALLOIDIN
E
CD81 KO + CTR AB
CD81 KO + CD9 AB
F
DONOR CELL
DiD
CD81 KO
ACCEPTOR CELL
WT GFP
24 hours
anti-CD9 ABs
2 hours
FIXATION & ANALYSIS
B
WT
C
% of TNT-connected cells
0.0013
CTR AB
CD9 AB
D
% of acceptors containing DiD vesicles
0.0335
G
<0.0001
H
0.9380

Figure 5: CD9 antibody treatment in WT cells and CD81 KO cells

A. Immunofluorescence of CD9 (green) and CD81 (red) in SH-SY5Y WT cells treated with control antibodies (CTR AB) or with antibodies anti-CD9 (CD9 AB) for 2 hours followed by PFA fixation and incubation with anti-CD81 (for CD9 AB samples) or anti-CD81 + anti-CD9 (for CTR AB samples) and appropriate fluorescent secondary antibodies. This representative image corresponds to the 3th to 4th slices of a stack comprising 12 slices for CTR AB and to the 3th to 4th slices of a stack comprising 11 slices for CD9 AB. Cells were also stained with phalloidin (magenta) and DAPI (blue) to visualize actin and nuclei respectively. The scale bars correspond to 10 µm.

B. Schematic of the experiment corresponding to the coculture of WT SH-SY5Y donor cells (DiD in yellow circles to stain the vesicles) and WT GFP-labeled acceptor cells, and the cocultured cells were treated with control antibodies (CTR AB) or with antibodies anti-CD9 (CD9 AB).

C. Graph of the % of TNT-connected cells in CTR AB or CD9 AB treatment in WT cells. Mean and standard deviation of the % of TNT-connected cells: CTR AB = 28.8 ± 1.32; CD9 AB = 37.4 ± 0.80. ** $p<0.0013$ for CTR AB versus CD9 AB for N=3.

D. Graph of the % of acceptor cells containing DiD vesicles of the cocultures of WT cells with CTR AB or CD9 AB treatment. Mean and standard deviation of the % of acceptor cells containing DiD vesicles: CTR AB = 27.7 ± 2.48; CD9 AB = 36.8 ± 3.03. * $p=0.0335$ for 2ry AB versus CD9 AB for N=3.

E. Immunofluorescence of CD9 (green) in SH-SY5Y CD81 KO cells treated with control antibodies (CTR AB) or with antibodies anti-CD9 (CD9 AB) for 2 hours followed by PFA fixation and incubation with anti-CD9 (for CTR AB samples) and appropriate fluorescent secondary antibodies. This representative image corresponds to the 3th to 4th slices of a stack comprising 10 slices for CTR AB and to the 5th to 6th slices of a stack comprising 12 slices for CD9 AB. Cells were also stained with phalloidin (magenta) and DAPI (blue) to visualize actin and nuclei respectively. Scale bars are 10 µm.

F. Schematic showing the coculture strategy adapted to the antibody treatment in SH-SY5Y CD81 KO cells. SH-SY5Y CD81 KO donor cells (DiD in yellow circles to stain the vesicles) were cocultured with WT GFP-labeled acceptor cells and all of them treated with control antibodies (CTR AB) or with antibodies anti-CD9 (CD9 AB).

G. Graph of the % of TNT-connected cells in the coculture and antibody treatment described in B. Mean and standard deviation of the % of TNT-connected cells: CTR AB = 28.8 ± 0.68; CD9 AB = 43 ± 2.23. **** $p<0.0001$ for CTR AB versus CD9 AB for N=3.

H. Graph of the % of acceptor cells containing DiD vesicles of the same experiment. Mean and standard deviation of the % of acceptor cells containing DiD vesicles: CTR AB = 20.6 ± 1.67; CD9 AB = 20.6 ± 2.16. ns $p=0.9380$ for CTR AB versus CD9 AB for N=3.

Figure 6

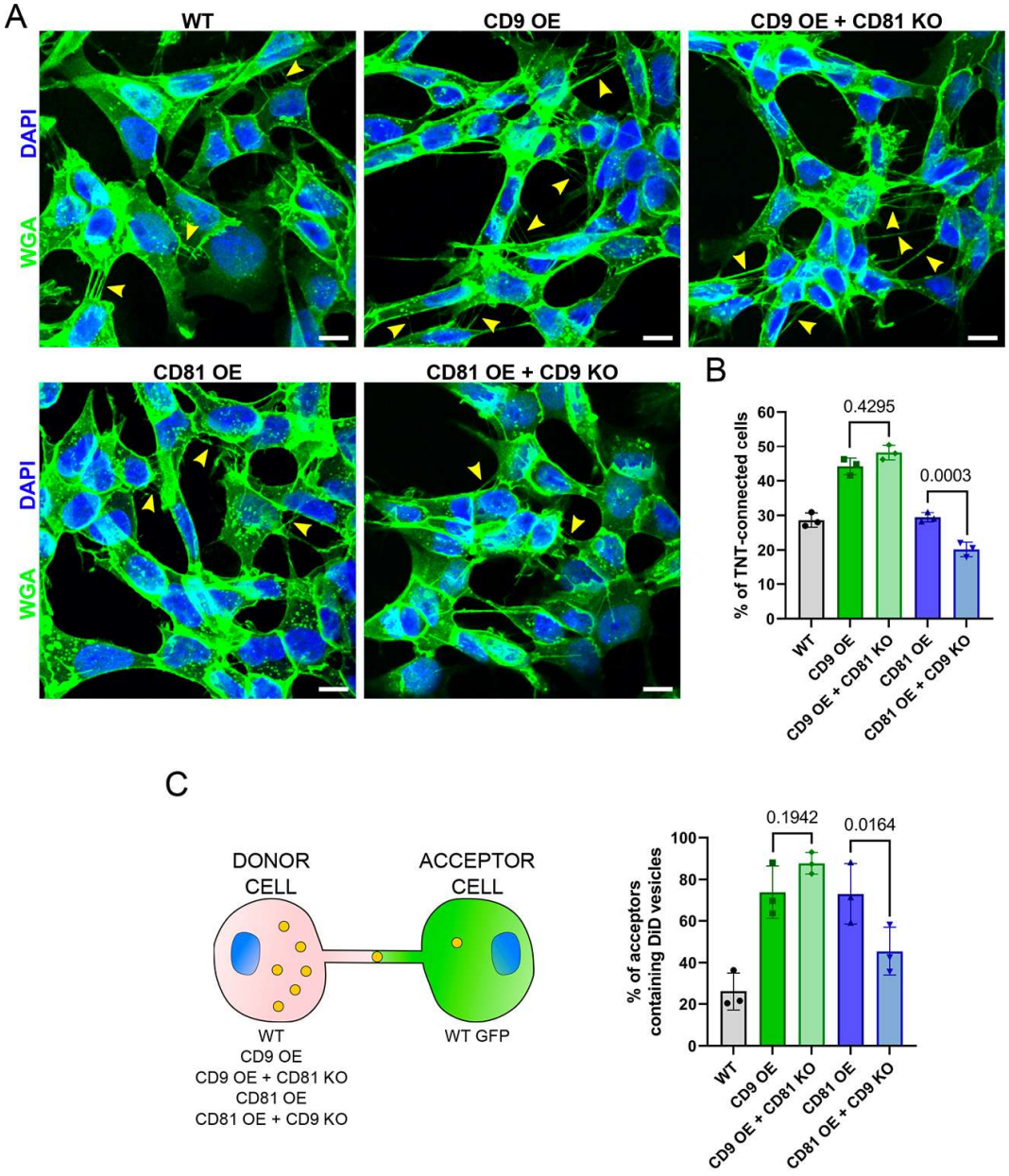
A
WT
CD9 OE
CD9 OE + CD81 KO
CD81 OE
CD81 OE + CD9 KO
DAPI
WGA
B
% of TNT-connected cells
0.4295
0.0003
WT
CD9 OE
CD9 OE + CD81 KO
CD81 OE
CD81 OE + CD9 KO
C
DONOR CELL
ACCEPTOR CELL
WT GFP
WT
CD9 OE
CD9 OE + CD81 KO
CD81 OE
CD81 OE + CD9 KO
% of acceptors containing DiD vesicles
0.1942
0.0164

Figure 6: CD9 and CD81 act successively in the formation of TNTs

A. Representative images of WT, CD9 OE, CD9 OE + CD81 KO, CD81 OE and CD81 OE + CD9 KO cells, stained with WGA-488 (green) and DAPI (blue). Yellow arrowheads show TNTs. Scale bars correspond to 10 μm.

B. Graph of the % of TNT-connected cells in the tetraspanin OE + KO cells. Mean and standard deviation of the % of TNT-connected cells, from 3 independent experiments: WT = 28.6 ± 2.05; CD9 OE = 44.2 ± 2.4; CD9 OE + CD81 KO = 48.2 ± 2.16; CD81 OE = 29.5 ± 1.36; CD81 OE + CD9 KO = 20.2 ± 2.09. ns p=0.4295 for CD9 OE versus CD9 OE + CD81 KO, *** p=0.0003 for CD81 OE versus CD81 OE + CD9 KO.

C. Coculture between tetraspanin OE + KO cells used as donors and WT GFP cells used as acceptors, as schematized on the left. The graph shows the % of acceptor cells containing DiD vesicles Mean and standard deviation of the % of acceptor cells containing DiD vesicles, from 3 independent experiments: WT = 26.1 ± 8.94; CD9 OE = 73.8 ± 12.64; CD9 OE + CD81 KO = 87.7 ± 5.11; CD81 OE = 73 ± 14.60; CD81 OE + CD9 KO = 45.4 ± 11.53. ns p=0.1942 for CD9 OE versus CD9 OE + CD81 KO, * p=0.0164 for CD81 OE versus CD81 OE + CD9 KO.

Figure 7

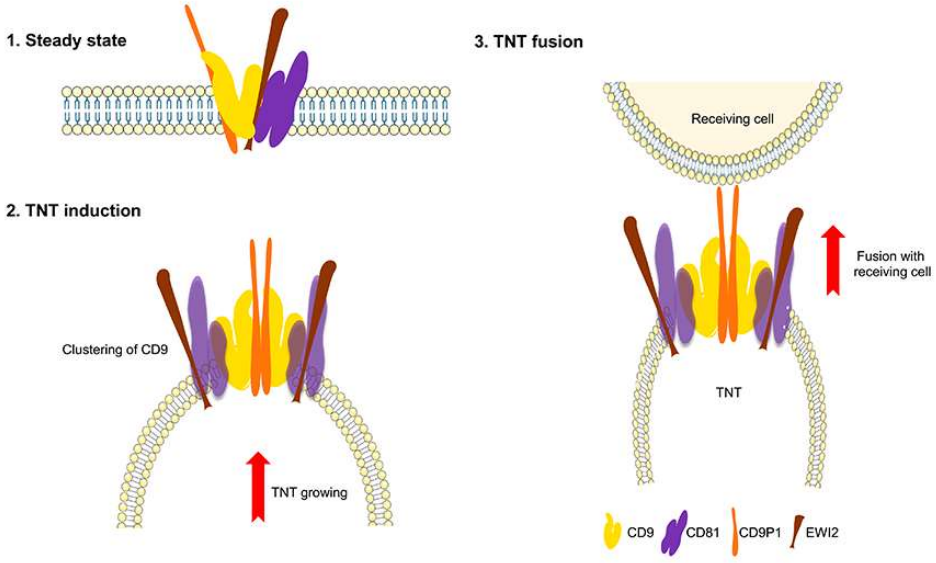
1. Steady state
2. TNT induction
Clustering of CD9
TNT growing
3. TNT fusion
Receiving cell
Fusion with receiving cell
TNT
CD9
CD81
CD9P1
EWI2

Figure 7: Model of CD9 and CD81 roles in TNT growth and fusion with opposing cell

1. At steady state, CD9 and CD81, surrounded by TEM, are in a conformation not inducing membrane curvature. 2. Upon specific TNT stimulating signal, CD9 undergoes conformation change and clustering, leading to membrane curvature and TNT protrusion. At this step, CD81 is not necessary, even though it is brought in the same TEM. 3. CD81 allows to bring together specific proteins involved in fusion with the opposing cell.

Figure S1

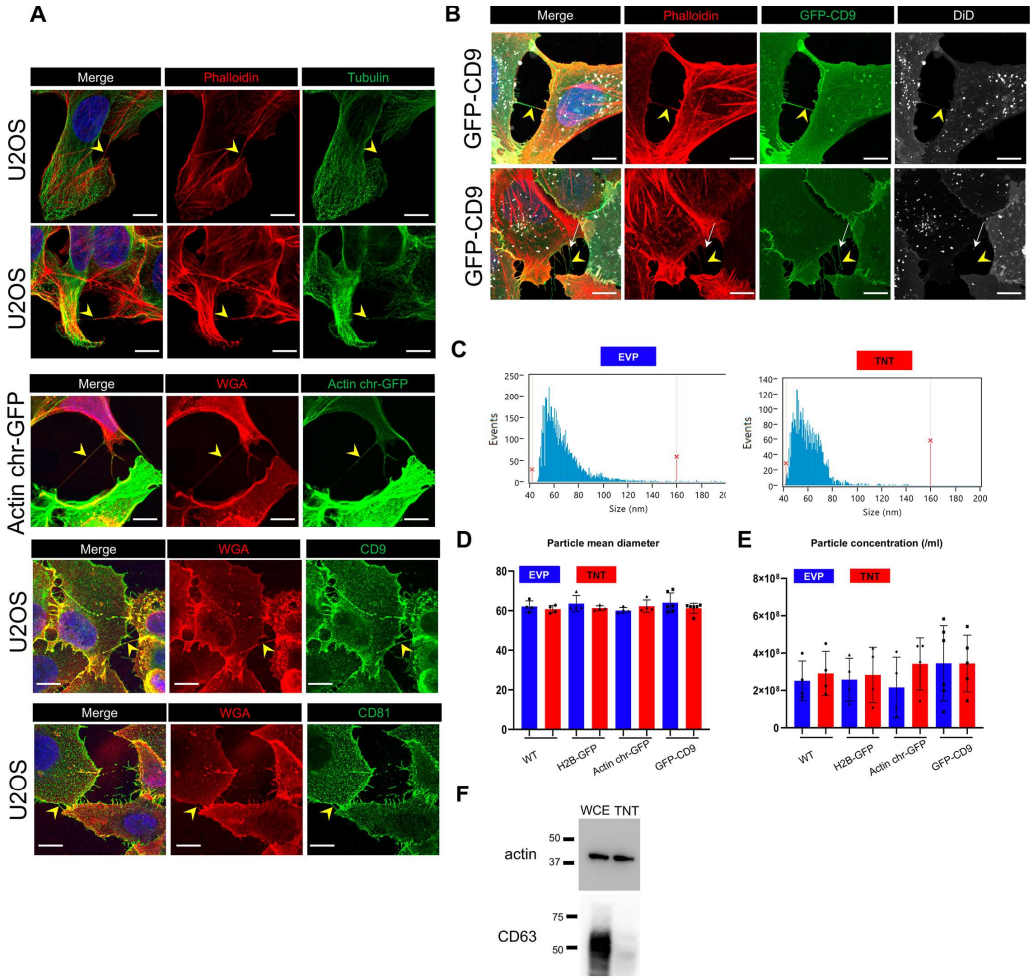
A
Merge
Phalloidin
Tubulin
U2OS
U2OS
Merge
WGA
Actin chr-GFP
Actin chr-GFP
Merge
WGA
CD9
U2OS
Merge
WGA
CD81
U2OS
B
Merge
Phalloidin
GFP-CD9
DiD
GFP-CD9
GFP-CD9
C
EVP
TNT
Events
Size (nm)
D
Particle mean diameter
EVP
TNT
WT
H2B-GFP
Actin chr-GFP
GFP-CD9
E
Particle concentration (/ml)
EVP
TNT
WT
H2B-GFP
Actin chr-GFP
GFP-CD9
F
WCE TNT
actin
CD63

Figure S1: Characterization of TNTs in U2OS cells

A. Representative immunofluorescence of TNTs in U2OS cells, expressing actin (stained with phalloidin, red in the two first lanes) without or with tubulin (green, lanes 1 and 2). Actin-chromodoby-GFP is also expressed in TNTs (lane 3). Lanes 5 and 6 show representative images of CD9 and CD81 in TNTs of U2OS cells. WGA (wheat germ agglutinin in red) labels cell surface of these non-permeabilized cells. The images in lanes 1 to 5 are respectively projections of 1, 3, 3, 2 and 1 slices of each stack. The yellow arrowheads point to TNTs, connecting two cells and not attached to the substrate. The scale bars are 10 μm.

B. Two examples of TNTs in GFP-CD9 expressing U2OS cells. TNTs are identified as containing actin (phalloidin in red), and DiD labels intracellular vesicles, sometimes found inside TNT as in the second lane (white arrow). The yellow arrowheads point to TNTs, scale bars are 10 μm.

C. Representative exemples of size distribution of EVPs and TNTs fractions.

D. Scatter dot plot representing mean size diameter of particles (with SD) of EVP and TNT fractions, depending on each cell line. At least 4 independent experiments were analyzed, each dot being one of them. No statistical difference was observed. Over 18 samples from all cell lines, mean particle diameter was 62.7 nm (SD : 3.8) for EVPs, 61.4 nm (SD 2.2) for TNTs.

E. Scatter dot plot representing mean particle concentration (with SD) of EVP and TNT fractions, depending on each cell line. At least 4 independent experiments were analyzed, each dot being one of them. No statistical difference was observed.

F. Western blot showing actin in WCE and TNT fraction, CD63 is used as loading control.

Figure S2

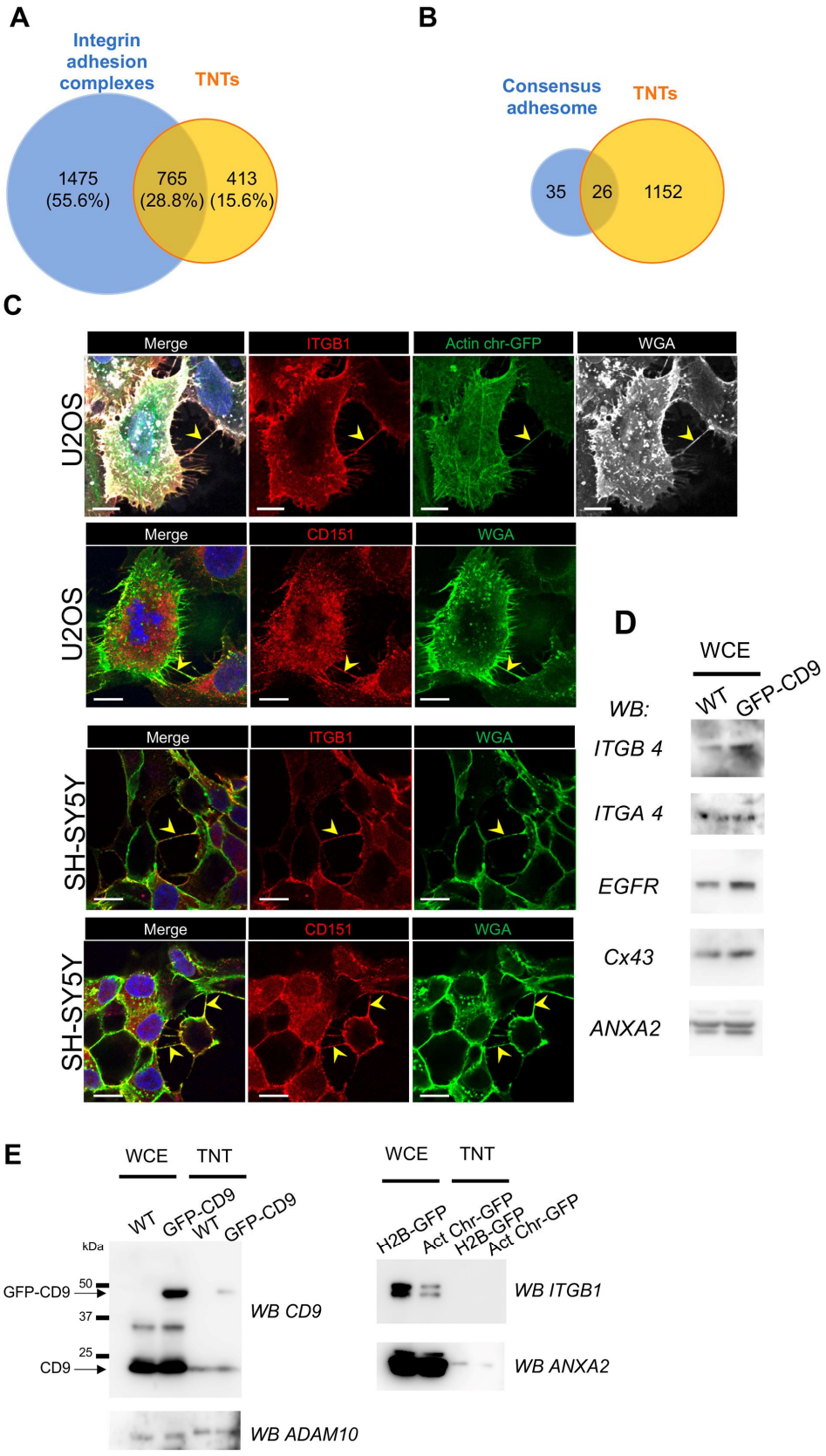
A
Integrin adhesion complexes
TNTs
1475 (55.6%)
765 (28.8%)
413 (15.6%)
B
Consensus adhesome
TNTs
35
26
1152
C
Merge
ITGB1
Actin chr-GFP
WGA
U2OS
Merge
CD151
WGA
U2OS
Merge
ITGB1
WGA
SH-SY5Y
Merge
CD151
WGA
SH-SY5Y
D
WCE
WB:
WT
GFP-CD9
ITGB 4
ITGA 4
EGFR
Cx43
ANXA2
E
WCE
TNT
WT
GFP-CD9
WT
GFP-CD9
kDa
GFP-CD9
50
37
25
CD9
WB CD9
WB ADAM10
WCE
TNT
H2B-GFP
Act Chr-GFP
H2B-GFP
Act Chr-GFP
WB ITGB1
WB ANXA2

Figure S2: Comparison of TNTome with Integrin adhesome and other cell proteins

A. Venn diagram showing common and exclusive proteins between Integrin adhesion complexes (blue circle) and TNTs (yellow circle). The percentages refer to total proteins.

B. Venn diagram showing common and exclusive proteins between consensus adhesome (blue circle) and TNTs (yellow circle).

C. Representative immunofluorescence pictures showing expression of ITGB1 and CD151 in TNTs of U2OS and SH-SY5Y as indicated on the left. Each picture is one upper slice of the stack, TNTs are further characterized by actin presence (actin chromobody-GFP, lane 1) or WGA labeling. The yellow arrowheads point to TNTs, scale bars are 10 □m.

D. Expression of TM proteins in U2OS whole cell extracts (WCE), which are not in TNTome. WB from WT or GFP-CD9 expressing cells, incubated with the antibodies indicated on the left. ANXA2 is used as loading control. WCE from all cell lines have been tested three times, two WCE are shown.

E. Comparative expression of proteins in WCE and TNTs from various U2OS cell lines. Left, CD9, GFP-CD9 and ADAM10 are compared using WT and GFP-CD9 expressing U2OS cells (using non reducing gels). Right, ITGB1 and ANXA2 are compared using H2B-GFP and Actin chromobodies-expressing cells (gels in reducing conditions).

Figure S3

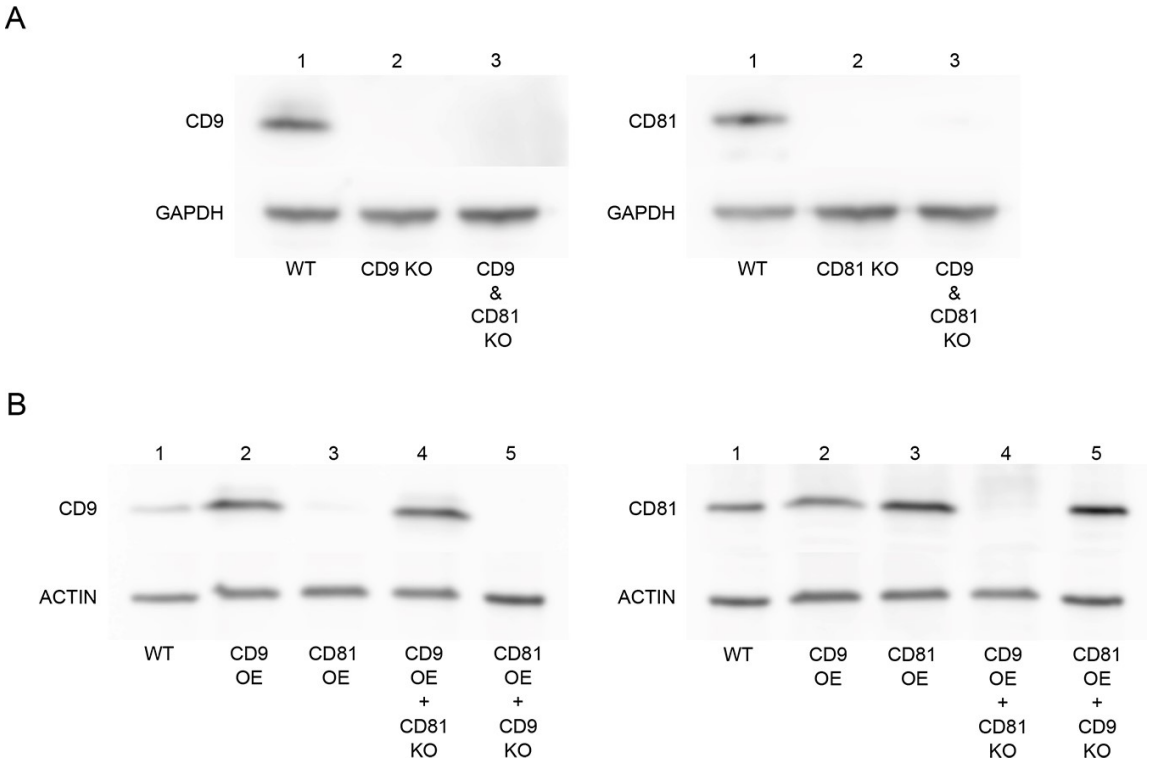
A
1
2
3
CD9
GAPDH
WT
CD9 KO
CD9 & CD81 KO
CD81
GAPDH
WT
CD81 KO
CD9 & CD81 KO
B
1
2
3
4
5
CD9
ACTIN
WT
CD9 OE
CD81 OE
CD9 OE + CD81 KO
CD81 OE + CD9 KO
CD81
ACTIN
WT
CD9 OE
CD81 OE
CD9 OE + CD81 KO
CD81 OE + CD9 KO

Figure S3: Western blot (WB) from the KO and OE of CD9 and or CD81 cell extracts.

A. Representative WB of the tetraspanin KO experiments blotted with CD9 (left blot) or CD81 (right blot) and GAPDH specific antibodies sequentially. Lines of the left blot correspond to 1: WT cells; 2: CD9 KO cells; 3: CD9 & CD81 KO cells. Lines of the right blot correspond to 1: WT cells; 2: CD81 KO cells; 3: CD9 & CD81 KO cells.

B. WB of the tetraspanin OE and OE + KO experiments blotted with CD9 (left blot) or CD81 (right blot) and actin specific antibodies sequentially. Lines of the left blot correspond to 1: WT cells; 2: CD9 OE cells; 3: CD81 OE cells; 4: CD9 OE + CD81 KO cells; CD81 OE + CD9 KO cells. Lines of the right blot correspond to 1: WT cells; 2: CD9 OE cells; 3: CD81 OE cells; 4: CD9 OE + CD81 KO cells; CD81 OE + CD9 KO cells

Figure S4

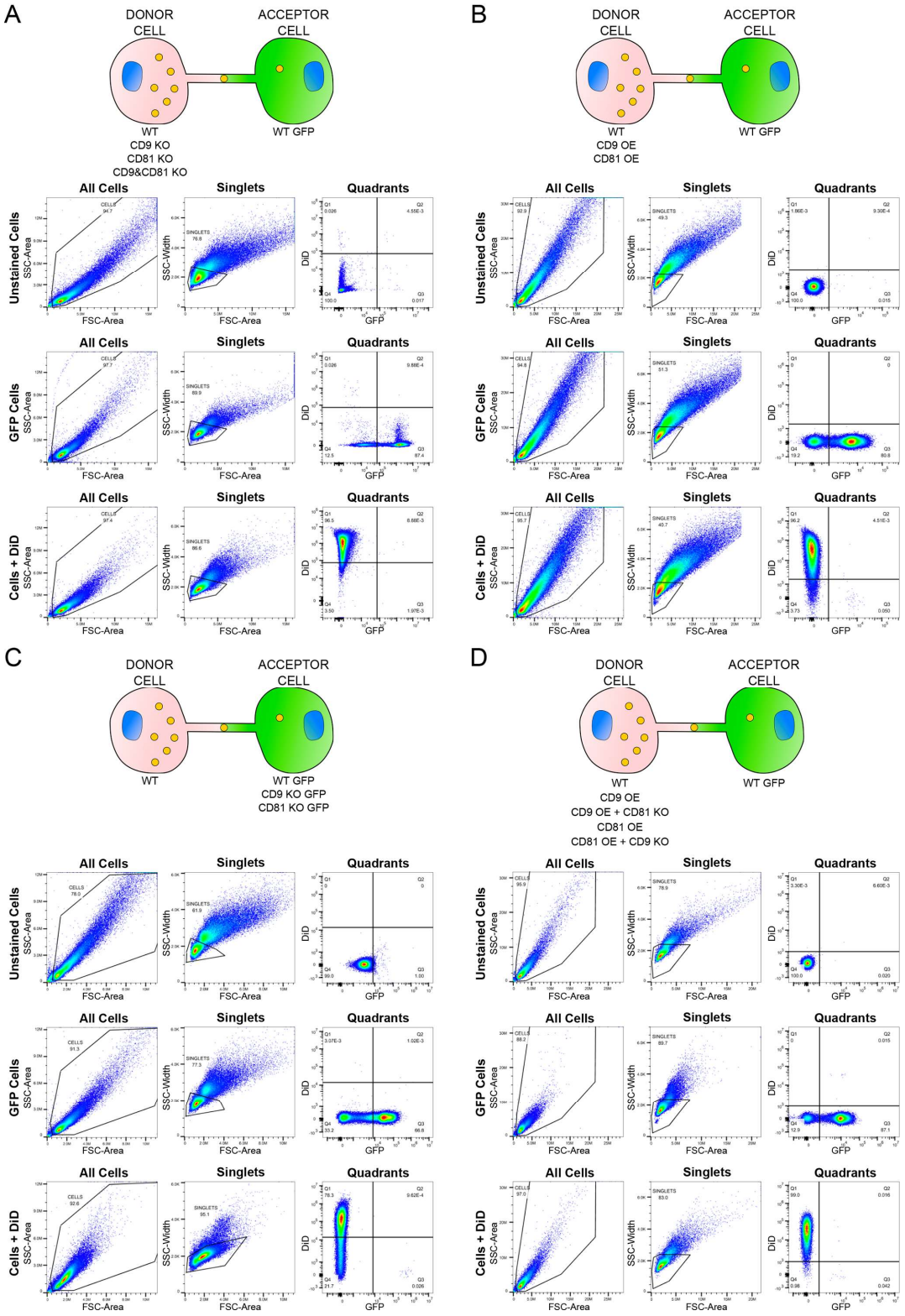
A
DONOR CELL
ACCEPTOR CELL
WT
CD9 KO
CD81 KO
CD9&CD81 KO
WT GFP
B
DONOR CELL
ACCEPTOR CELL
WT
CD9 OE
CD81 OE
WT GFP
C
DONOR CELL
ACCEPTOR CELL
WT
WT GFP
CD9 KO GFP
CD81 KO GFP
D
DONOR CELL
ACCEPTOR CELL
WT
CD9 OE
CD9 OE + CD81 KO
CD81 OE
CD81 OE + CD9 KO
WT GFP
All Cells
Singlets
Quadrants
Unstained Cells
GFP Cells
Cells + DiD
FSC-Area
SSC-Area
SSC-Width
DiD
GFP

Figure S4: Gate strategy of all the cocultures

A. Gate strategy of the coculture of tetraspanins KO cells used as donors. WT unstained cells, GFP cells and DiD+ cells were gated to select cells and exclude cellular debris, plotting SSC-Area (Y-axis) with FSC-Area (X-axis) (All Cells). Within the All Cells gate we selected for single cells to exclude doublets, plotting SSC-Width (Y-axis) with FSC-Area (X-axis) (Singlets). Within the Singlets gate the quadrants for DiD (Y-axis) and GFP (X-axis) were placed according to the position of the negative or positive populations. Schematic of the coculture is on top.

B. Gate strategy of the coculture of tetraspanins OE cells used as donors. The gate strategy follows the same principles explained in (A) and they were adapted to this coculture. Schematic of the coculture is on top.

C. Gate strategy of the coculture of tetraspanins KO cells used as acceptors. The gate strategy follows the same principles explained in (A) and they were adapted to this coculture. Schematic of the coculture is on top.

D. Gate strategy of the coculture of tetraspanins OE + KO cells. The gate strategy follows the same principles explained in (A) and they were adapted to this coculture. Schematic of the coculture is on top.

Figure S5

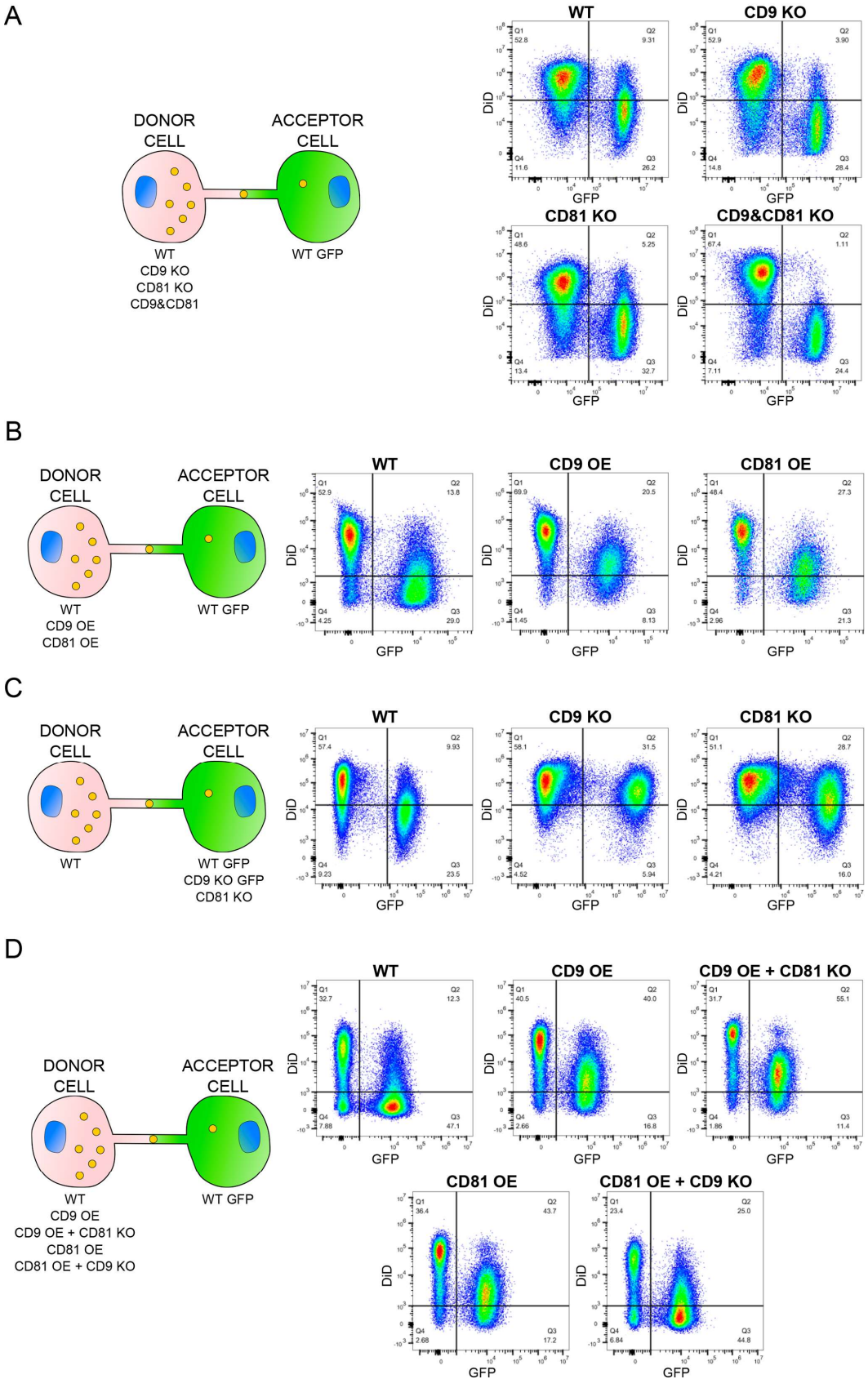
A
DONOR CELL
ACCEPTOR CELL
WT
CD9 KO
CD81 KO
CD9&CD81
WT GFP
WT
CD9 KO
CD81 KO
CD9&CD81
DiD
GFP
B
DONOR CELL
ACCEPTOR CELL
WT
CD9 OE
CD81 OE
WT GFP
WT
CD9 OE
CD81 OE
C
DONOR CELL
ACCEPTOR CELL
WT
WT GFP
CD9 KO GFP
CD81 KO
WT
CD9 KO
CD81 KO
D
DONOR CELL
ACCEPTOR CELL
WT
CD9 OE
CD9 OE + CD81 KO
CD81 OE
CD81 OE + CD9 KO
WT GFP
WT
CD9 OE
CD9 OE + CD81 KO
CD81 OE
CD81 OE + CD9 KO

Figure S5: Flow cytometry plots of all the results of all co-culture experiments

A. Coculture between tetraspanin KO cells used as donors loaded with DiD to stain the vesicles and WT GFP cells used as acceptors. Representative plots between the signal of DiD-labeled vesicles (Y-axis) and GFP-labeled acceptor cells (X-axis) of vesicle transfer in cells: WT, CD9 KO, CD81 KO and CD9 & CD81 KO. The second quadrant (Q2) represents the % of double positive cells and thus the acceptor cells that have received vesicles. The schematic of the coculture appears on the left.

B. Coculture between tetraspanin OE cells used as donors loaded with DiD to stain the vesicles and WT GFP cells used as acceptors. Representative plots between the signal of DiD-labeled vesicles (Y-axis) and GFP-labeled acceptor cells (X-axis) of vesicle transfer in cells: WT, CD9 OE and CD81 OE. The second quadrant (Q2) represents the % of double positive cells and thus the acceptor cells that have received vesicles. The schematic of the coculture appears on the left.

C. Coculture between WT cells used as donors loaded with DiD to stain the vesicles and tetraspanin KO GFP cells used as acceptors. Representative plots between the signal of DiD-labeled vesicles (Y-axis) and GFP-labeled acceptor cells (X-axis) of vesicle transfer in cells: WT, CD9 KO and CD81 KO. The second quadrant (Q2) represents the % of double positive cells and thus the acceptor cells that have received vesicles. The schematic of the coculture appears on the left.

D. Coculture between tetraspanin OE + KO cells used as donors loaded with DiD to stain the vesicles and WT GFP cells used as acceptors. Representative plots between the signal of DiD-labeled vesicles (Y-axis) and GFP-labeled acceptor cells (X-axis) of vesicle transfer in cells: WT, CD9 OE, CD9 OE + CD81 KO, CD81 OE and CD81 OE + CD9 KO. The second quadrant (Q2) represents the % of double positive cells and thus the acceptor cells that have received vesicles. The schematic of the coculture appears on the left.

Figure S6

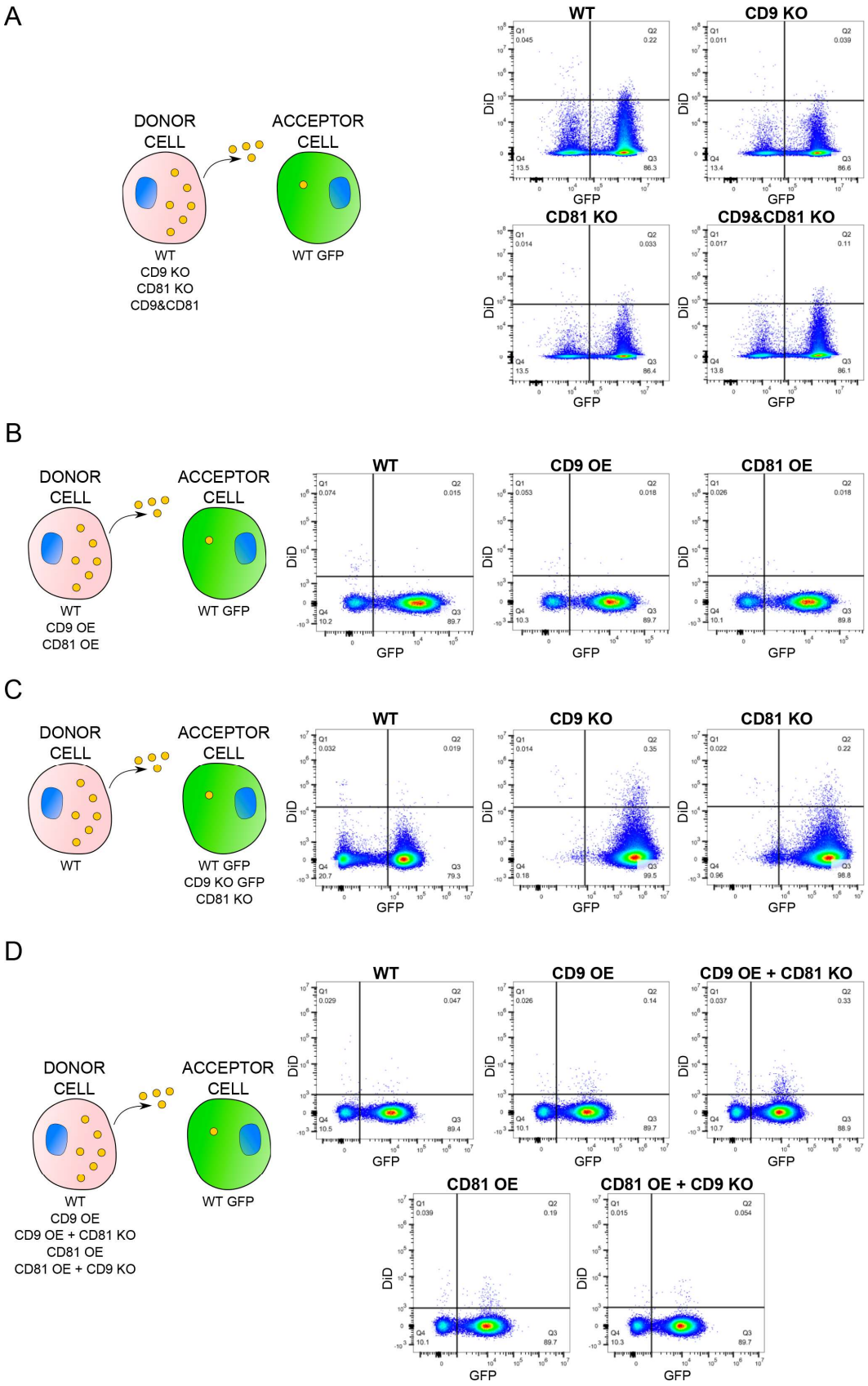
A
DONOR CELL
ACCEPTOR CELL
WT
CD9 KO
CD81 KO
CD9&CD81
WT GFP
WT
CD9 KO
CD81 KO
CD9&CD81 KO
DiD
GFP
B
DONOR CELL
ACCEPTOR CELL
WT
CD9 OE
CD81 OE
WT GFP
WT
CD9 OE
CD81 OE
C
DONOR CELL
ACCEPTOR CELL
WT
WT GFP
CD9 KO GFP
CD81 KO
WT
CD9 KO
CD81 KO
D
DONOR CELL
ACCEPTOR CELL
WT
CD9 OE
CD9 OE + CD81 KO
CD81 OE
CD81 OE + CD9 KO
WT GFP
WT
CD9 OE
CD9 OE + CD81 KO
CD81 OE
CD81 OE + CD9 KO

Figure S6: secretion of all the coculture experiments

A. Secretion of the coculture between tetraspanin KO cells used as donors loaded with DiD to stain the vesicles and WT GFP cells used as acceptors. Representative plots between the signal of DiD-labeled vesicles (Y-axis) and GFP-labeled acceptor cells (X-axis) of vesicle transfer by secretion in cells: WT, CD9 KO, CD81 KO and CD9 & CD81 KO. The second quadrant (Q2) represents the % of double positive cells and thus the acceptor cells that have received vesicles. Schematic of the secretion control of the coculture is on the left.

B. Secretion of the coculture between tetraspanin OE cells used as donors loaded with DiD to stain the vesicles and WT GFP cells used as acceptors. Representative plots between the signal of DiD-labeled vesicles (Y-axis) and GFP-labeled acceptor cells (X-axis) of vesicle transfer by secretion in cells: WT, CD9 OE and CD81 OE. The second quadrant (Q2) represents the % of double positive cells and thus the acceptor cells that have received vesicles. Schematic of the secretion control of the coculture is on the left.

C. Secretion of the coculture between WT cells used as donors loaded with DiD to stain the vesicles and tetraspanin KO GFP cells used as acceptors. Representative plots between the signal of DiD-labeled vesicles (Y-axis) and GFP-labeled acceptor cells (X-axis) of vesicle transfer by secretion in cells: WT, CD9 KO and CD81 KO. The second quadrant (Q2) represents the % of double positive cells and thus the acceptor cells that have received vesicles. Schematic of the secretion control of the coculture is on the left.

D. Secretion of the coculture between tetraspanin OE + KO cells used as donors loaded with DiD to stain the vesicles and WT GFP cells used as acceptors. Representative plots between the signal of DiD-labeled vesicles (Y-axis) and GFP-labeled acceptor cells (X-axis) of vesicle transfer by secretion in cells: WT, CD9 OE, CD9 OE + CD81 KO, CD81 OE and CD81 OE + CD9 KO. The second quadrant (Q2) represents the % of double positive cells and thus the acceptor cells that have received vesicles. Schematic of the secretion control of the coculture is on the left.

Figure S7

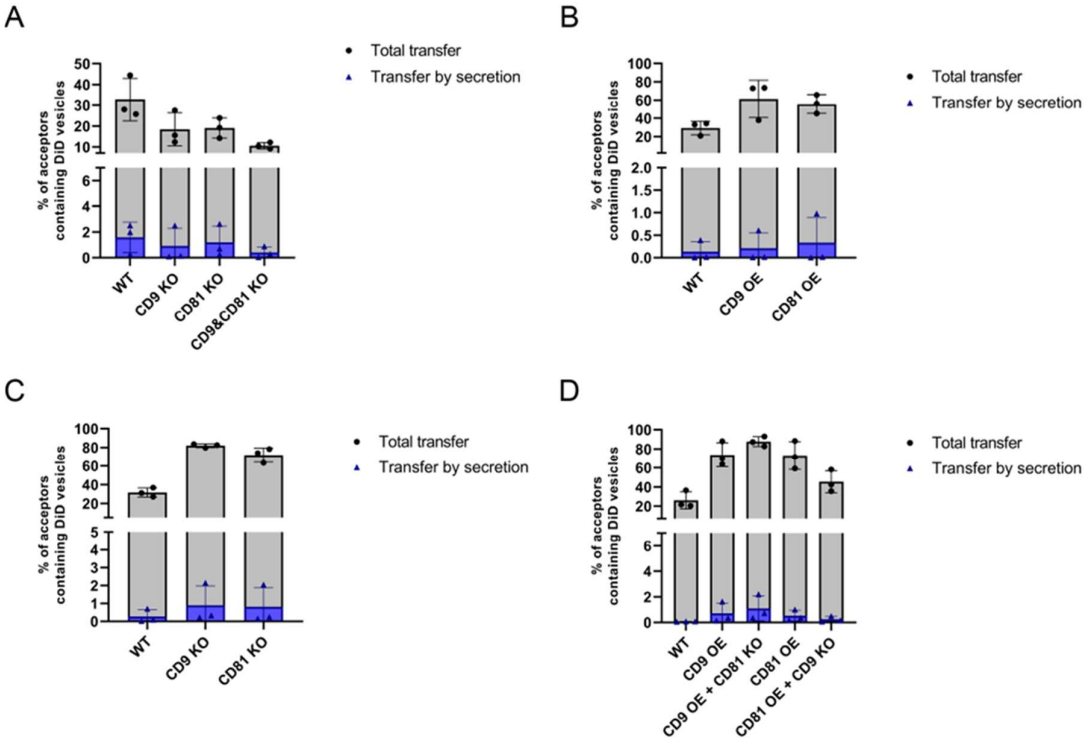
A
% of acceptors containing DiD vesicles
Total transfer
Transfer by secretion
WT
CD9 KO
CD81 KO
CD9&CD81 KO
B
% of acceptors containing DiD vesicles
Total transfer
Transfer by secretion
WT
CD9 OE
CD81 OE
C
% of acceptors containing DiD vesicles
Total transfer
Transfer by secretion
WT
CD9 KO
CD81 KO
D
% of acceptors containing DiD vesicles
Total transfer
Transfer by secretion
WT
CD9 OE
CD9 OE + CD81 KO
CD81 OE
CD81 OE + CD9 KO

Figure S7: Graphs of all co-culture experiments showing total transfer and transfer corresponding to secretion.

A. Graph % of acceptor cells containing DiD vesicles of the transfer by secretion of the coculture of tetraspanin KO cells used as donors. Mean and standard deviation of the % of acceptor cells containing DiD vesicles: WT = 1.6 ± 1.18; CD9 KO = 0.9 ± 1.38; CD81 KO = 1.2 ± 1.26; CD9 & CD81 KO = 0.4 ± 0.44 for N=3. Total transfer it is the same as in its corresponding figure (Figure 4A)

B. Graph corresponding to the % of acceptor cells containing DiD vesicles of the transfer by secretion of the coculture of tetraspanin OE cells used as donors. Mean and standard deviation of the % of acceptor cells containing DiD vesicles: WT = 0.14 ± 0.22; CD9 OE = 0.21 ± 0.34; CD81 OE = 0.33 ± 0.56 for N=3. Total transfer it is the same as in its corresponding figure (Figure 4B)

C. Graph corresponding to the % of acceptor cells containing DiD vesicles of the transfer by secretion of the coculture of tetraspanin KO cells used as acceptor. Mean and standard deviation of the % of acceptor cells containing DiD vesicles: WT = 0.27 ± 0.38; CD9 KO = 0.9 ± 1.08; CD81 KO = 0.82 ± 1.07 for N=3. Total transfer it is the same as in its corresponding figure (Figure 4C)

D. Graph corresponding to the % of acceptor cells containing DiD vesicles of the transfer by secretion of the coculture of tetraspanin OE + KO cells. Mean and standard deviation of the % of acceptor cells containing DiD vesicles: WT = 0.07 ± 0.02; CD9 OE = 0.71 ± 0.80; CD9 OE + CD81 KO = 1.09 ± 0.97; CD81 OE = 0.52 ± 0.42; CD81 OE + CD9 KO = 0.24 ± 0.22 for N=3. Total transfer it is the same as in its corresponding figure (Figure 7C)

Table 1: the full TNTome (1177 proteins), from 12 independent samples, proteins were conserved when present in more than 9 replicats, ranked in 4 quartiles (from higher to lower mean iBAQ) represented in different colors (orange Q1, green Q2, pink Q3, blue Q4). iBAQ of each sample is indicated for each protein.

Table 2: Cytoskeleton-associated proteins of the TNTome. Proteins identified by GO term analysis (cellular components), except those associated to proteasome, RNA and mitochondria, are ranked according to their quartile assignement (orange Q1, green Q2, pink Q3, blue Q4).

Table 3: Membrane-related proteins identified by GO term analysis (cellular components). Mitochondrial and other organelles membrane proteins have been discarded from GO analysis. Tab 1 lists all membrane and membrane-associated proteins, tab 2 only the integral membrane proteins, ranked according to their quartile assignement (orange Q1, green Q2, pink Q3, blue Q4) and from more abundant to less abundant. Integrins, Ephrin receptors, Cadherins and tetraspanin-related proteins are highlighted respectively in orange, red, dark gree and yellow as indicated in tab2.

Table 4: comparison of TNTome and Integrin adhesion complexes. Tab1 shows the common elements in integrin adhesion complexes (2240 proteins according to Horton et al, 2015) and in TNTome: 765 proteins listed in alphabetical order of the gene name (yellow background). On the right (blue background) are the 413 elements included exclusively in TNTome. Tab2 shows the 26 common elements in consensus adhesome (Horton 2015) and TNTome.

Table 5: TNT-only proteins. Tab1 (total) shows the 174 proteins present in TNT preparations and absent from EVPs. Tab2 (constitutive) shows the 89 TNT-only proteins without proteins described as mitochondrial, nuclear, ER or RNA-related. In yellow background are cytoskeleton-related proteins (20%).

Table 6: overlapping proteins between TNTs and EVPs. Tab1 (TOT TNT>EVP) shows the proteins more abundant in TNTs compared to EVPs, cleaned of nuclear, mitochondrial or RNA-related described proteins in tab2 (TNT>EVP). In yellow background are cytoskeleton-related proteins (29%).

Table 7: Common proteins between TNTome and protrusions from hCAD cells described in *Gousset et al., 2019*. The 190 proteins present in 2 samples of hCAD (mouse CAD cells treated with H2O2) were converted to their human ortholog, next compared to the 1177 proteins of table 1.

Results Annexes: Are NCAD and tetraspanin CD9 and/or CD81 interacting between them?

Results regarding the functionality of the TNTs controlled by NCAD suggested that this protein could somehow control the fusion of the TNTs with the opposing cell and there is when, following Dr. Christel Brou's advice, I decided to investigate if NCAD could have a relationship with the tetraspanin CD9 and CD81, proteins largely characterized in fusion processes (*Charrin et al., 2014*). One major thing that characterize tetraspanins it is their ability to interact with a vast number of molecules forming complexes at the membrane named Tetraspanin-Enriched Microdomains or "TEMs" (*Yáñez-Mó et al., 2009*). Therefore, I speculated that CD9 and/or CD81 could form TEMs and within them we may find NCAD interacting with one or both of these tetraspanins. To this end, I performed GFP-trap immunoprecipitation assays in neuronal SH-SY5Y cells overexpressing one of these proteins tagged to GFP (NCADGFP, CD9GFP, and CD81GFP) under conditions that would preserve tetraspanin-tetraspanin and tetraspanin-partner interactions (*Serru et al., 1999; Charrin et al., 2001*).

My results in one experiment showed that when using NCADGFP cells as a bait, this protein did not precipitate neither CD9 nor CD81 (*Figure Results Annexes 1A; IP*). This immunoprecipitation was validated by showing coprecipitation of GFP as positive control, no coprecipitation of tubulin as negative control and expected coprecipitation of α-catenin (*Figure Results Annexes 1A; IP*). CD9GFP cells as a bait showed the same result as they did not coprecipitate NCAD (*Figure Results Annexes 1B; IP*). Validation of the assay was shown by coprecipitation of GFP as positive control, no coprecipitation of tubulin as negative control and expected coprecipitation of the tetraspanin partner protein EWI-2 (*Stipp et al., 2001*) although no coprecipitation of CD81 was observed (*Figure Results Annexes 1B; IP*). Finally, coimmunoprecipitation of NCAD with CD81GFP also failed (*Figure Results Annexes 1C; IP*) in a valid immunoprecipitation shown by coprecipitation of GFP as positive control, no coprecipitation of tubulin as negative control and expected coprecipitation of CD9 and EWI-2 (the band near the height of EWI-2 in the GFPv sample should correspond to a stain) (*Figure Results Annexes 1C; IP*).

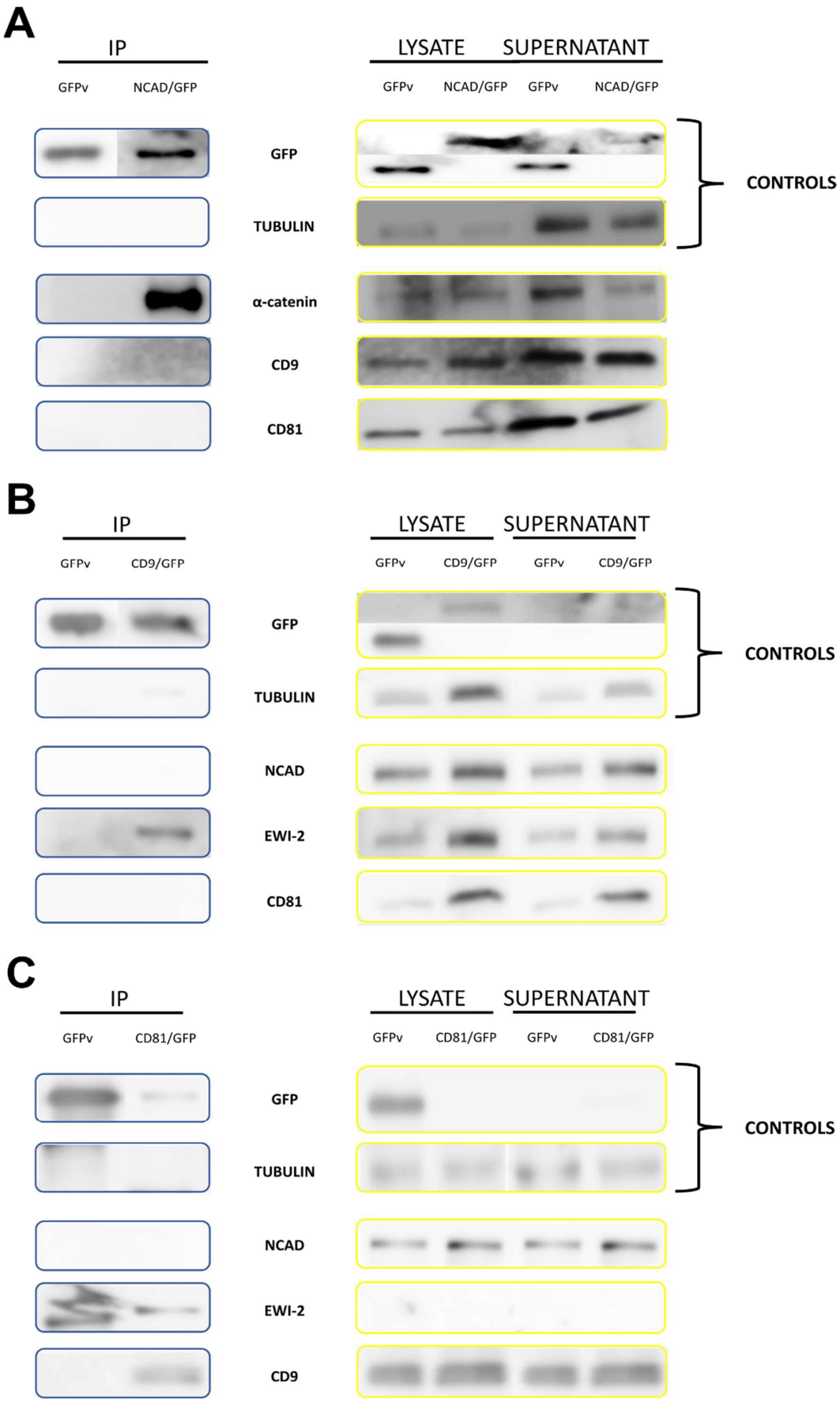
A
IP
GFPv
NCAD/GFP
LYSATE
SUPERNATANT
GFPv
NCAD/GFP
GFPv
NCAD/GFP
GFP
TUBULIN
α-catenin
CD9
CD81
CONTROLS
B
IP
GFPv
CD9/GFP
LYSATE
SUPERNATANT
GFPv
CD9/GFP
GFPv
CD9/GFP
GFP
TUBULIN
NCAD
EWI-2
CD81
CONTROLS
C
IP
GFPv
CD81/GFP
LYSATE
SUPERNATANT
GFPv
CD81/GFP
GFPv
CD81/GFP
GFP
TUBULIN
NCAD
EWI-2
CD9
CONTROLS

Figure 22. GFP-trap experiments on SH-SY5Y cells overexpressing NCADGFP, CD9GFP or CD81GFP.

(A) Western blot images of the GFP-trap on SH-SY5Y cells overexpressing NCADGFP or SH-SY5Y cells expressing GFP (GFPv for GFP vector). These samples were incubated sequentially in the same membrane with GFP, tubulin, α-catenin, CD9 or CD81 antibodies. The images delimited by a blue rectangle corresponds to those samples exposed to anti-GFP tagged beads (IP). The images delimited by a yellow rectangle correspond to the lysate samples (proteins extracted from the whole cell lysate of the bait cells before incubation with the beads) and supernatant samples (proteins that did not bind to the beads and remained in the follow-through after incubation with beads). (B) Western blot images of the GFP-trap on SH-SY5Y cells overexpressing CD9GFP or SH-SY5Y cells expressing GFP. These samples were incubated sequentially in the same membrane with GFP, tubulin, EWI-2 or CD81 antibodies. The images delimited by a blue rectangle corresponds to those samples exposed to anti-GFP tagged beads (IP). The images delimited by a yellow rectangle correspond to the lysate samples and supernatant samples. (C) Western blot images of the GFP-trap on SH-SY5Y cells overexpressing CD81GFP or SH-SY5Y cells expressing GFP. These samples were incubated sequentially in the same membrane with GFP, tubulin, EWI-2 or CD9 antibodies. The images delimited by a blue rectangle corresponds to those samples exposed to anti-GFP tagged beads (IP). The images delimited by a yellow rectangle correspond to the lysate samples and supernatant samples.

These results, although done just one time but interchanging all of the proteins of interest as a bait or as a prey, might indicate that interactions between NCAD and CD9 and/or CD81 would not occur on the neuronal SH-SY5Y cells or that the interactions are not stable enough or too minor to be detected this way. Thus, these data leaded me to decide that at that point the cadherin project and the tetraspanin project should be separated and that is way here I present two separated manuscripts.

Section 5: Discussion and perspectives

Since in the results section I have included the manuscripts with their corresponding discussions, this section will be devoted to a more general discussion of the most relevant aspects of the results that I have obtained during my PhD and of the possible future steps to follow in both projects.

Dual function of the cadherin-catenin complex in TNT regulation

The cadherin-catenin complex is formed by a cadherin (in this case NCAD) which binds through its cytoplasmic tail to p120-catenin and β-catenin, the latter associating with α-catenin. My project was conceived after the discovery of NCAD in between the iTNTs of neuronal cells (*Sartori-Rupp et al., 2019*), in which it was proposed and speculated that this molecule could have a role as a holder of the bundle of iTNTs, and therefore our idea was to study the role of this protein in TNTs, but we realized that although it is known in the literature that α-catenin is the link of cadherins to the actin cytoskeleton and that TNTs are supported by actin cytoskeleton, all previous studies had only paid attention to β-catenin, and only as a confirmation of the presence of cadherins based on colocalization of these two proteins (*Lokar et al., 2010*; *Jansens et al., 2017*). Therefore, I decided not only to study the role of NCAD in TNTs but also that of α-catenin and thus to know the set of processes of TNT formation controlled by the complex formed by these two proteins.

N-cadherin and α-catenin inhibit the formation of TNTs

My first aim it was to understand the influence of NCAD on the biogenesis of the TNTs. I showed that NCAD interference leaded to an increase of TNT-connected cells whereas the overexpression of NCAD provoked a huge decrease on the % of cells connected by TNTs This could be explained by two reasons, one of them purely physical by the phenotype of the cells depending on their NCAD expression and the other reason could be explained by the influence of cadherins on the actin cytoskeleton. On one hand, one could speculate that NCAD interference would lead to a failure of cell-to-cell adhesion and therefore that cells would be more scattered from each other, but, when NCAD is overexpressed this would make the cells to preferentially adhere to each other in an epithelial-like phenotype. This is indeed what I observed in both conditions and the physical distance between cells could therefore influence the formation of TNTs, which

by definition are membranous structures that connect cells. Although this could partially explain the decrease on TNT when NCAD is overexpressed (if cells are forming clusters and tight junctions between them, this could impair both mechanism of TNT formation), it is unlikely that the only reason why the cells interfered for NCAD would form more TNTs it is just because they are sparser. Indeed, the trypsin experiments on cells overexpressing NCAD revealed that although separating the cell bodies to visualize the TNTs, these cells still form less TNTs pointing to a much more complex regulation of NCAD on TNTs rather than the physical distances between cells. On the other hand, the influence of NCAD on the actin cytoskeleton could complete the explanation of the two different phenotypes regarding TNT number. The organization of the actin cytoskeleton on the adherens junctions relies on the establishment of an "actin belt" of parallel to the membrane actin filaments (*Cavey and Lecuit, 2009*) which presumably it is the opposite of what it is needed for TNT formation, since it is speculated that first, depolymerization of cortical actin should occur to create the place where protrusion could be formed and then filamentous actin could polymerize and would push out the membrane to deform it and form an initial protrusion that eventually would become in a TNT (*Ljubojevic et al., 2021*). So, one could speculate that when inhibited NCAD, the actin cytoskeleton would not be forming this belt and therefore, it could form microprotrusions that would evaginate the membrane and form TNTs (*Figure 23A*), but on the contrary, when NCAD is overexpressed, this molecule would inhibit the formation of these small protrusion by "sequestering" the actin cytoskeleton on the cadherin complexes (*Figure 23B*), thus explain the increase or decrease of TNTs when NCAD is knock down or overexpress respectively. When I check for the role of the downstream cadherin adaptor α-catenin on the biogenesis of TNTs, I observed that α-catenin interference or overexpression recapitulated NCAD interference or overexpression almost perfectly regarding the % of TNT-connected cells, which would imply that NCAD and α-catenin collaborate through the same or very similar mechanism on the biogenesis of TNTs (*Figure 23*).

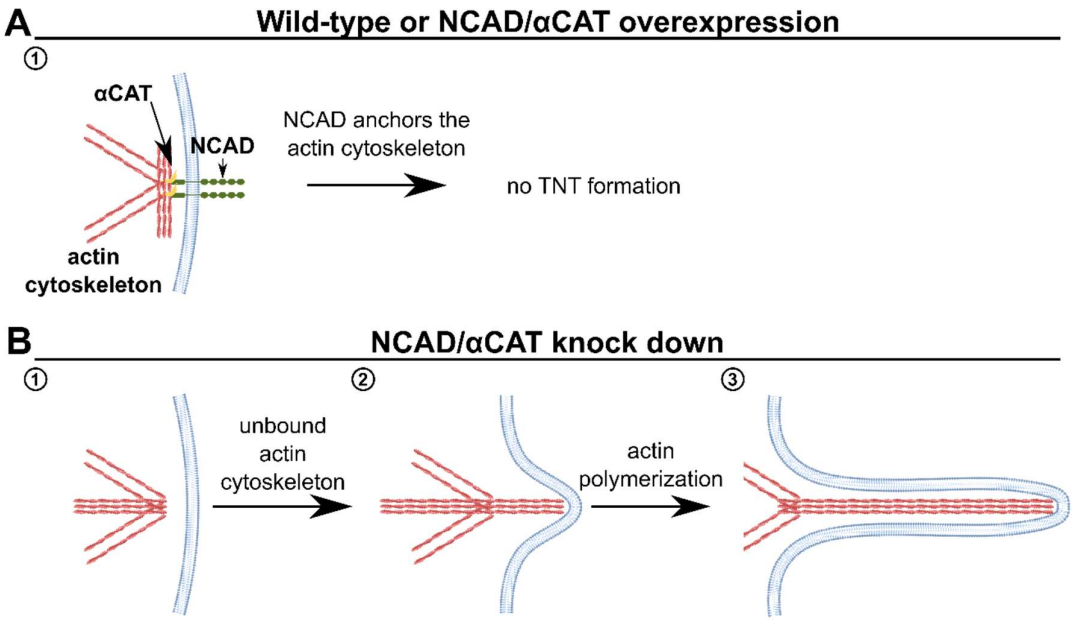

Figure 23. NCAD-α-catenin mechanism of formation of the TNTs.

(A) Schematics TNTs under wild-type or NCAD/α-catenin overexpression conditions. 1) NCAD would bind and anchor the actin cytoskeleton through α-catenin inhibiting the initial protrusion formation by actin filaments and the subsequent TNT formation. (B) Schematics TNTs under NCAD/α-catenin knock down conditions. 1) Actin cytoskeleton would not be anchored by the cadherin-catenin complex. 2) The actin filaments would be able to push outwards the membrane forming a microprotrusion. 3) Polymerization of filamentous actin would elongate this protrusion to form a TNT.

N-cadherin and α-catenin positively influence the functionality of the TNTs

Next, I checked for the functionality of these TNTs under NCAD interference or overexpression through a vesicle transfer assay in our coculture system (see Material & Methods section). Surprisingly, NCAD interference decreased the transfer of vesicle and NCAD overexpression increased this transfer, although the number of TNTs in interference or overexpression was completely opposite to the transfer results respectively. This was indeed remarkable, since normally an increase of cells connected by TNTs would logically increase the vesicle transfer between cells (*Zhu et al., 2018*; *Vargas et al., 2019*; *Dilsizoglu et al., 2019*; *Bhat et al., 2020*; *Pepe et al., 2022*). My data would mean that although NCAD interfered cells form more apparent TNTs, these structures are not functional, whereas NCAD overexpressing cells would form few TNTs but highly functional. As it was the case for TNT number, when I investigated the role of α-catenin on the functionality of the TNTs, I showed that again α-catenin interference and

overexpression replicated the phenotype of NCAD interference and overexpression respectively regarding vesicle transfer. This would confirm that α-catenin and NCAD collaborates positively on TNT functionality. But, how are NCAD and/or α-catenin regulating the functionality of the TNTs? On one hand, I measured the duration of the TNTs upon NCAD interference or overexpression, showing that when NCAD is knock down the duration of the TNTs tend to decrease whereas when we overexpress this protein, the duration of TNTs was highly enhanced. Therefore, this would mean that NCAD, as a cell-to-cell adhesion molecule, could serve as an anchor between iTNTs and/or TNT and opposing cell, which agrees with what it has been proposed by others (*Lokar et al., 2010*; *Jansens et al., 2017*), therefore facilitating the vesicle transfer. On the other hand, the Cryo-EM data obtained by Dr. Anna Pepe that the downregulation of NCAD or α-catenin increased the close-ended iTNTs in the bundle (which could be presumably in the process of extension or retraction) but the overexpression NCAD or α-catenin decreased the close-ended iTNTs. This data could reflect a defect on TNT fusion with the opposing cell when NCAD or α-catenin is knock down, in agreement with previous studies on cadherins and cell fusion (*Mège et al., 1992*; *Mbalaviele et al., 1995*; *Ishikawa et al., 2014*), which could explain why there is a decrease or increase on the transfer when NCAD or α-catenin are interfered or overexpressed. Thus, the presence of the cadherin-catenin complex could presumably serve as a holder of the TNTs with the opposing cell, facilitating the fusion of these structures, most probably indirectly by bringing the membranes close that fusion might occur and once fusion have happened, maintaining stably connected the TNT with the other cell (*Figure 24A*). On contrary, when NCAD or α-catenin is knock down, TNTs that are growing towards the opposing cell would not have the this “holder”, failing to adhere to the neighbor cell and presumably retracting (*Figure 24B*).

However, TNT counting is insufficient to establish the definition of TNT and although the vesicle transfer assay gives us a better insight of *bona fide* TNTs, further characterization of the molecular players on the step of protrusion formation and the subsequent fusion with the opposing cell is needed.

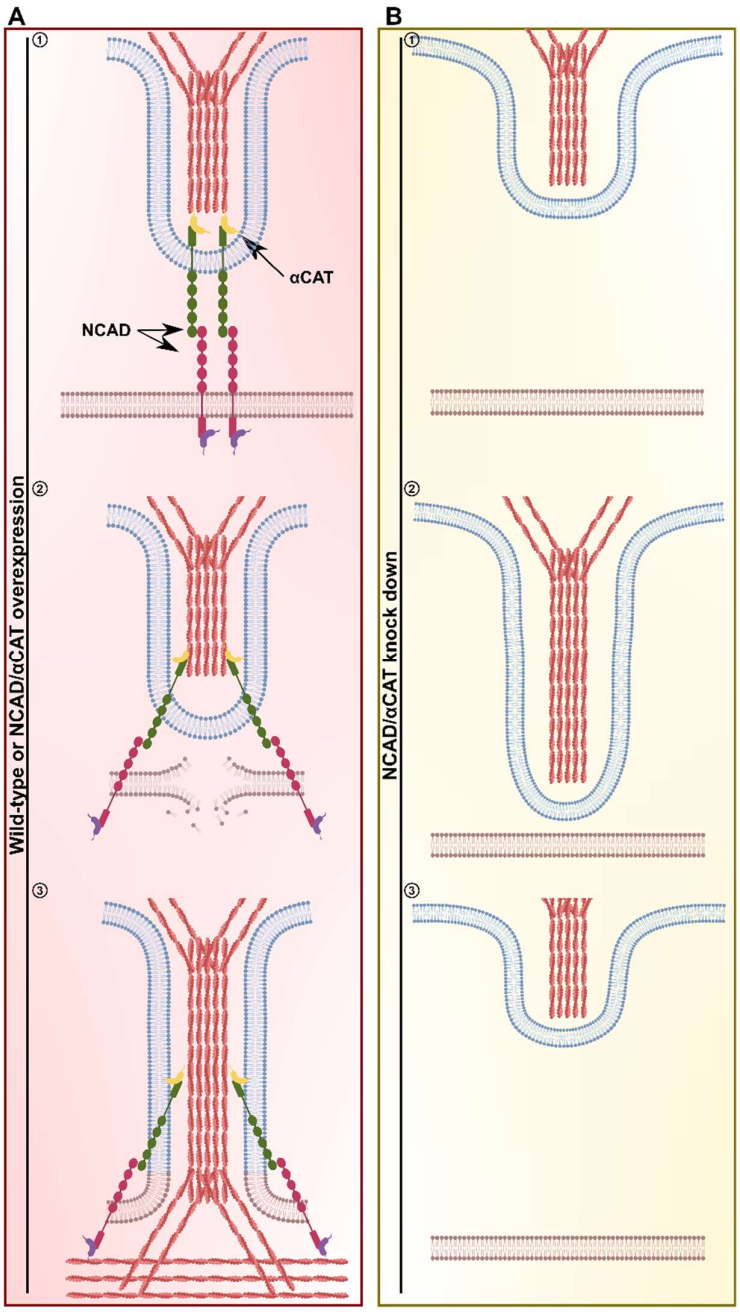

Figure 24. TNT functionality governed by NCAD and α-catenin.

(A) Schema of TNTs final formation under wild-type or NCAD/α-catenin overexpression conditions. 1) The TNT will reach a close proximity with the opposing cells and cadherins would engage. 2) Cadherins would bring and keep membranes in close proximity so fusion might occur by a yet unknown mechanism. 3) The open-ended TNT would be formed and maintain stable thought the cadherin-catenin complexes. (B) Schema of TNTs final formation under wild-type or NCAD/α-catenin knock down conditions. 1) The TNTs would approach to the opposing cells. 2) TNTs in these conditions might reach closer distance to interact through cell adhesion molecules. 3) The lack of NCAD and/or α-catenin would lead to a failure on the adhesion of the TNT with the opposing cell and therefore the TNT will retract.

α-Catenin is the downstream effector of N-cadherin in the regulation of the TNTs

Since the results of α-catenin interference and overexpression were totally in line with the results obtained in NCAD interference and overexpression and knowing that cadherins form complexes with α-catenin to link the actin cytoskeleton (*Mège and Ishiyama, 2017*), I decided to knock down α-catenin in cells overexpressing NCAD, showing that this cells increased their % of cells connected by TNTs but decreased the transfer, indicating that this knock down overcome the effect of the overexpression of NCAD and that α-catenin works downstream NCAD impairing the functionality of this cadherin when α-catenin is not present, data in agreement with previous studies (*Watabe-Uchida et al., 1998*; *Bajpai et al., 2009*). Finally, I cocultured cells overexpressing NCAD versus cells interfered for α-catenin, showing that this interference increased both the total number of cells connected by TNTs as well as cells heterotopically connected (NCAD overexpressing cells connected to α-catenin interfered cells), but decreased the vesicle transfer no matter if it is knock down in the donor or acceptor population. Overall, these last results would indicate that NCAD and α-catenin work in the same pathway in the regulation of the TNTs with α-catenin being downstream of N-cadherin and that cadherin-cadherin interactions occurs between TNTs and opposing cell.

Future perspectives

Although I was able to show the involvement of the cadherin-catenin complex on TNT regulation, there are still many possibilities to investigate in this regard, for both proteins that we investigated but also for the other members of this complex:

- Despite the fact that the decrease of the transfer when NCAD or α-catenin are knock down could be partially explained by the increase on close-ended iTNTs which could reflect a defect in the fusion of these TNTs, we for the moment don't have a direct prove about this. To this end, it would be very interesting to use Focus Ion Beam-Scanning Electron Microscopy (FIB-SEM) to visualize the contact area between TNT and opposing cell, as it has been done previously (*Sartori-Rupp et al., 2019*). By applying this technique, we could be able to investigate whether there is a decrease or increase of open TNTs when we interfere or the overexpress NCAD or α-catenin and therefore to give more direct evidences on the possible role of NCAD/α-catenin on TNT fusion.

- This present study it has been focused on neuronal cells that they do express NCAD. One interesting question it would be to asses whether this role of NCAD on TNTs is common to other cadherins or just specific to this protein or neuronal cells. To this end, other cellular models that do not express NCAD but for examples ECAD, could be used to investigate the specificity of the cadherin roles on TNTs.
- Although my experiments showed that NCAD interference affects negatively the stability of the TNTs by decreasing the duration of these structures and NCAD overexpression enhances this stability, this has not been yet demonstrated for α-catenin. Since all the experiments targeting α-catenin replicated the results regarding NCAD, it would be necessary to prove that the effect on the stability of the TNTs by NCAD it is also through α-catenin.
- Since α-catenin was the most straightforward cadherin adaptor to investigate in the regulation of the TNTs by the cadherin-catenin complex because it physically links this complex to the actin cytoskeleton which in turn in the core of the TNTs, this doesn't exclude a possible function of other catenins on TNT regulation. p120-Catenin have a central role in controlling the clustering of the cadherins (*Yap et al., 1998*), it prevents the recycling of the cadherins (*Hartsock and Nelson, 2012*) and strengthen the cadherin adhesion (*Thoreson et al., 2000*). Furthermore, p120-catenin also influence the actin cytoskeleton. This catenin favors the formation of filopodia by increasing CDC42 and Rac activity (*Grosheva et al., 2001*) and also inhibits RhoA activity (*Reynolds et al., 1996*). Here it is remarkable to say that we know from literature that CDC42 is a negative regulator of TNT formation (*Delage et al., 2016*), although we don't know yet the role of RhoA on TNTs (*Zhang et al., 2020*). Therefore, it is a very interesting member of the cadherin catenin complex to study, since it seems that the functions regarding cadherins (presence of cadherin at the membrane, strengthening adhesion) and actin cytoskeleton (activation of CDC42) would resemble the overexpression of NCAD. One could speculate that overexpressing NCAD would be followed by increased expression of p120-catenin to maintain the cadherin at the membrane and this enhanced expression of p120-catenin could eventually lead to an activation of CDC42 and inhibition of TNT formation, phenotype that I have described when NCAD is overexpressed. It could be worthy to overexpress and downregulate p120-catenin and measure TNT formation, vesicle transfer and

CDC42 activity. Furthermore, targeting p120-catenin could address other questions regarding NCAD expression and or location such as how NCAD it is sent or maintained at the right place. Since live imaging videos of cells overexpressing NCAD showed an accumulation of this protein at the tip/base of the TNTs, one may wonder if the presence and/or accumulation of NCAD in that precise location is depending on p120-catenin (which it would be based on the aforementioned roles of p120-catenin on clustering or recycling of the cadherins). Thus, if we overexpress or downregulate p120-catenin, in could be speculated that we would see an increased/decreased presence of NCAD at the membrane which could lead to an increased/decreased TNT stability.

- Finally, the last member of this complex, β-catenin, was initially discarded because it was demonstrated that TNT formation in neuronal cells it is through the Wnt/β-catenin independent pathway (*Vargas et al., 2019*) but this doesn't exclude a role of this protein in the cadherin-catenin regulation of TNTs. Since it links the cadherin to α-catenin, indeed it is a fundamental member of this complex. Through this interaction, targeting β-catenin would help us to understand better the function of α-catenin on the regulation of TNTs. Since α-catenin exists in the cell in two pools, one cytoplasmic and another cadherin bound (*Scott and Yap, 2006*), knocking out β-catenin could force α-catenin to only remain in the cytoplasm. By quantifying the number of TNTs and the vesicle transfer under this condition, we could relate the result with the presence or absence of α-catenin on the cadherin complex and therefore distinguish if the effects on TNTs by α-catenin it is through the cytoplasmic pool or the cadherin bound pool.

Tetraspanins CD9 and CD81 differentially regulate TNT formation

As stated in the introduction, the study of CD9 and CD81 tetraspanins aroused our interest because of being related to different membrane protrusive activities or being characterized in different membrane fusion processes, processes that are necessary for the formation of a functional TNT. In addition, Dr. Christel Brou's work on the TNTome revealed that these proteins are relatively abundant in TNTs. TNTome work and my work

on the regulation of the TNTs by CD9 and CD81 were done in parallel, therefore reinforcing our findings.

CD9, but not CD81, could regulate the formation of the TNTs

Intriguingly, these two tetraspanins which are very close in sequence, structure and function, showed a different role on TNT biogenesis. Whereas CD9 showed to be a positive regulator of the biogenesis or stability of the TNTs, CD81 didn't show to have a major role in these processes, although it is conceivable that CD81 could have a complementary role of CD9, because when both of them are knock out there is a huge decrease of the TNT-connected cells. CD9 increasing TNT formation would agree with its role on promoting the formation of other protrusions such as digitation junction (*Huang et al., 2018*) but on the other hand, CD81 not influencing TNT biogenesis is somehow contradictory because it was shown to promote microvilli formation (*Bari et al., 2011*), but different protrusions might be regulated differentially. Next, I decided to assess the mechanism by which CD9 was promoting TNT biogenesis. I speculated that, based on previous studies showing that CD9 molecular structure can cause membrane deformation (*Umeda et al., 2020*) and clustering of CD9 achieved through treating the cells with specific antibodies against this protein (*Nydegger et al., 2006*; *Khurana et al., 2007*; *Singethan et al., 2008*) leads to protrusion formation such as microvilli (*Singethan et al., 2008*), by treating my cells with anti-CD9 antibodies, CD9 clustering at specific places of the membrane could provoke membrane bending and evagination which could potentially lead to TNT formation. Indeed, just a short treatment with CD9 antibodies (2 hours) increased the the formation and/or stability of functional TNTs. These results lead me to hypothesize that CD9 would promote TNT initiation and this promotion could be through the aggregation of CD9 molecules that induce membrane curvature formation, deforming the membrane outwards, forming microprotrusions that presumably with the polymerization of actin filaments would grow towards an opposing cell to form a TNT (*Figure 25A*). Contrary, with the lack of CD9, membrane deformation at microdomains of the membrane would not be induce and therefore TNT formation would not be promoted (*Figure 25B*). In this process of formation controlled by CD9, it is conceivable that CD81 would have minimal influence (showed by the double knock of CD9 and CD81).

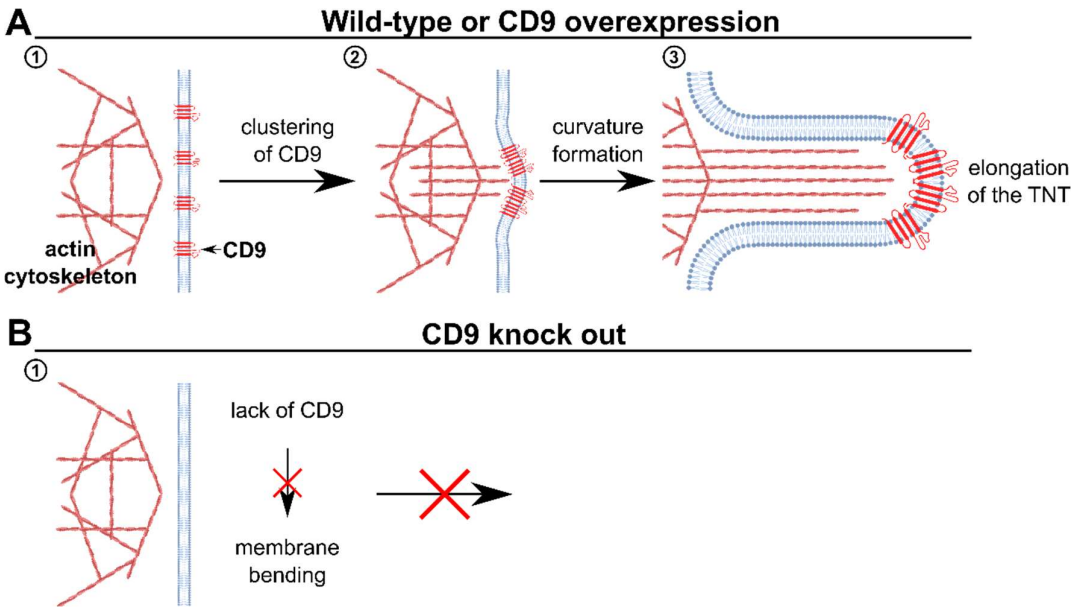

Figure 25. TNT initiation by CD9.

(A) Schematics representing TNTs under wild-type or CD9 overexpression conditions. 1) CD9 would be present at the membrane in its respective TEM. 2) Clustering of CD9 molecules would lead to membrane bending and initial protrusion formation. 3) Actin filaments polymerization would elongate the protrusion to form a TNT. (A) Schematics representing TNTs under wild-type or CD9 knock out conditions. 1) The absence of CD9 would impair the membrane curvature formation and inhibition of TNT formation.

CD81 rules in TNT functionality

Although it seemed that CD9 controlled the initiation of the formation of TNTs whereas CD81 not, I next investigated the potential role of these two tetraspanins on TNT functionality through our coculture assay. Here I knocked out or overexpressed CD9 or CD81 just in the donor population, showing that both CD9 knock out or CD81 knock out decreased the vesicle transfer whereas the overexpression of one or the other increased the transfer. When I knock out both CD9 and CD81 in the donor population this transfer dramatically decreased until levels much lower than the single knock out. On one hand, CD9 knock out or overexpression transfer results directly correlates with the number of TNTs that these cells would form (CD9 knock out cells form less TNTs therefore having less chances of transferring vesicles; CD9 overexpressing cells form more TNTs therefore having more chances of transferring vesicles) but also implies that CD9 is a positive regulator of all processes of TNT formation. On the other hand, the transfer results regarding CD81 are much more puzzling since this tetraspanin doesn't seem to affect

TNT initiation but it affects TNT functionality. Since by definition TNTs are open-ended channels (*Rustom et al., 2004*), which is indeed the case in my cellular model (*Sartori-Rupp et al., 2019*), this would signify that fusion might occur between TNT and opposing cell. Tetraspanins CD9 and CD81 have been well characterized to be involved in different cellular fusion events, such as sperm-egg fusion (*Rubinstein et al., 2006*) muscle cell fusion (*Charrin et al., 2013*) or multinucleated giant cells formation (*Takeda et al., 2003*). Despite this participation in fusion for CD9, my results would point to a minimal and, if so, complementary involvement of this tetraspanin on TNT fusion (showed by the double knock of CD9 and CD81). On the contrary, CD81 decrease or increase of vesicle transfer but no changes on TNT number when this protein is knock out or overexpress respectively would mean that CD81 is a positive regulator of TNT functionality and, considering the aforementioned function of this tetraspanin, it is conceivable that CD81 would be positively involved on TNT fusion from donor cells. The absence of changes on TNT number by CD81 levels of expression might exclude the involvement of this protein on TNT-opposing cell adhesion and therefore exclude its possible role in the stability of the TNTs. Indeed, when we repeated our CD9 antibody treatment this time on CD81 knock out cells it showed that still in these cells there is a huge induction of TNT formation (data that agrees with CD9 initiating the formation of these structure) but interestingly the transfer ability of these induced TNTs was impaired probably because of the lack of CD81, which would reinforce the idea of CD81 controlling the functionality (and presumably fusion) of the TNTs. One could speculate that the presence of CD81 in the cell that is sending the TNTs (which could be achieved by CD9 bringing CD81 to the right place) would promote the fusion of these structures by bringing in to the proximal zone TNT-opposing cell unknow fusion molecules that would destabilize the cell membrane allowing the lipids from both membranes to mix and fuse into an open channel (*Figure 26A*). Trans interaction between CD9 in oocyte an fusogenic proteins in sperm has been already described, which would support this model, but perhaps in this case with CD81 interacting in trans with an unknown fusion protein (*Ellerman et al., 2003*). Conversely, the absence of CD81 could provoke that these unknow fusion proteins would not be present at the tip and therefore the TNT (that presumably could adhere properly to the opposing cell) would not be able to fuse with the opposing membrane (*Figure 26B*).

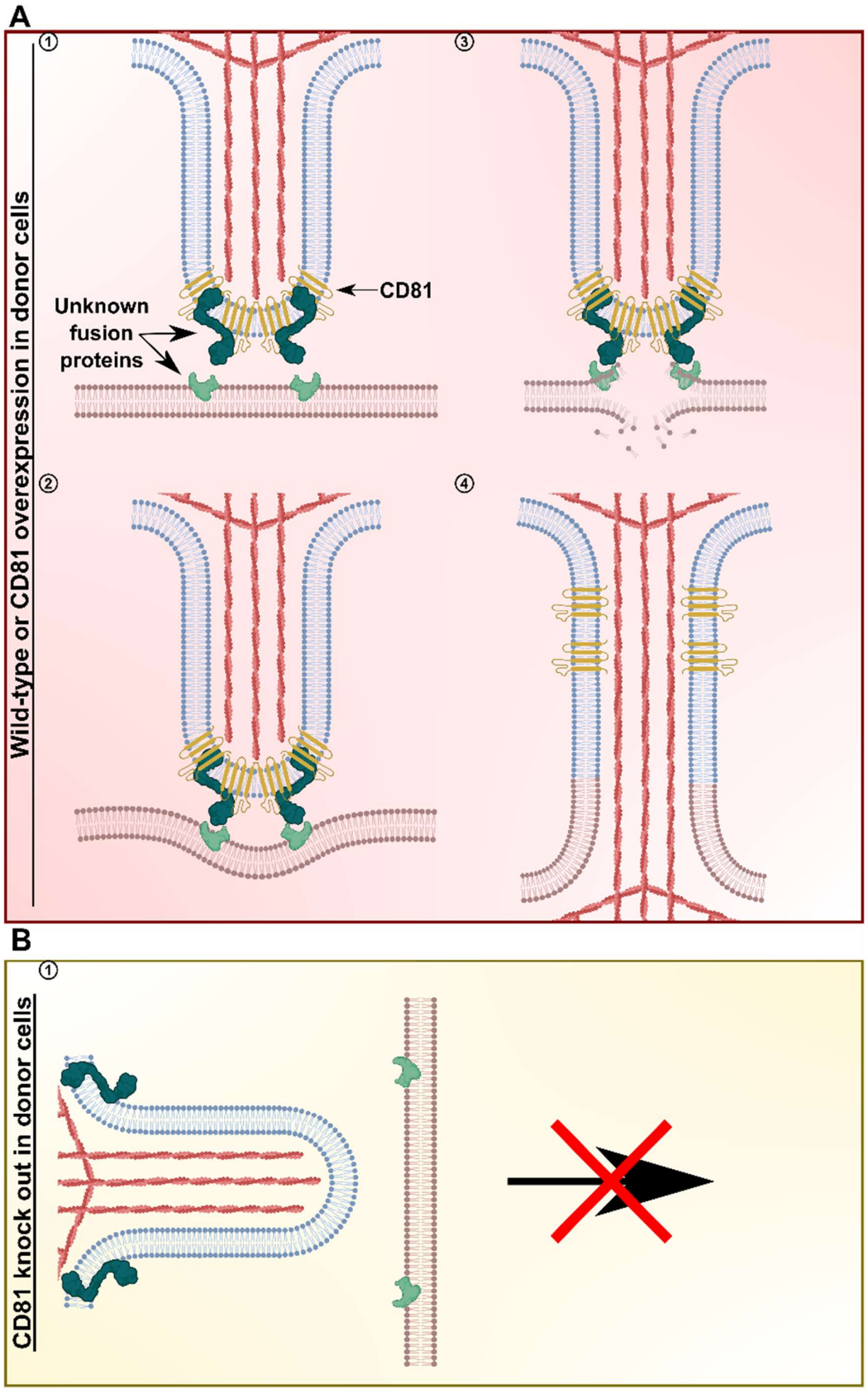
A
Wild-type or CD81 overexpression in donor cells
1
2
3
4
CD81
Unknown
fusion
proteins
B
CD81 knock out in donor cells
1

Figure 26. Control of TNT fusion by CD81 in donor cell.

(A) Representation of TNTs-fusion step under wild-type or CD81 overexpression conditions in donor cells. 1) CD81 presence of the TNTs would bring fusion proteins with them. 2) The membrane of the opposing cells would be pushed inwards by the TNT so the fusion molecules that interact with CD81 could interact with their counterparts. 3) Membrane fusion and lipid mixing would occur. 4) An open TNTs would be form. (B) Representation of TNTs-fusion step under CD81 knock out conditions in donor cells. 1) The lack of CD81 would impair the presence of fusion proteins on the contact area between TNT and opposing cell, therefore inhibiting TNT fusion.

Tetraspanins asymmetrically regulate the functionality of TNTs

Since my transfer experiments were targeting these tetraspanins specifically on donor cells, next I decided to knock out CD9 or CD81 in the acceptor population. Surprisingly, these knock outs in acceptor population resulted on a huge increase on the vesicle transfer for both CD9 or CD81 knock out. This differently behavior of this tetraspanins in donor or acceptor populations might indicate that there is an asymmetry in function and/or location whether they are on donor or acceptor cell. This phenotype it resembles sperm-egg fusion were at least in the case of CD9 it is fundamental on the oocyte (*Kaji et al., 2000*; *Le Naour et al., 2000*; *Miyado et al., 2000*) but it is not needed on the sperm (*Le Naour et al., 2000*). Alternatively, this aforementioned asymmetry could be caused by the conformation of the TEMs with the absence of CD9 or CD81 which could imply a change of associated partners (e.g. CD9P-1 or EWI-2) in the TEM or change in the lipidic composition of this TEMs, such as cholesterol, lipid described to be associated with these tetraspanins (*Charrin et al., 2003*). Here I hypothesize that when CD9 or CD81 is present in the membrane of the acceptor cell (in the schematics is only represented CD81 for simplicity) through the association with cholesterol would rigidify the membrane (*Caparotta and Masone, 2021*) avoiding the TNT to protrude and push the opposite membrane inwards (process need for drosophila myoblast fusion, *Lee and Chen, 2019*) and therefore impairing the TNT fusion (*Figure 27A*). This would imply that the formation of the TNTs or iTNTs it is directional, which means that TNTs or iTNTs are coming from one or the other cell, since this membrane rigidity in acceptor cell would not let this cell to provoke a membrane deformation impairing the formation of opposite directions TNTs or iTNTs. On contrary, CD9 or CD81 knock out could cause a dissipation of the cholesterol from the contact area allowing the TNT to invaginate into the opposing membrane and to produce the fusion of the TNT with the acceptor cell (*Figure 27B*).

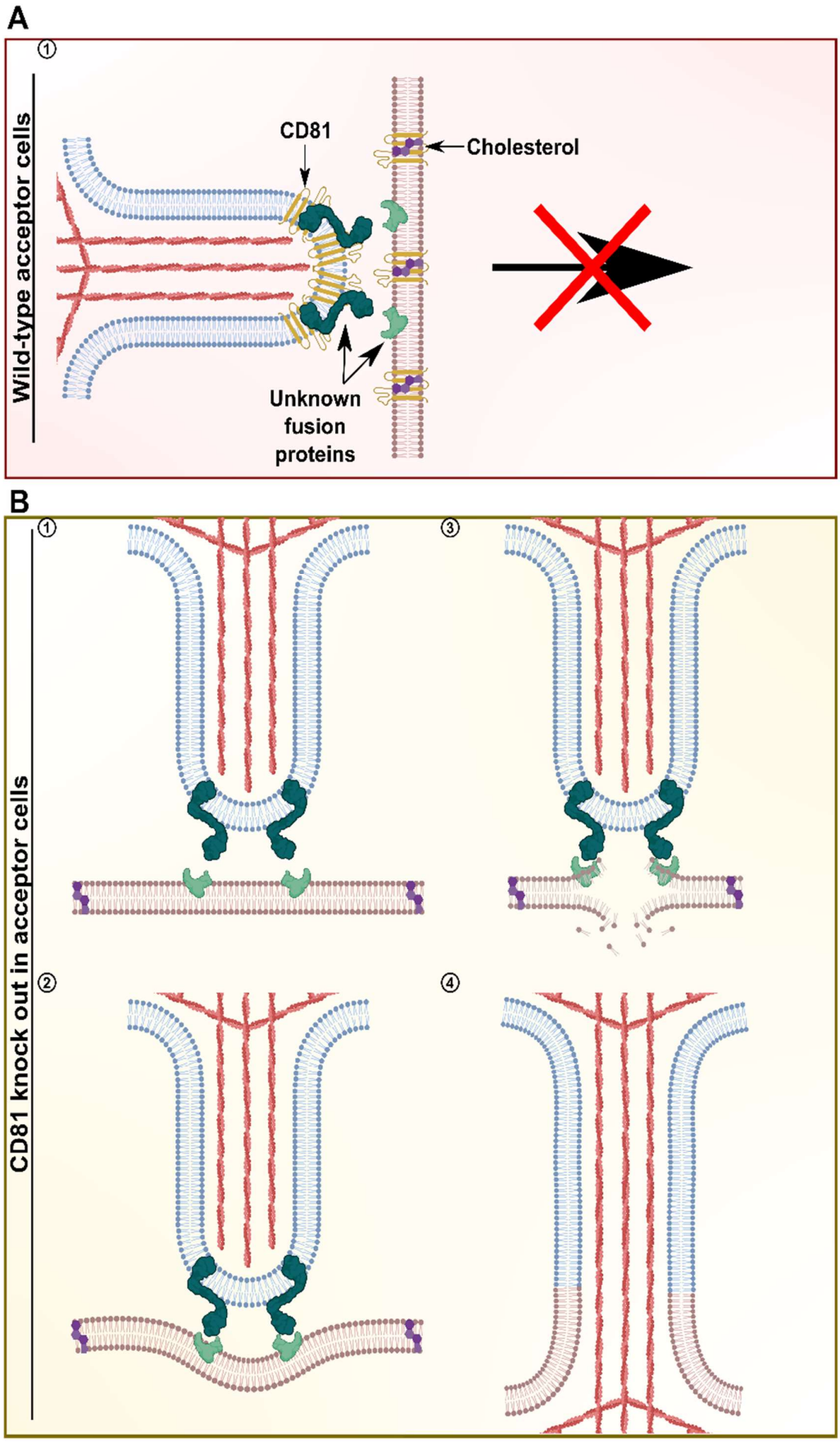
A
①
Wild-type acceptor cells
CD81
Cholesterol
Unknown
fusion
proteins
B
①
③
②
④
CD81 knock out in acceptor cells

Figure 27. Control of TNT fusion by CD81 in acceptor cell.

(A) Schematics of TNTs-fusion step under wild-type conditions in acceptor cells. 1) The presence of CD81 bound to cholesterol would rigidify the membrane avoiding the TNT to push inwards the opposing membrane and inhibiting the fusion. (B) Schematics of TNTs-fusion step under knock out conditions in acceptor cells. 1) The absence of CD81would diffuse cholesterol to other places of the membrane. 2) Without cholesterol in the opposing membrane, this would be pushed inwards by the TNT so the fusion molecules could interact with their counterparts. 3) Membrane fusion and lipid mixing would occur. 4) An open TNTs would be form.

My last step, since it seemed that these tetraspanins might regulate different processes of the TNT formation, was to unravel the biological processes of CD9 and CD81 on TNTs. To this end, I knocked out one of these tetraspanins in the cells overexpressing the other tetraspanin. Whereas the knockout of CD81 on cells overexpressing CD9 did not alter neither the % of cells connected by TNTs nor the vesicle transfer, the knockout of CD9 in cells overexpressing CD81 decreased both TNT number and vesicle transfer. Taking these results and those previously mentioned results together, I can conclude that both CD9 and CD81 are fundamental for the correct formation of a functional TNT, most probably with CD9 actin in the initiation of the formation of the TNT and CD81 on the last stages of the functionality of the TNTs (and presumably in the fusion of these structures with the opposing cells).

Future perspectives

Although this is the first study showing a specific and differential role of CD9 and CD81 on TNT formation and functionality there are a number of aspects that remain to be deciphered regarding the precise role of these tetraspanins in TNT biology:

- As I have mentioned in the previous results section, we want to confirm and expand the data that we have obtained regarding the regulation of TNTs by CD9 and CD81 and for this we have specific experiments in mind, some of them I am currently performing. To assess if the tetraspanins present in the donor cell or the ones present in the acceptor cell are important for the fusion with the opposite cell, I am going to perform two different sets of experiments: one in which we will co-culture donor cells KO for one of the tetraspanins versus acceptor cells KO for that same tetraspanin (e.g. CD9 KO cells versus CD9 KO cells or CD81 KO cells versus CD81 KO cells), and another in which we will co-culture donor cells KO for both tetraspanins versus acceptor cells KO for only one of the tetraspanins (e.g. CD9&CD81 KO cells versus CD9 KO cells or CD9&CD81 KO

cells versus CD81 KO cells). Knowing that the KO of these tetraspanins in the donor cells decreases the transfer while the KO of these tetraspanins in the acceptor cell increases this transfer, we can correlate the results obtained in these two experiments with the presence (or absence) and importance of the tetraspanins in the donor or acceptor cell.

On the other hand, in order to understand whether the presence of both tetraspanins or only one of them is necessary in the acceptor cell to enable fusion, I plan to perform experiments in which I will knock out one of the tetraspanins and overexpress the other in acceptor cells in coculture with WT cells.

- It is indeed intriguing that these two tetraspanins that are so similar in sequence, structure and functions (*Boucheix and Rubinstein, 2001*; *Umeda et al., 2020*) appear to have different roles on TNTs. Nevertheless, although being that similar they have some structural peculiarities. Whereas CD81 has a cholesterol pocket in between its transmembrane domain and by binding cholesterol it might impair its association with other proteins through a change in conformational state (*Zimmerman et al., 2016*), CD9 has also an inner lipidic cavity, but the conformational change is spontaneous. Therefore, the different roles of CD9 and CD81 on TNTs could be influenced by the cholesterol presence or absence on the initiation zone of the TNT or on the contact area between TNT and opposing cell. Since we have an already stablish workflow for the collection and analysis of TNTs established by Dr. Christel Brou (see TNTome preparation), it could be interesting to isolate TNTs and to precipitate CD9 or CD81 and analyze whether they can coprecipitate or not cholesterol. In this respect it could be interesting to assess the influence of cholesterol depletion on TNT formation and functionality. Alternatively, lipidic composition of the cells and specifically of TNTs can be investigated by performing immunofluorescence of lipids such as phosphatidylinositol or cholesterol.
- Since we have an already established Correlative-Cryo-EM workflow (*Sartori-Rupp et al., 2019*) by Dr. Anna Pepe, this tool would help us to understand the ultrastructure of the TNTs in the presence or absence of these tetraspanins. Similar to what we have done in my first project in the case of NCadherin we can assess whether we detect more or less close-ended TNTs, and if the architecture of the bundle of iTNTs it is affected. Furthermore, we could use FIB-SEM, especially in the case of CD81, to image the contact area between TNTs and the

opposing cell to visualize whether these TNTs are open or close in the different experimental conditions.

- As mentioned in the introduction, TEMs are formed by tetraspanins either associated between themselves or with other proteins (directly or indirectly) (*Charrin et al., 2014*). Between all the possible interactors, the tetraspanin CD9 and CD81 virtually obligated partners CD9P-1 and EWI-2, are the most interesting for me because of their roles in muscle cells fusion (*Charrin et al., 2013*) and their ability to bind the ERM complex that presumably would interact with the actin cytoskeleton providing a physical link tetraspanins-actin (*Sala-Valdés et al., 2006*). Therefore, investigating first CD9P-1 and EWI-2 and subsequently the ERM complex on TNT formation and functionality could reveal the mechanism by which CD9 and CD81 are regulating the TNTs.
- Since the discovery of iTNTs, this phenomenon could imply that in one apparent TNT there are different iTNTs from different cells forming this bundle, meaning that TNTs or iTNTs could be formed following a directionality. As I speculated previously, the results on the KO of the tetraspanins on acceptor cells and its possible relationship with cholesterol could suggest that indeed there is directional TNTs. Therefore, I propose to label actin in different colors in two different population of cells, one WT and another one rather cells knock out or overexpressing CD9 and/or CD81. This way, we would be able to distinguish which cell is forming the TNT (even if there is overlapping of both colors it could imply the presence of bidirectional TNTs) and how the different expression of these tetraspanins affects this directionality.
- In this section, I have discussed that CD9 could be a positive regulator of the initiation of the TNTs. However, the fact that we see more TNTs doesn't mean that there is more formation of these structures, because it could be that these structures are more or less stable (at therefore lasting more or less) with the different CD9 level of expression. Thus, to rule out the specific role of CD9 in TNT formation, here I propose to measure the duration of the TNTs by live imaging in the knock out or overexpression of this protein. Unlike for CD9, the same apparent number of TNTs in the knock out and overexpression of CD81 might mean that this protein is not involved on the stability of the TNTs.

- Tetraspanins CD9 and CD81 are just two members of a family composed by 33 proteins in mammals, so many other tetraspanins could have a role on TNT regulation. CD82 is an interesting member since it has been already characterized as a negative regulator of the digitation junction protrusions (*Huang et al., 2018*). Moreover, the detection of CD151 in the TNT fraction of our mass spectrometry analysis of the TNTome points to a possible role of this tetraspanin in TNT biology, But the member that most attracts my attention is CD63. Knowing that CD9 and CD81 are mainly markers of ectosomes whereas CD63 is mainly marking exosomes (*Mathieu et al., 2021*), could it be that CD63 have a different role (or any role at all) on TNT regulation compared to CD9 and CD81? Maybe targeting CD63 could give us more clues about the biogenesis of the TNTs.
- Finally, I believe it would be fundamental to characterize the membrane dynamics on the TNTs. For that, I propose to use Fluorescence Recovery After Photobleaching (FRAP) on the CD9GFP or CD81GFP cells, specifically on TNTs or at other places of the membrane. The objective would be to assess if the recovery of these proteins would be different on TNTs compared to other zone of the membrane, giving us and idea about the fluidity of the membrane on TNTs. It could be eventually investigated if the recovery of these tetraspanins it is unidirectional or bidirectional, which could indicate the presence (or not) of iTNTs with different orientation.

Are N-cadherin and CD9/CD81 pathways connected?

When we discovered that NCAD could have an effect on TNT fusion, I (following the advice of Dr. Christel Brou) started to be interested on the tetraspanin CD9 and CD81 because their role on different cellular fusion processes (*Le Naour et al., 2000*; *Takeda et al., 2003*; *Charrin et al., 2013*). Previous investigations have shown interaction of cadherins and tetraspanins, for example, the tetraspanin CD151 forms large adhesion complexes, including α3β1 integrin, CD151, PKCβII, RACK1, PTPμ, ECAD, β-catenin, α-catenin, and α-actinin and CD151 does not affect the ECAD–β-catenin complex, but stabilizes the α-catenin–α-actinin complex (*Chattopadhyay et al., 2003*). Other study, showed that the tetraspanin CD82 inhibits β-catenin tyrosine phosphorylation and stabilizes ECAD–β-catenin complexes (*Abe et al., 2008*). Also, it has been shown that ALCAM (Activated Leukocyte Cell Adhesion Molecule, a Ca^{2+} independent cell

adhesion molecule) directly associates with CD9 and ADAM17 on the leukocyte surface. CD9 induces upregulation of ALCAM interactions by 2 mechanism, augmented clustering of ALCAM molecules, and upregulation of ALCAM surface expression due to inhibition of ADAM17 sheddase activity (*Gilsanz et al., 2013*). Thus, I decided to investigate whether NCAD and CD9 and/or CD81 could interact on SH-SY5Y cells and if potentially they could form a complex that could regulate TNT formation and functionality.

N-cadherin does not seem to interact directly with CD9 and/or CD81

To this end, I performed GFP-trap experiments with cells overexpressing either NCAD, CD9 or CD81 (all of them tagged to GFP) with specific lysis buffer to preserve tetraspanin-to-tetraspanin interactions (*Serru et al., 1999*). Under these conditions, neither NCADGFP cells were able to precipitate CD9 or CD81, nor CD9GFP or CD81GFP cells were able to precipitate NCAD. The immunoprecipitation protocol was validated showing how NCADGFP cells did precipitate α-catenin, CD9GFP cells precipitated EWI-2 and CD81GFP cells precipitated both CD9 and CD81. The fact that CD9GFP did not precipitate CD81 is curious to say the least, but perhaps the GFP-tagged CD9 could somehow affect the CD9-CD81 interaction. With this result, I therefore decided to study NCAD and these tetraspanins as separate projects. However, it should be noted that I only performed these experiments once and therefore there are no replicates confirming these results, but it is conceivable, since the target proteins were not precipitated in either direction, that direct NCAD-CD9-CD81 interaction does not occur in SH-SY5Y cells.

Speculations and future perspectives

However, it exists the possibility that N-cadherin and the tetraspanins CD9 and CD81 indirectly interact by, speculating, ADAM10, a desintegrin and metalloprotease responsible for the cleavage of N-cadherin (*Reiss et al., 2005*) or either that these three proteins they could form complexes inside the TEMs without direct interaction. Thus, it could be interesting to try proximity ligation assay to if these molecules can be found in close proximity. But indeed, it might be that NCAD, CD9 and CD81 could have a relationship which would not imply physical interaction. We could speculate that these tetraspanins could have a role in the trafficking of NCAD as CD9 does with MHC proteins (*Rocha-Perugini et al., 2017*) or CD81 with CD19 (*Susa et al., 2020*), so a similar system

as previously used (*Mathieu et al., 2021*) could be applied to retain CD9 or CD81 at the level of the endoplasmic reticulum and asses if the membrane expression of NCAD it is affected. Alternatively, NCAD expression (localization and amount) could be checked by immunofluorescence in the knock out or overexpression of CD9 or CD81. If NCAD expression in the different conditions it is affected it could mean that the correct presence of NCAD requires a correct TEM composition. Moreover, the relatively abundance of these three proteins on the TNTome could mean that indeed they are important on TNT biology by regulating each other. Speculating, and comparing a similar result on TNT functionality for NCAD and CD81, I hypothesize that TNT formation would require CD9 to initiate the formation of the protrusion and that this molecule would eventually bring at the tip of the TNT both NCAD and CD81, then NCAD would engage homophilically with the NCAD of the opposing cell facilitating the adhesion and stabilization and CD81 could act subsequentially on the fusion of this TNT. Therefore, it would be necessary to check whether the expression (localization and amount) specifically on TNTs of CD9, CD81 or NCAD it is altered by the overexpression or knock out of one of the other proteins. Additionally, to know whether this hypothetical model could be true, I propose to perform immunofluorescence assays and live imaging in experiment concerning cells that would overexpress one of these proteins and knock out for one of the other (e.g. knock out CD9 in cells overexpressing NCAD or inversely; knock out CD81 in cells overexpressing NCAD or inversely). By this immunofluorescence and TNT counting and vesicle transfer we could potentially see what is the influence of one of this proteins to the other in terms of amount, location, formation and functionality of TNTs and by live imaging we could asses how it is the real time behavior of these molecules in the absence of the other, such as, if the trafficking of these proteins it is affected, if the location on TNTs it is altered or blocked while the TNT is forming or if they never reach their final location that we see on steady state conditions.

Section 6: Bibliography

Abe, K., Takeichi, M., 2008. EPLIN mediates linkage of the cadherin catenin complex to F-actin and stabilizes the circumferential actin belt. Proc Natl Acad Sci U S A 105, 13–19. https://doi.org/10.1073/pnas.0710504105

Abe, M., Sugiura, T., Takahashi, M., Ishii, K., Shimoda, M., Shirasuna, K., 2008. A novel function of CD82/KAI-1 on E-cadherin-mediated homophilic cellular adhesion of cancer cells. Cancer Lett 266, 163–170. https://doi.org/10.1016/j.canlet.2008.02.058

Abounit, Saïda, Bousset, L., Loria, F., Zhu, S., de Chaumont, F., Pieri, L., Olivo-Marin, J.-C., Melki, R., Zurzolo, C., 2016. Tunneling nanotubes spread fibrillar α-synuclein by intercellular trafficking of lysosomes. EMBO J 35, 2120–2138. https://doi.org/10.15252/embj.201593411

Abounit, Saida, Wu, J.W., Duff, K., Victoria, G.S., Zurzolo, C., 2016. Tunneling nanotubes: A possible highway in the spreading of tau and other prion-like proteins in neurodegenerative diseases. Prion 10, 344–351. https://doi.org/10.1080/19336896.2016.1223003

Abounit, S., Zurzolo, C., 2012. Wiring through tunneling nanotubes – from electrical signals to organelle transfer. Journal of Cell Science 125, 1089–1098. https://doi.org/10.1242/jcs.083279

Adar-Levor, S., Goliand, I., Elbaum, M., Elia, N., 2019. Studying the Spatial Organization of ESCRTs in Cytokinetic Abscission Using the High-Resolution Imaging Techniques SIM and Cryo-SXT, in: Culetto, E., Legouis, R. (Eds.), The ESCRT Complexes: Methods and Protocols, Methods in Molecular Biology. Springer, New York, NY, pp. 129–148. https://doi.org/10.1007/978-1-4939-9492-2_10

Alarcon-Martinez, L., Villafranca-Baughman, D., Quintero, H., Kacerovsky, J.B., Dotigny, F., Murai, K.K., Prat, A., Drapeau, P., Di Polo, A., 2020. Interpericyte tunnelling nanotubes regulate neurovascular coupling. Nature 585, 91–95. https://doi.org/10.1038/s41586-020-2589-x

Alberts, B., 2015. Molecular biology of the cell, Sixth edition. ed. Garland Science, Taylor and Francis Group, New York, NY.

Albiges-Rizo, C., Destaing, O., Fourcade, B., Planus, E., Block, M.R., 2009. Actin machinery and mechanosensitivity in invadopodia, podosomes and focal adhesions. Journal of Cell Science 122, 3037–3049. https://doi.org/10.1242/jcs.052704

Anastasiadis, P.Z., Moon, S.Y., Thoreson, M.A., Mariner, D.J., Crawford, H.C., Zheng, Y., Reynolds, A.B., 2000. Inhibition of RhoA by p120 catenin. Nat Cell Biol 2, 637–644. https://doi.org/10.1038/35023588

Andreu, Z., Yáñez-Mó, M., 2014. Tetraspanins in extracellular vesicle formation and function. Front Immunol 5, 442. https://doi.org/10.3389/fimmu.2014.00442

Angst, B.D., Marcozzi, C., Magee, A.I., 2001. The cadherin superfamily: diversity in form and function. Journal of Cell Science 114, 629–641. https://doi.org/10.1242/jcs.114.4.629

Antanavičiūtė, I., Rysevaitė, K., Liutkevičius, V., Marandykina, A., Rimkutė, L., Sveikatienė, R., Uloza, V., Skeberdis, V.A., 2014. Long-Distance Communication between Laryngeal Carcinoma Cells. PLoS One 9, e99196. https://doi.org/10.1371/journal.pone.0099196

Arduise, C., Abache, T., Li, L., Billard, M., Chabanon, A., Ludwig, A., Mauduit, P., Boucheix, C., Rubinstein, E., Le Naour, F., 2008. Tetraspanins regulate ADAM10-mediated cleavage of TNF-alpha and epidermal growth factor. J Immunol 181, 7002–7013. https://doi.org/10.4049/jimmunol.181.10.7002

Austefjord, M.W., Gerdes, H.-H., Wang, X., 2014. Tunneling nanotubes. Commun Integr Biol 7, e27934. https://doi.org/10.4161/cib.27934

Bajpai, S., Feng, Y., Krishnamurthy, R., Longmore, G.D., Wirtz, D., 2009. Loss of alpha-catenin decreases the strength of single E-cadherin bonds between human cancer cells. J Biol Chem 284, 18252–18259. https://doi.org/10.1074/jbc.M109.000661

Bari, R., Guo, Q., Xia, B., Zhang, Y.H., Giesert, E.E., Levy, S., Zheng, J.J., Zhang, X.A., 2011. Tetraspanins regulate the protrusive activities of cell membrane. Biochem Biophys Res Commun 415, 619–626. https://doi.org/10.1016/j.bbrc.2011.10.121

Bekirov, I.H., Needleman, L.A., Zhang, W., Benson, D.L., 2002. Identification and localization of multiple classic cadherins in developing rat limbic system. Neuroscience 115, 213–227. https://doi.org/10.1016/S0306-4522(02)00375-5

Benham-Pyle, B.W., Pruitt, B.L., Nelson, W.J., 2015. Cell adhesion. Mechanical strain induces E-cadherin-dependent Yap1 and β-catenin activation to drive cell cycle entry. Science 348, 1024–1027. https://doi.org/10.1126/science.aaa4559

Benjamin, J.M., Kwiatkowski, A.V., Yang, C., Korobova, F., Pokutta, S., Svitkina, T., Weis, W.I., Nelson, W.J., 2010. AlphaE-catenin regulates actin dynamics independently of cadherin-mediated cell-cell adhesion. J Cell Biol 189, 339–352. https://doi.org/10.1083/jcb.200910041

Berditchevski, F., Gilbert, E., Griffiths, M., Fitter, S., Ashman, L., Jenner, S., 2001. Analysis of the CD151·α3β1 Integrin and CD151·Tetraspanin Interactions by Mutagenesis. The Journal of biological chemistry 276, 41165–74. https://doi.org/10.1074/jbc.M104041200

Berditchevski, F., Odintsova, E., Sawada, S., Gilbert, E., 2002. Expression of the Palmitoylation-deficient CD151 Weakens the Association of α3β1 Integrin with the Tetraspanin-enriched Microdomains and Affects Integrin-dependent Signaling*. Journal of Biological Chemistry 277, 36991–37000. https://doi.org/10.1074/jbc.M205265200

Bhat, S., Ljubojevic, N., Zhu, S., Fukuda, M., Echard, A., Zurzolo, C., 2020. Rab35 and its effectors promote formation of tunneling nanotubes in neuronal cells. Sci Rep 10, 16803. https://doi.org/10.1038/s41598-020-74013-z

Boggon, T.J., Murray, J., Chappuis-Flament, S., Wong, E., Gumbiner, B.M., Shapiro, L., 2002. C-Cadherin Ectodomain Structure and Implications for Cell Adhesion Mechanisms. Science 296, 1308–1313. https://doi.org/10.1126/science.1071559

Bonnet, M., Maisonial-Besset, A., Zhu, Y., Witkowski, T., Roche, G., Boucheix, C., Greco, C., Degoul, F., 2019. Targeting the Tetraspanins with Monoclonal Antibodies in Oncology: Focus on Tspan8/Co-029. Cancers (Basel) 11, 179. https://doi.org/10.3390/cancers11020179

Boucheix, C., Benoit, P., Frachet, P., Billard, M., Worthington, R.E., Gagnon, J., Uzan, G., 1991. Molecular cloning of the CD9 antigen. A new family of cell surface proteins. J Biol Chem 266, 117–122.

Boucheix, C., Rubinstein, E., 2001. Tetraspanins. Cell Mol Life Sci 58, 1189–1205. https://doi.org/10.1007/PL00000933

Brinton, C.C., 1971. The properties of sex pili, the viral nature of "conjugal" genetic transfer systems, and some possible approaches to the control of bacterial drug resistance. CRC Crit Rev Microbiol 1, 105–160. https://doi.org/10.3109/10408417109104479

Brosseau, C., Colas, L., Magnan, A., Brouard, S., 2018. CD9 Tetraspanin: A New Pathway for the Regulation of Inflammation? Frontiers in Immunology 9.

Buckley, C.D., Tan, J., Anderson, K.L., Hanein, D., Volkmann, N., Weis, W.I., Nelson, W.J., Dunn, A.R., 2014. Cell adhesion. The minimal cadherin-catenin complex binds to actin filaments under force. Science 346, 1254211. https://doi.org/10.1126/science.1254211

Bukoreshtliev, N.V., Wang, X., Hodneland, E., Gurke, S., Barroso, J.F.V., Gerdes, H.-H., 2009. Selective block of tunneling nanotube (TNT) formation inhibits intercellular organelle transfer between PC12 cells. FEBS Lett 583, 1481–1488. https://doi.org/10.1016/j.febslet.2009.03.065

Caicedo, A., Fritz, V., Brondello, J.-M., Ayala, M., Dennemont, I., Abdellaoui, N., de Fraipont, F., Moisan, A., Prouteau, C.A., Boukhaddaoui, H., Jorgensen, C., Vignais, M.-L., 2015. MitoCeption as a new tool to assess the effects of mesenchymal stem/stromal cell mitochondria on cancer cell metabolism and function. Sci Rep 5, 9073. https://doi.org/10.1038/srep09073

Caneparo, L., Pantazis, P., Dempsey, W., Fraser, S.E., 2011. Intercellular bridges in vertebrate gastrulation. PLoS One 6, e20230. https://doi.org/10.1371/journal.pone.0020230

Cannon, K.S., Cresswell, P., 2001. Quality control of transmembrane domain assembly in the tetraspanin CD82. EMBO J 20, 2443–2453. https://doi.org/10.1093/emboj/20.10.2443

Caparotta, M., Masone, D., 2021. Cholesterol plays a decisive role in tetraspanin assemblies during bilayer deformations. Biosystems 209, 104505. https://doi.org/10.1016/j.biosystems.2021.104505

Castro-Castro, A., Marchesin, V., Monteiro, P., Lodillinsky, C., Rossé, C., Chavrier, P., 2016. Cellular and Molecular Mechanisms of MT1-MMP-Dependent Cancer Cell Invasion.

Annu Rev Cell Dev Biol 32, 555–576. https://doi.org/10.1146/annurev-cellbio-111315-125227

Cavallaro, U., Dejana, E., 2011. Adhesion molecule signalling: not always a sticky business. Nat Rev Mol Cell Biol 12, 189–197. https://doi.org/10.1038/nrm3068

Cavey, M., Lecuit, T., 2009. Molecular Bases of Cell–Cell Junctions Stability and Dynamics. Cold Spring Harb Perspect Biol 1, a002998. https://doi.org/10.1101/cshperspect.a002998

Cervantes, D.C., Zurzolo, C., 2021. Peering into tunneling nanotubes—The path forward. The EMBO Journal 40, e105789. https://doi.org/10.15252/embj.2020105789

Chang, M., Lee, O., Bu, G., Oh, J., Yunn, N.-O., Ryu, S.H., Kwon, H.-B., Kolomeisky, A.B., Shim, S.-H., Doh, J., Jeon, J.-H., Lee, J.-B., 2022. Formation of cellular close-ended tunneling nanotubes through mechanical deformation. Science Advances 8, eabj3995. https://doi.org/10.1126/sciadv.abj3995

Charrin, S., Jouannet, S., Boucheix, C., Rubinstein, E., 2014. Tetraspanins at a glance. Journal of Cell Science 127, 3641–3648. https://doi.org/10.1242/jcs.154906

Charrin, S., Latil, M., Soave, S., Polesskaya, A., Chrétien, F., Boucheix, C., Rubinstein, E., 2013. Normal muscle regeneration requires tight control of muscle cell fusion by tetraspanins CD9 and CD81. Nat Commun 4, 1674. https://doi.org/10.1038/ncomms2675

Charrin, S., Le Naour, F., Oualid, M., Billard, M., Faure, G., Hanash, S.M., Boucheix, C., Rubinstein, E., 2001. The major CD9 and CD81 molecular partner. Identification and characterization of the complexes. J Biol Chem 276, 14329–14337. https://doi.org/10.1074/jbc.M011297200

Charrin, S., le Naour, F., Silvie, O., Milhiet, P.-E., Boucheix, C., Rubinstein, E., 2009. Lateral organization of membrane proteins: tetraspanins spin their web. Biochem J 420, 133–154. https://doi.org/10.1042/BJ20082422

Charrin, S., Manié, S., Thiele, C., Billard, M., Gerlier, D., Boucheix, C., Rubinstein, E., 2003. A physical and functional link between cholesterol and tetraspanins. Eur J Immunol 33, 2479–2489. https://doi.org/10.1002/eji.200323884

Chastagner, P., Loria, F., Vargas, J.Y., Tois, J., I Diamond, M., Okafo, G., Brou, C., Zurzolo, C., 2020. Fate and propagation of endogenously formed Tau aggregates in neuronal cells. EMBO Mol Med 12, e12025. https://doi.org/10.15252/emmm.202012025

Chattopadhyay, N., Wang, Z., Ashman, L.K., Brady-Kalnay, S.M., Kreidberg, J.A., 2003. alpha3beta1 integrin-CD151, a component of the cadherin-catenin complex, regulates PTPmu expression and cell-cell adhesion. J Cell Biol 163, 1351–1362. https://doi.org/10.1083/jcb.200306067

Chatzi, C., Westbrook, G.L., 2021. Revisiting I-BAR Proteins at Central Synapses. Front Neural Circuits 15, 787436. https://doi.org/10.3389/fncir.2021.787436

Chauveau, A., Aucher, A., Eissmann, P., Vivier, E., Davis, D.M., 2010. Membrane nanotubes facilitate long-distance interactions between natural killer cells and target cells. Proc Natl Acad Sci U S A 107, 5545–5550. https://doi.org/10.1073/pnas.0910074107

Chen, J., Cao, J., 2021. Astrocyte-to-neuron transportation of enhanced green fluorescent protein in cerebral cortex requires F-actin dependent tunneling nanotubes. Sci Rep 11, 16798. https://doi.org/10.1038/s41598-021-96332-5

Claas, C., Stipp, C.S., Hemler, M.E., 2001. Evaluation of prototype transmembrane 4 superfamily protein complexes and their relation to lipid rafts. J Biol Chem 276, 7974–7984. https://doi.org/10.1074/jbc.M008650200

Collins, J.E., Legan, P.K., Kenny, T.P., MacGarvie, J., Holton, J.L., Garrod, D.R., 1991. Cloning and sequence analysis of desmosomal glycoproteins 2 and 3 (desmocollins): cadherin-like desmosomal adhesion molecules with heterogeneous cytoplasmic domains. J Cell Biol 113, 381–391. https://doi.org/10.1083/jcb.113.2.381

Colombo, M., Raposo, G., Théry, C., 2014. Biogenesis, Secretion, and Intercellular Interactions of Exosomes and Other Extracellular Vesicles. Annual Review of Cell and Developmental Biology 30, 255–289. https://doi.org/10.1146/annurev-cellbio-101512-122326

Connor, Y., Tekleab, S., Nandakumar, S., Walls, C., Tekleab, Y., Husain, A., Gadish, O., Sabbisetti, V., Kaushik, S., Sehrawat, S., Kulkarni, A., Dvorak, H., Zetter, B., R Edelman,

E., Sengupta, S., 2015. Physical nanoscale conduit-mediated communication between tumour cells and the endothelium modulates endothelial phenotype. Nat Commun 6, 8671. https://doi.org/10.1038/ncomms9671

Cordero Cervantes, D., Zurzolo, C., 2021. Peering into tunneling nanotubes-The path forward. EMBO J 40, e105789. https://doi.org/10.15252/embj.2020105789

Costanzo, M., Abounit, S., Marzo, L., Danckaert, A., Chamoun, Z., Roux, P., Zurzolo, C., 2013. Transfer of polyglutamine aggregates in neuronal cells occurs in tunneling nanotubes. J Cell Sci 126, 3678–3685. https://doi.org/10.1242/jcs.126086

Daly, C.A., Hall, E.T., Ogden, S.K., 2022. Regulatory mechanisms of cytoneme-based morphogen transport. Cell. Mol. Life Sci. 79, 119. https://doi.org/10.1007/s00018-022-04148-x

Davis, M.A., Reynolds, A.B., 2006. Blocked acinar development, E-cadherin reduction, and intraepithelial neoplasia upon ablation of p120-catenin in the mouse salivary gland. Dev Cell 10, 21–31. https://doi.org/10.1016/j.devcel.2005.12.004

Delage, E., Cervantes, D.C., Pénard, E., Schmitt, C., Syan, S., Disanza, A., Scita, G., Zurzolo, C., 2016. Differential identity of Filopodia and Tunneling Nanotubes revealed by the opposite functions of actin regulatory complexes. Sci Rep 6, 39632. https://doi.org/10.1038/srep39632

Desir, S., Dickson, E.L., Vogel, R.I., Thayanithy, V., Wong, P., Teoh, D., Geller, M.A., Steer, C.J., Subramanian, S., Lou, E., 2016. Tunneling nanotube formation is stimulated by hypoxia in ovarian cancer cells. Oncotarget 7, 43150–43161. https://doi.org/10.18632/oncotarget.9504

Desir, S., O'Hare, P., Vogel, R.I., Sperduto, W., Sarkari, A., Dickson, E.L., Wong, P., Nelson, A.C., Fong, Y., Steer, C.J., Subramanian, S., Lou, E., 2018. Chemotherapy-Induced Tunneling Nanotubes Mediate Intercellular Drug Efflux in Pancreatic Cancer. Sci Rep 8, 9484. https://doi.org/10.1038/s41598-018-27649-x

Desprat, N., Supatto, W., Pouille, P.-A., Beaurepaire, E., Farge, E., 2008. Tissue deformation modulates twist expression to determine anterior midgut differentiation in Drosophila embryos. Dev Cell 15, 470–477. https://doi.org/10.1016/j.devcel.2008.07.009

Dilna, A., Deepak, K.V., Damodaran, N., Kielkopf, C.S., Kagedal, K., Ollinger, K., Nath, S., 2021. Amyloid-β induced membrane damage instigates tunneling nanotube-like conduits by p21-activated kinase dependent actin remodulation. Biochim Biophys Acta Mol Basis Dis 1867, 166246. https://doi.org/10.1016/j.bbadis.2021.166246

Dilsizoglu Senol, A., Pepe, A., Grudina, C., Sassoon, N., Reiko, U., Bousset, L., Melki, R., Piel, J., Gugger, M., Zurzolo, C., 2019. Effect of tolytoxin on tunneling nanotube formation and function. Sci Rep 9, 5741. https://doi.org/10.1038/s41598-019-42161-6

Dilsizoglu Senol, A., Samarani, M., Syan, S., Guardia, C.M., Nonaka, T., Liv, N., Latour-Lambert, P., Hasegawa, M., Klumperman, J., Bonifacino, J.S., Zurzolo, C., 2021. α-Synuclein fibrils subvert lysosome structure and function for the propagation of protein misfolding between cells through tunneling nanotubes. PLoS Biol 19, e3001287. https://doi.org/10.1371/journal.pbio.3001287

Domhan, S., Ma, L., Tai, A., Anaya, Z., Beheshti, A., Zeier, M., Hlatky, L., Abdollahi, A., 2011. Intercellular communication by exchange of cytoplasmic material via tunneling nano-tube like structures in primary human renal epithelial cells. PLoS One 6, e21283. https://doi.org/10.1371/journal.pone.0021283

Drees, F., Pokutta, S., Yamada, S., Nelson, W.J., Weis, W.I., 2005. Alpha-catenin is a molecular switch that binds E-cadherin-beta-catenin and regulates actin-filament assembly. Cell 123, 903–915. https://doi.org/10.1016/j.cell.2005.09.021

Dubois, F., Jean-Jacques, B., Roberge, H., Bénard, M., Galas, L., Schapman, D., Elie, N., Goux, D., Keller, M., Maille, E., Bergot, E., Zalcman, G., Levallet, G., 2018. A role for RASSF1A in tunneling nanotube formation between cells through GEFH1/Rab11 pathway control. Cell Communication and Signaling 16, 66. https://doi.org/10.1186/s12964-018-0276-4

Dubuisson, J., Helle, F., Cocquerel, L., 2008. Early steps of the hepatitis C virus life cycle. Cellular Microbiology 10, 821–827. https://doi.org/10.1111/j.1462-5822.2007.01107.x

Dupont, M., Souriant, S., Balboa, L., Vu Manh, T.-P., Pingris, K., Rousset, S., Cougoule, C., Rombouts, Y., Poincloux, R., Ben Neji, M., Allers, C., Kaushal, D., Kuroda, M.J., Benet, S., Martinez-Picado, J., Izquierdo-Useros, N., Sasiain, M.D.C., Maridonneau-Parini, I., Neyrolles, O., Vérollet, C., Lugo-Villarino, G., 2020. Tuberculosis-associated IFN-I induces Siglec-1 on tunneling nanotubes and favors HIV-1 spread in macrophages. Elife 9, e52535. https://doi.org/10.7554/eLife.52535

Ellerman, D.A., Ha, C., Primakoff, P., Myles, D.G., Dveksler, G.S., 2003. Direct Binding of the Ligand PSG17 to CD9 Requires a CD9 Site Essential for Sperm-Egg Fusion. Mol Biol Cell 14, 5098–5103. https://doi.org/10.1091/mbc.E03-04-0244

Eugenin, E.A., Gaskill, P.J., Berman, J.W., 2009. Tunneling nanotubes (TNT) are induced by HIV-infection of macrophages: a potential mechanism for intercellular HIV trafficking. Cell Immunol 254, 142–148. https://doi.org/10.1016/j.cellimm.2008.08.005

Faix, J., Rottner, K., 2006. The making of filopodia. Curr Opin Cell Biol 18, 18–25. https://doi.org/10.1016/j.ceb.2005.11.002

Feigelson, S.W., Grabovsky, V., Shamri, R., Levy, S., Alon, R., 2003. The CD81 Tetraspanin Facilitates Instantaneous Leukocyte VLA-4 Adhesion Strengthening to Vascular Cell Adhesion Molecule 1 (VCAM-1) under Shear Flow*. Journal of Biological Chemistry 278, 51203–51212. https://doi.org/10.1074/jbc.M303601200

Ferrari, R., Martin, G., Tagit, O., Guichard, A., Cambi, A., Voituriez, R., Vassilopoulos, S., Chavrier, P., 2019. MT1-MMP directs force-producing proteolytic contacts that drive tumor cell invasion. Nat Commun 10, 4886. https://doi.org/10.1038/s41467-019-12930-y

Filloux, A., 2010. A Variety of Bacterial Pili Involved in Horizontal Gene Transfer. Journal of Bacteriology 192, 3243–3245. https://doi.org/10.1128/JB.00424-10

Fykerud, T.A., Knudsen, L.M., Totland, M.Z., Sørensen, V., Dahal-Koirala, S., Lothe, R.A., Brech, A., Leithe, E., 2016. Mitotic cells form actin-based bridges with adjacent cells to provide intercellular communication during rounding. Cell Cycle 15, 2943–2957. https://doi.org/10.1080/15384101.2016.1231280

Gallop, J.L., 2020. Filopodia and their links with membrane traffic and cell adhesion. Semin Cell Dev Biol 102, 81–89. https://doi.org/10.1016/j.semcdb.2019.11.017

Gilsanz, A., Sánchez-Martín, L., Gutiérrez-López, M.D., Ovalle, S., Machado-Pineda, Y., Reyes, R., Swart, G.W., Figdor, C.G., Lafuente, E.M., Cabañas, C., 2013. ALCAM/CD166 adhesive function is regulated by the tetraspanin CD9. Cell Mol Life Sci 70, 475–493. https://doi.org/10.1007/s00018-012-1132-0

Gousset, K., Schiff, E., Langevin, C., Marijanovic, Z., Caputo, A., Browman, D.T., Chenouard, N., de Chaumont, F., Martino, A., Enninga, J., Olivo-Marin, J.-C., Männel, D., Zurzolo, C., 2009. Prions hijack tunnelling nanotubes for intercellular spread. Nat Cell Biol 11, 328–336. https://doi.org/10.1038/ncb1841

Grisard, E., Nevo, N., Lescure, A., Doll, S., Corbé, M., Jouve, M., Lavieu, G., Joliot, A., Nery, E.D., Martin-Jaular, L., Théry, C., 2022. Homosalate boosts the release of tumour-derived extracellular vesicles with protection against anchorage-loss property. Journal of Extracellular Vesicles 11, e12242. https://doi.org/10.1002/jev2.12242

Grosheva, I., Shtutman, M., Elbaum, M., Bershadsky, A.D., 2001. p120 catenin affects cell motility via modulation of activity of Rho-family GTPases: a link between cell-cell contact formation and regulation of cell locomotion. J Cell Sci 114, 695–707. https://doi.org/10.1242/jcs.114.4.695

Grudina, C., Kouroupi, G., Nonaka, T., Hasegawa, M., Matsas, R., Zurzolo, C., 2019. Human NPCs can degrade α-syn fibrils and transfer them preferentially in a cell contact-dependent manner possibly through TNT-like structures. Neurobiol Dis 132, 104609. https://doi.org/10.1016/j.nbd.2019.104609

Gumbiner, B.M., 2005. Regulation of cadherin-mediated adhesion in morphogenesis. Nat Rev Mol Cell Biol 6, 622–634. https://doi.org/10.1038/nrm1699

Gupton, S.L., Gertler, F.B., 2007. Filopodia: the fingers that do the walking. Sci STKE 2007, re5. https://doi.org/10.1126/stke.4002007re5

Haimovich, G., Dasgupta, S., Gerst, J.E., 2020. RNA transfer through tunneling nanotubes. Biochemical Society Transactions 49, 145–160. https://doi.org/10.1042/BST20200113

Haimovich, G., Ecker, C.M., Dunagin, M.C., Eggan, E., Raj, A., Gerst, J.E., Singer, R.H., 2017. Intercellular mRNA trafficking via membrane nanotube-like extensions in mammalian cells. Proceedings of the National Academy of Sciences 114, E9873–E9882. https://doi.org/10.1073/pnas.1706365114

Halbleib, J.M., Nelson, W.J., 2006. Cadherins in development: cell adhesion, sorting, and tissue morphogenesis. Genes Dev. 20, 3199–3214. https://doi.org/10.1101/gad.1486806

Hall, J.E., Guyton, A.C., 2011. Guyton and Hall textbook of medical physiology, 12th ed. ed. Saunders/Elsevier, Philadelphia, Pa.

Hanna, S.J., McCoy-Simandle, K., Leung, E., Genna, A., Condeelis, J., Cox, D., 2019. Tunneling nanotubes, a novel mode of tumor cell–macrophage communication in tumor cell invasion. J Cell Sci 132, jcs223321. https://doi.org/10.1242/jcs.223321

Hanna, S.J., McCoy-Simandle, K., Miskolci, V., Guo, P., Cammer, M., Hodgson, L., Cox, D., 2017. The Role of Rho-GTPases and actin polymerization during Macrophage Tunneling Nanotube Biogenesis. Sci Rep 7, 8547. https://doi.org/10.1038/s41598-017-08950-7

Harrison, O.J., Jin, X., Hong, S., Bahna, F., Ahlsen, G., Brasch, J., Wu, Y., Vendome, J., Felsovalyi, K., Hampton, C.M., Troyanovsky, R.B., Ben-Shaul, A., Frank, J., Troyanovsky, S.M., Shapiro, L., Honig, B., 2011. The Extracellular Architecture of Adherens Junctions Revealed by Crystal Structures of Type I Cadherins. Structure 19, 244–256. https://doi.org/10.1016/j.str.2010.11.016

Hartsock, A., Nelson, W.J., 2012. Competitive regulation of E-cadherin juxtamembrane domain degradation by p120-catenin binding and Hakai-mediated ubiquitination. PLoS One 7, e37476. https://doi.org/10.1371/journal.pone.0037476

Hase, K., Kimura, S., Takatsu, H., Ohmae, M., Kawano, S., Kitamura, H., Ito, M., Watarai, H., Hazelett, C.C., Yeaman, C., Ohno, H., 2009. M-Sec promotes membrane nanotube formation by interacting with Ral and the exocyst complex. Nat Cell Biol 11, 1427–1432. https://doi.org/10.1038/ncb1990

Hatta, K., Okada, T.S., Takeichi, M., 1985. A monoclonal antibody disrupting calcium-dependent cell-cell adhesion of brain tissues: possible role of its target antigen in animal

pattern formation. Proc Natl Acad Sci U S A 82, 2789–2793. https://doi.org/10.1073/pnas.82.9.2789

Hayakawa, K., Esposito, E., Wang, X., Terasaki, Y., Liu, Y., Xing, C., Ji, X., Lo, E.H., 2016. Transfer of mitochondria from astrocytes to neurons after stroke. Nature 535, 551–555. https://doi.org/10.1038/nature18928

Hayashi, S., Takeichi, M., 2015. Emerging roles of protocadherins: from self-avoidance to enhancement of motility. Journal of Cell Science 128, 1455–1464. https://doi.org/10.1242/jcs.166306

Hazan, R.B., Kang, L., Roe, S., Borgen, P.I., Rimm, D.L., 1997. Vinculin is associated with the E-cadherin adhesion complex. J Biol Chem 272, 32448–32453. https://doi.org/10.1074/jbc.272.51.32448

He, J., Sun, E., Bujny, M.V., Kim, D., Davidson, M.W., Zhuang, X., 2013. Dual Function of CD81 in Influenza Virus Uncoating and Budding. PLOS Pathogens 9, e1003701. https://doi.org/10.1371/journal.ppat.1003701

Hekmatshoar, Y., Nakhle, J., Galloni, M., Vignais, M.-L., 2018. The role of metabolism and tunneling nanotube-mediated intercellular mitochondria exchange in cancer drug resistance. Biochemical Journal 475, 2305–2328. https://doi.org/10.1042/BCJ20170712

Hemler, M.E., 2014. Tetraspanin proteins promote multiple cancer stages. Nat Rev Cancer 14, 49–60. https://doi.org/10.1038/nrc3640

Hemler, M.E., 2003. Tetraspanin proteins mediate cellular penetration, invasion, and fusion events and define a novel type of membrane microdomain. Annu Rev Cell Dev Biol 19, 397–422. https://doi.org/10.1146/annurev.cellbio.19.111301.153609

Higginbottom, A., Quinn, E.R., Kuo, C.-C., Flint, M., Wilson, L.H., Bianchi, E., Nicosia, A., Monk, P.N., McKeating, J.A., Levy, S., 2000. Identification of Amino Acid Residues in CD81 Critical for Interaction with Hepatitis C Virus Envelope Glycoprotein E2. Journal of Virology 74, 3642–3649. https://doi.org/10.1128/JVI.74.8.3642-3649.2000

Hirano, S., Takeichi, M., 2012. Cadherins in Brain Morphogenesis and Wiring. Physiological Reviews 92, 597–634. https://doi.org/10.1152/physrev.00014.2011

Hong, I.-K., Jeoung, D.-I., Ha, K.-S., Kim, Y.-M., Lee, H., 2012. Tetraspanin CD151 Stimulates Adhesion-dependent Activation of Ras, Rac, and Cdc42 by Facilitating Molecular Association between β1 Integrins and Small GTPases*. Journal of Biological Chemistry 287, 32027–32039. https://doi.org/10.1074/jbc.M111.314443

Hua, K., Ferland, R.J., 2018. Primary cilia proteins: ciliary and extraciliary sites and functions. Cell. Mol. Life Sci. 75, 1521–1540. https://doi.org/10.1007/s00018-017-2740-5

Huang, C., Fu, C., Wren, J.D., Wang, X., Zhang, F., Zhang, Y.H., Connel, S.A., Chen, T., Zhang, X.A., 2018. Tetraspanin-enriched Microdomains Regulate Digitation Junctions. Cell Mol Life Sci 75, 3423–3439. https://doi.org/10.1007/s00018-018-2803-2

Huber, A.H., Stewart, D.B., Laurents, D.V., Nelson, W.J., Weis, W.I., 2001. The cadherin cytoplasmic domain is unstructured in the absence of beta-catenin. A possible mechanism for regulating cadherin turnover. J Biol Chem 276, 12301–12309. https://doi.org/10.1074/jbc.M010377200

Huber, O., Krohn, M., Kemler, R., 1997. A specific domain in alpha-catenin mediates binding to beta-catenin or plakoglobin. J Cell Sci 110 (Pt 15), 1759–1765. https://doi.org/10.1242/jcs.110.15.1759

Ichii, T., Takeichi, M., 2007. p120-catenin regulates microtubule dynamics and cell migration in a cadherin-independent manner. Genes to Cells 12, 827–839. https://doi.org/10.1111/j.1365-2443.2007.01095.x

Irigoín, F., Badano, J.L., 2011. Keeping the balance between proliferation and differentiation: the primary cilium. Curr Genomics 12, 285–297. https://doi.org/10.2174/138920211795860134

Ishii, M., Iwai, K., Koike, M., Ohshima, S., Kudo-Tanaka, E., Ishii, T., Mima, T., Katada, Y., Miyatake, K., Uchiyama, Y., Saeki, Y., 2006. RANKL-induced expression of tetraspanin CD9 in lipid raft membrane microdomain is essential for cell fusion during osteoclastogenesis. J Bone Miner Res 21, 965–976. https://doi.org/10.1359/jbmr.060308

Ishii, T., Ruiz-Torruella, M., Ikeda, A., Shindo, S., Movila, A., Mawardi, H., Albassam, A., Kayal, R.A., Al-Dharrab, A.A., Egashira, K., Wisitrasameewong, W., Yamamoto, K.,

Mira, A.I., Sueishi, K., Han, X., Taubman, M.A., Miyamoto, T., Kawai, T., 2018. OC-STAMP promotes osteoclast fusion for pathogenic bone resorption in periodontitis via up-regulation of permissive fusogen CD9. FASEB J 32, 4016–4030. https://doi.org/10.1096/fj.201701424R

Ishikawa, A., Omata, W., Ackerman, W.E., Takeshita, T., Vandré, D.D., Robinson, J.M., 2014. Cell fusion mediates dramatic alterations in the actin cytoskeleton, focal adhesions, and E-cadherin in trophoblastic cells. Cytoskeleton (Hoboken) 71, 241–256. https://doi.org/10.1002/cm.21165

Itoh, M., Nagafuchi, A., Moroi, S., Tsukita, S., 1997. Involvement of ZO-1 in cadherin-based cell adhesion through its direct binding to alpha catenin and actin filaments. J Cell Biol 138, 181–192. https://doi.org/10.1083/jcb.138.1.181

Jansens, R.J.J., Tishchenko, A., Favoreel, H.W., 2020. Bridging the Gap: Virus Long-Distance Spread via Tunneling Nanotubes. J Virol 94, e02120-19. https://doi.org/10.1128/JVI.02120-19

Jansens, R.J.J., Van den Broeck, W., De Pelsmaeker, S., Lamote, J.A.S., Van Waesberghe, C., Couck, L., Favoreel, H.W., 2017. Pseudorabies Virus US3-Induced Tunneling Nanotubes Contain Stabilized Microtubules, Interact with Neighboring Cells via Cadherins, and Allow Intercellular Molecular Communication. Journal of Virology 91, e00749-17. https://doi.org/10.1128/JVI.00749-17

Kabaso, D., Lokar, M., Kralj-Iglič, V., Veranič, P., Iglič, A., 2011. Temperature and cholera toxin B are factors that influence formation of membrane nanotubes in RT4 and T24 urothelial cancer cell lines. Int J Nanomedicine 6, 495–509. https://doi.org/10.2147/IJN.S16982

Kaji, K., Oda, S., Miyazaki, S., Kudo, A., 2002. Infertility of CD9-Deficient Mouse Eggs Is Reversed by Mouse CD9, Human CD9, or Mouse CD81; Polyadenylated mRNA Injection Developed for Molecular Analysis of Sperm–Egg Fusion. Developmental Biology 247, 327–334. https://doi.org/10.1006/dbio.2002.0694

Kaji, K., Oda, S., Shikano, T., Ohnuki, T., Uematsu, Y., Sakagami, J., Tada, N., Miyazaki, S., Kudo, A., 2000. The gamete fusion process is defective in eggs of Cd9-deficient mice. Nat Genet 24, 279–282. https://doi.org/10.1038/73502

Kardash, E., Reichman-Fried, M., Maître, J.-L., Boldajipour, B., Papusheva, E., Messerschmidt, E.-M., Heisenberg, C.-P., Raz, E., 2010. A role for Rho GTPases and cell-cell adhesion in single-cell motility in vivo. Nat Cell Biol 12, 47–53; sup pp 1-11. https://doi.org/10.1038/ncb2003

Karlas, A., Machuy, N., Shin, Y., Pleissner, K.-P., Artarini, A., Heuer, D., Becker, D., Khalil, H., Ogilvie, L.A., Hess, S., Mäurer, A.P., Müller, E., Wolff, T., Rudel, T., Meyer, T.F., 2010. Genome-wide RNAi screen identifies human host factors crucial for influenza virus replication. Nature 463, 818–822. https://doi.org/10.1038/nature08760

Khattar, K.E., Safi, J., Rodriguez, A.-M., Vignais, M.-L., 2022. Intercellular Communication in the Brain through Tunneling Nanotubes. Cancers (Basel) 14, 1207. https://doi.org/10.3390/cancers14051207

Khurana, S., Krementsov, D.N., de Parseval, A., Elder, J.H., Foti, M., Thali, M., 2007. Human immunodeficiency virus type 1 and influenza virus exit via different membrane microdomains. J Virol 81, 12630–12640. https://doi.org/10.1128/JVI.01255-07

Kitadokoro, K., Bordo, D., Galli, G., Petracca, R., Falugi, F., Abrignani, S., Grandi, G., Bolognesi, M., 2001. CD81 extracellular domain 3D structure: insight into the tetraspanin superfamily structural motifs. EMBO J 20, 12–18. https://doi.org/10.1093/emboj/20.1.12

Knudsen, K.A., Soler, A.P., Johnson, K.R., Wheelock, M.J., 1995. Interaction of alpha-actinin with the cadherin/catenin cell-cell adhesion complex via alpha-catenin. J Cell Biol 130, 67–77. https://doi.org/10.1083/jcb.130.1.67

Kobielak, A., Pasolli, H.A., Fuchs, E., 2004. Mammalian formin-1 participates in adherens junctions and polymerization of linear actin cables. Nat Cell Biol 6, 21–30. https://doi.org/10.1038/ncb1075

Koch, P.J., Walsh, M.J., Schmelz, M., Goldschmidt, M.D., Zimbelmann, R., Franke, W.W., 1990. Identification of desmoglein, a constitutive desmosomal glycoprotein, as a member of the cadherin family of cell adhesion molecules. Eur J Cell Biol 53, 1–12.

Korenkova, O., Pepe, A., Zurzolo, C., 2020. Fine intercellular connections in development: TNTs, cytonemes, or intercellular bridges? Cell Stress 4, 30–43. https://doi.org/10.15698/cst2020.02.212

Kovalenko, O.V., Yang, X., Kolesnikova, T.V., Hemler, M.E., 2004. Evidence for specific tetraspanin homodimers: inhibition of palmitoylation makes cysteine residues available for cross-linking. Biochem J 377, 407–417. https://doi.org/10.1042/BJ20031037

Kretschmer, A., Zhang, F., Somasekharan, S.P., Tse, C., Leachman, L., Gleave, A., Li, B., Asmaro, I., Huang, T., Kotula, L., Sorensen, P.H., Gleave, M.E., 2019. Stress-induced tunneling nanotubes support treatment adaptation in prostate cancer. Sci Rep 9, 7826. https://doi.org/10.1038/s41598-019-44346-5

Kumar, A., Kim, J.H., Ranjan, P., Metcalfe, M.G., Cao, W., Mishina, M., Gangappa, S., Guo, Z., Boyden, E.S., Zaki, S., York, I., García-Sastre, A., Shaw, M., Sambhara, S., 2017. Influenza virus exploits tunneling nanotubes for cell-to-cell spread. Sci Rep 7, 40360. https://doi.org/10.1038/srep40360

Lachambre, S., Chopard, C., Beaumelle, B., 2014. Preliminary characterisation of nanotubes connecting T-cells and their use by HIV-1. Biol Cell 106, 394–404. https://doi.org/10.1111/boc.201400037

Lau, L.-M., Wee, J.L., Wright, M.D., Moseley, G.W., Hogarth, P.M., Ashman, L.K., Jackson, D.E., 2004. The tetraspanin superfamily member CD151 regulates outside-in integrin αIIbβ3 signaling and platelet function. Blood 104, 2368–2375. https://doi.org/10.1182/blood-2003-12-4430

Le Naour, F., Rubinstein, E., Jasmin, C., Prenant, M., Boucheix, C., 2000. Severely Reduced Female Fertility in CD9-Deficient Mice. Science 287, 319–321. https://doi.org/10.1126/science.287.5451.319

Lechler, T., 2012. Adherens Junctions and Stem Cells, in: Harris, T. (Ed.), Adherens Junctions: From Molecular Mechanisms to Tissue Development and Disease, Subcellular Biochemistry. Springer Netherlands, Dordrecht, pp. 359–377. https://doi.org/10.1007/978-94-007-4186-7_15

Leckband, D.E., le Duc, Q., Wang, N., de Rooij, J., 2011. Mechanotransduction at cadherin-mediated adhesions. Current Opinion in Cell Biology, Cell-to-cell contact and extracellular matrix 23, 523–530. https://doi.org/10.1016/j.ceb.2011.08.003

Lee, D.M., Chen, E.H., 2019. Drosophila Myoblast Fusion: Invasion and Resistance for the Ultimate Union. Annu Rev Genet 53, 67–91. https://doi.org/10.1146/annurev-genet-120116-024603

Li, Z.P., Paterlini, A., Glavier, M., Bayer, E.M., 2021. Intercellular trafficking via plasmodesmata: molecular layers of complexity. Cell Mol Life Sci 78, 799–816. https://doi.org/10.1007/s00018-020-03622-8

Lien, W.-H., Klezovitch, O., Vasioukhin, V., 2006. Cadherin–catenin proteins in vertebrate development. Current Opinion in Cell Biology, Cell-to-cell contact and extracellular matrix 18, 499–506. https://doi.org/10.1016/j.ceb.2006.07.001

Linder, S., 2009. Invadosomes at a glance. Journal of Cell Science 122, 3009–3013. https://doi.org/10.1242/jcs.032631

Liu, K., Ji, K., Guo, L., Wu, W., Lu, H., Shan, P., Yan, C., 2014. Mesenchymal stem cells rescue injured endothelial cells in an in vitro ischemia-reperfusion model via tunneling nanotube like structure-mediated mitochondrial transfer. Microvasc Res 92, 10–18. https://doi.org/10.1016/j.mvr.2014.01.008

Ljubojevic, N., Henderson, J.M., Zurzolo, C., 2021. The Ways of Actin: Why Tunneling Nanotubes Are Unique Cell Protrusions. Trends Cell Biol 31, 130–142. https://doi.org/10.1016/j.tcb.2020.11.008

Lokar, M., Iglič, A., Veranič, P., 2010. Protruding membrane nanotubes: attachment of tubular protrusions to adjacent cells by several anchoring junctions. Protoplasma 246, 81–87. https://doi.org/10.1007/s00709-010-0143-7

Lou, E., Fujisawa, S., Morozov, A., Barlas, A., Romin, Y., Dogan, Y., Gholami, S., Moreira, A.L., Manova-Todorova, K., Moore, M.A.S., 2012. Tunneling nanotubes provide a unique conduit for intercellular transfer of cellular contents in human malignant pleural mesothelioma. PLoS One 7, e33093. https://doi.org/10.1371/journal.pone.0033093

Lu, J., Zheng, X., Li, F., Yu, Y., Chen, Z., Liu, Z., Wang, Z., Xu, H., Yang, W., 2017. Tunneling nanotubes promote intercellular mitochondria transfer followed by increased invasiveness in bladder cancer cells. Oncotarget 8, 15539–15552. https://doi.org/10.18632/oncotarget.14695

Lu, J.J., Yang, W.M., Li, F., Zhu, W., Chen, Z., 2019. Tunneling Nanotubes Mediated microRNA-155 Intercellular Transportation Promotes Bladder Cancer Cells' Invasive and Proliferative Capacity. Int J Nanomedicine 14, 9731–9743. https://doi.org/10.2147/IJN.S217277

Lucas, W.J., Ding, B., Van Der Schoot, C., 1993. Plasmodesmata and the supracellular nature of plants. New Phytologist 125, 435–476. https://doi.org/10.1111/j.1469-8137.1993.tb03897.x

Maecker, H.T., Todd, S.C., Levy, S., 1997. The tetraspanin superfamily: molecular facilitators. The FASEB Journal 11, 428–442. https://doi.org/10.1096/fasebj.11.6.9194523

Maeda, S., Tsukihara, T., 2011. Structure of the gap junction channel and its implications for its biological functions. Cell Mol Life Sci 68, 1115–1129. https://doi.org/10.1007/s00018-010-0551-z

Masciopinto, F., Campagnoli, S., Abrignani, S., Uematsu, Y., Pileri, P., 2001. The small extracellular loop of CD81 is necessary for optimal surface expression of the large loop, a putative HCV receptor. Virus Research 80, 1–10. https://doi.org/10.1016/S0168-1702(01)00245-3

Mathieu, M., Martin-Jaular, L., Lavieu, G., Théry, C., 2019. Specificities of secretion and uptake of exosomes and other extracellular vesicles for cell-to-cell communication. Nat Cell Biol 21, 9–17. https://doi.org/10.1038/s41556-018-0250-9

Mathieu, M., Névo, N., Jouve, M., Valenzuela, J.I., Maurin, M., Verweij, F.J., Palmulli, R., Lankar, D., Dingli, F., Loew, D., Rubinstein, E., Boncompain, G., Perez, F., Théry, C., 2021. Specificities of exosome versus small ectosome secretion revealed by live intracellular tracking of CD63 and CD9. Nat Commun 12, 4389. https://doi.org/10.1038/s41467-021-24384-2

Mbalaviele, G., Chen, H., Boyce, B.F., Mundy, G.R., Yoneda, T., 1995. The role of cadherin in the generation of multinucleated osteoclasts from mononuclear precursors in murine marrow. J Clin Invest 95, 2757–2765. https://doi.org/10.1172/JCI117979

McCrea, P.D., Gu, D., 2010. The catenin family at a glance. Journal of Cell Science 123, 637–642. https://doi.org/10.1242/jcs.039842

McKinney, M.C., Kulesa, P.M., 2011. In Vivo Calcium Dynamics During Neural Crest Cell Migration and Patterning Using GCaMP3. Dev Biol 358, 309–317. https://doi.org/10.1016/j.ydbio.2011.08.004

Mège, R.-M., Gavard, J., Lambert, M., 2006. Regulation of cell–cell junctions by the cytoskeleton. Current Opinion in Cell Biology, Cell-to-cell contact and extracellular matrix 18, 541–548. https://doi.org/10.1016/j.ceb.2006.08.004

Mege, R.M., Goudou, D., Diaz, C., Nicolet, M., Garcia, L., Geraud, G., Rieger, F., 1992. N-cadherin and N-CAM in myoblast fusion: compared localisation and effect of blockade by peptides and antibodies. J Cell Sci 103 (Pt 4), 897–906. https://doi.org/10.1242/jcs.103.4.897

Mège, R.M., Ishiyama, N., 2017. Integration of Cadherin Adhesion and Cytoskeleton at Adherens Junctions. Cold Spring Harb Perspect Biol 9, a028738. https://doi.org/10.1101/cshperspect.a028738

Meşe, G., Richard, G., White, T.W., 2007. Gap Junctions: Basic Structure and Function. Journal of Investigative Dermatology 127, 2516–2524. https://doi.org/10.1038/sj.jid.5700770

Metzelaar, M.J., Wijngaard, P.L., Peters, P.J., Sixma, J.J., Nieuwenhuis, H.K., Clevers, H.C., 1991. CD63 antigen. A novel lysosomal membrane glycoprotein, cloned by a screening procedure for intracellular antigens in eukaryotic cells. J Biol Chem 266, 3239–3245.

Miller, J., Fraser, S.E., McClay, D., 1995. Dynamics of thin filopodia during sea urchin gastrulation. Development 121, 2501–2511. https://doi.org/10.1242/dev.121.8.2501

Miyado, K., Yamada, G., Yamada, S., Hasuwa, H., Nakamura, Y., Ryu, F., Suzuki, K., Kosai, K., Inoue, K., Ogura, A., Okabe, M., Mekada, E., 2000. Requirement of CD9 on the Egg Plasma Membrane for Fertilization. Science 287, 321–324. https://doi.org/10.1126/science.287.5451.321

Monk, P.N., Partridge, L.J., 2012. Tetraspanins: gateways for infection. Infect Disord Drug Targets 12, 4–17. https://doi.org/10.2174/187152612798994957

Moschoi, R., Imbert, V., Nebout, M., Chiche, J., Mary, D., Prebet, T., Saland, E., Castellano, R., Pouyet, L., Collette, Y., Vey, N., Chabannon, C., Recher, C., Sarry, J.-E., Alcor, D., Peyron, J.-F., Griessinger, E., 2016. Protective mitochondrial transfer from bone marrow stromal cells to acute myeloid leukemic cells during chemotherapy. Blood 128, 253–264. https://doi.org/10.1182/blood-2015-07-655860

Mrkonjic, S., Destaing, O., Albiges-Rizo, C., 2017. Mechanotransduction pulls the strings of matrix degradation at invadosome. Matrix Biol 57–58, 190–203. https://doi.org/10.1016/j.matbio.2016.06.007

Mukherjee, A., Melamed, S., Damouny-Khoury, H., Amer, M., Feld, L., Nadjar-Boger, E., Sheetz, M.P., Wolfenson, H., 2022. α-Catenin links integrin adhesions to F-actin to regulate ECM mechanosensing and rigidity dependence. J Cell Biol 221, e202102121. https://doi.org/10.1083/jcb.202102121

Mulens-Arias, V., 2021. Dissecting the Inorganic Nanoparticle-Driven Interferences on Adhesome Dynamics. Journal of Nanotheranostics 2, 174–195. https://doi.org/10.3390/jnt2030011

Naphade, S., Sharma, J., Gaide Chevronnay, H.P., Shook, M.A., Yeagy, B.A., Rocca, C.J., Ur, S.N., Lau, A.J., Courtoy, P.J., Cherqui, S., 2015. Brief reports: Lysosomal cross-

correction by hematopoietic stem cell-derived macrophages via tunneling nanotubes. Stem Cells 33, 301–309. https://doi.org/10.1002/stem.1835

Nelson, W.J., Nusse, R., 2004. Convergence of Wnt, beta-catenin, and cadherin pathways. Science 303, 1483–1487. https://doi.org/10.1126/science.1094291

Nobes, C.D., Hall, A., 1995. Rho, rac, and cdc42 GTPases regulate the assembly of multimolecular focal complexes associated with actin stress fibers, lamellipodia, and filopodia. Cell 81, 53–62. https://doi.org/10.1016/0092-8674(95)90370-4

Nydegger, S., Khurana, S., Krementsov, D.N., Foti, M., Thali, M., 2006. Mapping of tetraspanin-enriched microdomains that can function as gateways for HIV-1. J Cell Biol 173, 795–807. https://doi.org/10.1083/jcb.200508165

Obata, S., Sago, H., Mori, N., Rochelle, J.M., Seldin, M.F., Davidson, M., St John, T., Taketani, S., Suzuki, S.T., 1995. Protocadherin Pcdh2 shows properties similar to, but distinct from, those of classical cadherins. Journal of Cell Science 108, 3765–3773. https://doi.org/10.1242/jcs.108.12.3765

Ohno, H., Hase, K., Kimura, S., 2010. M-Sec: Emerging secrets of tunneling nanotube formation. Communicative and Integrative Biology 3, 231–233. https://doi.org/10.4161/cib.3.3.11242

Okafo, G., Prevedel, L., Eugenin, E., 2017. Tunneling nanotubes (TNT) mediate long-range gap junctional communication: Implications for HIV cell to cell spread. Sci Rep 7, 16660. https://doi.org/10.1038/s41598-017-16600-1

Önfelt, B., Nedvetzki, S., Benninger, R.K.P., Purbhoo, M.A., Sowinski, S., Hume, A.N., Seabra, M.C., Neil, M.A.A., French, P.M.W., Davis, D.M., 2006. Structurally Distinct Membrane Nanotubes between Human Macrophages Support Long-Distance Vesicular Traffic or Surfing of Bacteria. The Journal of Immunology 177, 8476–8483. https://doi.org/10.4049/jimmunol.177.12.8476

Ooi, Y.S., Stiles, K.M., Liu, C.Y., Taylor, G.M., Kielian, M., 2013. Genome-Wide RNAi Screen Identifies Novel Host Proteins Required for Alphavirus Entry. PLOS Pathogens 9, e1003835. https://doi.org/10.1371/journal.ppat.1003835

Oren, R., Takahashi, S., Doss, C., Levy, R., Levy, S., 1990. TAPA-1, the target of an antiproliferative antibody, defines a new family of transmembrane proteins. Mol Cell Biol 10, 4007–4015. https://doi.org/10.1128/mcb.10.8.4007-4015.1990

Ortin-Martinez, A., Yan, N.E., Tsai, E.L.S., Comanita, L., Gurdita, A., Tachibana, N., Liu, Z.C., Lu, S., Dolati, P., Pokrajac, N.T., El-Sehemy, A., Nickerson, P.E.B., Schuurmans, C., Bremner, R., Wallace, V.A., 2021. Photoreceptor nanotubes mediate the in vivo exchange of intracellular material. EMBO J 40, e107264. https://doi.org/10.15252/embj.2020107264

Osswald, M., Jung, E., Sahm, F., Solecki, G., Venkataramani, V., Blaes, J., Weil, S., Horstmann, H., Wiestler, B., Syed, M., Huang, L., Ratliff, M., Karimian-Jazi, K., Kurz, F., Schmenger, T., Lemke, D., Gömmel, M., Pauli, M., Liao, Y., Winkler, F., 2015. Brain tumor cells interconnect to a functional and resistant network. Nature Published online 04 November. https://doi.org/10.1038/nature16071

Overduin, M., Harvey, T.S., Bagby, S., Tong, K.I., Yau, P., Takeichi, M., Ikura, M., 1995. Solution structure of the epithelial cadherin domain responsible for selective cell adhesion. Science 267, 386–389. https://doi.org/10.1126/science.7824937

Ozawa, M., Baribault, H., Kemler, R., 1989. The cytoplasmic domain of the cell adhesion molecule uvomorulin associates with three independent proteins structurally related in different species. EMBO J 8, 1711–1717.

Pasquier, J., Guerrouahen, B.S., Al Thawadi, H., Ghiabi, P., Maleki, M., Abu-Kaoud, N., Jacob, A., Mirshahi, M., Galas, L., Rafii, S., Le Foll, F., Rafii, A., 2013. Preferential transfer of mitochondria from endothelial to cancer cells through tunneling nanotubes modulates chemoresistance. Journal of Translational Medicine 11, 94. https://doi.org/10.1186/1479-5876-11-94

Peinado, H., Portillo, F., Cano, A., 2004. Transcriptional regulation of cadherins during development and carcinogenesis. Int J Dev Biol 48, 365–375. https://doi.org/10.1387/ijdb.041794hp

Pepe, A., Pietropaoli, S., Vos, M., Barba-Spaeth, G., Zurzolo, C., 2022. Tunneling nanotubes provide a route for SARS-CoV-2 spreading. Sci Adv 8, eabo0171. https://doi.org/10.1126/sciadv.abo0171

Peters, W.S., Jensen, K.H., Stone, H.A., Knoblauch, M., 2021. Plasmodesmata and the problems with size: Interpreting the confusion. Journal of Plant Physiology 257, 153341. https://doi.org/10.1016/j.jplph.2020.153341

Pinto, G., Brou, C., Zurzolo, C., 2020. Tunneling Nanotubes: The Fuel of Tumor Progression? Trends Cancer 6, 874–888. https://doi.org/10.1016/j.trecan.2020.04.012

Pinto, G., Saenz-de-Santa-Maria, I., Chastagner, P., Perthame, E., Delmas, C., Toulas, C., Moyal-Jonathan-Cohen, E., Brou, C., Zurzolo, C., 2021. Patient-derived glioblastoma stem cells transfer mitochondria through tunneling nanotubes in tumor organoids. Biochem J 478, 21–39. https://doi.org/10.1042/BCJ20200710

Pisani, F., Castagnola, V., Simone, L., Loiacono, F., Svelto, M., Benfenati, F., 2022. Role of pericytes in blood–brain barrier preservation during ischemia through tunneling nanotubes. Cell Death Dis 13, 1–14. https://doi.org/10.1038/s41419-022-05025-y

Pokutta, S., Drees, F., Takai, Y., Nelson, W.J., Weis, W.I., 2002. Biochemical and structural definition of the l-afadin- and actin-binding sites of alpha-catenin. J Biol Chem 277, 18868–18874. https://doi.org/10.1074/jbc.M201463200

Qian, X., Karpova, T., Sheppard, A.M., McNally, J., Lowy, D.R., 2004. E-cadherin-mediated adhesion inhibits ligand-dependent activation of diverse receptor tyrosine kinases. EMBO J 23, 1739–1748. https://doi.org/10.1038/sj.emboj.7600136

Ramakrishnan, A.-B., Cadigan, K.M., 2017. Wnt target genes and where to find them. F1000Res 6, 746. https://doi.org/10.12688/f1000research.11034.1

Ramírez-Weber, F.A., Kornberg, T.B., 1999. Cytonemes: cellular processes that project to the principal signaling center in Drosophila imaginal discs. Cell 97, 599–607. https://doi.org/10.1016/s0092-8674(00)80771-0

Reiss, K., Maretzky, T., Ludwig, A., Tousseyn, T., de Strooper, B., Hartmann, D., Saftig, P., 2005. ADAM10 cleavage of N-cadherin and regulation of cell-cell adhesion and beta-

catenin nuclear signalling. EMBO J 24, 742–752. https://doi.org/10.1038/sj.emboj.7600548

Resnik, N., Erman, A., Veranič, P., Kreft, M.E., 2019. Triple labelling of actin filaments, intermediate filaments and microtubules for broad application in cell biology: uncovering the cytoskeletal composition in tunneling nanotubes. Histochem Cell Biol 152, 311–317. https://doi.org/10.1007/s00418-019-01806-3

Reynolds, A.B., Daniel, J., McCrea, P.D., Wheelock, M.J., Wu, J., Zhang, Z., 1994. Identification of a new catenin: the tyrosine kinase substrate p120cas associates with E-cadherin complexes. Mol Cell Biol 14, 8333–8342. https://doi.org/10.1128/mcb.14.12.8333-8342.1994

Reynolds, A.B., Daniel, J.M., Mo, Y.Y., Wu, J., Zhang, Z., 1996. The novel catenin p120cas binds classical cadherins and induces an unusual morphological phenotype in NIH3T3 fibroblasts. Exp Cell Res 225, 328–337. https://doi.org/10.1006/excr.1996.0183

Rimm, D.L., Koslov, E.R., Kebriaei, P., Cianci, C.D., Morrow, J.S., 1995. Alpha 1(E)-catenin is an actin-binding and -bundling protein mediating the attachment of F-actin to the membrane adhesion complex. Proc Natl Acad Sci U S A 92, 8813–8817.

Roberts, A.G., Oparka, K.J., 2003. Plasmodesmata and the control of symplastic transport. Plant, Cell & Environment 26, 103–124. https://doi.org/10.1046/j.1365-3040.2003.00950.x

Rocha-Perugini, V., Martínez Del Hoyo, G., González-Granado, J.M., Ramírez-Huesca, M., Zorita, V., Rubinstein, E., Boucheix, C., Sánchez-Madrid, F., 2017. CD9 Regulates Major Histocompatibility Complex Class II Trafficking in Monocyte-Derived Dendritic Cells. Mol Cell Biol 37, e00202-17. https://doi.org/10.1128/MCB.00202-17

Rous, B.A., Reaves, B.J., Ihrke, G., Briggs, J.A.G., Gray, S.R., Stephens, D.J., Banting, G., Luzio, J.P., 2002. Role of Adaptor Complex AP-3 in Targeting Wild-Type and Mutated CD63 to Lysosomes. MBoC 13, 1071–1082. https://doi.org/10.1091/mbc.01-08-0409

Routledge, D., Scholpp, S., 2019. Mechanisms of intercellular Wnt transport. Development 146, dev176073. https://doi.org/10.1242/dev.176073

Rubinstein, E., Ziyyat, A., Prenant, M., Wrobel, E., Wolf, J.-P., Levy, S., Le Naour, F., Boucheix, C., 2006a. Reduced fertility of female mice lacking CD81. Dev Biol 290, 351–358. https://doi.org/10.1016/j.ydbio.2005.11.031

Rubinstein, E., Ziyyat, A., Wolf, J.-P., Le Naour, F., Boucheix, C., 2006b. The molecular players of sperm–egg fusion in mammals. Seminars in Cell & Developmental Biology, The Wnt Signaling Pathway and Embryonic Polarity 17, 254–263. https://doi.org/10.1016/j.semcdb.2006.02.012

Rustom, A., Saffrich, R., Markovic, I., Walther, P., Gerdes, H.-H., 2004. Nanotubular Highways for Intercellular Organelle Transport. Science 303, 1007–1010. https://doi.org/10.1126/science.1093133

Sáenz-de-Santa-María, I., Bernardo-Castiñeira, C., Enciso, E., García-Moreno, I., Chiara, J.L., Suarez, C., Chiara, M.-D., 2017. Control of long-distance cell-to-cell communication and autophagosome transfer in squamous cell carcinoma via tunneling nanotubes. Oncotarget 8, 20939–20960. https://doi.org/10.18632/oncotarget.15467

Saiz, M.L., Rocha-Perugini, V., Sánchez-Madrid, F., 2018. Tetraspanins as Organizers of Antigen-Presenting Cell Function. Front Immunol 9, 1074. https://doi.org/10.3389/fimmu.2018.01074

Sala-Valdés, M., Ursa, A., Charrin, S., Rubinstein, E., Hemler, M.E., Sánchez-Madrid, F., Yáñez-Mó, M., 2006. EWI-2 and EWI-F link the tetraspanin web to the actin cytoskeleton through their direct association with ezrin-radixin-moesin proteins. J Biol Chem 281, 19665–19675. https://doi.org/10.1074/jbc.M602116200

Sanabria, H., Swulius, M.T., Kolodziej, S.J., Liu, J., Waxham, M.N., 2009. βCaMKII Regulates Actin Assembly and Structure *. Journal of Biological Chemistry 284, 9770–9780. https://doi.org/10.1074/jbc.M809518200

Sartori-Rupp, A., Cordero Cervantes, D., Pepe, A., Gousset, K., Delage, E., Corroyer-Dulmont, S., Schmitt, C., Krijnse-Locker, J., Zurzolo, C., 2019. Correlative cryo-electron microscopy reveals the structure of TNTs in neuronal cells. Nat Commun 10, 342. https://doi.org/10.1038/s41467-018-08178-7

Satir, P., Christensen, S.T., 2007. Overview of Structure and Function of Mammalian Cilia. Annual Review of Physiology 69, 377–400. https://doi.org/10.1146/annurev.physiol.69.040705.141236

Scheffer, K.D., Gawlitza, A., Spoden, G.A., Zhang, X.A., Lambert, C., Berditchevski, F., Florin, L., 2013. Tetraspanin CD151 mediates papillomavirus type 16 endocytosis. J Virol 87, 3435–3446. https://doi.org/10.1128/JVI.02906-12

Schiller, C., Diakopoulos, K.N., Rohwedder, I., Kremmer, E., von Toerne, C., Ueffing, M., Weidle, U.H., Ohno, H., Weiss, E.H., 2013. LST1 promotes the assembly of a molecular machinery responsible for tunneling nanotube formation. J Cell Sci 126, 767–777. https://doi.org/10.1242/jcs.114033

Scott, J.A., Yap, A.S., 2006. Cinderella no longer: alpha-catenin steps out of cadherin's shadow. J Cell Sci 119, 4599–4605. https://doi.org/10.1242/jcs.03267

Seigneuret, M., Delaguillaumie, A., Lagaudrière-Gesbert, C., Conjeaud, H., 2001. Structure of the tetraspanin main extracellular domain. A partially conserved fold with a structurally variable domain insertion. J Biol Chem 276, 40055–40064. https://doi.org/10.1074/jbc.M105557200

SERRU, V., François, L.N., BILLARD, M., AZORSA, D.O., LANZA, F., BOUCHEIX, C., RUBINSTEIN, E., 1999. Selective tetraspan–integrin complexes (CD81/α4β1, CD151/α3β1, CD151/α6β1) under conditions disrupting tetraspan interactions. Biochemical Journal 340, 103–111. https://doi.org/10.1042/bj3400103

Shapiro, L., Weis, W.I., 2009. Structure and Biochemistry of Cadherins and Catenins. Cold Spring Harb Perspect Biol 1, a003053. https://doi.org/10.1101/cshperspect.a003053

Sharma, M., Subramaniam, S., 2019. Rhes travels from cell to cell and transports Huntington disease protein via TNT-like protrusion. J Cell Biol 218, 1972–1993. https://doi.org/10.1083/jcb.201807068

Silvie, O., Rubinstein, E., Franetich, J.-F., Prenant, M., Belnoue, E., Rénia, L., Hannoun, L., Eling, W., Levy, S., Boucheix, C., Mazier, D., 2003. Hepatocyte CD81 is required for

Plasmodium falciparum and Plasmodium yoelii sporozoite infectivity. Nat Med 9, 93–96. https://doi.org/10.1038/nm808

Singethan, K., Müller, N., Schubert, S., Lüttge, D., Krementsov, D.N., Khurana, S.R., Krohne, G., Schneider-Schaulies, S., Thali, M., Schneider-Schaulies, J., 2008. CD9 Clustering and Formation of Microvilli Zippers Between Contacting Cells Regulates Virus-Induced Cell Fusion. Traffic 9, 924–935. https://doi.org/10.1111/j.1600-0854.2008.00737.x

Smith, I.F., Shuai, J., Parker, I., 2011. Active Generation and Propagation of Ca2+ Signals within Tunneling Membrane Nanotubes. Biophys J 100, L37–L39. https://doi.org/10.1016/j.bpj.2011.03.007

Sowinski, S., Jolly, C., Berninghausen, O., Purbhoo, M.A., Chauveau, A., Köhler, K., Oddos, S., Eissmann, P., Brodsky, F.M., Hopkins, C., Önfelt, B., Sattentau, Q., Davis, D.M., 2008. Membrane nanotubes physically connect T cells over long distances presenting a novel route for HIV-1 transmission. Nat Cell Biol 10, 211–219. https://doi.org/10.1038/ncb1682

Stephan, J., Eitelmann, S., Zhou, M., 2021. Approaches to Study Gap Junctional Coupling. Frontiers in Cellular Neuroscience 15.

Stipp, C.S., Kolesnikova, T.V., Hemler, M.E., 2003a. Functional domains in tetraspanin proteins. Trends in Biochemical Sciences 28, 106–112. https://doi.org/10.1016/S0968-0004(02)00014-2

Stipp, C.S., Kolesnikova, T.V., Hemler, M.E., 2003b. EWI-2 regulates α3β1 integrin–dependent cell functions on laminin-5. J Cell Biol 163, 1167–1177. https://doi.org/10.1083/jcb.200309113

Stipp, C.S., Kolesnikova, T.V., Hemler, M.E., 2001. EWI-2 is a major CD9 and CD81 partner and member of a novel Ig protein subfamily. J Biol Chem 276, 40545–40554. https://doi.org/10.1074/jbc.M107338200

Su, L.K., Vogelstein, B., Kinzler, K.W., 1993. Association of the APC tumor suppressor protein with catenins. Science 262, 1734–1737. https://doi.org/10.1126/science.8259519

Susa, K.J., Seegar, T.C., Blacklow, S.C., Kruse, A.C., 2020. A dynamic interaction between CD19 and the tetraspanin CD81 controls B cell co-receptor trafficking. eLife 9, e52337. https://doi.org/10.7554/eLife.52337

Suyama, K., Shapiro, I., Guttman, M., Hazan, R.B., 2002. A signaling pathway leading to metastasis is controlled by N-cadherin and the FGF receptor. Cancer Cell 2, 301–314. https://doi.org/10.1016/s1535-6108(02)00150-2

Suzuki, S., Sano, K., Tanihara, H., 1991. Diversity of the cadherin family: evidence for eight new cadherins in nervous tissue. Cell Regul 2, 261–270.

Takeda, Y., Kazarov, A.R., Butterfield, C.E., Hopkins, B.D., Benjamin, L.E., Kaipainen, A., Hemler, M.E., 2006. Deletion of tetraspanin Cd151 results in decreased pathologic angiogenesis in vivo and in vitro. Blood 109, 1524–1532. https://doi.org/10.1182/blood-2006-08-041970

Takeda, Y., Tachibana, I., Miyado, K., Kobayashi, M., Miyazaki, T., Funakoshi, T., Kimura, H., Yamane, H., Saito, Y., Goto, H., Yoneda, T., Yoshida, M., Kumagai, T., Osaki, T., Hayashi, S., Kawase, I., Mekada, E., 2003. Tetraspanins CD9 and CD81 function to prevent the fusion of mononuclear phagocytes. J Cell Biol 161, 945–956. https://doi.org/10.1083/jcb.200212031

Takeichi, M., 2018. Historical review of the discovery of cadherin, in memory of Tokindo Okada. Development, Growth & Differentiation 60, 3–13. https://doi.org/10.1111/dgd.12416

Takeichi, M., 1990. Cadherins: A Molecular Family Important in Selective Cell-Cell Adhesion. Annual Review of Biochemistry 59, 237–252. https://doi.org/10.1146/annurev.bi.59.070190.001321

Takeichi, M., 1977. Functional correlation between cell adhesive properties and some cell surface proteins. J Cell Biol 75, 464–474. https://doi.org/10.1083/jcb.75.2.464

Tang, V.W., Brieher, W.M., 2012. α-Actinin-4/FSGS1 is required for Arp2/3-dependent actin assembly at the adherens junction. J Cell Biol 196, 115–130. https://doi.org/10.1083/jcb.201103116

Tardivel, M., Bégard, S., Bousset, L., Dujardin, S., Coens, A., Melki, R., Buée, L., Colin, M., 2016. Tunneling nanotube (TNT)-mediated neuron-to neuron transfer of pathological Tau protein assemblies. Acta Neuropathol Commun 4, 117. https://doi.org/10.1186/s40478-016-0386-4

Teddy, J.M., Kulesa, P.M., 2004. In vivo evidence for short- and long-range cell communication in cranial neural crest cells. Development 131, 6141–6151. https://doi.org/10.1242/dev.01534

Thayanithy, V., Dickson, E.L., Steer, C., Subramanian, S., Lou, E., 2014. Tumor-stromal cross talk: direct cell-to-cell transfer of oncogenic microRNAs via tunneling nanotubes. Transl Res 164, 359–365. https://doi.org/10.1016/j.trsl.2014.05.011

The Cadherin Superfamily, n.d.

Théry, C., Witwer, K.W., Aikawa, E., Alcaraz, M.J., Anderson, J.D., Andriantsitohaina, R., Antoniou, A., Arab, T., Archer, F., Atkin-Smith, G.K., Ayre, D.C., Bach, J.-M., Bachurski, D., Baharvand, H., Balaj, L., Baldacchino, S., Bauer, N.N., Baxter, A.A., Bebawy, M., Beckham, C., Bedina Zavec, A., Benmoussa, A., Berardi, A.C., Bergese, P., Bielska, E., Blenkiron, C., Bobis-Wozowicz, S., Boilard, E., Boireau, W., Bongiovanni, A., Borràs, F.E., Bosch, S., Boulanger, C.M., Breakefield, X., Breglio, A.M., Brennan, M.Á., Brigstock, D.R., Brisson, A., Broekman, M.L., Bromberg, J.F., Bryl-Górecka, P., Buch, S., Buck, A.H., Burger, D., Busatto, S., Buschmann, D., Bussolati, B., Buzás, E.I., Byrd, J.B., Camussi, G., Carter, D.R., Caruso, S., Chamley, L.W., Chang, Y.-T., Chen, C., Chen, S., Cheng, L., Chin, A.R., Clayton, A., Clerici, S.P., Cocks, A., Cocucci, E., Coffey, R.J., Cordeiro-da-Silva, A., Couch, Y., Coumans, F.A., Coyle, B., Crescitelli, R., Criado, M.F., D'Souza-Schorey, C., Das, S., Datta Chaudhuri, A., de Candia, P., De Santana, E.F., De Wever, O., del Portillo, H.A., Demaret, T., Deville, S., Devitt, A., Dhondt, B., Di Vizio, D., Dieterich, L.C., Dolo, V., Dominguez Rubio, A.P., Dominici, M., Dourado, M.R., Driedonks, T.A., Duarte, F.V., Duncan, H.M., Eichenberger, R.M., Ekström, K., EL Andaloussi, S., Elie-Caille, C., Erdbrügger, U., Falcón-Pérez, J.M., Fatima, F., Fish, J.E., Flores-Bellver, M., Försönits, A., Frelet-Barrand, A., Fricke, F., Fuhrmann, G., Gabrielsson, S., Gámez-Valero, A., Gardiner, C., Gärtner, K., Gaudin, R., Gho, Y.S., Giebel, B., Gilbert, C., Gimona, M., Giusti, I., Goberdhan, D.C., Görgens, A., Gorski, S.M., Greening, D.W., Gross, J.C., Gualerzi, A., Gupta, G.N., Gustafson, D.,

Handberg, A., Haraszti, R.A., Harrison, P., Hegyesi, H., Hendrix, A., Hill, A.F., Hochberg, F.H., Hoffmann, K.F., Holder, B., Holthofer, H., Hosseinkhani, B., Hu, G., Huang, Y., Huber, V., Hunt, S., Ibrahim, A.G.-E., Ikezu, T., Inal, J.M., Isin, M., Ivanova, A., Jackson, H.K., Jacobsen, S., Jay, S.M., Jayachandran, M., Jenster, G., Jiang, L., Johnson, S.M., Jones, J.C., Jong, A., Jovanovic-Talisman, T., Jung, S., Kalluri, R., Kano, S., Kaur, S., Kawamura, Y., Keller, E.T., Khamari, D., Khomyakova, E., Khvorova, A., Kierulf, P., Kim, K.P., Kislinger, T., Klingeborn, M., Klinke, D.J., Kornek, M., Kosanović, M.M., Kovács, Á.F., Krämer-Albers, E.-M., Krasemann, S., Krause, M., Kurochkin, I.V., Kusuma, G.D., Kuypers, S., Laitinen, S., Langevin, S.M., Languino, L.R., Lannigan, J., Lässer, C., Laurent, L.C., Lavieu, G., Lázaro-Ibáñez, E., Le Lay, S., Lee, M.-S., Lee, Y.X.F., Lemos, D.S., Lenassi, M., Leszczynska, A., Li, I.T., Liao, K., Libregts, S.F., Ligeti, E., Lim, R., Lim, S.K., Linē, A., Linnemannstöns, K., Llorente, A., Lombard, C.A., Lorenowicz, M.J., Lörincz, Á.M., Lötvall, J., Lovett, J., Lowry, M.C., Loyer, X., Lu, Q., Lukomska, B., Lunavat, T.R., Maas, S.L., Malhi, H., Marcilla, A., Mariani, J., Mariscal, J., Martens-Uzunova, E.S., Martin-Jaular, L., Martinez, M.C., Martins, V.R., Mathieu, M., Mathivanan, S., Maugeri, M., McGinnis, L.K., McVey, M.J., Meckes, D.G., Meehan, K.L., Mertens, I., Minciacchi, V.R., Möller, A., Møller Jørgensen, M., Morales-Kastresana, A., Morhayim, J., Mullier, F., Muraca, M., Musante, L., Mussack, V., Muth, D.C., Myburgh, K.H., Najrana, T., Nawaz, M., Nazarenko, I., Nejsum, P., Neri, C., Neri, T., Nieuwland, R., Nimrichter, L., Nolan, J.P., Nolte-'t Hoen, E.N., Noren Hooten, N., O'Driscoll, L., O'Grady, T., O'Loghlen, A., Ochiya, T., Olivier, M., Ortiz, A., Ortiz, L.A., Osteikoetxea, X., Østergaard, O., Ostrowski, M., Park, J., Pegtel, D.M., Peinado, H., Perut, F., Pfaffl, M.W., Phinney, D.G., Pieters, B.C., Pink, R.C., Pisetsky, D.S., Pogge von Strandmann, E., Polakovicova, I., Poon, I.K., Powell, B.H., Prada, I., Pulliam, L., Quesenberry, P., Radeghieri, A., Raffai, R.L., Raimondo, S., Rak, J., Ramirez, M.I., Raposo, G., Rayyan, M.S., Regev-Rudzki, N., Ricklefs, F.L., Robbins, P.D., Roberts, D.D., Rodrigues, S.C., Rohde, E., Rome, S., Rouschop, K.M., Rughetti, A., Russell, A.E., Saá, P., Sahoo, S., Salas-Huenuleo, E., Sánchez, C., Saugstad, J.A., Saul, M.J., Schiffelers, R.M., Schneider, R., Schøyen, T.H., Scott, A., Shahaj, E., Sharma, S., Shatnyeva, O., Shekari, F., Shelke, G.V., Shetty, A.K., Shiba, K., Siljander, P.R.-M., Silva, A.M., Skowronek, A., Snyder, O.L., Soares, R.P., Sódar, B.W., Soekmadji, C., Sotillo, J., Stahl, P.D., Stoorvogel, W., Stott, S.L., Strasser, E.F., Swift, S., Tahara, H., Tewari, M., Timms, K., Tiwari, S., Tixeira, R., Tkach, M., Toh, W.S., Tomasini, R., Torrecilhas, A.C., Tosar, J.P., Toxavidis, V., Urbanelli, L., Vader, P., van

Balkom, B.W., van der Grein, S.G., Van Deun, J., van Herwijnen, M.J., Van Keuren-Jensen, K., van Niel, G., van Royen, M.E., van Wijnen, A.J., Vasconcelos, M.H., Vechetti, I.J., Veit, T.D., Vella, L.J., Velot, É., Verweij, F.J., Vestad, B., Viñas, J.L., Visnovitz, T., Vukman, K.V., Wahlgren, J., Watson, D.C., Wauben, M.H., Weaver, A., Webber, J.P., Weber, V., Wehman, A.M., Weiss, D.J., Welsh, J.A., Wendt, S., Wheelock, A.M., Wiener, Z., Witte, L., Wolfram, J., Xagorari, A., Xander, P., Xu, J., Yan, X., Yáñez-Mó, M., Yin, H., Yuana, Y., Zappulli, V., Zarubova, J., Žėkas, V., Zhang, J., Zhao, Z., Zheng, L., Zheutlin, A.R., Zickler, A.M., Zimmermann, P., Zivkovic, A.M., Zocco, D., Zuba-Surma, E.K., 2018. Minimal information for studies of extracellular vesicles 2018 (MISEV2018): a position statement of the International Society for Extracellular Vesicles and update of the MISEV2014 guidelines. J Extracell Vesicles 7, 1535750. https://doi.org/10.1080/20013078.2018.1535750

Thiery, J.P., Brackenbury, R., Rutishauser, U., Edelman, G.M., 1977. Adhesion among neural cells of the chick embryo. II. Purification and characterization of a cell adhesion molecule from neural retina. J Biol Chem 252, 6841–6845.

Thoreson, M.A., Anastasiadis, P.Z., Daniel, J.M., Ireton, R.C., Wheelock, M.J., Johnson, K.R., Hummingbird, D.K., Reynolds, A.B., 2000. Selective Uncoupling of P120ctn from E-Cadherin Disrupts Strong Adhesion. J Cell Biol 148, 189–202.

Tilney, L.G., Cooke, T.J., Connelly, P.S., Tilney, M.S., 1991. The structure of plasmodesmata as revealed by plasmolysis, detergent extraction, and protease digestion. J Cell Biol 112, 739–747. https://doi.org/10.1083/jcb.112.4.739

Tilney, L.G., Portnoy, D.A., 1989. Actin filaments and the growth, movement, and spread of the intracellular bacterial parasite, Listeria monocytogenes. Journal of Cell Biology 109, 1597–1608. https://doi.org/10.1083/jcb.109.4.1597

Umeda, R., Satouh, Y., Takemoto, M., Nakada-Nakura, Y., Liu, K., Yokoyama, T., Shirouzu, M., Iwata, S., Nomura, N., Sato, K., Ikawa, M., Nishizawa, T., Nureki, O., 2020. Structural insights into tetraspanin CD9 function. Nat Commun 11, 1606. https://doi.org/10.1038/s41467-020-15459-7

van Spriel, A.B., de Keijzer, S., van der Schaaf, A., Gartlan, K.H., Sofi, M., Light, A., Linssen, P.C., Boezeman, J.B., Zuidscherwoude, M., Reinieren-Beeren, I., Cambi, A., Mackay, F.,

Tarlinton, D.M., Figdor, C.G., Wright, M.D., 2012. The Tetraspanin CD37 Orchestrates the α4β1 Integrin–Akt Signaling Axis and Supports Long-Lived Plasma Cell Survival. Science Signaling 5, ra82–ra82. https://doi.org/10.1126/scisignal.2003113

Vargas, J.Y., Loria, F., Wu, Y.-J., Córdova, G., Nonaka, T., Bellow, S., Syan, S., Hasegawa, M., van Woerden, G.M., Trollet, C., Zurzolo, C., 2019. The Wnt/Ca2+ pathway is involved in interneuronal communication mediated by tunneling nanotubes. EMBO J 38, e101230. https://doi.org/10.15252/embj.2018101230

Victoria, G.S., Zurzolo, C., 2017. The spread of prion-like proteins by lysosomes and tunneling nanotubes: Implications for neurodegenerative diseases. J Cell Biol 216, 2633–2644. https://doi.org/10.1083/jcb.201701047

Vignais, M.-L., Caicedo, A., Brondello, J.-M., Jorgensen, C., 2017. Cell Connections by Tunneling Nanotubes: Effects of Mitochondrial Trafficking on Target Cell Metabolism, Homeostasis, and Response to Therapy. Stem Cells Int 2017, 6917941. https://doi.org/10.1155/2017/6917941

Wang, H.-X., Kolesnikova, T.V., Denison, C., Gygi, S.P., Hemler, M.E., 2011. The C-terminal tail of tetraspanin protein CD9 contributes to its function and molecular organization. J Cell Sci 124, 2702–2710. https://doi.org/10.1242/jcs.085449

Wang, X., Bukoreshtliev, N.V., Gerdes, H.-H., 2012. Developing Neurons Form Transient Nanotubes Facilitating Electrical Coupling and Calcium Signaling with Distant Astrocytes. PLOS ONE 7, e47429. https://doi.org/10.1371/journal.pone.0047429

Wang, X., Gerdes, H.-H., 2015. Transfer of mitochondria via tunneling nanotubes rescues apoptotic PC12 cells. Cell Death Differ 22, 1181–1191. https://doi.org/10.1038/cdd.2014.211

Wang, X., Veruki, M.L., Bukoreshtliev, N.V., Hartveit, E., Gerdes, H.-H., 2010. Animal cells connected by nanotubes can be electrically coupled through interposed gap-junction channels. Proceedings of the National Academy of Sciences 107, 17194–17199. https://doi.org/10.1073/pnas.1006785107

Wang, Y., Cui, J., Sun, X., Zhang, Y., 2011. Tunneling-nanotube development in astrocytes depends on p53 activation. Cell Death Differ 18, 732–742. https://doi.org/10.1038/cdd.2010.147

Wang, Y.A., Yu, X., Silverman, P.M., Harris, R.L., Egelman, E.H., 2009. The Structure of F-Pili. Journal of Molecular Biology 385, 22–29. https://doi.org/10.1016/j.jmb.2008.10.054

Watabe-Uchida, M., Uchida, N., Imamura, Y., Nagafuchi, A., Fujimoto, K., Uemura, T., Vermeulen, S., van Roy, F., Adamson, E.D., Takeichi, M., 1998. alpha-Catenin-vinculin interaction functions to organize the apical junctional complex in epithelial cells. J Cell Biol 142, 847–857. https://doi.org/10.1083/jcb.142.3.847

Watkins, S.C., Salter, R.D., 2005. Functional Connectivity between Immune Cells Mediated by Tunneling Nanotubules. Immunity 23, 309–318. https://doi.org/10.1016/j.immuni.2005.08.009

Weber, P.A., Chang, H.-C., Spaeth, K.E., Nitsche, J.M., Nicholson, B.J., 2004. The Permeability of Gap Junction Channels to Probes of Different Size Is Dependent on Connexin Composition and Permeant-Pore Affinities. Biophys J 87, 958–973. https://doi.org/10.1529/biophysj.103.036350

Wittig, D., Wang, X., Walter, C., Gerdes, H.-H., Funk, R.H.W., Roehlecke, C., 2012. Multi-level communication of human retinal pigment epithelial cells via tunneling nanotubes. PLoS One 7, e33195. https://doi.org/10.1371/journal.pone.0033195

Wood, B.M., Baena, V., Huang, H., Jorgens, D.M., Terasaki, M., Kornberg, T.B., 2021. Cytonemes with complex geometries and composition extend into invaginations of target cells. J Cell Biol 220, e202101116. https://doi.org/10.1083/jcb.202101116

Wood, M.N., Ishiyama, N., Singaram, I., Chung, C.M., Flozak, A.S., Yemelyanov, A., Ikura, M., Cho, W., Gottardi, C.J., 2017. α-Catenin homodimers are recruited to phosphoinositide-activated membranes to promote adhesion. Journal of Cell Biology 216, 3767–3783. https://doi.org/10.1083/jcb.201612006

Yamada, M., Sumida, Y., Fujibayashi, A., Fukaguchi, K., Sanzen, N., Nishiuchi, R., Sekiguchi, K., 2008. The tetraspanin CD151 regulates cell morphology and intracellular

signaling on laminin-511. The FEBS Journal 275, 3335–3351. https://doi.org/10.1111/j.1742-4658.2008.06481.x

Yamada, S., Pokutta, S., Drees, F., Weis, W.I., Nelson, W.J., 2005. Deconstructing the cadherin-catenin-actin complex. Cell 123, 889–901. https://doi.org/10.1016/j.cell.2005.09.020

Yáñez-Mó, M., Barreiro, O., Gordon-Alonso, M., Sala-Valdés, M., Sánchez-Madrid, F., 2009. Tetraspanin-enriched microdomains: a functional unit in cell plasma membranes. Trends in Cell Biology 19, 434–446. https://doi.org/10.1016/j.tcb.2009.06.004

Yang, X.H., Richardson, A.L., Torres-Arzayus, M.I., Zhou, P., Sharma, C., Kazarov, A.R., Andzelm, M.M., Strominger, J.L., Brown, M., Hemler, M.E., 2008. CD151 Accelerates Breast Cancer by Regulating α6 Integrin Function, Signaling, and Molecular Organization. Cancer Research 68, 3204–3213. https://doi.org/10.1158/0008-5472.CAN-07-2949

Yap, A.S., Niessen, C.M., Gumbiner, B.M., 1998. The juxtamembrane region of the cadherin cytoplasmic tail supports lateral clustering, adhesive strengthening, and interaction with p120ctn. J Cell Biol 141, 779–789. https://doi.org/10.1083/jcb.141.3.779

Yauch, R.L., Berditchevski, F., Harler, M.B., Reichner, J., Hemler, M.E., 1998. Highly Stoichiometric, Stable, and Specific Association of Integrin α3β1 with CD151 Provides a Major Link to Phosphatidylinositol 4-Kinase, and May Regulate Cell Migration. MBoC 9, 2751–2765. https://doi.org/10.1091/mbc.9.10.2751

Yauch, R.L., Kazarov, A.R., Desai, B., Lee, R.T., Hemler, M.E., 2000. Direct extracellular contact between integrin alpha(3)beta(1) and TM4SF protein CD151. J Biol Chem 275, 9230–9238. https://doi.org/10.1074/jbc.275.13.9230

Yoshida-Noro, C., Suzuki, N., Takeichi, M., 1984. Molecular nature of the calcium-dependent cell-cell adhesion system in mouse teratocarcinoma and embryonic cells studied with a monoclonal antibody. Developmental Biology 101, 19–27. https://doi.org/10.1016/0012-1606(84)90112-X

Yu, M., Yuan, X., Lu, C., Le, S., Kawamura, R., Efremov, A.K., Zhao, Z., Kozlov, M.M., Sheetz, M., Bershadsky, A., Yan, J., 2017. mDia1 senses both force and torque during F-actin filament polymerization. Nat Commun 8, 1650. https://doi.org/10.1038/s41467-017-01745-4

Zhang, C., Scholpp, S., 2019. Cytonemes in development. Current Opinion in Genetics & Development, Developmental mechanisms, patterning and evolution 57, 25–30. https://doi.org/10.1016/j.gde.2019.06.005

Zhang, K., Sun, Z., Chen, X., Zhang, Yifan, Guo, A., Zhang, Yan, 2021. Intercellular transport of Tau protein and β-amyloid mediated by tunneling nanotubes. Am J Transl Res 13, 12509–12522.

Zhang, S., Kazanietz, M.G., Cooke, M., 2020. Rho GTPases and the emerging role of tunneling nanotubes in physiology and disease. Am J Physiol Cell Physiol 319, C877–C884. https://doi.org/10.1152/ajpcell.00351.2020

Zhu, G.-Z., Miller, B.J., Boucheix, C., Rubinstein, E., Liu, C.C., Hynes, R.O., Myles, D.G., Primakoff, P., 2002. Residues SFQ (173-175) in the large extracellular loop of CD9 are required for gamete fusion. Development 129, 1995–2002. https://doi.org/10.1242/dev.129.8.1995

Zhu, S., Bhat, S., Syan, S., Kuchitsu, Y., Fukuda, M., Zurzolo, C., 2018. Rab11a–Rab8a cascade regulates the formation of tunneling nanotubes through vesicle recycling. Journal of Cell Science 131, jcs215889. https://doi.org/10.1242/jcs.215889

Zhu, S., Victoria, G.S., Marzo, L., Ghosh, R., Zurzolo, C., 2015. Prion aggregates transfer through tunneling nanotubes in endocytic vesicles. Prion 9, 125–135. https://doi.org/10.1080/19336896.2015.1025189

Zimmerman, B., Kelly, B., McMillan, B.J., Seegar, T.C.M., Dror, R.O., Kruse, A.C., Blacklow, S.C., 2016. Crystal Structure of a Full-Length Human Tetraspanin Reveals a Cholesterol-Binding Pocket. Cell 167, 1041-1051.e11. https://doi.org/10.1016/j.cell.2016.09.056